



HAL
open science

Rôle des cavéoles dans la régulation des contraintes biophysiques membranaires et implication dans la formation de tunnels transendothéliaux induits par une inhibition de RhoA

Camille Morel

► **To cite this version:**

Camille Morel. Rôle des cavéoles dans la régulation des contraintes biophysiques membranaires et implication dans la formation de tunnels transendothéliaux induits par une inhibition de RhoA. Human health and pathology. Université Paris Cité, 2021. English. NNT : 2021UNIP7338 . tel-04114633

HAL Id: tel-04114633

<https://theses.hal.science/tel-04114633v1>

Submitted on 2 Jun 2023

HAL is a multi-disciplinary open access archive for the deposit and dissemination of scientific research documents, whether they are published or not. The documents may come from teaching and research institutions in France or abroad, or from public or private research centers.

L'archive ouverte pluridisciplinaire **HAL**, est destinée au dépôt et à la diffusion de documents scientifiques de niveau recherche, publiés ou non, émanant des établissements d'enseignement et de recherche français ou étrangers, des laboratoires publics ou privés.

Université de Paris

École doctorale BioSPC (ED 562)

Unité des Toxines Bactériennes, Département de Microbiologie, Institut Pasteur, Paris.

**Role of caveolae in the regulation of membrane biophysical constraints
and involvement in the formation of transendothelial tunnels induced by
RhoA inhibition**

Par Camille Morel

Thèse de Doctorat de Microbiologie Cellulaire

Dirigée par Emmanuel Lemichez

Présentée et soutenue publiquement à Paris le 13/12/2021

Devant un jury composé de :

Isabelle Martin Verstraete Pr, Université de Paris et Institut Pasteur	Présidente du Jury
Anne Blangy DR, CNRS et Université de Montpellier	Rapportrice
Pierre Nassoy DR, CNRS et Université de Bordeaux	Rapporteur
Ewa Paluch Pr, Université de Cambridge	Examinatrice
Kheya Sengupta DR, Université d'Aix-Marseille	Examinatrice
Aurélien Roux Pr, Université de Genève	Examineur
Cécile Leduc CR, CNRS et Institut Jacques Monod	Membre invitée
Emmanuel Lemichez DR, Inserm et Institut Pasteur	Directeur de thèse

Abstract (English)

Several bacterial pathogens compromise the endothelial barrier function by triggering the opening of transendothelial (TEM) tunnels up to 20 μm wide. *In vivo*, this phenomenon has been associated with the dissemination of *Staphylococcus aureus* expressing the epidermal differentiation inhibitor (EDIN) via the hematogenous route and the appearance of gelatinous edema induced by the edema toxin from *Bacillus anthracis*. The opening of TEMs occurs concurrently to the spreading of endothelial HUVEC cells due to a relaxation of the actomyosin cytoskeleton induced by the inhibition of the small GTPase RhoA. The physical principle of liquid dewetting offers a theoretical framework that describes primary mechanical forces underlying the opening and widening of TEMs. In this model, the spreading of EDIN-intoxicated cells increases the membrane tension, leading to the opening of TEM. Then, enlargement of TEM tunnels is limited by the membrane rigidity and blocked thanks to the formation of an ezrin-driven formation of stiff actomyosin cable that accounts for line tension forces. TEM formation induces a combination of positive and negative membrane curvatures, which is sensed by the I-BAR domain proteins MIM/ABBA. Their accumulation around TEMs triggers an Arp2/3-driven actin polymerization leading to membrane wave expansion and resealing of tunnels.

Caveolae are cup-shaped invaginations of the plasma membrane known to deploy immediately in response to the increase of membrane tension. In this work, we have investigated the involvement of caveolae components, notably caveolin1 (cav1) and cavin1/PTRF, for nucleation and opening of TEMs. We report the presence of caveolae pits at the ventral side of the plasma membrane of endothelial cells subjected to ExoC3, although with a 2-fold decrease in their density. By a siRNA-based approach, we then established the importance of CAV1 and CAVIN1/PTRF in limiting the proportion of cells with TEMs and density of TEMs per cell. This aligns well with data showing the importance of caveolin1 and cavin1/PTRF in preventing the spreading of cells. Using a quantitative approach of TEM dynamics analysis, we record a dramatic increase of the speed of opening of TEMs and consequently their maximal size in siCAV1 cells, as compared to control and CAVIN1/PTRF KD conditions. Data framed in the theoretical cellular dewetting model, show that silencing of caveolin1 increases the effective membrane tension by 2-fold and reduces the effective bending rigidity by 3-fold, compared with control. The 1.5-fold decrease of membrane bending rigidity in siPTRF HUVECs can likely be attributed to a concomitant decrease of

caveolin1 protein level. In parallel, we have measured a decrease of cell volume and therefore cell height in both siCAV1 and siCAVIN conditions, which likely promote the apposition of membranes for nucleation of TEMs and account for an increase of TEM density in these conditions.

In conclusion, we elucidate a new role of caveolin1 independent from the formation of caveolae that specifically restrains the widening of TEMs possibly through its insertion in the inner leaflet of the plasma membrane.

Keywords :_caveolae, RhoA, mono-ADPribosylation, toxin, endothelium, caveolin1, cavin1, transendothelial macroaperture, TEM, membrane tension, membrane bending rigidity

Résumé (français)

Plusieurs pathogènes bactériens compromettent la fonction de barrière endothéliale en déclenchant l'ouverture de tunnels transendothéliaux dans les cellules (TEM). Ces TEM sont des structures dynamiques qui peuvent atteindre un diamètre de près de 20 micromètres. *In vivo*, ce phénomène a été associé à la dissémination de la bactérie *Staphylococcus aureus* qui exprime et produit l'inhibiteur de différenciation épidermique (EDIN) par voie hématogène. La formation de TEM corrèle également avec l'apparition d'un œdème gélatineux induit par la toxine œdematogène de *Bacillus anthracis*. Le processus de formation des TEM se décompose en trois phases.

L'ouverture des TEM se produit en même temps que l'étalement des cellules endothéliales HUVEC. Ceci est dû à la relaxation du cytosquelette d'actomyosine induite par l'inhibition de la GTPase RhoA, qui est spécifiquement ciblée par la toxine EDIN. Une autre toxine, l'ExoC3, est analogue à la toxine EDIN. L'exoC3 est produite par la bactérie *Clostridium botulinum* et cible spécifiquement RhoA. Ces deux toxines partagent le même mécanisme d'action.

Le principe physique du démouillage d'un liquide offre un cadre théorique qui décrit les forces mécaniques sous-jacentes à l'ouverture et l'élargissement des TEM. Le démouillage d'un liquide est un processus au cours duquel un liquide est forcé de s'étaler sur une surface non mouillable. Ceci induit la nucléation et la croissance de patch secs. La matière qui se rétracte de ses patchs secs forme alors une bordure courbée qui encercle le TEM. Par la suite, le liquide se décompose alors en goutellettes : un phénomène qui est irréversible. Dans le modèle de démouillage des cellules, les cellules sont apparentées à un liquide. L'étalement des cellules intoxiquées par l'EDIN augmente la tension de la membrane cellulaire, ce qui conduit à l'ouverture du TEM. La deuxième étape du processus de formation du TEM intervient après son élargissement. En effet, l'élargissement des tunnels TEM est limité par la rigidité de la membrane. Il est bloqué grâce à la formation d'un câble d'actin et de myosine rigide, également piloté par l'ezrin. Ce câble est non élastique et rend compte des forces de tension de ligne.

La dernière étape du processus de formation des TEM est la refermeture. La formation des TEM induit une combinaison de courbures positives et négatives de la membrane. Ces courbures sont rapidement détectées par les protéines du domaine I-BAR missing-in-

metastasis (MIM) et ABBA. Leur accumulation autour des TEMs déclenche une polymérisation de l'actine pilotée par Arp2/3.

Ceci conduit à l'expansion des ondes membranaires d'un bord du TEM jusqu'à son extrémité opposée. Ceci mène à la refermeture des tunnels.

Les cavéoles sont des invaginations de la membrane plasmique mesurant 60 à 80 nanomètres de diamètre. Elles sont composées de plusieurs protéines, qui sont impliquées dans la formation, la stabilisation et la dynamique de ces structures à la membrane plasmique. Les protéines cavéolines sont insérées dans la membrane plasmique et sont essentielles pour la formation de cavéoles invaginées. Il en est de même pour les protéines cytosoliques cavéolines qui sont nécessaires à la formation des cavéoles. D'autres protéines accessoires comme l'ATPase EHD2 permettent la stabilisation de la cavéole à la membrane plasmique, mais ne sont pas essentielles pour la formation des cavéoles. Les cavéoles sont très riches dans les cellules qui sont constamment soumises à un stress mécanique, comme les cellules endothéliales et les cellules musculaires. Du fait de leur présence importante dans ce type de cellules, elles sont associées à de nombreuses pathologies vasculaires et musculaires. Des mutations des protéines essentielles cavéolines ont été décrites comme impliquées dans des pathologies comme la dystrophie musculaire de Duchenne. Les cavéoles sont également nombreuses dans les cellules adipocytaires et sont donc associées à des pathologies telles que des lipodystrophies.

Les cavéoles présentent de nombreux rôles, comme dans le trafic des lipides à la membrane plasmique, l'endocytose ou encore de nombreux processus cellulaires. Notamment, elles sont connues pour se déployer immédiatement en réponse à l'augmentation de la tension membranaire. En effet, il a été montré qu'à la suite d'un choc osmotique qui induit une augmentation de la tension membranaire, les cavéoles se désassemblent. Elles ont donc un rôle de protection de la membrane plasmique contre une éventuelle rupture membranaire induite par un stress mécanique.

Dans ce travail de thèse, nous avons étudié l'implication des composants des cavéoles, notamment caveolin1 et la cavéoline1/PTRF, qui sont les isoformes majeures des cavéoles dans les cellules endothéliales. Nous avons étudié leur rôle dans la nucléation et l'ouverture des TEM induits par une inhibition de RhoA par la toxine EDIN et la toxine ExoC3.

En utilisant des expériences de microscopie électronique, nous rapportons la présence de cavéoles sur la face ventrale de la membrane plasmique de cellules endothéliales contrôles et de cellules endothéliales traitées à l'ExoC3. Nous avons observé que la forme, la taille et la composition des cavéoles est identiques dans les cellules contrôles et traitées à l'ExoC3. Nous avons noté que la densité des cavéoles est divisée par deux dans les cellules endothéliales traitées à l'ExoC3. Par une approche d'inactivation de gène par siRNA qui ciblent spécifiquement CAV1 et CAVIN1/PTRF, nous avons ensuite établi l'importance de ces deux protéines, la cavéoline1 et la cavin1/PTRF dans la limitation de la proportion de cellules présentant des TEMs. De plus, nous avons montré que la densité de TEMs induits par l'exoC3 est augmentée dans les cellules inactivées soit pour la cavéoline1 soit pour la cavin1.

Ceci s'aligne bien avec les données montrant l'importance de cav1 et cavin1/PTRF dans la prévention de l'étalement des cellules. En effet nous avons pu montrer que la déplétion des cavéoles par un traitement siCAV1 ou siCAVIN1/PTRF, induit une augmentation de l'air des cellules endothéliales intoxiquées. Nous avons également montré que le volume de ces cellules décroît. Ceci suggère que la hauteur des cellules traitées par siRNA ciblant CAV1 ou CAVIN1/PTRF diminue suite à un traitement à la l'ExoC3. Ceci favorise probablement l'apposition des membranes pour la nucléation des TEMs et explique une augmentation de la densité des TEMs dans ces conditions. Nous faisons ici l'hypothèse que cet affinement des cellules est responsable de la nucléation de TEMs observée dans ces conditions.

Nous avons par la suite réalisé des expériences de microscopie à fluorescence sur cellules vivantes afin d'observer la dynamique de formation des tunnels transendothéliaux. En utilisant une approche bioinformatique quantitative d'analyse de la dynamique des ces TEMs, nous enregistrons une augmentation spectaculaire de la vitesse d'ouverture des TEMs dans les cellules inactivées pour la cavéoline1. De plus, cette augmentation de vitesse d'ouverture corrèle avec une augmentation de la taille maximale des TEMs dans ces cellules siCAV1, par rapport aux conditions de contrôle et de siPTRF.

Les données interprétées par le modèle théorique de démouillage cellulaire, montrent que la déplétion de cav1 augmente la tension effective de la membrane de 2 fois et réduit la rigidité effective de courbure de 3 fois, par rapport aux cellules contrôles. La diminution de 1,5 fois de la rigidité de flexion de la membrane dans les HUVECs siPTRF peut probablement être attribuée à une diminution concomitante du niveau de cav1.

Nous avons effectué des expériences préliminaires de mesure de la rigidité membranaire en utilisant la méthode d'aspiration par micropipette couplée à l'extraction d'un

tube de membrane plasmique par pince optique. Les résultats suggèrent que le traitement d'inactivation de la cavéoline1 diminue la rigidité de la membrane. Ces résultats sont en accord avec les prédictions du modèle de démouillage cellulaire.

En conclusion, nous montrons que les cavéoles sont impliquées dans le contrôle de l'étalement et du volume cellulaire, lorsque les cellules sont intoxiquées. Nous concluons que c'est cet effet sur la forme des cellules qui est responsable de la nucléation des TEMs.

Nous élucidons également un nouveau rôle de la cavéoline1 dans le contrôle des paramètres physiques de la membrane plasmique, et notamment de la rigidité membranaire. Nous concluons que ce rôle de la cavéoline1 est indépendant de la formation des cavéoles et restreint spécifiquement l'élargissement des TEMs probablement par son insertion dans le feuillet interne de la membrane plasmique.

Remerciements

Tout d'abord je souhaiterais remercier les membres de mon comité de thèse, d'avoir accepté de relire ces pages et pour être présent le jour de ma soutenance afin d'évaluer les travaux de ces trois années de thèse. J'espère qu'ils vous plairont.

J'aimerais ensuite remercier Emmanuel Lemichez, mon directeur de thèse. Vous m'avez fait découvrir les tunnels ou les trous (personne n'a jamais vraiment compris la différence, soyons honnêtes). Ensemble nous avons pu apprendre plein de chose sur les cavéoles et s'émerveiller devant leurs photos. Merci d'avoir trouvé mes images d'IF toujours plus belles et de m'avoir fait confiance pour compter les innombrables TEMs. Merci d'avoir voulu aller toujours plus loin et d'avoir eu des idées un peu folles (que je n'ai pas toutes testées d'ailleurs, j'avoue...). Surtout, merci d'avoir été là quand je pensais que je n'étais pas capable de faire une thèse et de science. Vous m'avez fait découvrir ce que c'est de travailler avec passion. Merci aussi pour votre enthousiasme à toutes épreuves, car oui, des épreuves il y en a eu ! Merci aussi pour toutes les collaborations que vous m'avez poussée à faire, vous aviez raison : « pour que les gens s'intéressent à un projet, il fallait leur faire la danse du ventre ». Merci aussi pour tous les paris que vous avez perdus : j'attends avec impatience toutes les pizzas qui vont avec (au nombre de 3, je n'oublie rien). En bref, merci mille fois, pour tout. J'espère qu'au bout de 3 ans j'ai réussi à vous convaincre et si ce n'est pas le cas, j'espère au moins vous avoir embrouiller, parce qu'il faut bien se le dire « on ne tue pas une poule avec une crotte d'éléphant ».

Cécile, MERCI ! Parce que tu m'as fait découvrir la physique des cellules et parce que tu me l'as surtout traduite en langage d'humain lambda. Je me souviens encore de notre première réunion : j'avais rejoint l'unité depuis peu. Vous étiez tellement passionnés que je n'ai pas osé vous dire que je n'avais pas compris un mot pendant 2h de réunion. Grâce à toi le sentiment de vide ultime qui m'a envahie alors, a aujourd'hui disparu. Cela dit, pour moi la physique gardera toujours ses parts d'ombres (notamment les équations dans lesquels il y a autre chose que des chiffres, et la courbure Gaussienne, qui m'a traumatisée). Mais surtout merci pour ce manuscrit qui ne serait pas ce qu'il est sans toi. Merci pour tes ces innombrables corrections, suggestions et commentaires nocturnes, pour ces allers-retours et pour tous tes conseils WhatsApp. Merci de m'avoir secouée à le finir et d'avoir suggéré un jury du tonnerre ! Merci pour les millions de conseils et de tubes que tu m'as donné pour la microscopie. Tu m'as vraiment fait aimer ça et j'espère qu'on pourra retravailler ensemble un jour pour jouer avec des gros microscopes très chers et faire des

images incroyables. Merci aussi parce que sans toi le monde ne saurait pas à quel point les filaments intermédiaires sont importants. Un jour promis, je travaillerai dessus !

Je remercie également toutes les membres toxbac : Meng, Landry, Yu, Emma, Diane, Elea, Serena, Maud et Daniel. Marie-Anne, si notre rencontre m'a marqué à jamais, je n'ai pas l'intention de me souvenir de notre séparation : tu seras toujours dans mon cœur. Merci pour ton écoute, ta présence, tes conseils et toutes tes anecdotes qui me font tant rêver. Amel merci pour avoir été là pour répondre à mes questions de science, de manip et de gestion. Merci aussi de m'avoir sauvée de la tâche de la réparation du Pxi ! Kloé, merci mille fois. D'une part pour avoir un K dans ton prénom et ensuite parce que tu as été une stagiaire exemplaire : au labo comme en dehors. Merci pour ces verres (trop ?) et pour ces moments de rigolades. Aujourd'hui ton stage est fini mais tu resteras mon amie, alors merci.

Merci à tous mes collaborateurs, Nishit et Matthieu Piel, Feng et Patricia Bassereau, Eline et Stéphane Vassilopoulos, sans qui cette thèse n'aurait pas été possible. David, merci mille fois de m'avoir expliqué encore et encore la théorie du dewetting : merci pour ces heures de réunion pour ta bonne humeur et ton travail dans cette jolie histoire ! Un grand merci aussi à la Team Cossart et à vous tous, qui m'avez accompagnée lors de mon changement de thèse. Cette thèse est aussi la vôtre. Merci à Thomthom pour toutes ces analyses statistiques qui ont mis des étoiles dans ma thèse. Grâce à toi j'ai un peu moins peur des stats, alors on peut te féliciter chaleureusement. Merci pour ces heures passées à essayer de comprendre ce que je faisais, et merci de m'avoir fait rire autant, tu rends les stats bien plus agréables. J'attends mon petit tour de Paris en Mustang avec impatience, et la bière que tu me dois depuis 6 mois. Dr Lemerle, merci d'être venue seule à ce magnifique congrès EMBO : je ne m'y serais pas autant amusé sans toi ! Les manip qu'on a faites ensemble ont été fun et enrichissantes : merci pour toutes ces discussions cavéolaires accompagnée de muffins incroyables. Merci pour le Genepi qui a fait tellement de bien (ou de mal ?). Merci de m'avoir prêté ton chat quand j'avais besoin de câlins, compagnie et coup de griffes. Merci aussi pour cette conversation « harcèlement » qui m'a aidé à faire cette thèse. Grâce à toi je me suis sentie comprise : oui cav1 et cavin1 ça se ressemble, mais ce n'est pas la même chose. Merci pour cette aprèm de comptage de cavéoles qui restera gravé : déjà parce que je n'avais jamais vu une cavéole aplatie avant et ensuite parce que maintenant j'ai besoin de nouvelles lunettes. Tes images ont fait pleurer mes yeux de douleurs, j'espère qu'elles feront pleurer mes reviewers de joie.

Spéciale dédicace à mes tigrisses, pour toutes ces pauses Thé-caféO et malheureusement tous les gâteaux qui vont avec. Grâce à vous je n'ai pas perdu un seul kilo... Merci pour ce groupe WhatsApp de l'enfer, qui retrace la vie et les potins du labo :

avec ce qu'il y a dedans, on pourrait écrire un livre, dont Pay serait le PI. Pay, merci d'avoir été une si bonne collègue. Je ne te dirai qu'une chose : c'est CIAO (drop the mic'). Maud, tu as été le soleil du labo. Ta bonne humeur et ton humour n'ont pas d'égal (et tant mieux). Merci pour tes snaps de vie, qui rythme mes journées et me font tellement rire : j'en suis sûre tu as de l'avenir ! Merci pour les cadeaux PokémonGo et pour ton soutien dans ce combat. Je n'oublierai pas ton concert privé de Johnny dans la salle de ma soutenance. Merci pour ton aide à la rédaction de cette thèse, elle a été essentielle. Merci pour tous ces blots, pour les manips RTK interminables et ADPr qu'on a mis trop de temps à comprendre et que je n'aurais pas pu faire sans toi. Tu as de l'or scientifique entre les mains, crois-moi. Merci pour les poissons d'avril, bien que ça n'ait fait rire personne. Serena, merci parce que tu as été là du début à la fin de cette thèse. Merci pour ces heures passées ensemble et pour tes manips du siècle. Merci parce que grâce à toi j'ai appris l'italien, enfin, j'ai surtout appris à crier fort. Tes expressions ont été une bouffée d'air frais dans ce labo (qui sent le Laemmlli). Les filles, merci pour ce ski-trip qui a été exceptionnellement drôle, rempli de chute, de fromage et de boule de neige. Que ça soit bien clair : c'est maintenant une obligation annuelle, un peu comme payer ses impôts à temps (Pay ?).

Mili, merci pour ces journées de rédaction interminables et pour ma concentration que tu as su garder au max malgré toutes les feintes que j'ai développé pour échapper à ton œil avisé de maman de rédac. Merci pour ces pics de stress que tu as contrés a coup de cookies, de kinder surprise et de Playmobil et de moments « calls » qui m'ont fait oublier les aléas de la thèse un instant. Merci d'avoir été mon writting buddy et d'avoir pris soin de moi malgré mes moments d'absence (de 4 ans ?) et surtout d'avoir été là quand ça n'allait pas : on se fait de nouveaux souvenirs.

Je ne pouvais pas t'accorder qu'une seule ligne. Pay, tu as été une de mes meilleures rencontres. J'ai eu besoin de toi tout au long de cette thèse et je resterai là jusqu'à ce que tu finisses la tienne. Merci pour ces soirées de folie qu'on a passées ensemble, je pense que je ne serai plus jamais capable de sortir sans toi. On a tellement rigolé, nos bêtises vont me manquer atrocement. Merci pour ces week-ends camions qui n'ont aucun sens, mais qu'on va continuer de faire. Merci de m'avoir accompagnée pour une nuit au sommet du Semnoz, là où tu as découvert que nos sacs de couchages étaient confort à +15°C, lorsqu'il en faisait -6°C dehors. C'était magnifique, mais on a bien cru qu'on ne passerait pas la nuit (c'était sans « comté » sur les trésors et Justin Bieber). Mais attends, si je pars dans 2 mois, et que toi tu pars dans 1 an, comment on va faire pour sortir danser l'une sans l'autre ? Les calculs sont pas bons Kevin !!

T9, tu as été un bon camarade de Shifumi (surtout tu perds tout le temps, sauf le premier et je te remercie de l'avoir gagné celui-là), même s'il va te falloir encore un peu de pratique pour expliquer les règles du jeu. Que nenni ! Ça viendra quand tu grandiras. Merci pour la vraie gentillesse dont tu fais preuve : c'est si rare. Merci aussi de me supporter : ça aussi, c'est rare. Je suis contente de faire Bonnie si tu fais Clyde. Merci pour tes schémas, abréviations et biblio : je n'y serais pas arrivé sans toi. Pour finir merci d'avoir essayé (sans succès) de faire des blagues plus drôles que le miennes.

Jazmin : merci d'avoir été là ça dans les coups durs, merci pour ces discussions, pour ces toutes ces pauses café qui ont été une vraie échappatoire. Merci d'être mon amie, toujours. Merci d'avoir cassé la centri chez Pascale, ça me fait toujours autant rire. Je t'attends pour visiter le Costa-Rica, Besote chica ! Akié, merci pour ces appels sans fin, ces dimanches de bonheur et ces semaines passées chez toi, à chanter à tue-tête. Merci pour m'avoir appris ta version du Poker Blinders et de m'avoir accompagnée tout au long de ma thèse. Tu es comme une sœur pour moi. Merci à Mousst, Pauline, Moumou et Zinzi pour votre soutien, votre présence et vos conseils et à tous les copains que je ne peux pas citer par manque de place : je vous aime !

Merci à toute ma famille qui est toujours là pour moi, qui invite mes collègues à manger des raclettes et qui m'accueille à bras ouvert quand je rentre « en province » pour skier et respirer. Merci Mam's pour avoir mis tant d'entrain à essayer de comprendre ce que je fais, sans jamais y arriver. Merci à ma sœur préférée pour supporter mes absences et ma non implication dans les cadeaux de Noël. Merci aussi pour avoir veillé sur Henry.

Merci aussi à toi. Et merci à tous les autres que j'oublie par manque de place. Vous êtes dans mon cœur !

Comme l'a dit Albert Einstein : "La théorie, c'est quand on sait tout et que rien ne fonctionne. La pratique, c'est quand tout fonctionne et que personne ne sait pourquoi. Ici, nous avons réuni théorie et pratique : Rien ne fonctionne... et personne ne sait pourquoi !"

« Choisissez un travail que vous aimez
et vous n'aurez pas à travailler
un seul jour de votre vie. »

Confucius

Table of contents

ABSTRACT (ENGLISH)	2
RESUME (FRANÇAIS)	4
REMERCIEMENTS	8
TABLE DES MATIÈRES	13
LIST OF ABBREVIATIONS	16
LIST OF FIGURES	21
I. INTRODUCTION	23
1. CYTOSKELETON AND PLASMA MEMBRANE	26
1.1. CYTOSKELETON	26
1.1.1. Actin	27
1.1.1.1. Steady state of actin polymerization	27
1.1.1.2. Actin nucleation	28
1.1.1.3. Actin polymerization	29
1.1.1.4. Organization of actin filaments and networks	30
1.1.2. Regulation of actin cytoskeleton by RhoGTPases	33
1.1.2.1. RhoA signalling and its effectors	34
1.1.2.1. Rac1/Cdc 42 signalling and their effectors	35
1.2. PLASMA MEMBRANE	37
1.2.1. Composition	37
1.2.2. Physical properties of membranes	42
1.2.2.1. Bending rigidity	42
1.2.2.2. Plasma membrane tension	49
1.2.3. Controlling and measuring membrane physical properties	54
1.2.3.1. Micropipette aspiration	55
1.2.3.2. Tether pulling experiments	56
1.2.3.3. Combination of micropipette aspiration and optical tweezers	58
1.2.3.4. A lipid probe to measure membrane tension	59
2. CAVEOLAE	60
2.1.1. Caveolae: structure, composition and organization	60
2.1.1.1. Caveolins	62
2.1.1.2. Cavins	65
2.1.1.1. EHD2 and accessory proteins	67
2.1.1.2. Lipids	68
2.1.2. Caveolae biogenesis	69
2.1.3. Role and function of caveolae	71
2.1.3.1. Caveolae in lipids trafficking	71
2.1.3.2. Caveolae as mechanoprotectors	73
2.1.3.3. Caveolae as endocytic carrier	78
2.1.3.4. Caveolae in cell signalling	79
2.1.4. Pathologies related to caveolae	81
2.1.4.1. Cav1 and vascular pathologies	82

2.1.4.2.	Caveolae and microbial pathogenesis	82
2.1.5.	Caveolae and endothelium	85
3.	TRANSCELLULAR TUNNELS AND THE ENDOTHELIUM	86
3.1.	IN PHYSIOLOGY.....	86
3.2.	IN PATHOLOGIES.....	93
3.2.1.	Transendothelial macroapertures tunnels induction.....	94
3.2.1.1.	Transendothelial cell tunnels macroapertures opening.....	97
3.2.1.2.	Stabilization.....	101
3.2.1.3.	Closure	102
3.2.2.	Analogies of the cellular dewetting model	103
II.	<u>MATERIALS AND METHODS.....</u>	<u>105</u>
1.	CELL CULTURE.....	106
1.1.	SIRNA TRANSFECTION	106
1.2.	DNA ELECTROPORATION	106
1.3.	CELL INTOXICATION.....	107
2.	MORPHOLOGICAL ANALYSIS	107
2.1.	IMMUNOFLUORESCENCE	107
2.2.	VIDEO MICROSCOPY	107
2.3.	CELL VOLUME MEASUREMENT.....	108
2.4.	VARIATION OF SUBSTRATE COMPLIANCE USING HYDROGELS.....	108
2.5.	TRANSMISSION ELECTRON MICROSCOPY.....	109
3.	BIOCHEMISTRY ANALYSIS	111
3.1.	WESTERN BLOT ANALYSIS	111
4.	BENDING RIGIDITY MEASUREMENTS.....	111
4.1.	PMS FORMATION.....	111
4.2.	TETHER EXTRACTION, MICROPIPETTE ASPIRATION AND FORCE MEASUREMENT.....	111
5.	STATISTICAL ANALYSIS.....	112
6.	PHYSICAL MODELING	113
III.	<u>CONTEXT AND AIM OF THE STUDY</u>	<u>117</u>
1.	CONTEXT	118
2.	AIM OF THE THESIS	120
IV.	<u>RESULTS.....</u>	<u>121</u>
1.	ENDOTHELIAL CELL TREATMENT WITH RHOA INHIBITING TOXIN ALTERS CAVEOLAE DENSITY AT THE PLASMA MEMBRANE. 122	
2.	CAVEOLAE COMPONENTS LIMIT THE FORMATION OF TEMS	126
3.	CELL SPREADING INCREASE OF STIFF SUBSTRATE AND CONTROL OF TEMS FORMATION	ERREUR ! SIGNET NON DEFINI.
4.	CAVEOLIN1 AND CAVIN1/PTRF IN THE CONTROL OF CELL SPREADING.....	135
5.	CAVEOLIN1 AND CAVIN1/PTRF IN THE CONTROL OF CELL VOLUME.....	136
6.	DIFFERENTIAL IMPACT OF CAVIN1/PTRF AND CAVEOLIN1 ON TEM DYNAMICS	139
7.	DIFFERENTIAL IMPACT OF CAVEOLIN AND CAVIN ON MEMBRANE RIGIDITY	143
V.	<u>DISCUSSION.....</u>	<u>145</u>
VI.	<u>CONCLUSION, PERSPECTIVES.....</u>	<u>149</u>

8. CAVEOLINS VS CAVEOLAE IN SIGNALLING PROCESSES	150
9. MEMBRANE MECHANICAL PROPERTIES	152
9.1. IMPACT OF CHOLESTEROL DEPLETION AND PERTURBATION OF PM LIPID COMPOSITION.....	152
9.2. LIPIDOMIC ANALYSIS.....	153
9.3. PROBING MEMBRANE MECHANICAL PROPERTIES OF THE PLASMA MEMBRANE	153
10. CELL SHAPE	154
11. PHYSIOLOGY AND PATHOPHYSIOLOGY PROCESSES.....	154
11.1. OTHER TOXINS	154
11.2. <i>IN VITRO</i> SYNTHETIC BLOOD VESSELS.....	154
11.3. <i>IN VIVO</i> ANIMAL MODELS.....	155
<u>VII. BIBLIOGRAPHY</u>	<u>156</u>
<u>VIII. ANNEXE</u>	<u>185</u>
1. DHA-PHOSPHOLIPIDS CONTROL MEMBRANE FUSION AND TRANSCellular TUNNEL DYNAMICS.....	186
1.1. ABSTRACT	ERREUR ! SIGNET NON DEFINI.
1.2. INTRODUCTION	ERREUR ! SIGNET NON DEFINI.
1.3. RESULTS	ERREUR ! SIGNET NON DEFINI.
1.4. DISCUSSION.....	ERREUR ! SIGNET NON DEFINI.
1.5. MATERIALS AND METHODS	ERREUR ! SIGNET NON DEFINI.
1.6. REFERENCES	ERREUR ! SIGNET NON DEFINI.
1.7. FIGURE LEGENDS	ERREUR ! SIGNET NON DEFINI.
1.8. SUPPLEMENTARY FILES.....	ERREUR ! SIGNET NON DEFINI.
2. DEWETTING: FROM PHYSICS TO THE BIOLOGY OF INTOXICATED CELLS.....	186
2.1. ABSTRACT	36
2.2. INTRODUCTION	38
2.3. PHYSICAL MODEL OF CELLULAR DEWETTING	40
2.4. CHARACTERISTICS OF CELL DEWETTING	41
2.4.1. Driving force.....	42
2.4.2. Line tension.....	44
2.4.3. Nucleation.....	46
2.4.4. Maximum size	47
2.4.5. Rim formation	49
2.4.6. Viscous dissipation and opening dynamics.....	49
2.4.7. Closure	51
2.5. FUTURE DEVELOPMENTS AND CONCLUSIONS.....	52
2.5.1. Critical thickness.....	52
2.5.2. Spinodal dewetting.....	53
2.5.3. Irregular and soft substrates	54
2.6. ACKNOWLEDGEMENTS.....	55

List of abbreviations

ABP: actin binding protein
ADF: actin depolymerizing factor
ADP: adenosine diphosphate
AFM: atomic force microscopy
Arp: actin related protein
ATP: adenosine triphosphate
BAR: Bin/Amphiphysin/Rvs
BSA: bovin serum albumin
CAM: cell adhesion molecule
CaMKII: calcium-calmodulin-dependent protein kinase II
Cav1: caveolin 1
Cdc42: cell division cycle 42
COP: coat protein
CSD: caveolin scaffolding domain
CTRL: control
DHA: docosahexaenoic acid
DNA: deoxynucleic acid
DOPC: 1,2-dioleoyl-snglycero-3-phosphocholine
DRM: detergent resistant membrane
ECM: extracellular matrix
Ect2: epithelial cell transforming 2
EDIN: epidermal differentiation inhibitor
EF: edema factor
EGF: epidermal growth factor
EHD2: EH-domain containing 2
Ena: drosophila melanogaster Enabled
eNOS: endothelial nitric oxide synthase
Epac: exchange protein directly activated by cAMP
ER: endoplasmic Reticulum
ERK: extracellular-signal-regulated kinase
ERM: ezrin–radixin–moesin
ESCRT: endosomal sorting complex required for transport
ET: oedematogenic toxin
ExoC3: C3 exoenzyme

F-actin: filamentous actin
F-BAR: Fes/CIP4 homology- bin/Amphysin/Rvs
FA: fatty acids
FAK: focal adhesion kinase
FBS: foetal bovine serum
FGF: fibroblast growth factor
FH1: formin homology 1
FH2: formin homology 2
FITC: Fluorescein isothiocyanate
FLIM: fluorescence lifetime imaging microscopy
FLNA: Filamin A
FRAP: fluorescence-recovery-after-photobleaching
G-actin: Globular actin
GAP: GTPase activating protein
GD3: ganglioside 3
GDI: guanine nucleotide dissociation inhibitor
GDP: guanosine diphosphate
GEF: guanine nucleotide exchange factor
GFP: green fluorescent protein
GM: monosialodihexosylganglioside
GPL: glycerophospholipid
GSL: glycosphingolipid
GTP: guanosine triphosphate
GUV: giant unilamellar vesicle
H2AX: H2A histone family member X
HEK: human embryonic kidney
HEPES: 4-(2-hydroxyethyl)-1-piperazineethanesulfonic acid
HIV: human immunodeficiency virus
HMDS: hexamethyldisilazane
HR: helical region
HRP: horseradish peroxidase
HUVEC: human umbilical vein endothelial cell
I-BAR: inverse homology-bin/Amphysin/Rvs
IAA: iodoacetic acid
ICAM: intercellular adhesion molecule
IRSp53: insulin receptor substrate p53 protein
KD: knock-down

KO: Knock-out
LARG: leukemia-associated Rho guanine nucleotide exchange factor
LFG: lifeguard
LT: lethal toxin
lysoPC: lysophosphatidylcholine
LZD: leucine zipper-like domain
MBS: myosin binding subunit
mDia: mammalian homolog of diaphanous
Mfsd2a: major facilitator superfamily domain containing 2A
MIM: missing in metastasis
MLC: myosin light chain
MLCK myosin light chain kinase
MRLC: myosin regulatory light chain
M β CD: methyl- β -cyclodextrin
mTOR: mammalian target of rapamycin
mTORC: mammalian target of rapamycin complex
MURC: muscle-restricted coiled-coil protein
MW: molecular weight
NBD: nucleotide-binding domain
NPF: nucleation promoting factors
OA: oleic acid
PA: phosphatidic acid
PAK: p21-activated kinase
PBS: phosphate-buffered saline
PC: phosphatidylcholine
pCMV: porcine cytomegalovirus
PDMS: poly(dimethylsiloxan)
PE: phosphatidylethanolamine
PEST: proline (P), glutamic acid (E), serine (S), threonine (T)
PFA: paraformaldehyde
PG: Phosphatidylglycerol
PI: phosphatidylinositol
PI3K: phosphoinositide-3-kinase
PIP: phosphatidylinositol phosphate
PIP2: phosphatidylinositol4,5-bisphosphate
PKA: protein Kinase A
PKC: protein kinase C

PLD2: phospholipase D2
PLs: Phospholipids
PM: plasma membrane
PMS: plasma membrane spheres
pol1: polymerase 1
PP1: type 1 protein phosphatase
PS: phosphatidylserine
PTRF: polymerase I and transcript release factor
PUFA: polyunsaturated fatty acids
PV1: plasmalemma vesicle protein 1
PVLAP: plasmalemmal vesicle associated protein
Rac1: Ras-related C3 botulinum toxin substrate 1
Rap: Ras proximate
Ras: rat sarcoma
rDNA: ribosomal desoxyribonucleic acid
Rho: Ras homolog
RNA: ribonucleic acid
ROCK: Rho-associated kinase
ROI: regions of interest
RT: room temperature
Sar1: secretion associated Ras related GTPase 1
SC: Schlemm's canal
SDPR: serum deprivation response protein
SDS: sodium dodecyl sulfate
SFM: serum free medium
SFMc: serum free medium complete
siRNA: small interfering RNA
SNARE: soluble N-éthylmaleimide-sensitive-factor attachment protein receptor
SRBC: serum deprivation response-related gene product that binds to c-kinase
SV40: simian virus 40
TAZ: transcriptional coactivator with PDZ-binding motif
TBS-T: tris-buffer saline supplemented with tween 20
TEM: transendothelial macroaperture
TNF- α : tumor necrosis factor α
TRITC: tetramethylrhodamine
VASP: vasodilator-stimulated phosphoprotein
VE-cadherin: vascular endothelial cadherin

VEGF: vascular endothelial growth factor

WASP: Wiskott–Aldrich syndrome protein

WAVE: WASP-like verprolin homologous protein

WH2: WASP-homology 2

WT: wild type

YAP: yes-associated protein

List of figures

Figure 1. Animal cell.....	26
Figure 2. Kinetics of single actin filament assembly.....	27
Figure 3. Distinct actin filament organizations.....	29
Figure 4. Actin filaments organization in a moving eukaryotic cell.....	31
Figure 5. Rho GTPases regulation.....	34
Figure 6. Fluid mosaic model.....	37
Figure 7. Lipids composition and diversity.....	39
Figure 8. Liquid-disordered and liquid-ordered phases.....	40
Figure 9. Lipid composition of the endomembrane system.....	41
Figure 10. Example of membrane deformations.....	44
Figure 11. Membrane curvature and lipid packing defects and variety of lipid shape.....	45
Figure 12. The structure of BAR domain proteins.....	48
Figure 13. Thermal fluctuation of a giant vesicle observed in phase contrast.....	50
Figure 14. Scheme depicting the main method to characterize the effective PM tension.....	55
Figure 15. Model of a tube pulled out of a flat membrane and its force-extension curve ..	57
Figure 16. Scheme depicts the equilibrium of forces on a blebbing membrane.....	58
Figure 17. Tether pulling experiment on a GUV controlled by micropipette aspiration.....	59
Figure 18. Fluorescence lifetime of the FliptR probe reports membrane tension changes	60
Figure 19. Caveolae.....	61
Figure 20. Caveolae structure.....	62
Figure 21. Caveolin1 structure.....	64
Figure 22. Cavins structure.....	65
Figure 23. Schematic model of caveolin biogenesis.....	71
Figure 24. Caveolae flattening induced by osmotic shock.....	74
Figure 25. Schematic model of the flattening of the caveolae.....	76
Figure 26. Proposed model for the caveolin-mediated uptake of <i>L. monocytogenes</i> membrane protrusions.....	84
Figure 27. Formation of transcellular tunnels in endothelial cells during transcytosis.....	86
Figure 28. Diapedesis process of leucocytes.....	88
Figure 29. Transcellular pore closure is initiated by novel ventral lamellipodia.....	89
Figure 30. Schlemm's canal endothelium present pores.....	90
Figure 31. Fenestrae of rat liver sinusoidal endothelium.....	92
Figure 32. Formation of transendothelial macroapertures.....	94
Figure 33. Inhibition of RhoA triggers transendothelial macroapertures formation.....	97
Figure 34. Local force application by the tip of an atomic force microscope cantilever is sufficient to induce transcellular tunnels in endothelial cells.....	98
Figure 35. Physical process of liquid dewetting compared to biological cellular dewetting.....	100
Figure 36. Organization of the actomyosin cytoskeleton along transendothelial macroapertures edges.....	101
Figure 37. Transendothelial macroaperture closure mechanisms.....	103
Figure 38. Principle of cell volume measurement.....	108
Figure 39. Variation of tissue stiffness in physiology.....	109
Figure 40. Unroofing of cells for transmission electron microscopy.....	110

Figure 41. Density of caveolae at plasma membrane decreases upon RhoA inhibition by ExoC3 from <i>C. botulinum</i>	124
Figure 42. Immunogold labelling of GFP-Cav1.	125
Figure 43. Density of caveolae at the plasma membrane of HUVEC control or treated 24h with ExoC3, quantified on transmission electron micrographs	126
Figure 44. Depletion of structural components of caveolae by siRNA effectively reduces the level of targeted proteins.	127
Figure 45. Controls of RhoA mono-ADP ribosylation.	127
Figure 46. Control of siRNA efficacy in RhoA mono-ADP ribosylation experiments.....	128
Figure 47. TEM density increases in CAV1 or cavin1/PTRF siRNA-treated cells.	129
Figure 48. TEM density increases in CAV1 or cavin1/PTRF siRNA-treated cells.	129
Figure 49. TEM density increases in CAV1 or cavin1/PTRF siRNA-treated cells.	130
Figure 50. In HUVEC intoxicated with the EDIN from <i>S. aureus</i> , TEM density increases in CAV1 or cavin1/PTRF siRNA-treated cells.	131
Figure 51. TEM density increases in siEHD2 or siFLNA treated cells.....	132
Figure 52. Variations of cell spreading and percentage of TEM formation in HUVEC plated on matrix of different compliance.	134
<i>Figure 53. Example of a confocal micrographs of cells show the spreading determination process.....</i>	<i>135</i>
Figure 54. Cavin1/PTRF plays key role in the control of the spreading of HUVEC.	136
Figure 55. Cavin1/PTRF plays key role in the control of the volume of HUVEC.	138
Figure 56. Heatmap of TEMs opening in HUVEC	139
Figure 57. Caveolin1 controls parameters of speed of TEM opening and maximal size.	140
Figure 58. Caveolin1 controls effective membrane bending rigidity and tension.....	142
Figure 59. Caveolin1 controls effective membrane bending rigidity and tension.....	142
Figure 60. Caveolin1 controls effective membrane rigidity and tension	144



I. Introduction

I joined the laboratory of Dr Lemichez during the second year of my PhD thesis. My thesis work was conducted within the frame of the research conducted in the host laboratory on the description of cellular dewetting theory formulated by David Gonzalez-Rodriguez, Françoise Brochard-Wyart and colleagues in 2012 (Gonzalez-Rodriguez et al., 2012). This theory draws a phenomenological analogy between the process of formation of transendothelial cell macroaperture (TEM) tunnels and the phenomenon of viscous liquid dewetting, i.e. nucleation and enlargement of a dry patch within a viscous liquid film under tension. It is a well-known phenomenon that has been extensively studied by Pr Françoise Brochard-Wyart and Pr Gilles de Gennes. This theory is more generally part of the description of physical phenomena at the micrometric scale relatively independent of Newtonian forces and essentially based on several forces encompassing surface tension, interfacial forces and viscoelasticity. The beauty of such a description of TEM dynamics by a simplified physical model is that it offers a framework to challenge the model and thereby decipher important cellular parameters at play. For example, in the liquid film the dry patch retracts until complete dewetting of the liquid film whereas in a cell TEMs reach a maximal size. This led us to discover that cells built a stiff actomyosin cable that encircle TEMs thereby blocking enlargement (Stefani et al., 2011). The disruption of the cable leads to a resume growth of TEMs indicating that the forces at play in TEM opening do not vanish during TEM enlargement, as previously postulated, but are rather counter-acted by the force generated by the cable along the TEM circumference.

At the time I enter the field, two remarkable studies rendered possible to address questions on the implication of membrane bending rigidity and tension in the dynamics of TEMs. The study by Pinot and colleagues had unveiled the remarkable contribution of polyunsaturated fatty acids (Docosahexaenoic acid, DHA) in facilitating membrane bending and fusion, thereby facilitating membrane endocytosis (Pinot et al., 2014). The other study conducted by Sinha and colleagues reported that caveolae membrane invaginations forming a reservoir of plasma membrane prone to deploy to counteract an acute increase of membrane tension, thereby protecting membrane from rupturing (Sinha et al., 2011). Of importance in this study, they showed that absence of caveolae is responsible for a linear increase of membrane tension as a function of the increasing traction forces applied to the membrane. The host laboratory took advantage of these two findings to challenge hypothesis of the implication of membrane tension and bending rigidity physical parameters postulated in the cellular dewetting model. While modulation of lipid composition at the plasma membrane was the object of the thesis work of Meng-Chen TSAI (see accompanied manuscript in reviewing), I studied the contribution of caveolin1 and cavin1-dependent

formation of caveolae pits in the dynamics of TEMs (manuscript under writing). During my thesis, I also participated in the writing of a review describing the different biophysical analogies of liquid dewetting in living systems.

The two complementary approaches show that it is possible to modulate the size and density of TEMs in endothelial cells, which may be of importance in physiology and during intoxication processes. The massive incorporation of DHA in the plasma membrane (an acyl chain essential in diet), for example, leads to an increase in the frequency of formation of TEMs, which is expected for an acyl chain able of promoting membrane fusion. Moreover, this leads to a compensatory phenomenon of reduction in the size of TEMs to ensure an overall conservation of opening surfaces at the scale of the cell population. This homeostatic regulation associated to a disequilibrium of hyper-unsaturation of phospholipid acyl chains remains to be defined. I could further document a cross-talk between RhoA signalling and caveolae. Loss of RhoA activity leads to a 2-fold reduction of caveolae at the plasma membrane. Nevertheless, ablation of caveolae components, either caveolin1 or cavin1 leads to an increase the density of TEMs per cell and massive enlargement of the size of TEMs in caveolin1 depleted cells. Further consistent with a differential role of cavin1 and caveolin1, I have documented a role of cavin1 in limiting the spreading of cells while caveolin1 is more implicated in the regulation of cell shape, i.e. adjustment of cell volume during cell spreading. Finally, through determination of TEM dynamics parameters combined with direct measurement of membrane physical parameters, I have brought evidences that caveolin1 control parameter of membrane rigidity contrary to cavin1. These findings and implication in the understanding of cellular dewetting phenomenon are discussed in my thesis manuscript after an introduction that is aimed at presenting a large number of concepts involved in the understanding of the whole phenomenon of cellular dewetting.

My introduction is divided in three chapters. In a first chapter, I characterize the properties of plasma membrane and its coupling to the actin cytoskeleton and introduce the physical parameters that will be later used in the course of my thesis. In a second chapter, I provide a state-of-the-art knowledge on caveolae, in order to later show how my PhD work brings new insights on their cellular functions. In a third chapter, I finally introduce the toxins that I worked with and introduce the context of the study on TEMs. Then I describe my PhD work divided in 4 sections: II. Material and Methods, III. Context, IV. Results, V. Discussion. These sections aim at being merged in order to form the main text of an article. Finally, I conclude my thesis in the section VI. and provide perspectives for my PhD work. The manuscripts that I co-authored are added in the annex (VII).

1. CYTOSKELETON AND PLASMA MEMBRANE

A cell is defined as the basic unit of life and animal cells can be divided in three main compartments. Cellular matter is physically defined by a plasma membrane (PM) in tight interaction with the cytoskeleton. The cytoskeleton is a complex, dynamic network of interlinking protein filaments present in the cytoplasm of all cells. The cytoplasm contains many organelles, including the nucleus, the endoplasmic reticulum (ER) and the Golgi apparatus. The nucleus of the cell supports all information in the form of deoxyribonucleic acid (DNA) (Albert et al. 1995). In this first chapter, we will focus on the cytoskeleton, that maintains the cell shape and confers its mechanical properties to the cell and the PM, a semi-permeable barrier that regulates the flow of molecules in and out of the cell (**Fig. 1**).

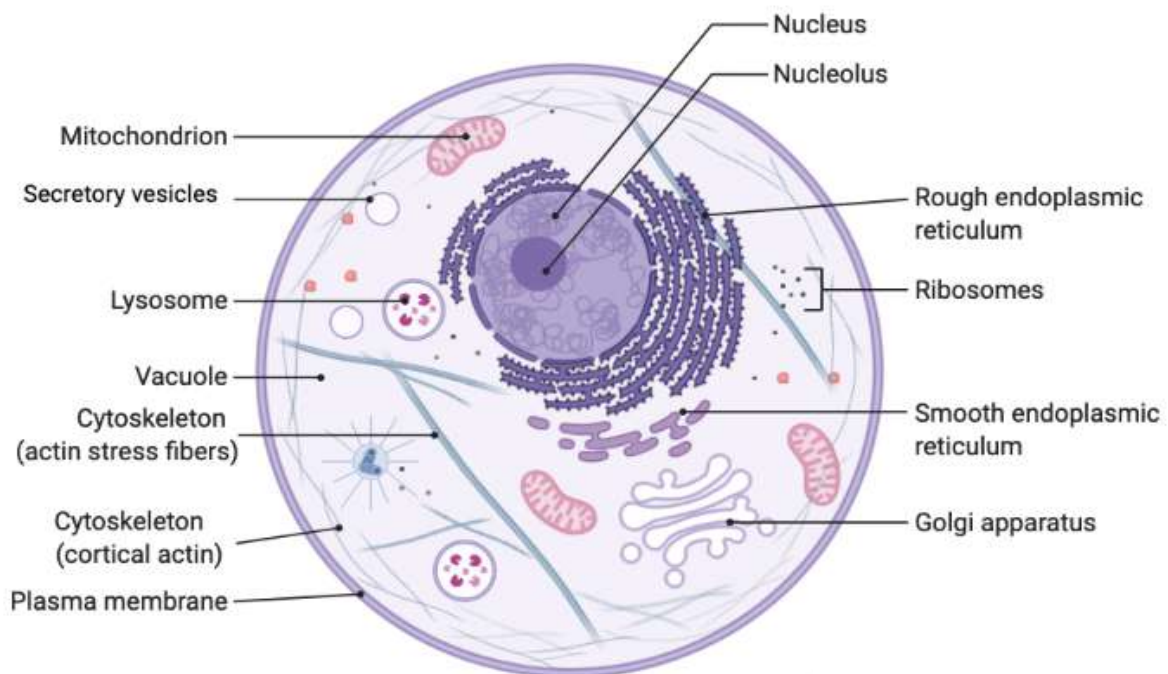


Figure 1. Animal cell

Scheme of an animal cell and its main intracellular constituents, notably the actin cytoskeleton and the plasma membrane.

1.1. CYTOSKELETON

The cytoskeleton supports the general cell shape and its resistance to deformation. It is involved in various cellular processes such as cell adhesion, migration, division and trafficking. It is composed of filaments that assemble mainly in the cytoplasm of cells and that can be divided in 3 classes: the actin filaments, the microtubules, and the intermediate filaments.

1.1.1. Actin

Actin is the major constituent of the cell cytoskeleton and was discovered in 1942 (Straub et Feuer 1950). Actin is a globular monomeric protein (G-actin) that assembles into a two-strand filamentous structure (F-actin), with two distinct ends referred to as barbed and pointed ends. In cells, the balance between free G-actin monomers and F-actin filaments is tightly controlled by various actin binding proteins (ABP). *In vitro*, at steady state, the rate of G-actin addition (polymerization) at the barbed end is balanced by the rate of G-actin loss (depolymerization) at the pointed end, therefore no net filament growth occurs. The resulting concentration of free ATP-G-actin is called critical concentration. When the concentration of G-actin is above the critical concentration, actin filaments grow. Conversely, when the concentration of free ATP-G-actin is below the critical concentration, actin filaments disassemble. Proteins that alter the critical concentration impair the dynamics of actin filaments. The formation of actin filaments can be divided in 3 steps: the nucleation, the elongation and the steady state (**Fig. 2**).

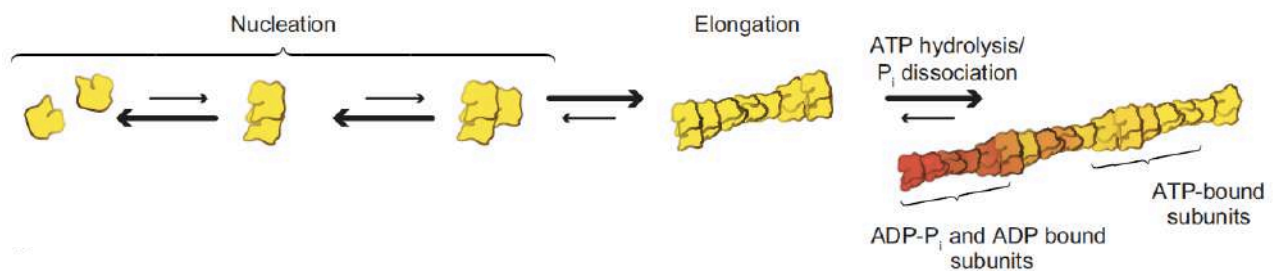


Figure 2. Kinetics of single actin filament assembly.

Actin polymerization from the pool of actin monomers happens in two phases. First, nucleation, is the formation of dimers and trimers. This is followed by rapid elongation at the more dynamic end, the barbed end, ATP hydrolysis in the filament, and phosphate dissociation.

1.1.1.1. Steady state of actin polymerization

The main model for actin polymerization stands only *in vitro*, in the absence of ABPs (except profilin). It depicts that the transition between G-actin and F-actin forms is dependent on ATP hydrolysis. During the last step of actin filament formation *i.e.* the steady state, unstable ADP-bound actin monomers dissociate from the pointed end while more stable ATP-actin monomers associate to the growing barbed end of filament. As a result, actin filament assembly is a polar mechanism called treadmilling, during which actin polymerization occurs at one end (barbed end) while concomitant actin disassembly occurs

at the other end (pointed end) implicating a non-variation of the length of the filament (Wegner 1976).

Another aspect of the polymerization/depolymerization process is the intervention of various capping proteins to prevent assembly and disassembly at the barbed end of the filament. Gelsolin is a severing protein that binds along actin filaments and breaks them into two segments (Yin, Albrecht, et Fattoum 1981). It then remains attached to the barbed end of the severed filaments acting as a capping protein blocking actin polymerization (Bryan et Kurth 1984; Wegner et al. 1994). Of note, capping and severing of actin filaments by gelsolin can be inhibited through its interaction with phosphatidylinositol phosphate (PIP) or phosphatidylinositol (4,5)-bisphosphate (PIP₂) (Yu et al. 1992).

1.1.1.2. Actin nucleation

During the nucleation, three monomers of G-actin associate to initiate a filament. The actin related protein complex (Arp2/3) and formins are two major known actin filament nucleators (**Fig. 3**). The Arp2/3 complex is an assembly of 7 proteins that nucleates the branching of new filaments from the side of a pre-existing filament (Mullins, Heuser, et Pollard 1998) (Svitkina et Borisy 1999). Arp2/3 mediated actin assembly is regulated by various nucleation promoting factors (NPF) such as the Wiskott–Aldrich syndrome protein (WASP) and WASP-like verprolin homologous protein (WAVE) family proteins, whose activation is induced by the small GTPases cell division cycle 42 (Cdc42) and Rac, respectively (Alekhina, Burstein, et Billadeau 2017).

Conversely, formins are thought to nucleate linear actin bundles through their C-terminal formin homology domains 1 and 2 (FH1FH2)(Chesarone, DuPage, et Goode 2010) (Pruyne et al. 2002). *In vitro*, the FH1 domain of formins interacts with another ABP, profilin, promoting nucleation of filaments independently of the Arp2/3 complex (Sagot et al. 2002) (Paul et Pollard 2008).

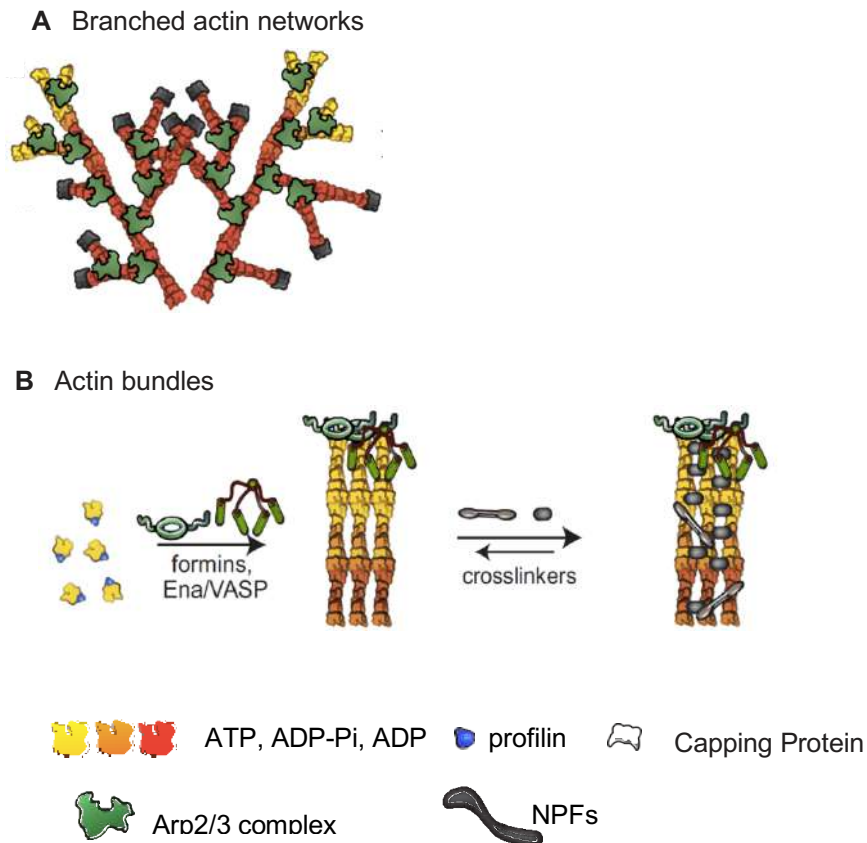


Figure 3. Distinct actin filament organizations.

(A) a branched actin network results from the autocatalytic branching activity of the Arp2/3 complex. Activated by nucleation promoting factors, NPFs, the Arp2/3 complex generates a branched network from the side of a preexisting actin filament. (B) short crosslinkers tightly pack unbranched filaments, such as those generated by formins or Ena/VASP proteins, into stiff, straight bundles (Adapted from Blanchoin et al., 2014).

1.1.1.3. Actin polymerization

The FH1FH2 domain of formins is also involved in the second steps of filaments formation, *i.e.* the elongation, notably by protecting the barbed-end of filaments from capping (Zigmond et al. 2003). During the elongation, subunits of actin monomers are added at both ends of the filament although the rate of G-actin subunits incorporation is higher at the barbed-end. The elongation is modulated by various ABP such as profilin that interacts with both formins and actin monomers. Profilin promotes ADP to ATP nucleotide exchange on actin monomers. As a consequence, it triggers the addition of ATP-actin monomers at the barbed end of the filament (Romero et al. 2004). In addition, profilin promotes disassembly of actin filaments by sequestering G-actin monomers, thereby blocking their association with the barbed ends and promoting disassembly from the pointed ends of actin filaments (Ressad et al. 1999).

In opposition, through their binding to ADP-actin monomers, ABP belonging to the actin depolymerizing factor (ADF)/cofilin family inhibit the exchange of ADP to ATP and favor actin depolymerization at the pointed end of the filament (Carlier et al. 1997; dos Remedios et al. 2003; Ressad et al. 1999).

All these actin regulatory proteins usually display more than one define activity thereby being differently implicated in the formation of diverse actin networks.

1.1.1.4. Organization of actin filaments and networks

Actin filaments interact with each other to form different networks, like lamellipodia, filopodia or stress fibers, each having distinct roles and localization (**Fig. 4**).

Lamellipodia

Lamellipodia are branched actin networks found at the edges of the cells, promoting sheet-like extensions responsible for the cell migration and adhesion to the extracellular matrix (ECM). Hence, these protrusions push the cell forward allowing the cell to be motile. Lamellipodia formation is an Arp2/3-dependent mechanism of actin polymerization (**Fig. 4**) (Mullins et al. 1998) (Svitkina et Borisy 1999). Their formation is regulated by the GTPase Ras-related C3 botulinum toxin substrate 1 (Rac1). This small GTPase belonging to the ras sarcoma (Ras) superfamily is responsible for the formation of focal adhesion in the lamellipodia, at the leading edge of the cell (Nobes et Hall 1995).

Filopodia

Filopodia are thin actin-rich membrane protrusions with a typical diameter of 100 to 300 nm, allowing cells to probe their extracellular environment. Therefore, they are involved in numerous cellular processes, including cell migration and guidance. Filopodia contain actin filaments arranged in parallel bundles cross-linked by proteins such as fascin, and emerging from lamellipodia (**Fig. 4**) (Svitkina et al. 2003; Vignjevic et al. 2006; Yamashiro-Matsumura et Matsumura 1986). In this model, during filopodia formation, the global regulator Cdc42 binds to and activates the WASP protein leading to Arp2/3 activation and thereby actin nucleation (Pellegrin et Mellor 2005). Another model suggests that filopodia can be formed in absence of Arp2/3 and regulators (Steffen et al. 2006).

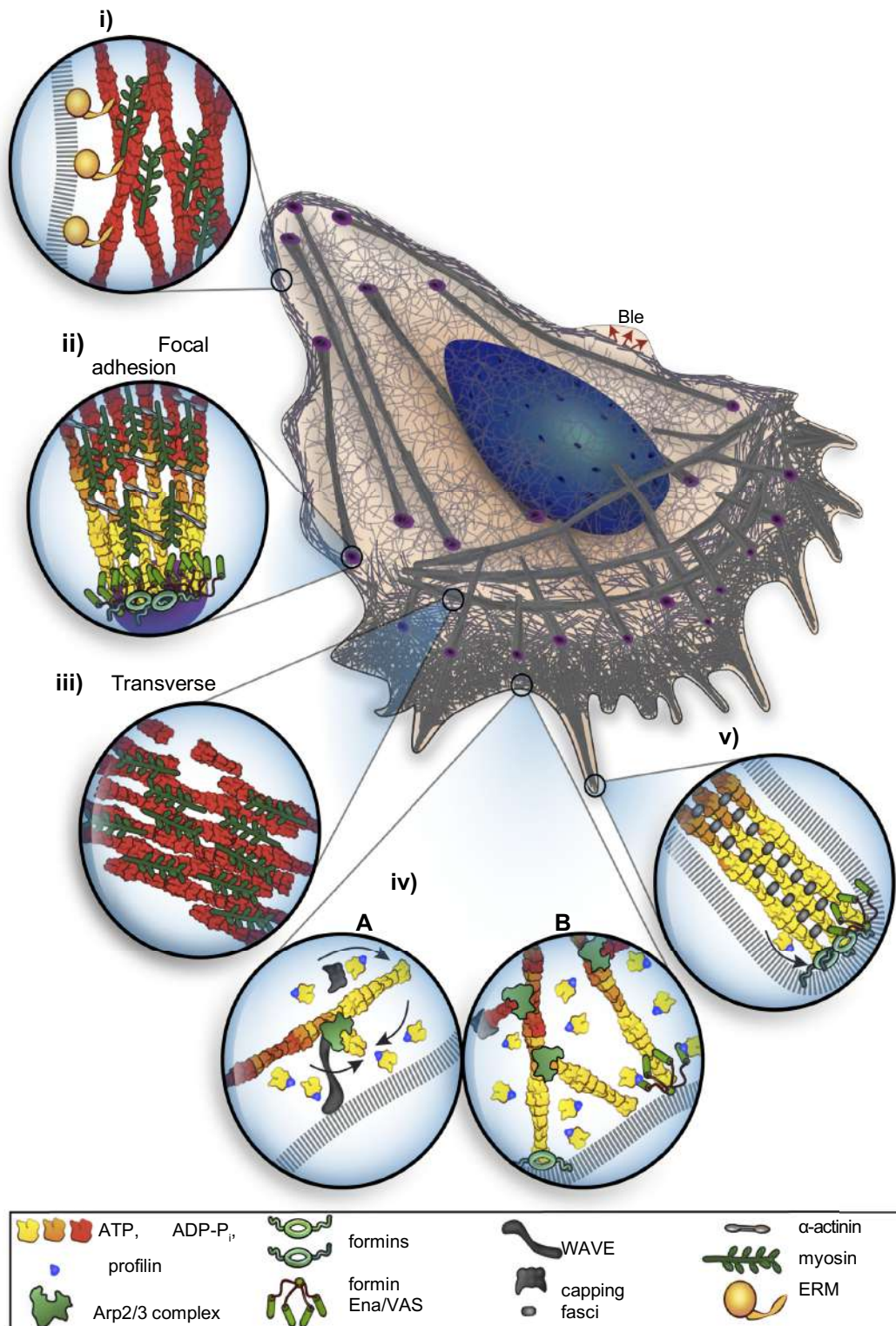


Figure 4. Actin filaments organization in a moving eukaryotic cell.

The scheme depicts the architectural specificities of different regions of the cell. Actin filaments form networks such as filopodia, lamellipodia and actin stress fibers attached to focal adhesion. Underneath the PM is located the actin cortex. These networks present distinct roles and localization in the cell (Adapted from Blanchoin et al., 2014).

Hence, filopodia can be formed by actin filaments and next nucleated at their tips by formins mammalian homolog of diaphanous (mDia) 2. This can be followed by barbed end elongation and eventually filament bundling (Dent et al. 2007; Schirenbeck et al. 2005).

However, it has also been proposed that filopodia formed *via* mDia2 emerged from long lamellipodial filaments that converge into bundles (Yang et al. 2007).

In fibroblast the *Drosophila melanogaster* Enabled protein (Ena)/vasodilator-stimulated phosphoprotein (VASP) family proteins appear to play a central role in uncapping and elongation of filopodia (Bear et al. 2002). Indeed, depletion of capping proteins impair lamellipodia formation thereby favoring the formation of filopodia. However, in Ena/VASP deficient cells, the depletion of capping proteins is not sufficient for filopodia formation, indicating that Ena/VASP is required to activate functions downstream of actin filament elongation (Mejillano et al. 2004).

Stress fibers

Stress fibers are contractile bundles of 10 to 30 actin filaments (Cramer, Siebert, et Mitchison 1997). They are involved in cell adhesion, contraction and migration as well as cell morphology. They are composed of actin and non-muscular myosin (Weber et Groeschel-Stewart 1974) and can be cross-linked by various proteins, the main ones being α -actinin (Lazarides et Burridge 1975) and filamin (Wang et Singer 1977) (**Fig. 4**).

There are 3 types of stress fibers: the transvers arc, the dorsal and the ventral stress fibers (Small et al. 1998). The two last ones are linked to focal adhesions, which are dynamic structures that link the cytoskeleton to the ECM. They are composed of integrins and actin-binding linkers, such as vinculin, talin or filamin A (FLNA) (Brakebusch et Fässler 2003). Focal adhesions newly form at the leading edge of the cells, allowing cell to migrate and to adhere. Initially, they are small focal complexes that next mature into proper focal adhesions *via* the recruitment of linker proteins involved in adhesion. The transition of focal complexes into mature focal adhesions requires the activation of myosin II-driven contractility by the Ras homolog (Rho)-associated kinase (ROCK). Focal adhesions are individual mechanosensors that assemble in response to an external local mechanical force, in a mDia1-dependent and ROCK-independent mechanism (Riveline et al. 2001). Formation of mature focal adhesions is highly dependent on the formation of stress fibers and have a major role in mechanotransduction as they are implicated in force transmission (Geiger, Spatz, et Bershadsky 2009).

Dorsal stress fibers assembled by formins are associated to focal adhesions at one end, whereas ventral stress fibers are connected to focal adhesions at both ends. Ventral stress fibers, most prominent actomyosin bundles, are generated from the association by the end of dorsal stress fibers or/and transverse arcs (Hotulainen et Lappalainen 2006).

Their formation is regulated by ROCK signalling pathway, more precisely via RhoA (Ridley et al. 1992) (See 1.1.2. “Regulation of actin cytoskeleton by Rho GTPases”). Transvers arcs emerge from lamellipodia to the center of the cells. Their formation is dependent on myosin and actin bundles, that are generated by Arp2/3 complex.

Recently, a new mechanism by which stress fibers can be formed *de novo* from the actin cortex, without requirement of pre-existing actomyosin bundles, has been reported (Lehtimäki et al. 2021). These stress fibers are integrated in the cell cortex and assemble preferentially underneath the nucleus. In this process, non-muscle myosin II is responsible for the reorganization of cortical actin meshwork into regular bundles, which promotes nascent focal adhesions and subsequent stabilization of the cortical stress fibers.

Forces exerted on the cells can be sensed by mechanosensors and translated by mechanotransducers in biochemical signals within the cells. In most of the cases, mechanotransducers are stretch-sensitive ion channels, signalling molecules and integrins. These actors promote cytoskeletal rearrangement, and subsequently regulate cell deformation. Here we will focus on the RhoGTPases, which are the main signalling regulators of the actin cytoskeleton.

1.1.2. Regulation of actin cytoskeleton by RhoGTPases

Rho GTPases are proteins found in all eukaryotic cells belonging to the RAS superfamily (Bernards 2005). They have been implicated in various cell processes including extracellular signal transduction, cytokinesis, cell motility, cell-cell and cell-extracellular matrix adhesion and morphogenesis. They are best known for their ability to induce dynamic rearrangements of the PM-associated actin cytoskeleton as they are involved in many signal transduction pathways (Aspenström, Fransson, et Saras 2004) (Govek, Newey, et Van Aelst 2005). Rho was first discovered in 1985 and Rho-like proteins have been extensively studied ever since (Madaule et Axel 1985). Few years later, the G protein RhoC was identified as a target of *Clostridium botulinum* exoenzyme C3 (ExoC3) which induces Rho ADP-ribosylation and affects actin microfilaments (Chardin et al. 1989). The most characterized RhoGTPases are RhoA, Cdc42 and Rac1 (**Fig. 5**).

The shared feature of all these GTPases is their ability to act as molecular switches, oscillating between an active form when bound to GTP and an inactive form when bound to GDP. Various upstream regulatory proteins can control RhoGTPases activity. First, the guanine nucleotide exchange factors (GEFs) catalyze the exchange of GDP for GTP leading

to conformational changes into an active GTP-bound form (Schmidt et Hall 1998), whereas GTPase activating proteins (GAPs) are able to stimulate the intrinsic GTPase activity leading to their inactivation following GTP hydrolysis into GDP (Bernards 2003). Eventually, the guanine nucleotide dissociation inhibitor (GDI) sequesters the GDP-bound form of some GTPases in the cytosol (Olofsson 1999). It is in their active GTP-bound state that the Rho GTPases perform their regulatory functions through a conformation-specific interaction with their effector proteins. Rho GTPase regulates a huge diversity of downstream effectors and most effectors are regulated by multiple Rho GTPases, resulting in an elaborate cross-talk. In this chapter we will focus on RhoA, cdc42 and Rac1, the three most studied Rho GTPases, their effectors and subsequent cellular functions (**Fig. 5**).

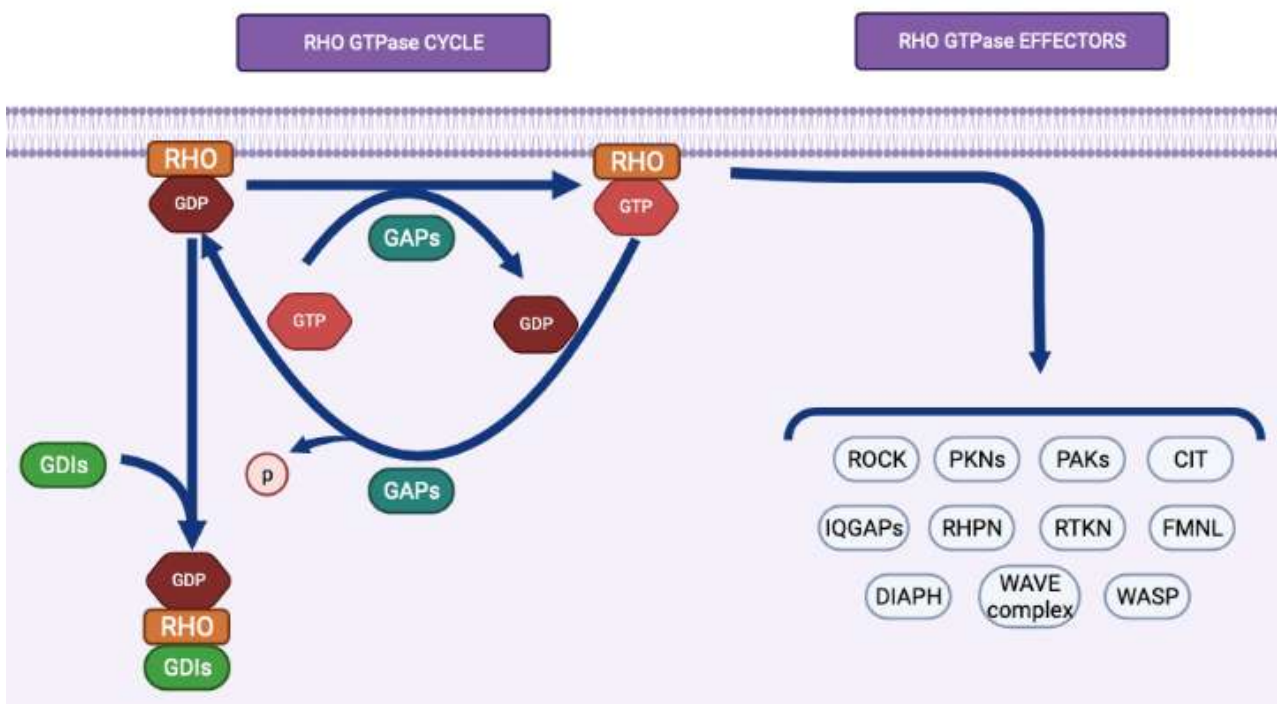


Figure 5. Rho GTPases regulation.

The small Rho GTPases are monomeric proteins of 21 kDa, which function as molecular switches that cycles between “on” and “off” conformations when bound to either GTP or GDP, respectively. They regulate various signal transduction pathways and their downstream effectors, and are controlled by diverse upstream regulators.

1.1.2.1. RhoA signalling and its effectors

RhoA is an actin regulator that share 85% homology with the other two main classical Rho GTPases: RhoB and C. However, as RhoC, the active form of RhoA localizes at the PM while RhoB localizes in late endosomal compartments (Adamson, Paterson, et Hall 1992). RhoA is responsible for the formation of focal adhesion and actin stress fibers (Ridley

et Hall 1992) and therefore promotes actin polymerization and bundling, leading to enhanced actomyosin cytoskeleton contractility.

Although Rho GTPases display a large array of effectors, RhoA most characterized effectors are the protein kinases ROCK and mDia.

They phosphorylate many proteins involved in the stabilization of actin filaments and in the actomyosin contractility. For instance, ROCK regulates the LIM kinases which phosphorylate and inhibit the actin severing protein cofilin/ADF resulting in an increased number of actin filaments (Maekawa et al. 1999; Olson et Sahai 2009). In addition, ROCK inhibits the myosin light chain (MLC) phosphatase subunit MYPT1, thereby having an action on the myosin regulatory subunit (ML20) to promote actin–myosin contractility (Kimura et al. 1996; Mizutani et al. 2009; Riento et Ridley 2003). In fibroblast, RhoA activation promotes MLC-II phosphorylation, followed by a gain of cell contractility notably due to stress fibers formation (Burrige et Chrzanowska-Wodnicka 1996). Stress fibers formation also requires the formin mDia that mediates actin nucleation and polymerization into straight filaments (Li et Higgs 2003; Watanabe et al. 1999).

Other Rho effectors include members of the ezrin–radixin–moesin (ERM) proteins. These proteins associate with the cell PM where they mediate Rho-dependent actin cytoskeleton remodeling (Tan et al. 2008). Recent progress has been made in deciphering the importance of inverse – Bin/Amphiphysin/Rvs (I-BAR) domain containing proteins for a targeting of the Ezrin ERM-protein family member to curved membranes (Tsai et al. s. d.)

1.1.2.1. Rac1/Cdc 42 signalling and their effectors

Contrasting with RhoA, Rac1 and Cdc42 activation primarily leads to the formation of protrusive actin-rich lamellipodia and filopodia membrane protrusions respectively (Ridley et Hall 1992; Nobes et Hall 1995; Etienne-Manneville et Hall 2002). Although they both activate the Arp2/3 complex through Wiskott–Aldrich syndrome protein (WASP) family proteins, their mechanism of actin nucleation and regulation are different.

Indeed, active Rac1 is found at the leading edge of lamellipodia (Machacek et al. 2009) and depletion of Rac1 inhibits the formation of lamellipodia formation (Tan et al. 2008; Wells et al. 2004) and has a strong impact on cell motility (Steffen et al. 2013), while a local enrichment of active Rac1 is sufficient to induce lamellipodia formation (Wu et al. 2009). Rac1 promotes the activation of WASP-like verprolin homologous protein (WAVE) that interacts with both profilin and Arp2/3 complex, thereby promoting polymerization of branched actin networks (Eden et al. 2002; Ho et al. 2004; Innocenti et al. 2004).

The most known effector of RAC1 is p21-activated kinase (PAK), that belongs to the family of serine/threonine kinases. Active PAK phosphorylates MLC-kinase (MLCK) resulting in its inactivation. As a consequence, a decrease of actomyosin contractility is observed. This likely contributes to the antagonism observed between RhoA and Rac1 for actin cytoskeleton organization into contractile stress fibers versus actin-rich membrane protrusions (Ridley et al. 1992).

Cdc42 promotes the activation of N-WASP effectors that interact with Arp2/3 and G-actin through their WASP-homology 2 (WH2) domains (Eden et al. 2002; Ho et al. 2004; Innocenti et al. 2004). Cdc42, unlike RAC1, initiates the formation of unbranched bundles of actin filaments in filopodia, that are suggested to originate from a branched network initiated by the crosstalk between Cdc42 and Arp2/3 (Svitkina et al. 2003). As observed with Rac1, Cdc42 can also activate PAK, decreasing actomyosin contractility.

Cell migration is dependent on the formation of protrusion at the leading edge of cells and on the concomitant retraction of their rear. This process is tightly regulated by the local activation and inactivation of several Rho GTPases. In fibroblast, RhoA and Rac1/Cdc42 are activated simultaneously at the leading edge of migrating cells with a delay of 40 seconds (Machacek et al. 2009). This indicates that the formation of lamellipodia is a coordinated work between different Rho GTPases. RhoA seems to initiate the actin polymerization at the front of migrating cells, with Rac1 and Cdc42 being involved in reinforcing adhesion junctions. Moreover, RhoA is also positioned at the cell rear to promote contractility.

Due to their essential role in the regulation of the actin cytoskeleton, RhoGTPases are common targets for pathogens during infectious processes, especially for highly pathogenic bacteria, such as *Salmonella*, *Listeria*, *Escherichia coli* or even Gram positive bacteria *Clostridium botulinum* and *Staphylococcus aureus*. These bacteria produce an arsenal of virulence factors, including toxins, specifically targeting RhoGTPases, to disrupt epithelial or endothelial barriers and successfully invade their hosts (Lemichiez et Aktories 2013), 2013). Few examples will be described in the chapter 3 of this thesis (“Transendothelial macroapertures”).

1.2. PLASMA MEMBRANE

1.2.1. Composition

The PM a 10 nm thick bilayer mainly composed of proteins, sugar and phospholipids. The bilayer is made of two leaflets of phospholipids facing each other. It has been defined as a fluid mosaic model in which proteins are inserted. (**Fig. 6** (Singer et Nicolson 1972)).

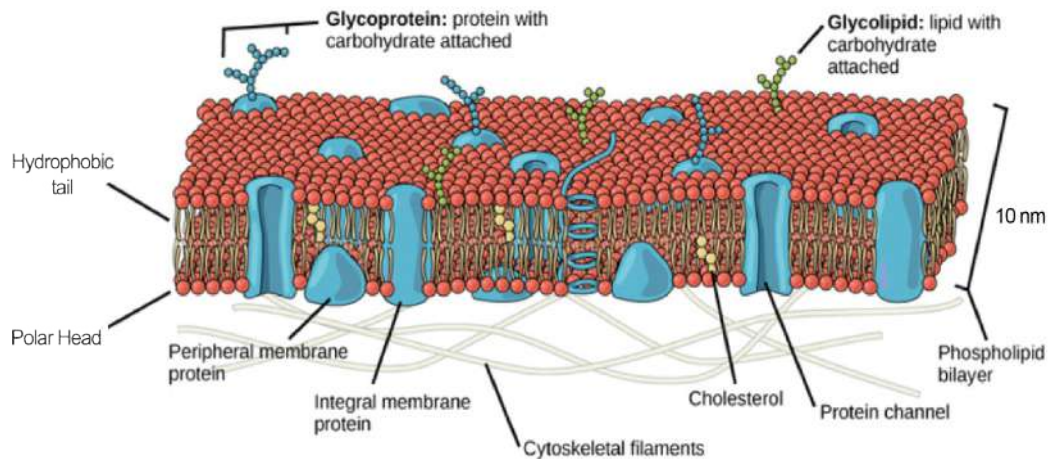


Figure 6. Fluid mosaic model.

Scheme representing the plasma membrane, which is composed of a lipid bilayer and various proteins inserted into it. extracted and adapted from <https://bio.libretexts.org/@go/page/12739>.

Phospholipid composition

Phospholipids are amphiphilic molecules: they are formed of a hydrophilic head and an hydrophobic tail, which is composed of saturated or unsaturated fatty acids (FA). There are three main families of phospholipids: (i) the glycerophospholipids (GPLs), which are the most abundant in the PM, (ii) the sphingolipids, and (iii) the sterols with the cholesterol which plays key role in rigidifying the PM (**Fig. 7**).

- (i) GPLs are composed of two fatty acyl chains link by a glycerol backbone to a polar head that can be a phosphatidic acid (PA), phosphatidylethanolamine (PE) phosphatidylcholine (PC) phosphatidylserine (PS), phosphatidylglycerol (PG) or phosphatidylinositol (PI). The polar head can be removed to generate a PA.
- (ii) Sphingolipids are the second most abundant lipids in the cell and are composed of a sphingoid base that links a fatty acyl chain to the polar head of the lipid. The acyl chains of sphingolipids tend to be longer than those of GPLs (Grösch, Schiffmann, et Geisslinger 2012). The main sphingolipids are ceramides, sphingomyelins, and glycosphingolipids and gangliosides.

- (iii) Sterols, and mainly cholesterol in mammalian cells, are the major non-polar lipids of the PM. They are composed of a steroid backbone with 4 fused carbon rings, a hydroxyl head group and a short hydrocarbon tail. The steroid backbone of sterols provides a high rigidity to PM in which it is inserted. Each polar head can be associated to various acyl chains, thereby generating a large array of lipids (**Fig. 7**; (Harayama et Riezman 2018)).

Fatty acyl chains are different in length as well as in number of unsaturation. We distinguish mono- and polyunsaturated fatty acids (PUFAs) such as oleic acid (OA) and docosahexaenoic acid (DHA) from saturated FA like the palmitic acid (**Fig. 7**). The main source of omega-3 PUFAs is the diet. The ratio between n-6 and n-3 PUFAs, provided by the diet, is essential to maintain healthy physiological processes and can be modified by microorganism of the microbial flora. Among them, DHA an essential omega-3 transported by the lipid transporter major facilitator superfamily domain containing 2A (Mfsd2a), which is found at the luminal PM of endothelial cells. From there it delivers DHA in the form of lysophosphatidylcholine (lysoPC) into the brain. Besides DHA, Mfsd2a is thought to transport lysoPCs with long-chain FA *i.e.* with more than 14-carbons, such as lysoPC oleate and palmitate. Mfsd2a knock-out (KO) mice present low levels of DHA in the brain and smaller brain than wild type (WT) mice (Nguyen et al. 2014).

In PUFA, the position of the double bonds is also a way to classify PL. Polar head group can associate to a variety of acyl chains annotated as follows: (XX:Y, n-Z), where XX is the carbon number of the chain, Y is the number of double bonds and Z indicates the position of the first double bond from the end (**Fig. 7**). Sphingolipids are usually more saturated than GPLs (Grösch et al. 2012). For instance, the mono-unsaturation in OA induces a kink in the acyl chain and thus, OA occupy a larger space than saturated PL. Furthermore, the ratio between the size of the polar head and level of FA saturation is responsible for the global geometry of PL (Vanni et al. 2014) (Pinot et al. 2014)4). Interestingly, direct interaction between PUFAs and voltage-gated ion channels such as K⁺, Na⁺, Ca²⁺ and H⁺ has been described. According to the nature of the channel, the regulatory effects could be negative or positive (reviewed by Elinder and Liin in 2017).

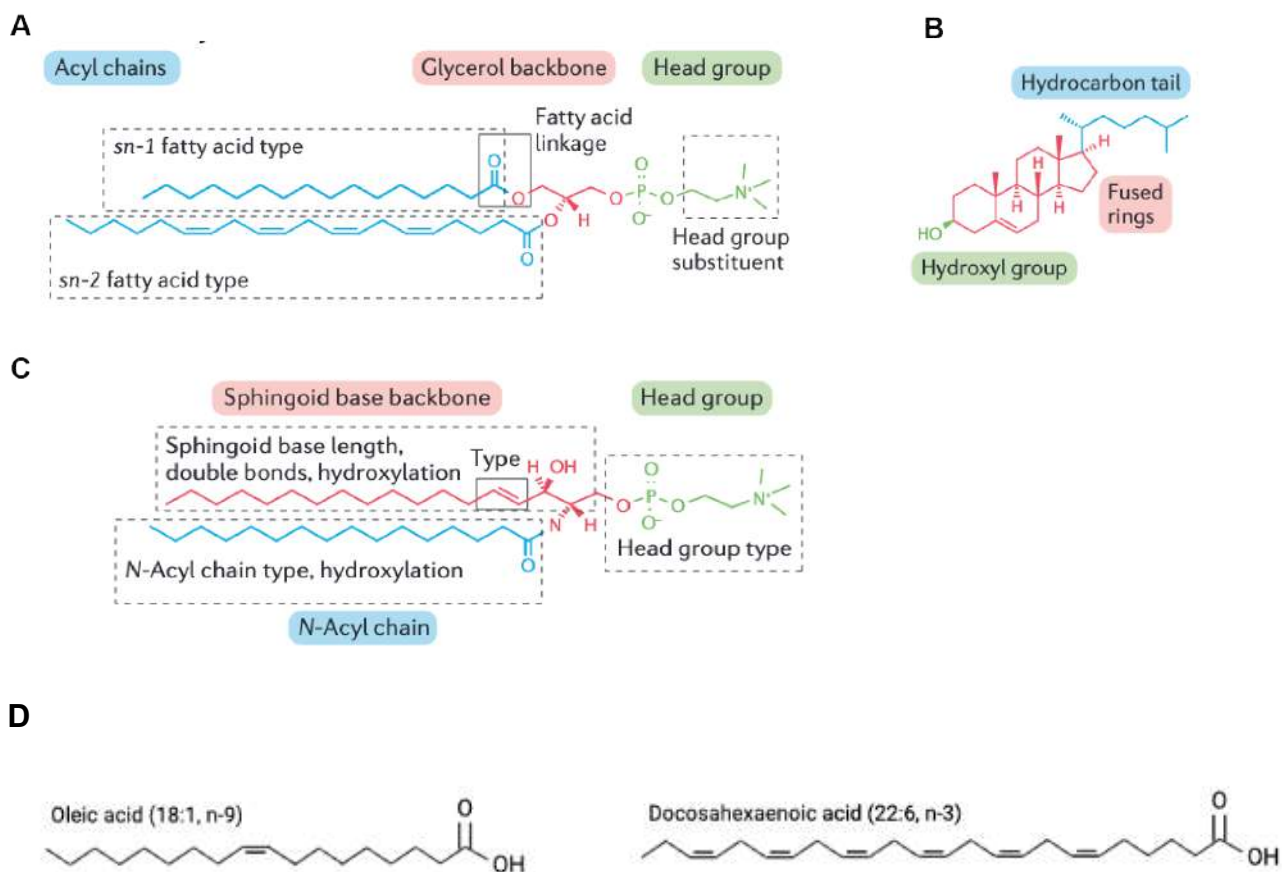
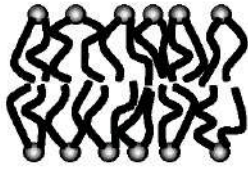


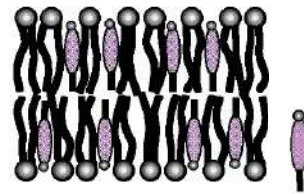
Figure 7. Lipids composition and diversity.

Lipids are made of a polar head group that can be classified in 3 groups according to their backbone: A) glycerophospholipids B) Sterols or C) Sphingolipids. D) example of a two omega-3, a polyunsaturated fatty acid, the docosahexaenoic (DHA) with 22 carbons, 6 unsaturation and their positions (22:6, 3) and a monounsaturated fatty acid, the oleic acid (OA; 18:1,9)(adapted from (Harayama et Riezman 2018)).

In aqueous medium, lipid bilayers of biological membranes exist in different physical states characterized by the lateral organization, the molecular order and the mobility of the lipid molecules within the bilayer. Lipids packing can be described using acyl chain order parameter. In the fluid phase known as liquid-disordered phase, lipids with a low value of order parameter form a bilayer phase of low order and high mobility and are mainly PUFAs. It is thought that most of the membrane is in the liquid-disordered phase (Raghupathy et al., 2015). Interestingly, the addition of cholesterol enhances acyl chain order in liquid-disordered membranes (van Meer, Voelker, et Feigenson 2008). By contrast, bilayers formed of long-chain saturated lipids, like sphingomyelin, adopt a solid-like phase of high order and low mobility. Addition of cholesterol, renders the solid-like membrane more mobile, turning it into a liquid-like phase. This phase is called the liquid-ordered (L_o) phase as the order still remains high (**Fig. 8**)(Eeman et Deleu 2010).



Fluid, liquid-disordered phase (L_d)



Fluid, liquid-ordered phase (L_o).

Figure 8. Liquid-disordered and liquid-ordered phases.

Scheme illustrating two physical states that can adopt a lipid bilayer in aqueous medium (adapted from (Eeman et Deleu 2010)).

It has been proposed that PM lipids contribute to the spatial organization of membrane proteins via the same thermodynamic forces that drive the separation of liquid-ordered and liquid-disordered phases in model membranes (Lingwood et Simons 2010; Schroeder, London, et Brown 1994). Liquid-ordered or disordered domains can be visualized by two-color super-resolution microscopy, when marked with different lipid-linked peptides such as the cholera toxin subunit or transmembrane peptide probes associated to fluorescent proteins (Stone et al. 2017).

The level of acyl chain saturations has an impact on the phase separation process in membranes. In liquid-ordered domains, lipids are highly packed, and their acyl chains are ordered promoting rigid domains. These ones are mainly composed of saturated lipids, such as sphingolipids and cholesterol, which represent up to 50% of the whole PM lipids (van Meer et al. 2008) (Gerl et al. 2012). In liquid disorder domains, lipids are preferentially mono- or poly-unsaturated and less packed, thereby increasing the fluidity of membranes and melting point. This phase separation is responsible for the formation of rigid domains in the PM, that are resistant to detergents and often called lipids rafts or preferably detergent resistant membrane domains, that refers to a biochemical definition. PM is known to be asymmetric *i.e.* the inner leaflet and the outer leaflet display variation in protein and lipid composition. The outer leaflet contains mainly PC and sphingomyelin. In contrast, PI, PS and PE localize in the inner leaflet. The cholesterol is thought to be evenly distributed throughout the two membrane leaflets (Harayama et Riezman 2018).

PM composition is tightly regulated. A huge diversity in lipids and proteins composition is observed in the different endomembranes compartments compared with the PM. This difference of composition largely defined various compartments including:

membrane from the endoplasmic reticulum (ER), the nuclear membrane, the Golgi apparatus, the mitochondria and the endo-lysosomes.

For instance, proteins found in the membranes of the ER and the Golgi apparatus contain sorting signals, which are like molecular zip codes that specify their final destination. Cholesterol is a major constituent of PM whereas it is only present at low level in endomembranes. Similarly, sphingomyelin is highly enriched in the Golgi compartment network and PM. Vesicular trafficking allows highly regulated exchanges of lipids and proteins between the PM and internal membranes (**Fig. 9**, (Casares, Escribá, et Rosselló 2019)).

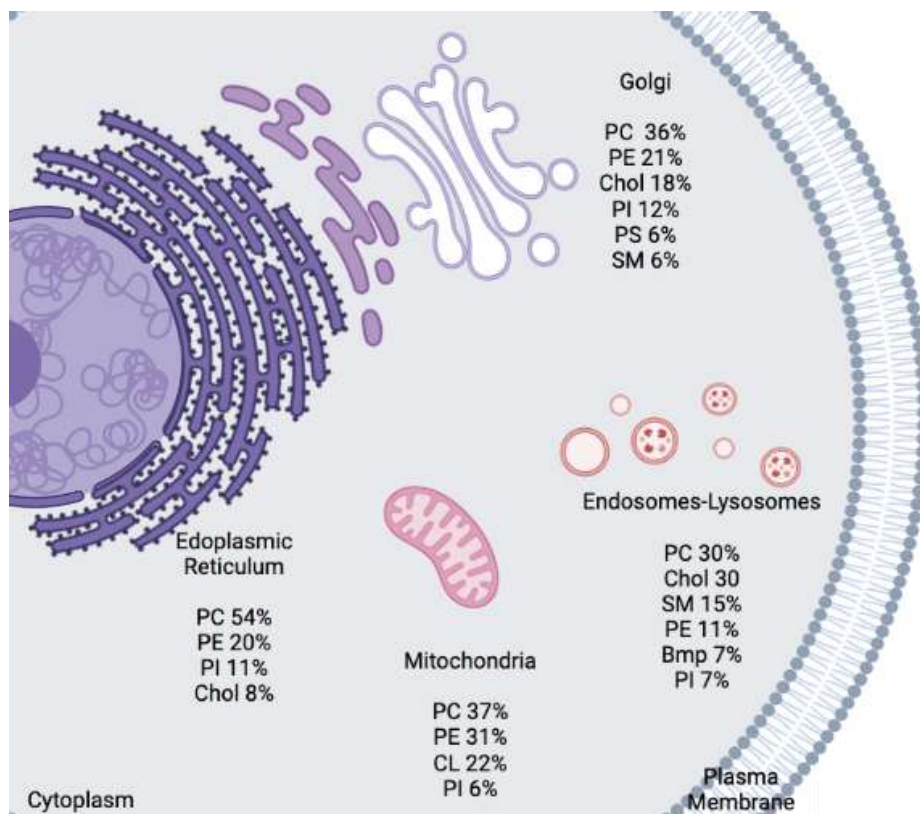


Figure 9. Lipid composition of the endomembrane system.

The main lipid constituents and the proportion they account for in the membrane are listed for each organelle (in percentage). BmP: bis(monoacylglycero)phosphate; Chol: cholesterol; CL: cardiolipin; PC: phosphatidylcholine; PE: phosphatidylethanolamine; PI: phosphatidylinositol; PS: phosphatidylserine; SM: Sphingomyelin (adapted from Casares et al. 2019).

Protein composition

The PM is also composed of proteins, which account for 50% of the total weight of the PM, and that defines its structure. Proteins can be either intrinsic, spanning the entire membrane or extrinsic and being located either in the inner or the outer leaflet of the PM. Transmembrane proteins comprise ion channels, such as Ca^{2+}/K^{+} pumps, enzyme or transporters that control the exchange of large molecules, such as fatty acids. Conversely, extrinsic proteins are mainly involved in the interaction with lipids or with other proteins found

on each side of the PM. The fluid mosaic aspect of the PM demonstrated by Singer and Nicolson allows lateral diffusion of the proteins inserted in the PM.

Transmembrane proteins are involved in the transport of various molecules through the membrane. As an example, glucose transporters allow the translocation of glucose molecules across the PM (Navale et Paranjape 2016).

Proteins together with lipids can also interact to deform the PM leading to invaginations that can transport molecules during endo- or exocytosis processes. As an example, patches of clathrin, forming a well-known honeycomb-like structure, are able to bend the PM into coated pits (Saffarian 2009; Kirchhausen et al. 2014) triggering endocytosis. Clathrin-mediated endocytosis is the major route of mammalian receptors endocytosis (Bitsikas, Corrêa, et Nichols 2014; Watts et Marsh 1992). As discussed in chapter “2.3.1 Role and function of caveolae”, another type of membrane-coat driven PM invagination, namely caveolae, adopt a cup-shape, whose role in endocytosis has been described during mitosis (Boucrot et al. 2011) or shown to be involved in the entry of the Simian Virus 40 into the cell (Pelkmans, Kartenbeck, et Helenius 2001). Interestingly, many studies have described an enrichment of potassium and calcium channels in caveolae, with Ca^{2+} pumps shown to be 18-25 fold higher in caveolae, as compared to the whole plasma membrane (Kristensen, Rasmussen, et Juel 2008)(Maguy, Hebert, et Nattel 2006) (Daniel, El-Yazbi, et Cho 2006) (Bergdahl et Swärd 2004) (Taggart 2001).

1.2.2. Physical properties of membranes

The lipid bilayer intrinsic mechanical properties can be characterized by four elasticity moduli that describe the response of the bilayer to compression/expansion, bending, and extension, that can be triggered by lipids or proteins composition and insertion in the PM. Here I will focus in more details on the bending and extension of membrane, which are the main properties relevant for my work.

1.2.2.1. Bending rigidity

Physical description

Bending is the result of the force that curves the membrane out of its plane. The curvature energy per unit area for purely lipidic membrane is given by the Helfrich's law (Helfrich 1973):

$$F_{bending} = \frac{\kappa}{2} (C_1 + C_2 - C_0)^2 + \kappa_{C_1, C_2}$$

where C_1 and C_2 are the principale membrane curvatures, C_0 is the spontaneous membrane curvature that occurs spontaneously at room temperature due to thermal fluctuations, κ the bending modulus and K the Gaussian bending modulus. The Gauss-Bonnet theorem states that the integration of the Gaussian curvature over the surface without an edge is invariant under any deformation that is not involved with topological transformations. That is why this term is often neglected. However, it is fundamental for topological transitions like fusion or fission (Rueda-Contreras et al. 2021).

Order of magnitude

In the case of purely lipidic membranes, the bending modulus κ depends on the lipid composition and typically ranges between 5-20 times the thermal energy $k_B T$ for membranes in a fluid state, where k_B is the Boltzmann constant and T is the absolute temperature (Marsh 2006). In that case, membrane curvature occurs without external forces thanks to thermal fluctuations. Membranes composed of PUFAs display lower bending rigidity than membranes made of saturated fatty acids (Pinot et al. 2014). The bending modulus of membranes composed of PUFAs and cholesterol is between 20-30 $k_B T$ (Pan, Tristram-Nagle, et Nagle 2009). The bending modulus of membrane domains mainly composed of cholesterol and sphingolipids is about 60 $k_B T$ (Roux et al. 2005).

Cholesterol is an essential component of eukaryotic cell membranes and a key molecule in controlling membrane fluidity and organization among other functions. Cholesterol was described to stiffen saturated lipid membranes but has no stiffening effect on membranes composed of unsaturated lipids, such as 1,2-dioleoyl-snglycero-3-phosphocholine (DOPC). However, it has been shown recently that cholesterol can locally increase the bending rigidity of DOPC membranes, similar to saturated membranes, by increasing the bilayer's packing density. This points to a scale-dependent manifestation of membrane properties, highlighting the need to reassess cholesterol's role in controlling membrane bending rigidity over mesoscopic length and time scales of important biological functions (Chakraborty et al. 2020). In contrast to the known effect of cholesterol on membrane stiffness of lipid bilayers, Byfield and colleagues observed that cholesterol depletion of bovine aortic endothelial cells resulted in a significant decrease in membrane bending rigidity and a corresponding increase in the value of the elastic coefficient of the membrane, i.e. the Young's modulus, indicating that cholesterol-depleted cells are stiffer than control cells. An increase in cellular cholesterol to a level higher than that of normal cells, however, had no effect. Although cholesterol depletion had no apparent effect on F-

actin, disrupting F-actin with latrunculin A abrogated the stiffening effect, suggesting that cholesterol depletion increases the stiffness of the membrane by altering the properties of the submembrane F-actin and/or its attachment to the membrane (Byfield et al. 2004).

Mechanisms to bend the PM.

Membrane curvature can be induced at various scale (i) through the introduction of spontaneous curvature, (ii) through protein oligomerization, (iii) through protein scaffolding, (iv) through protein-protein crowding, (v) through cytoskeletal rearrangements (**Fig. 10**) (McMahon et Gallop 2005) (Campelo, McMahon, et Kozlov 2008:200).

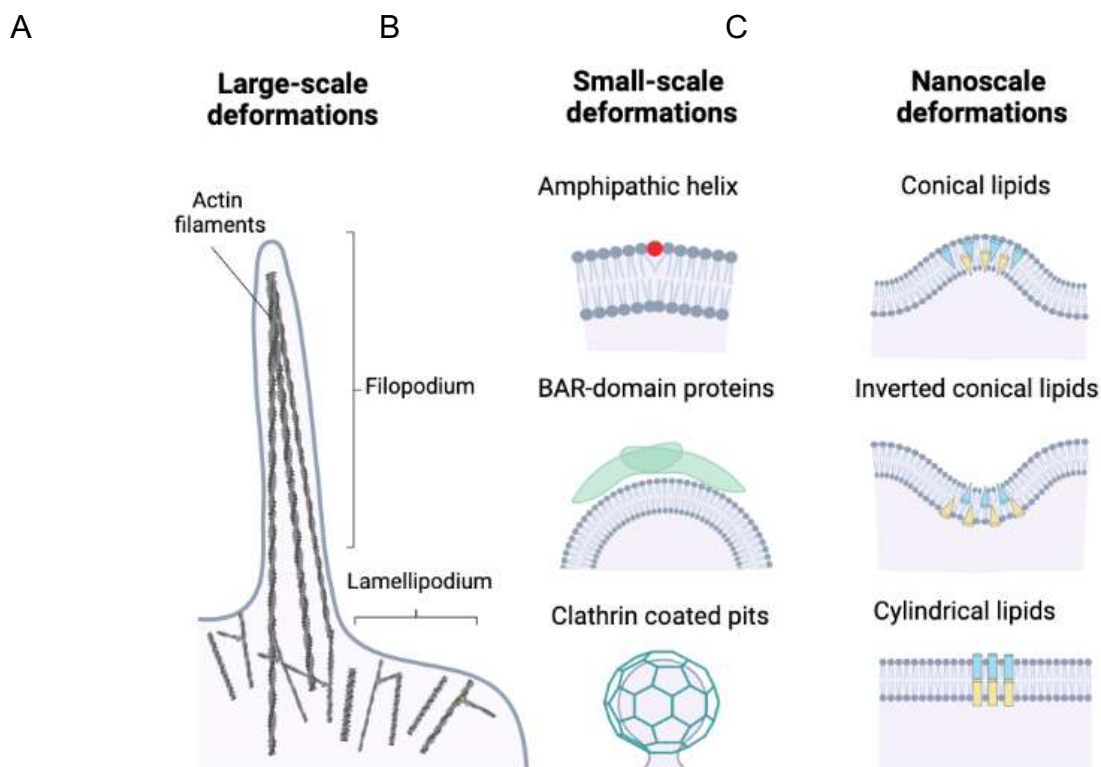


Figure 10. Example of membrane deformations.

Membranes bending occurs at various scales and can be induced by numerous actors. The cell cytoskeleton is responsible for large scale deformations while, bending proteins and lipid composition are responsible for lower scale deformation of the membrane (adapted from (McMahon et Boucrot 2015)).

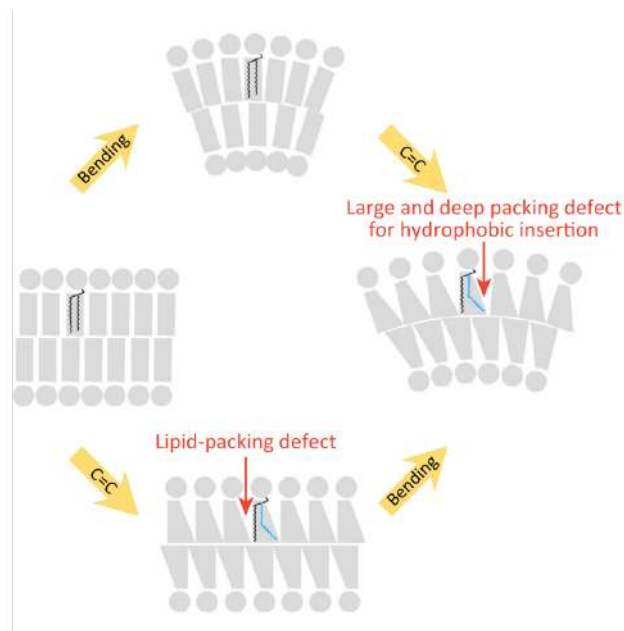
(i) Introduction of spontaneous curvature

In the case of biological membranes, we can distinguish two kinds of PM membrane curvatures that can be generated by lipids changes or bending proteins.

Upon positive curvature, the polar heads of lipids in the convex side are more separated and gaps form in between, trigger lipid packing defects that could acts as binding site for membrane anchoring proteins. Phospholipids with large polar head groups such as PI fit better in the convex side, reducing both the area of packing defects and exposure of hydrophobic acyl chains. On the concave side where negative curvature is created, the

phospholipid packing is high, therefore insertion of phospholipids with small head groups or single acyl chain are favored (**Fig. 11A**) (Antonny et al. 2015). Indeed, phospholipids can be categorized according to their intrinsic shape. There are cylinder shapes, like PC or PS, inverted cone-shaped lipids, mainly PE and PA, or conical lipids such as PI and lysoPC, which depend on the area ratio of the polar group and acyl chain (Peetla, Vijayaraghavalu, et al. 2013) (**Fig. 11B**).

A



B

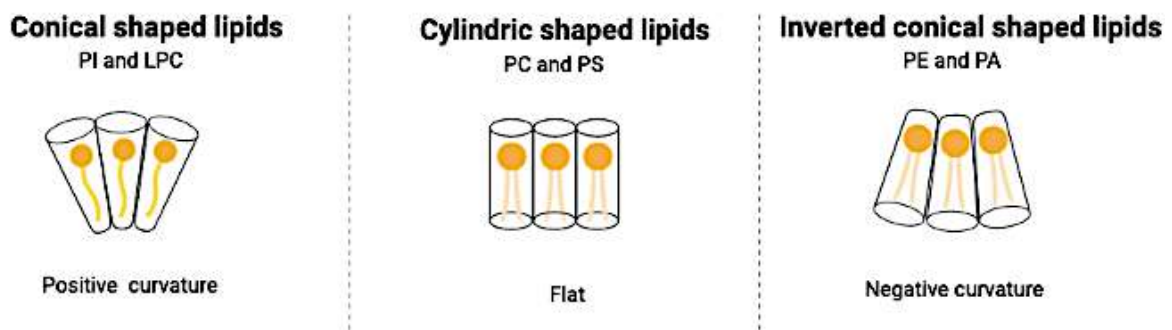


Figure 11. Membrane curvature and lipid packing defects and variety of lipid shape.

(A) Positive curvature locates in the convex side, where the head groups of PL separate to form gaps, the lipid packing defects. Negative curvature locates at the concave side, where head groups of PL are compressed. (Antonny et al., 2015). (B) Conical lipids induce positive curvature whereas inverted conical lipids promote negative curvature. Cylinders are responsible for flat membranes (adapted from (McMahon et Boucrot 2015; Peetla et al. 2013)).

Spontaneous curvature can also be created by insertion of proteins. Transmembrane proteins such as ion channels and transporters have an intrinsic conical or inverted conical shape that can bend membranes. Cell-sized giant unilamellar vesicles (GUVs) containing the voltage-gated potassium uptake system KvAP, were shown to be specifically enriched in KvAP in tubes, suggesting a greater enrichment in highly curved membranes. Fluorescence

recovery after photobleaching (FRAP) has shown that proteins freely diffuse through the neck between the tube and GUV, suggesting that membrane shape is involved in the proper targeting of transmembrane proteins (Aimon et al. 2014). The concentration of high-curvature-sensing and -inducing proteins, such as the secretion associated Ras related GTPase 1 (Sar1), the ESCRT complex or sorting nexin proteins, is also important for the organization of ER exit sites or endosomal sorting and recycling (Cullen et Korswagen 2011; Okamoto et al. 2012).

(ii) Protein oligomerization

Clathrins can self-assemble into rigid, curved shell-like structures. They impose their curvature on the PM, triggering the formation of the well-known honeycomb-shaped pits. Coat proteins such as clathrin and coat protein (COP) proteins stabilize membrane curvature during vesicle budding (Kirchhausen 2000; McMahon et Boucrot 2011). Their bending capacity depends on the rigidity of the coat and the transmission of this shape to the membrane (Čopič et al. 2012). In cells, curvature is commonly found at the level of vesicles such as caveolae or clathrin coated pits.

Membrane scission is essential to the budding of these vesicles from the PM as in the case of clathrin pits, or from the ER or Golgi for COPI and COPII vesicles.

High concentrations of hydrophobic insertions at the neck of these vesicles supports their fission, as it is the case for Sar1 and epsin localized at COPII and clathrin vesicles respectively (Boucrot et al. 2011:201; Lee et al. 2005). Epsin insertion occurs in the outer part of the PM, meaning that the tip of the wedge is in the center of the bilayer which generates a small radius of curvature (Ford et al. 2002).

Another example is dynamins, which are GTPases that mechanically drive membrane fission and deform membranes into tubules, through a helical coat that encircles the tubule. Dynamin polymerization occurs on preformed tubes at high concentration (12 μM). *In vivo*, physiological concentrations ranges between a few hundred nM and a few tens μM , allowing dynamin to acts either as a curvature sensor or as a curvature inducer. Consequently, dynamin nucleation could be regulated by membrane curvature *in vivo* (Roux et al. 2010). Interestingly, polyunsaturated PLs increased the ability of dynamin and endophilin to deform and vesiculate synthetic membranes. When cells incorporated polyunsaturated fatty acids into PLs, the plasma membrane became more amenable to deformation endocytosis increase, in particular, under conditions in which cholesterol was limiting. Polyunsaturated PLs adapted their conformation to membrane curvature.

Thus, by reducing the energetic cost of membrane bending and fission, polyunsaturated PLs may help to support rapid endocytosis (Pinot et al. 2014).

Caveolins are integral membrane proteins that oligomerize, thereby facilitating the formation or stabilization of curvature at caveolae (Parton et Simons 2007). Cavins, which are cytosolic proteins interacting with caveolins, were also proposed to induce membrane curvature (Hayer et al. 2010), together with Pacsin and the EH-domain containing 2 protein (EHD2) (Daumke et al. 2007) (Plomann, Wittmann, et Rudolph 2010).

(iii) Scaffolding proteins

Scaffolding by peripheral proteins triggers membrane bending whereby the shape of the membrane-binding interface is imposed on the membrane. As an example, Bin/Amphiphysin/Rvs (BAR) domain proteins are central regulators of membrane deformation, which they can impose in a local density dependent-manner (Peter et al. 2004). The large BAR-domain containing protein family can sense positive and negative membrane curvature. Among them, BAR and Fes/CIP4 homology-BAR (F-BAR) domains are banana-shaped dimers containing positively charged residues on their concave side, which interacts with negatively charged lipids (**Fig. 12A**) (Peter et al. 2004).

They can sense and impose positive membrane curvature to the PM. As an example, the BAR protein endophilin nucleates its scaffolds at the ends of a membrane tube, contrary to a weaker curving protein centaurin, which binds evenly along the tube's length. Therefore, the nature of local protein–membrane interactions can affect the specific localization of proteins on membrane-remodeling sites (Simunovic et al. 2016). Conversely, inverse BAR-domain containing proteins are zeppelin-shaped homodimers. They sense and generate negative membrane curvature through their positively charged residues on their convex side, and for some of them, through their amphipathic helices. I-BAR-domain proteins harbor a lipid-binding domain together with a WH2 domain that interacts with G-actin. These domains promote the polymerization of actin filaments involved in the formation of protrusions such as filopodia and lamellipodia (Saarikangas et al. 2009; Suetsugu et al. 2006; Zhao, Pykäläinen, et Lappalainen 2011)(Lin et al. 2005). The most well-known proteins of the family are missing-in-metastasis (MIM), ABBA and the insulin receptor substrate p53 protein (IRSp53). Through their I-BAR domains, they induce a negative curvature of PIP2-enriched membranes by binding within the tubular structure (**Fig. 12B**) (Mattila et al. 2007). In addition, PIP2 can stabilize I-BAR protein assembly of I-BAR protein at the PM (Jarín et al. 2021).

The shape of the coating can be spherical as in the case of clathrins, or tubular for the wells of F-BAR domain proteins (McMahon et Gallop 2005). Typical radii of these structures range from 30 nm in the case of F-BAR domains to 120 nm for spherical coats. (McMahon et Mills 2004) (Masuda et Mochizuki 2010).

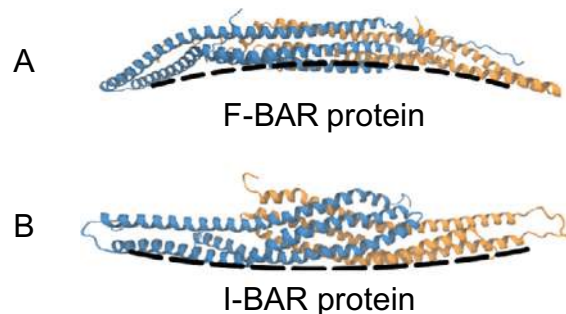


Figure 12. The structure of BAR domain proteins.

Representative members of the BAR protein family, each subunit is denoted by a different color. Shown are (A) the F-BAR protein FCh2 with positive intrinsic curvature (red-colored N-terminal amphipathic helices were added by hand) and (B) the I-BAR protein IRSp53 with negative intrinsic curvature (Adapted from Simunovic et al., 2016).

(iv) Protein-protein crowding

Another model described in GUVs propose that protein-protein crowding of the PM trigger bending (Stachowiak et al. 2012) although the contribution of this mechanism is still unclear (Kozlov et al. 2014). By correlating membrane tubulation with measurements of protein densities, Stachowiak and colleagues showed *in vitro* that lateral pressure generated by collisions between bound proteins drives bending and that a coverage above 20% is sufficient to bend membranes. Proteins unrelated to membrane curvature, such as green fluorescent protein (GFP), can also bend membranes when sufficiently concentrated. A highly efficient mechanism by which the crowded protein environment on the surface of cellular membranes can contribute to membrane shape changes at least *in vitro*.

(v) Cytoskeletal rearrangement

At a macroscopic scale, the cytoskeleton supports cell membrane bending, as it is the case in large organelles such as the Golgi or the ER. Formation of filopodia and lamellipodia upon cell migration also induce PM curvature. The actin cytoskeleton promotes a specific arrangement of the plasma membrane during phagocytosis with the production of membrane ruffles or in specialized cellular shapes (neurons or visual cones) (Sheetz 2001) (Rohn et Baum 2010). Active membrane pulling by kinesins, dynein and myosin motors also induces considerable membrane reorganization and supports some of the organelle morphologies (Leduc et al. 2010).

1.2.2.2. Plasma membrane tension

Physical description

The physical model explaining the properties of lipid membranes establishes that the elastic energy of a membrane depends on its tension, as well as changes in membrane area, local curvature and bending rigidity (Helfrich et Servuss 1984). Membrane tension is defined as the energy associated to the increase of area when a membrane is stretched: $\Delta F = \sigma \Delta A$, where ΔA is the increase of area and σ the membrane tension. It has the dimension of a force per unit of length and is usually expressed in mN/m.

In the case of GUVs, when the vesicles are not under tension, the membrane fluctuates: the observed area does not correspond to the real area of the surface but to the projected area (**Fig. 13B**). Only the deformations of longer wavelengths are optically visible (**Fig. 13A**). Consequently, when a fluctuating vesicle is pulled, the membrane fluctuations are first unfolded, without changing the projected area. The energy density of a fluid and fluctuating vesicle associated with the tension, using as an excess of area the relative variation between the real area and the projected area is then given by the sum of the curvature term and the tension is related to the bending rigidity by the following equation (Helfrich et Servuss 1984):

$$\sigma \simeq \frac{\kappa}{l^2} \exp\left(\frac{8\pi\kappa}{kT} \frac{A - A_p}{A}\right)$$

where σ the membrane tension, κ the bending rigidity, A is the real area and A_p the projected area, and l a microscopic cut-off (Helfrich 1985)(**Fig. 13C**).

The greater the difference between the actual area and the projected area is, the lower the tension and the more the membrane is fluctuating. Therefore, at low tension, these membrane fluctuations could act as membrane reservoir.

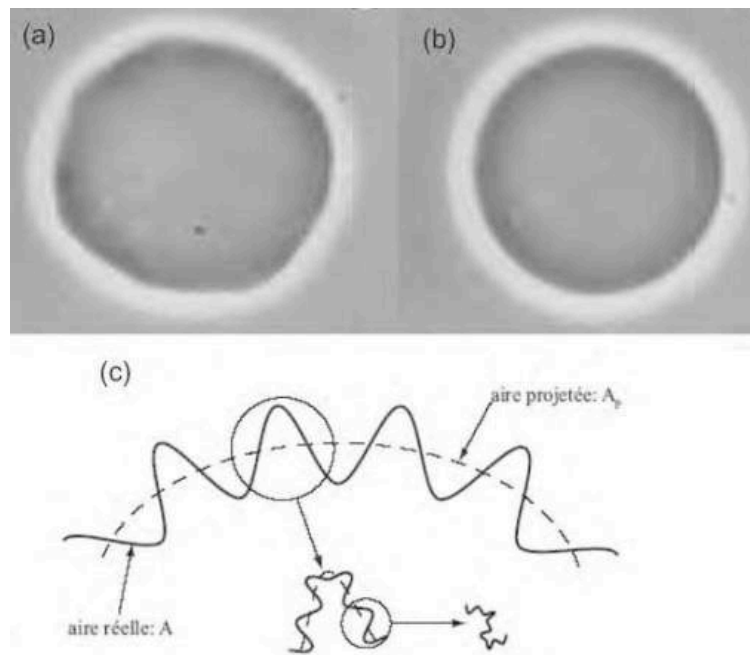


Figure 13. Thermal fluctuation of a giant vesicle observed in phase contrast

(A) vesicle subjected to thermal fluctuations of large amplitude that fold the membrane (the tension of the membrane is then very low; (B) tense vesicle whose shape is now spherical. (C) schematic representation of a fluctuating membrane at all spatial scales. The real area A is in continuous line and the projected area A_p in dashed lines (from (Girard, Prost, et Bassereau 2005)).

In cells, the parameter of “membrane tension” is more complicated to define when dealing with PM. In a simple membrane model, like a GUVs, tension can be described by the lateral in-plane tension in the lipid bilayer. In cells, the tension depends not only on the membrane but also on the adhesion of the underlying cytoskeleton. The cellular membrane tension or effective tension is defined as the sum of the two contributions: the membrane contribution and the contribution coming from the cortical tension that take in account the adhesion of the actomyosin cytoskeleton (Sens et Plastino 2015):

$$\sigma_{\text{cell}} = \sigma_{\text{membrane}} + \sigma_{\text{cortex}} .$$

Source of cortical tension

Cortical actin is linked to the PM mainly through the ERM protein family (Fehon, McClatchey, et Bretscher 2010). Among them, the ezrin, whose activation is dependent on its phosphorylation, is reduced in spread adherent cells compared to round cells during differentiation (De Belly et al. 2021).

In addition, ezrin attachment to F-actin occurs in multiple site, whose number increase in the presence of PIP2 in the PM (Braunger et al. 2014). Because of its interaction with the PM and cortex, membrane-cortex attachments decrease in absence of ezrin, which subsequently decrease actin protrusion formation essential for cell migration, suggesting a role for ezrin in the regulation of cortical tension (Diz-Muñoz et al. 2010). Mice expressing a

phosphomimetic mutant of the ezrin in T-cells show an increase of T-cells PM tension that consequently impair lymphocytes migration through the endothelium (Liu et al. 2012).

The cytoskeleton maintains cell membrane tension by connecting to the bilayer at regular intervals, and it imposes macroscopic shapes by providing an underlying scaffold (Doherty et McMahon 2008).

Functional role

Cellular membrane tension was shown to be implicated (i) in the regulation of cell migration, (ii) cell signalling, (iii) cell trafficking, (iv) cell differentiation and (v) cell division, in a possible mechanical feedback from PM to cytoskeleton.

(i) Cell migration

Effective membrane tension is an important player in actin-dependent protrusions in cells, likely filopodia, lamellipodia and blebs (Sens et Plastino 2015). Indeed, a decrease of membrane tension is responsible for the formation of unorganized lamellipodia composed of short filaments impairing cell movement (Raucher et Sheetz 2000). Conversely, an increase of membrane tension promotes actin polymerization resulting in longer filaments geared in the direction of movement, promoting cell motility (Batchelder et al. 2011).

Blebs are spherical structures resulting from detachment of the PM from the underlying cortex, or from increased intracellular pressure. They can be instrumental for cell migration in various cell types such as germ cells in zebrafish (Charras et Paluch 2008) (Diz-Muñoz et al. 2010).

(ii) Cell signalling

Various cell types such as fibroblast, neurons and neutrophils, submitted to osmotic shocks modifying their intracellular volume, show a high cell tension (Pontes et al. 2017) (Dai et al. 1998) (Diz-Muñoz et al. 2016). Indeed, rapidly after an osmotic shock, epithelial cell volume and tension change to balance differences in intra- and extracellular osmotic pressures. Interestingly, after the initial response, tension and volume recover from an hypoosmotic shock but not following hyperosmotic shocks and remain coupled.

When the cell volume dramatically increases following hypoosmotic shock, the cell first responds by depolymerizing the cytoskeleton to drive membrane unfolding, which results in a release of membrane surface area. The cell recovers its initial volume through the activation of ion channels, as the cytoskeleton is still disrupted. The volume is then completely recovered with actin repolymerization, which refolds the membrane, under the

control of the mammalian target of rapamycin (mTOR) signalling. Thereby, the coupling between tension and volume is actively regulated by the cytoskeleton, ion channels and mTOR signalling to maintain a quantitative relation between volume and tension well described by passive physical mechanisms (Roffay et al. 2021).

(iii) Cell trafficking

Cells compensate an increase of effective PM tension induced by hypo-osmotic shock by promoting exocytosis, thereby bringing the excess of membrane area stored in reservoirs, such as protrusions and vesicles, to the PM. On the contrary, when tension drops, the size of the reservoir increases removing excess membrane from the PM to restore its basal tension (Raucher et Sheetz 1999). To this aim, it was proposed that the loss of membrane–actin contacts reduces the effective PM tension and promotes endocytosis (Pietuch, Brückner, et Janshoff 2013). Clathrin assembly is responsible for the formation of coated pits in normal conditions. However, when cells face a rise of PM tension, clathrin assembly is not sufficient to properly invaginate the PM, and actin polymerization mediated by Rac1 and Arp2/3 GTPases then take over to complete the invagination process (Boulant et al. 2011). Equivalently, caveolae have been shown to play a role in PM tension regulation as they can flatten under cell stretching or osmotic shock, to increase PM area (Sinha et al. 2011). For more information of caveolae role in mechanobiology please refer to “2.3.1.2 Caveolae as mechanoprotectors”).

Interestingly, for typical cellular membrane tension ($\sim 10^{-5}$ N/m), dynamin do not deform membranes into tubules, as its polymerization force is overcome by high PM tension. This suggests that recruitment of proteins to the membrane can be controlled by tuning cellular membrane tension, and could explain how endocytosis is up-regulated when plasma membrane tension is reduced (Roux et al. 2010).

(iv) Cell differentiation

Effective PM tension also plays a central role in differentiation, during which embryonic stem cells face morphological changes regulated by a decrease in effective PM tension and cell spreading. This reduction is driven by a β -catenin-mediated lessening in RhoA activity and facilitates the endocytosis of FGF signalling components, which activate the extracellular signaled kinase (ERK) signalling and promote differentiation (Bergert et al. 2021:202; De Belly et al. 2021).

(v) Cell division

In mouse oocytes, the effective tension drops during meiotic maturation and strengthens upon fertilization. In metaphase II, the egg is polarized with a difference of tension between the meiotic spindle cortex and the opposite cortex, suggesting the assembly of a stiffer cortical domain promoting asymmetric cytokinesis. Actin, myosin-II, and the ERM family of proteins are enriched in these cortical domains and modulate mechanical properties in oocytes, contributing to cell polarity and meiosis (Larson et al. 2010).

Mechanical feedback

Cytoskeletal rearrangements, together with PM remodeling, affect PM tension involved in a mechanical feedback between PM and actin cytoskeleton. As an example, phagocytosis induces the formation of pseudopods following actin remodeling. This leads to an unfolding of membrane reservoirs and a subsequent increase of the effective PM tension triggering pseudopod extension (Masters et al. 2013). In a 3D matrix, rear retraction and durotaxis are controlled by the accumulation of caveolae, which form in response to low membrane tension. Subsequently, caveolae activate RhoA signalling to control local F-actin organization, contractility and promote rear retraction (Hetmanski et al. 2019).

In neutrophils, effective PM tension doubles during leading-edge protrusion, thereby serving as a long-range inhibitor of Rac activation and subsequent actin assembly outside the leading edge. As a result, the formation of secondary fronts is inhibited and the spread of the existing front is promoted (Houk et al. 2012:20). This inhibition of actin assembly is the result of an increase of PM tension that acts through phospholipase D2 (PLD2) and the mammalian target of rapamycin complex 2 (mTORC2). In the absence of this pathway, neutrophils exhibit larger leading edges, higher membrane tension, and defects in chemotaxis (Diz-Muñoz et al. 2016).

Interestingly, cholesterol depletion was also shown to enhance PM tension in red blood cells, promoting cell PM rupture in a cytoskeletal-independent manner (Biswas et al. 2019:201).

Tension distribution across the cell

Whether membrane tension is widespread, or a local event is still unclear. Studies suggest that formation of high-tension domains in the cells, for instance during protrusion formation at the leading edge, generate a local tension that is sensed at the other pole of the cell.

As a response, a decrease of PM tension account for inhibitory effects at the other pole of the cell, thereby lowering PM at the rear (Houk et al. 2012) (Lieber et al. 2013:20) (Diz-Muñoz et al. 2016) In addition, ECM can also play a role in the propagation of PM tension as a gradient in membrane tension between the front and rear of cancer cell can be observed when cells migrate on a rigidity gradient (Hetmanski et al. 2019). Indeed, because of its 2D fluid nature, the PM allows lipid diffusion in the bilayer, but lipid domains and proteins bending the PM or interacting with the cytoskeleton could acts as barrier in the PM and may impair the lipid flow, thereby generating regions of different tensions. Similarly, PM bending may induce variation of PM tension, promoting inhomogeneity of PM tension (Kozlov et Chernomordik 2015).

1.2.3. Controlling and measuring membrane physical properties

Measuring cellular membrane tension is challenging, especially in cells displaying membrane tension gradients. For this reason, it is common to simply probe the impact of a variation of in-plane membrane tension induced by osmotic shocks. Indeed, hypoosmotic increase cell surface area and subsequent PM tension, whereas hyperosmotic shock trigger cell shrinkage and decrease PM tension. They have been widely use in cell mechanobiology to investigate the role of membrane tension in cell processes, including clathrin-mediated endocytosis, caveolae multiple function and more globally to probe cell mechanistic (Riggi et al. 2019) (Ferguson et al. 2017; Guo et al. 2015; Pietuch et al. 2013) .

Several methods exist to control or measure the cell tension and the bending rigidity. Among others, atomic force microscopy (AFM), cell compression, micropipette aspiration or chemical sensors are commonly used (**Fig. 14**) (Diz-Muñoz, Weiner, et Fletcher 2018). In this part we will focus on some of these methods, mainly the micropipette aspiration, the tether pulling experiments and the use of a lipid probe sensing the PM tension variations which correspond to the techniques I used during my thesis.

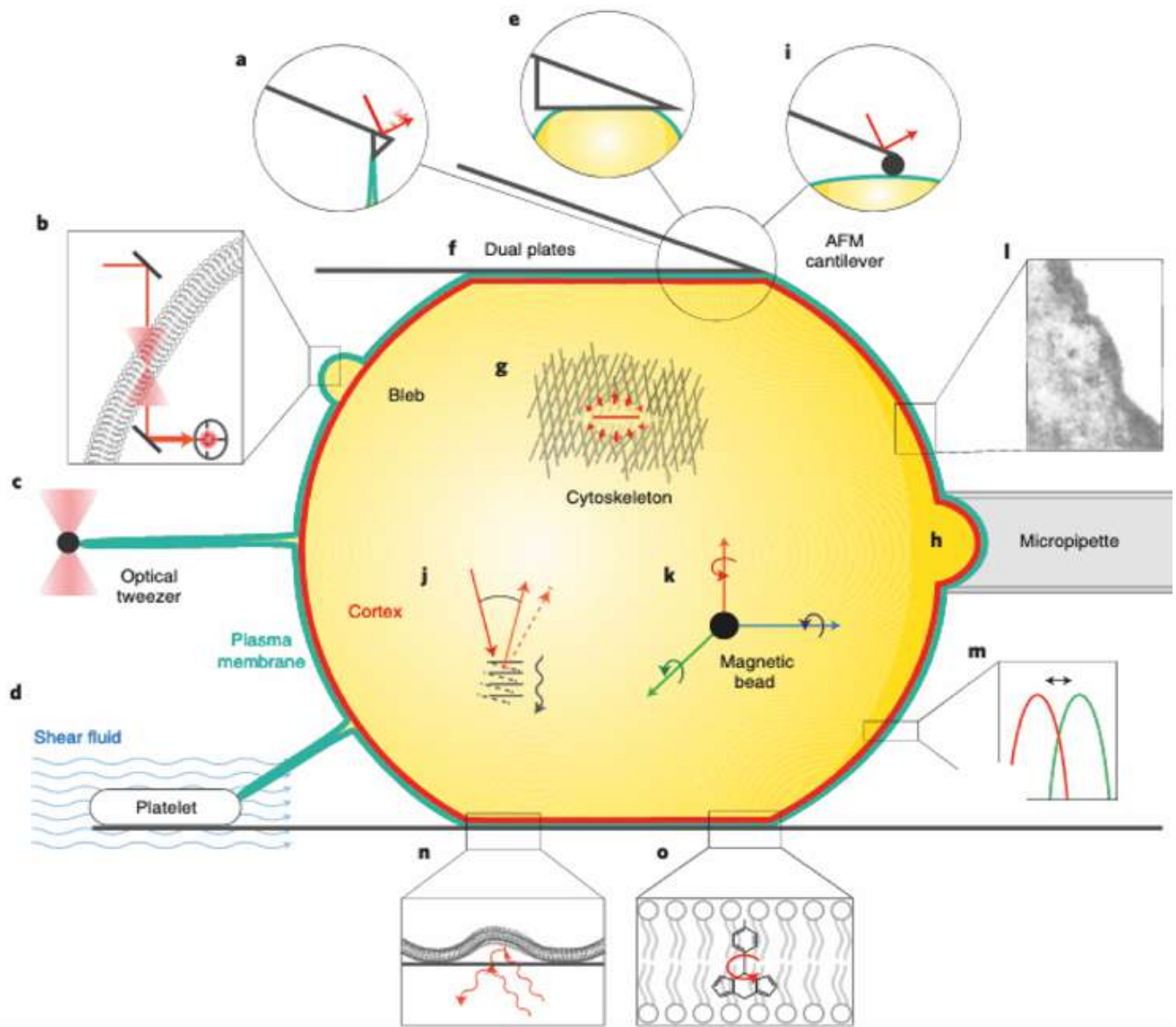


Figure 14. Scheme depicting the main method to characterize the effective PM tension.

a, Tether pulling using AFM. **b**, Interferometric particle detection using optical tweezers. **c**, Tether pulling using optical or magnetic tweezers. **d**, Tether pulling using shear fluid. **e**, AFM compression with a flat cantilever. **f**, Dual plate compression. **g**, Laser ablation. **h**, Micropipette aspiration. **i**, AFM indentation. **j**, Brillouin microscopy. **k**, Magnetic twisting cytometry. **l**, Electron microscopy. **m**, Fluorescence microscopy. **n**, Flicker spectroscopy. **o**, FlipoR technology (Diz-Muñoz et al. 2018).

1.2.3.1. Micropipette aspiration

Micropipette aspiration has been first used in 1979 on erythrocytes (Waugh et Evans 1979). This technic allows to fix the cellular tension using the hydrostatic pressure. A glass micropipette with a typical diameter of 3 to 5 μm is connected to a water reservoir whose height varies to apply a suction pressure to a vesicle or a detached cell, which is then aspirated inside the micropipette, forming a tongue-like projection in the pipette.

Using Laplace's law, the membrane tension can be deduced from the aspiration pressure applied to the cell R_c , the radius of the pipet R_p and the radius of the cell,:

$$\sigma = \frac{P_e - P_i}{2 \left(\frac{1}{R_p} - \frac{1}{R_c} \right)}$$

P_e is the pressure outside the pipet and P_i the pressure inside the pipet. This law can only be applied if the tongue of the vesicle inside the pipet is longer than the radius of the pipet R_p (Hochmuth 2000).

1.2.3.2. Tether pulling experiments

Membrane tension can be measured by the use of tether pulling experiments using optical tweezers. In tethers extraction, the tube can be considered as cylinder. The static force f_0 necessary to pull a tube, depends on the balance between membrane tension and bending rigidity:

$$f_0 = 2 \pi \sqrt{2 \sigma \kappa} ,$$

where σ is the membrane tension and κ the bending rigidity. Knowing the bending rigidity, it is then possible to measure the membrane tension and *vice et versa*.

Interestingly, in adherent GUV whose tension is not controlled by micropipette aspiration, the force needed to pull a membrane tube depends on the length of the tube since pulling a long tube deplete the membrane reservoir in the vesicle and therefore continuously increases membrane tension (Cuvelier et al. 2005).

From a theoretical point of view, a model of a tube pulled out of a flat membrane has been numerically solved by Derenyi et al. When the tube is formed, the flat membrane is deformed into a catenoïd whose force needed to elongate the tube linearly depend on the tube length. Once the tether has been pulled, the force becomes independent from its length (**Fig. 15A**). The transition between the flat membrane and the tether is accompanied by a force overshoot (Derenyi, Julicher, et Prost 2002), which was also been observed experimentally (**Fig. 15B**) (Koster et al. 2005).

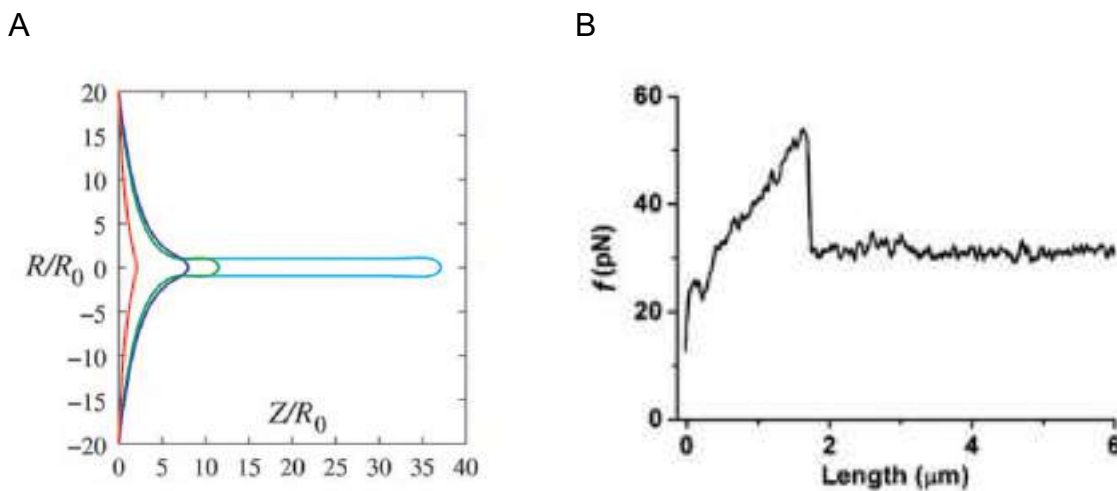


Figure 15. Model of a tube pulled out of a flat membrane and its force-extension curve

(A) shape of a tether pulled with a membrane of tension $\sigma = 5.10^{-5}$ N/m and bending rigidity $\kappa = 10$ KBT. Different lengths are represented (normalized by the tube radius R_0). The red curve corresponds to a nascent tube whereas the blue curve represent the established tether (Derenyi et al. 2002). (B) Representative force-extension curve at fixed tension of 1.3×10^{-5} N/m, with the overshoot (Roux et al. 2005).

There are different techniques to extract tubes from membrane. Tethers were first observed on adherent red blood cells submitted to shear stress (Hochmuth, Mohandas, et Blackshear 1973). Tubes can also be extracted by an AFM tip (Gumí-Audenis et al. 2018), by optical tweezers (Roux et al. 2005) or molecular motors pulling tubes from GUV along microtubules (Koster et al. 2003; Leduc et al. 2004; Roux et al. 2002). These tubes were pulled from GUVs of complex lipid composition, as well as biological membranes purified from the Golgi complex (Roux et al. 2002). Leduc et al., provided direct observation and quantification of the accumulation of motors at the tip of tubes, which promote tube formation. In addition, for a given membrane tension, they determined that it exists a threshold in motor density on the vesicle, below which no tubes can be formed (Leduc et al. 2004). Moreover, using optical tweezers it was shown that lipid composition differs between the tubes and the vesicles. Tube fission is observed when phase separation is generated in the tubes suggesting that lipid sorting depend on both membrane curvature and phase separation (Roux et al. 2005).

When tubes are pulled directly from cells, then the force necessary to pull a tube depends on the effective tension which is the some of the membrane tension and the adhesion of the cytoskeleton. Dai & Sheetz showed that pulling tubes from cellular blebs allows to separate the contribution to the tension coming from the membrane and the one originated from the adhesion of the cytoskeleton (Dai et Sheetz 1999). Indeed, blebs do not contain an actin cortex as depicted in **figure 16**. When the membrane tension term is subtracted from the apparent membrane tension over the cytoskeleton, the membrane-

cytoskeleton adhesion term can be estimated. In both cell systems they studied, the membrane-cytoskeleton adhesion was the major factor in generating the tether force. According to the cell type and the level of cytoskeleton adhesion, the apparent tension varies between 0.01 to 0.3mN/m.

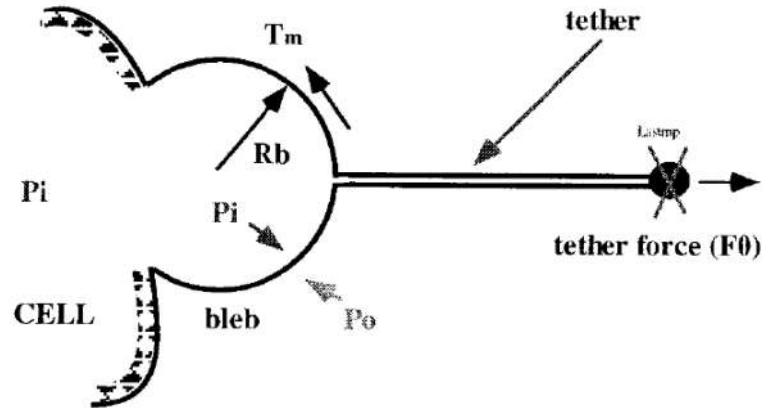


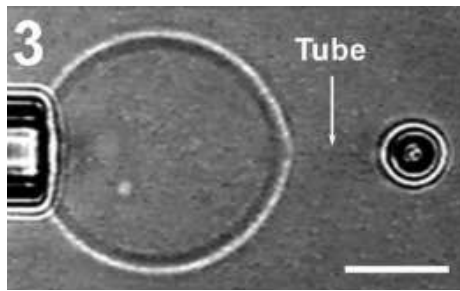
Figure 16. Scheme depicts the equilibrium of forces on a blebbing membrane.

Pi: pressure inside the cell, Po : pressure outside the cell which is equal to the atmospheric pressure (from (Dai et Sheetz 1999)).

1.2.3.3. Combination of micropipette aspiration and optical tweezers

When combined, micropipette aspiration and optical tweezers allow to control the membrane tension and measure the force needed to pull and hold the PM tube. This combination allows to perform bending rigidity measurements (Roux et al. 2005). Indeed, by studying the impact of an increase of the membrane tension, imposed by an increase of the aspiration in the micropipette, on the force necessary to pull a tube a tube: $f_0 = 2 \pi \sqrt{2 \sigma \kappa}$, the value of the bending rigidity can be deduced from the slope of the curves f vs. $\sqrt{\sigma}$ as depicted in **figure 17** (Roux et al. 2005).

A



B

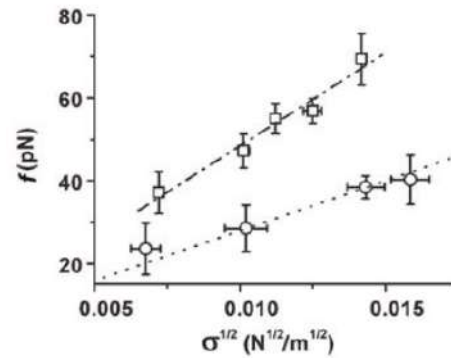


Figure 17. Tether pulling experiment on a GUV controlled by micropipette aspiration.

(A) Micrograph of the tether extraction experiment where the vesicle is held by a micropipette aspiration system while tether is extracted by optical tweezer trapping a bead. Scale bar 10 μm . (B) Linear variation of the force (f) necessary to pull a membrane tube from a GUV in the liquid ordered phase (squares) and liquid disordered phase (circles) as a function of the square root of the membrane tension ($\sqrt{\sigma}$). Line slopes are proportional to the square root of the bending rigidities ($\sqrt{\kappa}$) (Extracted from (Roux et al. 2005)).

In a simple model of GUV, the bending rigidity depends on the lipid composition. Consequently, the force is independent of the tether length and only weakly affected by the speed of extraction, with a fast relaxation to its static value f_0 . In plasma membrane spheres devoid of actin cytoskeleton, relaxation of the force occurs in two times: the short time corresponds to intermonolayer frictions, while the long time correlates to a diffusion process inside the membrane tube and is on the same order of magnitude of cytoskeleton remodeling. Therefore, tethers need to be pulled slowly to allow time to relax (Campillo et al., 2013). In cells, because of the presence of cortex and proteins inserted to the PM and the cytoskeleton, the tether force depends strongly on the speed of tube pulling (Sens et Plastino 2015)

1.2.3.4. A lipid probe to measure membrane tension

Recently, a great advance has been made to measure the PM tension in cells in a simple way, by the use of a lipid probe, FlipoR. This fluorescent probe spontaneously inserts into the PM of cells and is only fluorescent when inserted in the membrane. There, it responds to PM tension variation by changing its conformation. Indeed, it senses changes of the organization of the lipid bilayer through changes of the twist angle and polarization between the two twisted dithienothiophenes of the mechanophore. Therefore its planarization changes its fluorescence lifetime, which can then be measured by fluorescence lifetime imaging microscopy (FLIM) (**Fig. 18**) (Colom et al. 2018).

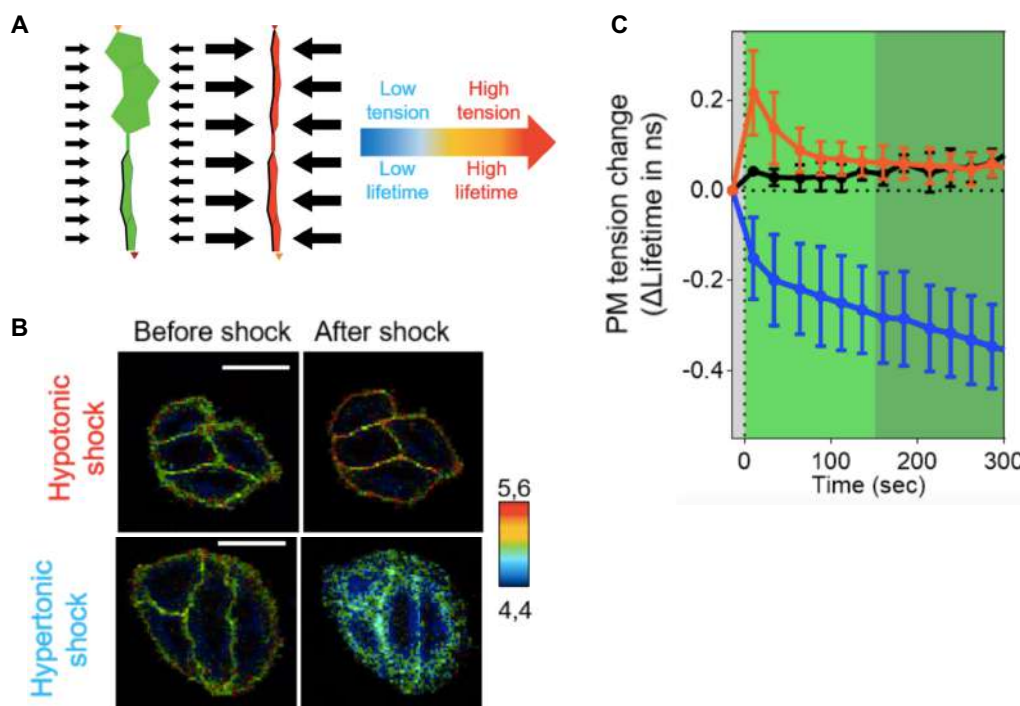


Figure 18. Fluorescence lifetime of the FliptR probe reports membrane tension changes

(A) The scheme depicts in green the FliptR molecule under low tension. Pressure along the axis of the FliptR probe planarize molecule (red molecule), leading to changes in fluorescence lifetime. (B) FLIM images of FliptR lifetime values (colorscale) of cells subjected to osmotic shocks. (C) Dynamics of the change of tension as measured by FliptR lifetime (grey : before shock; light green : short-term response; dark green : long-term response; red curve : hypoosmotic shock, blue curve : hyperosmotic shock, black curve : isotonic condition) (adapted from (Colom et al. 2018; Roffay et al. 2021)).

2. CAVEOLAE

Caveolae were first described in 1950 by Palade and Yamada. Multiple functions have now been assigned to omega-shaped caveolae and their components, as well as involvement of caveolin1 (cav1) in several host-pathogen interactions and of caveolin1 mutations in several human diseases. They contribute to signalling, transcytosis, endocytosis, cell migration, mechanical sensing, lipid and cholesterol transport, tumor suppression and induction (Goetz et al. 2008) (Goetz et al. 2008; Parton and Simons, 2007; Sens and Turner, 2005).

2.1. CAVEOLAE: STRUCTURE, COMPOSITION AND ORGANIZATION.

Palade and Yamada made the first observations by electron microscopy of small cave-like invaginations in various cell types that they named caveolae (**Fig. 19A**). In contrast to clathrin-coated pits, these membrane invaginations were first described as cup-shaped uncoated invaginations of similar but irregular size of 50 to 100 nm in diameter, compared to clathrin-coated pits (Palade 1953) (Yamada 1955).

Indeed “uncoated” caveolae turned out to be surrounded by striated structures on their cytoplasmic side (**Fig. 19B,C**). Then, Rothberg et al. identified the essential protein caveolin1 as the major component of caveolae (Rothberg et al. 1992). A caveola it is composed of 144 molecules of caveolins, which are evolutionarily conserved integral membrane proteins (Kirkham et al. 2008).

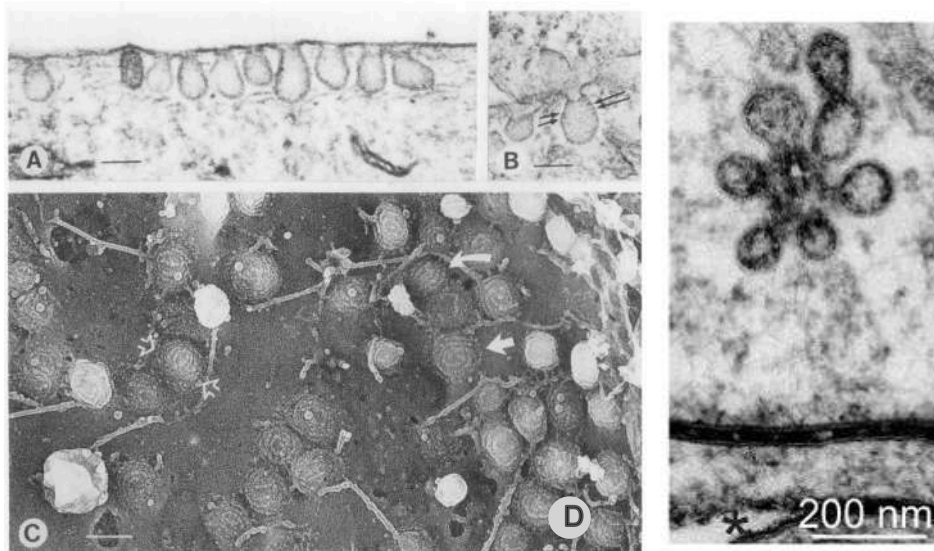


Figure 19. Caveolae

When observed by EM, caveolae can form cup-shaped invaginations at the PM (**A**) with a striated coat (**B, C**). Eventually they can assemble into superstructures called rosettes (**D**) (adapted from (Echarri et Del Pozo 2015; Rothberg et al. 1992)).

A few years later, Hansen and Nichols identified cavin family proteins involved in stabilizing caveolae structures through their interaction with cav1 (Hansen et Nichols 2010). Caveolae are thus defined by the specific array of proteins, which forge them, together with their enrichment in cholesterol, glycosphingolipids and sphingomyelins forming so called detergent-resistant PM domains enriched in cholesterol, glycosphingolipids and sphingomyelins (**Fig. 20**) (Monier et al. 1995; Anderson 1998).

Caveolae are present in most mammalian cell types with the exception of lymphocytes and neurons, although all cells express cav1. Whether cav1 has a specific role in addition to its structural function of specific detergent-resistant PM and flask-shaped pits remains to be fully understood and is the object of present thesis work. In fibroblasts, adipocytes, endothelial cells, and muscle cells, caveolae can cover up to 40% of the PM surface. They can also assemble into multicaveolar superstructures referred to as rosettes (**Fig. 19D**) (Thorn et al. 2003; Parton et Simons 2007).

In this chapter, we will focus on caveolar structures and their content in lipids and proteins, namely cav1, cavin1/PTRF, and EHD2, and their associated physiological roles and functions.

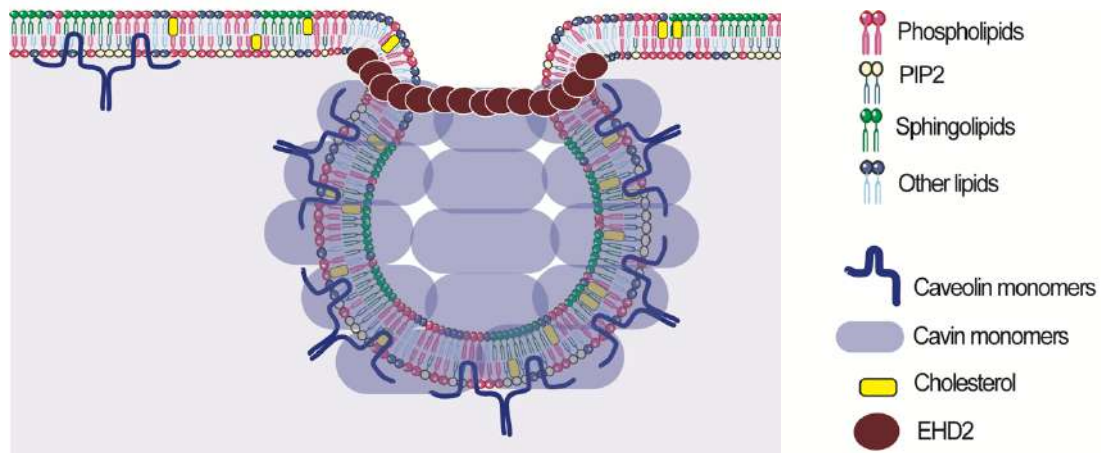


Figure 20. Caveolae structure.

Caveolae are composed of specific array of proteins, the main ones being the integral membrane caveolins monomers that can assemble with cavins complexes coating the caveolae. EHD2 is an ATPase localized at the neck of the caveolae and plays a role for neck constriction. Caveolae have also a specific detergent-resistant PM composition.

2.1.1. Caveolins

Caveolins were primarily defined by their association with detergent-resistant domains and caveolae. However, they can serve as scaffolds in non-detergent resistant domains of the PM. For example, caveolins are found in lipid droplets (Pol et al. 2005), cell-matrix adhesion (Nethe et al. 2010), non-PM membranes and notably in the secretory pathway (Pelkmans et al. 2004) (Botos et al. 2008) (Muriel et al. 2011; Ritz et al. 2011). In addition, they have been implicated in mitochondrial function (Bosch et al. 2011) (Fridolfsson et al. 2012; Simón et al. 2020).

The first protein identified as an essential component of caveolae was named caveolin1 because of its close association with the caveolar pit (Rothberg et al. 1992). Later, two other isoforms of caveolins were described: caveolin2 and caveolin3 (Scherer et al. 1996) (Way et Parton 1995). All caveolins are very similar in structure and exhibit conserved domains. In particular, the N-terminus harbors a caveolin signature motif 'FEDVIAEP' together with the oligomerization domain (Scherer et al. 1996) (Tang et al. 1996). In addition, caveolins C-terminal domains can be all palmitoylated, thereby allowing their interaction with membraneous subdomains (Dietzen, Hastings, et Lublin 1995) (Kwon et al. 2015). Together, caveolins interact with cavin proteins to form a stable, invaginated caveolar pit.

Caveolin 1

Cav1 is observed on the membrane of the trans-Golgi apparatus, indicating that it localizes at the PM, as well as at internal vesicular membranes (Kurzchalia et al. 1992). Expression of cav1 in a prokaryotic host lacking intracellular membrane system, such as the ER and Golgi apparatus, drives the formation of cav1-positive cytoplasmic vesicles. These vesicles are equivalent in size and cav1 density, to caveolae found in eukaryotic cells. Moreover, this heterologous expression of caveolae generates a membrane domain with a distinct lipid composition, although bacterial cell membranes typically lack cholesterol (Walser et al. 2012).

Cav1 is a small 21-kDa protein composed of 178 amino acids (aa). It consists in a C-terminal amphipathic helical domain and a N-terminal extended disordered domain. Both these domains face the cytoplasmic compartment (Parton et al. 2021), while a central alpha-helical hairpin domain is thought to contribute to membrane anchorage (**Fig. 21A**) (Glenney et al. 1992). In front of the intramembrane region, cav1 harbors an essential domain called the cav1 scaffolding domain (CSD, amino acids 82-101) (**Fig. 21B**). It is responsible for the oligomerization of cav1, as well as the interaction of cav1 with other proteins, such as cavin. In addition, cav1-CSD binds one to two cholesterol molecules (Murata et al. 1995). Giancotti's group has shown that the N-terminal part of cav1 presents a key tyrosine residue at position 14 (Tyr14) which phosphorylation is implicated in many regulatory processes that cav1 C-terminal ends can be palmitoylated on multiple cysteine residues (**Fig. 21B**) (Dietzen et al. 1995).

Two isoforms of cav1, α and β , had been thought to be generated by alternative translation initiation sites of an mRNA. They form homo-oligomers at the PM where they can interact with heterotrimeric G proteins (Monier et al. 1996) (Scherer et al. 1996) (Sargiacomo et al. 1993) (Parton et al. 2021). Interestingly, the depletion of cav1 leads to a decrease in cavin1/PTRF level. This is also possibly true for other cav1-interacting proteins, such as filamin A (Hill et al. 2008) (Ravid et al. 2008). As the major isoform of caveolin in endothelial cells, cav1 will be the isoform studied in this thesis.

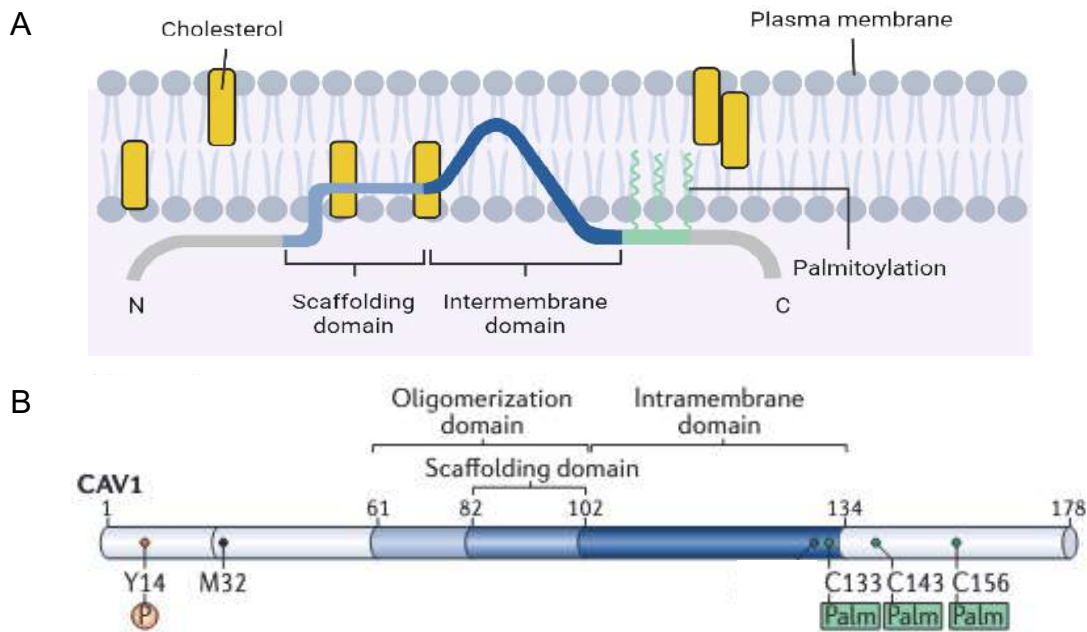


Figure 21. Caveolin1 structure.

Cav1 is an integral membrane protein with a hairpin domain that allows it insertion in the inner leaflet of the PM. Both the N- and C-terminal domains face the cytoplasm. Numbers above the lines correspond to the amino acid in mammalian cav1. Cav1 is composed of a caveolin scaffolding domain (CSD) interacting with cholesterol and proteins. The starting Met of CAV1 is shown in black (M32). Cav1 can be phosphorylated on its tyrosin 14 residue (Y14-P, in red). Palmitoylation (Palm) sites in CAV1 are indicated on its C-terminal part on three cysteins (in green, C133, C143, C156) (adapted from (Parton et del Pozo 2013)).

Other caveolins

Caveolin2 consists in 161 aa and is co-expressed with cav1 in most cell types forming stable hetero-oligomers (Scherer et al. 1996). When expressed alone, cav2 forms mono- or dimers and cannot reach the PM (Mora et al. 1999). This indicates that cav1 may also fulfil a sorting function for trafficking of proteins and lipids to the PM. Like cav1, cav2 is expressed in 2 isoforms α and β , the latter being the shorter version. However, to date, little is known about their respective functions in cells (Scherer et al. 1996).

Caveolin3 is composed of 151 aa and is a muscle-specific protein found at the sarcolemma (Way et Parton 1995; Tang et al. 1996). Cav3 can form hetero-oligomers with cav1 in cardiomyocytes, leading to the formation of mixed caveolae (Volonte et al. 2008). Cav3 is important for myotube formation. It associates with the dystrophin-glycoprotein complex (DGC), which is known to link the ECM to the actin cytoskeleton, thus ensuring the structural stability of the PM (Dalkilic et Kunkel 2003). Cav3 is associated with many muscular dystrophies as detailed in chapter "2.3.4 Caveolae-related pathologies" of this thesis.

Only cav1 and cav3 are able form caveolae at the PM and deletion of either of these two proteins impairs caveolae formation (Fra et al. 1995; Capozza et al. 2005).

2.1.2. Cavins

The first evidence of the existence of cavins appeared in 2001 in a study where Vinten et al. demonstrated the presence of a protein associated with caveolae (Vinten et al., 2001). Cavins are cytosolic proteins that interact together to form hetero-oligomeric complexes, recruited to the PM *via* cav1 (Aboulaich et al. 2004) (McMahon et al. 2009) (Liu et al. 2008). There are 4 isoforms of cavins annotated cavin1/PTRF to cavin4.

They are homologous proteins found in all tissues, with the exception of cavin4, which is specific to muscle (Liu et al. 2014) (Hansen et al. 2013).

Cavins harbor a positively charged α helical structure in two clearly delineated helical regions (HR). HR1 and HR2 confer the ability to bind PI and PS to cavins (Gustincich et al. 1999) (Kovtun et al. 2014). Indeed, cavin1 possesses an essential undecad repeat sequence (UC1) for caveolar localization and promotes membrane remodelling through binding to PS (Tillu et al. 2018). It is also through their HR domains that cavins 2, 3, and 4 can trimerize with cavin1/PTRF, forming striations on the surface of caveolae (Gambin et al. 2014:201). In addition, cavins undergo numerous post-translational modifications, such as palmitoylation and phosphorylation. They all harbor PEST motifs (rich in proline, glutamic acid, serine, and threonine), indicating high sensitivity to proteolysis (Kovtun et al. 2015). Cavin1/PTRF, 2, and 3 contain a leucine zipper domain typically involved in DNA binding. Cavin1/PTRF and 4 contain nuclear localization signals (Fig. 22) (Aboulaich et al. 2004) (Bastiani et al. 2009).

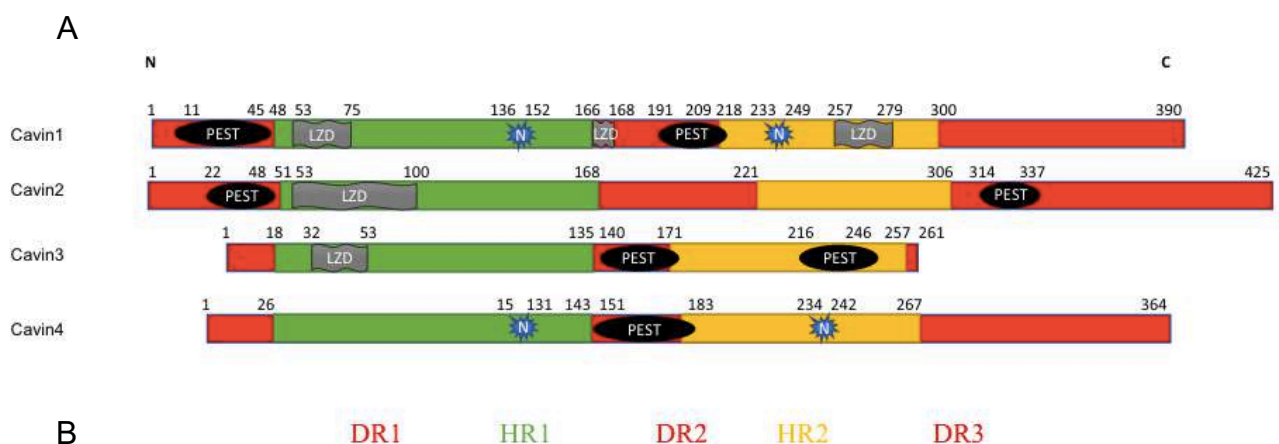


Figure 22. Cavins structure.

Cavins present two conserved, basic and positively charged helical regions (HR) 1 and 2 (HR1 and HR2) separated by disordered and non-conserved regions DR1, 2 and 3. They all present a proline, glutamic acid, serine, and threonine-rich domain (PEST); a leucine zipper-like domain (LZD). Cavin 1 and 4 also present nuclear localization signals (N) (Nassar et al. 2015).

Cavin1/PTRF was originally described in a yeast two-hybrid screen, as a RNA polymerase transcription regulatory factor (PTRF), where it was shown to interact with Pol1 and TFF1 (Jansa et al. 1998). The first link between cavin1/PTRF and caveolae was established in adipocytes (Vinten et al. 2001) (Vinten et al. 2005) and then in other tissues such as skeletal and cardiac muscle, smooth vascular and intestinal muscle, as well as in endothelial cells and perineural sheath cells (Voldstedlund, Vinten, et Trantum-Jensen 2001). Later, cavin1/PTRF was identified by proteomics as a putative caveolar protein, essential for the formation and proper function of caveolae (Hill et al. 2008).

In both cell culture systems and animal models, it has been demonstrated that caveolae formation is dramatically reduced upon cavin1/PTRF depletion. Cavin1/PTRF depletion also decreases the association of actin with detergent resistant domains, suggesting a role for cavin1/PTRF in actin regulation. In addition, cavin1/PTRF is essential for the formation of caveolae in mammalian cells in all tissues, and its distribution is very close to that of cav1 (Hill et al. 2008; Liu et al. 2008; Liu et Pilch 2008). Upon cavin1/PTRF depletion, cav1 remains at the PM, where it exhibits an increased lateral mobility and an accelerated lysosomal degradation (Hill et al. 2008).

Cavin1/PTRF is the only homo-oligomer that associates with caveolae at the PM through its interaction with cav1 and the predominant lipids phosphatidyl serine (PS) and phosphatidylinositol (4,5)-bisphosphate (PIP2). Interestingly, cavin1/PTRF does not interact with caveolae in the Golgi apparatus or with mutant forms of caveolins (Bastiani et al. 2009) (Hansen et al. 2013; Hill et al. 2008). Cavin1/PTRF rather serves as a base for the other cavins to be incorporated into the caveolar coat (Bastiani et al. 2009). The caveolar coat is formed of approximately 50 cavin molecules, where cavin1/PTRF associates with either cavin2 or cavin3 as trimers, at a ratio of 2 to 3 molecules of cavin1/PTRF for one molecule of cavin2 or cavin3 (Gambin et al. 2014) (Ludwig et al. 2013).

Cavin2 was initially identified in platelets as a PS-binding protein and later as a serum deprivation response protein (SDPR) (Burgener et al. 1990; Gustincich et Schneider 1993) (McMahon et al. 2009). Depletion of cavin2 impairs caveolae formation, likely due to a loss of cavin1/PTRF recruitment to the PM. On the other hand, cavin2 overexpression results in extensive PM tubulation, suggesting a role for cavin2 in PM curvature or curvature sensing (Hansen et al. 2009).

In vivo, cavin2 plays a critical role for caveolae formation in adipocytes and in mouse lung endothelial cells, yet it is not essential in cardiac endothelium and other tissues. This difference of implication in different endothelia suggests that endothelial caveolae are

heterogeneous (Hansen et al. 2013). Interestingly, when cavin2 is depleted in mouse lung endothelial cells, cav1 and cavin1/PTRF relocate to non-invaginated caveolae, suggesting that caveolae can flatten (Hansen et al. 2013).

Cavin3, also known as Sdr-related gene product that binds to C-kinase (SRBC), was discovered in 1997 (Izumi et al. 1997). Cavin3 is highly expressed in the heart but can also be found in the brain and liver, in contrast to other cavin proteins (Bastiani et al. 2009). Like cavin2, cavin3 is able to bind to PS and is overexpressed during serum starvation. It is also able to associate with cavin1/PTRF in caveolae (Aboulaich et al. 2004).

Cavin4 was the last identified protein of the cavin family. It is mainly found in the sarcolemmal caveolae of muscle cells, hence its other name: muscle-restricted coiled-coil protein (MURC). It was initially described as a free cytosolic protein (Ogata et al. 2008). However, like other members of the cavin family, it was shown later that cavin4 interacts with cavin1/PTRF to form complexes that stabilize caveolae. In caveolae-associated muscle diseases, the distribution of the sarcolemmal cavin4 is strongly perturbed upon pathological mutations in human cav3, as discussed in the chapter 2.1.4.1 and in Bastiani et al. 2009.

2.1.3. EHD2 and accessory proteins

Although not essential for caveolae formation, other accessory proteins stabilize and regulate caveolar structures. Among them, Eps 15 homology containing domain 2 (EHD2) was shown to interact with caveolae in human adipocytes (Aboulaich et al. 2004) and to colocalize with cav1 in epithelial cells (Hansen, Howard, et Nichols 2011).

EHD2 is an ATPase that associates with stable invaginated caveolae. It localizes at the neck of the pit, where it forms a ring composed of 14 monomers that contributes to stabilize caveolae at the PM, in an ATP-dependent manner (Stoeber et al. 2012). The N-terminus of EHD2 harbors a nucleotide-binding domain (NBD) responsible for ATP binding and its oligomerization. Indeed, the loop in the NBD as well as the ATP binding site are required for caveolar localization of EHD2 (Daumke et al. 2007). The N-terminal domain also regulates the targeting and stabilization of the protein at the caveolar neck (Shah et al. 2014). The C-terminal domain of EHD2 hosts the EH domain of the protein which can interact with pacsin 2 to stabilize caveolae and is similar to those present in many proteins involved in endocytosis (Daumke et al. 2007).

High levels of EHD2 cause distortion and loss of endogenous caveolae. Conversely, depletion of EHD2 destabilizes caveolae, increasing their dynamics and endocytosis (Morén et al. 2012). Outside of caveolae, EHD2 can translocate into the nucleus where it regulates transcription of genes involved in cell cycle and division (Torrino et al. 2018). For more information, please see "2.3.3.2. Caveolae as mechanosensors and mechanoprotectors".

At the PM, EHD2 also associates with pacsins to stabilize caveolae. Pacsin 1, 2 and 3, are F-BAR-domain proteins promoting caveolae budding. While pacsin2 is ubiquitous, pacsin1 is found in neurons and pacsin3 localizes to muscle cells (Plomann et al. 1998) (Ritter et al. 1999). Their depletion alters caveolae morphology, suggesting a role for pacsins in membrane curvature during caveolae formation likely through their F-BAR domains (Hansen et al. 2011), see "1.2.2.1 BAR-domain proteins" for more details on BAR-domain proteins. Similarly, pacsin2, through its F-BAR domain, interacts with cav1 and recruits the GTPase-protein dynamin2 to the PM, which allows caveolae budding and thereby promoting their fission (Senju et al. 2011).

2.1.4. Lipids

Caveolae have their own specific lipid composition, which differentiates them from other membrane invaginations. Indeed, they form clusters of ordered lipid detergent resistant domains. Compared with the rest of the PM, caveolae are enriched in cholesterol and glycosphingolipids, especially GM1 and GM3 gangliosides, and sphingomyelin. In addition, lipid density is higher in caveolae than in the rest of the PM (Örtegren et al. 2004).

The shape of caveolae results in the bending of the PM which defines caveolae and PM lipid composition. Therefore, lateral tension imposed on the membrane by external, cytoskeletal, or osmotic forces triggers the flattening of caveolae, which has an impact on lipid distribution at PM (Ariotti et al. 2014) (Sinha et al. 2011)

Importantly, cholesterol is present in a very large amount in caveolae pits and consequently plays a very significant role. Indeed, a caveola has up to 22,000 cholesterol molecules (Örtegren et al. 2004). Therefore, cholesterol depletion causes both flattening of caveolae (Rothberg et al. 1992) and dissociation of cavins from the PM (Hill et al. 2008) (Breen et al. 2012). Cholesterol molecules are likely to be targeted to caveolae through their interaction with cav1, as cav1 harbors a consensus cholesterol recognition and interaction motif that significantly enriches cholesterol in the caveolar domain (Epanand, Sayer, et Epanand

2005). Outside of caveolae, cav1 can be found in scaffolding domains at the PM. The formation of these domains could balance the pool of inaccessible cholesterol (sequestered within these caveolin-enriched domains) and accessible cholesterol (freely diffusing in the PM) (Fielding et Fielding 2001), probably through cav1 phosphorylation, which also mediates internalization of proteins such as integrins (Meng et al. 2017, del Pozo et al. 2005). Other lipids such as PS could be similarly regulated (Ariotti et al. 2014).

As briefly mentioned previously, cavins bind to lipids through their HR1 domains. Specifically, they interact with PS and PIP2 in the PM, which are enriched in the cytoplasmic leaflet of caveolae (Fairn et al. 2011) (Fujita et al. 2009). Interestingly, PS depletion reduces EM-detectable caveolae, suggesting that PS is involved in caveolae stability and formation (Hirama et al. 2017). Similarly, cav1 depletion alters cellular lipid composition and impact PS distribution at the PM (Ariotti et al. 2014). In addition, cav1 regulates the global lipid composition of the PM. Indeed, under conditions of extra load of lipids in the PM, cells lacking cav1 exhibit an aberrant trafficking of glycosphingolipids (GSLs) and cholesterol through the Golgi-ER system. As a result, these lipids accumulate in lysosomes (Cheng et al. 2015).

2.2. CAVEOLAE BIOGENESIS

Cav1 is synthesized at the ER in a signal recognition molecule dependent manner (Monier et al. 1995), as an integral membrane protein. From there, it quickly oligomerizes and forms small highly mobile cav1-complexes (Hayer et al. 2010). Accumulation of cav1 complexes at the ER redirects them to lipid droplets. Consequently, these complexes are rapidly transfer to the Golgi apparatus in a COP-II dependent export system. In the Golgi, larger complexes are formed, decreasing their mobility. Thus, large cav1-complexes become more stable and sodium dodecyl sulfate (SDS) resistant, pointing to their association with lipids found in detergent resistant domains. Indeed, formation of these complexes is accelerated by cholesterol addition and is inhibited by glycosphingolipids depletion (Pol et al. 2005). From the Golgi apparatus, these cav1-positive exocytic carrier bud in a cholesterol-dependent fashion and directly travel as a vesicle to the PM (Tagawa et al. 2005) (Hayer et al. 2010). Their trafficking also involves the soluble N-éthylmaleimide-sensitive-factor attachment protein receptor (SNARE) protein syntaxin-6 that drives the delivery of cav1, GPI-anchored protein and GM1 to the PM (Choudhury et al. 2006).

It has also been suggested that cav1 proteins can transit to the PM as small complexes of oligomers, in a non-caveolar pathway (**Fig. 23**) (Khater et al. 2019).

Once at the PM, caveolae localize in specific domains enriched in cholesterol sphingomyelin, GM1/3 and ganglioside 3 (GD3)(Örtegren et al. 2004). They are associated with GPI-lipid cargos and transport rafts components to the PM. After vesicle fusion to the PM, GPI-anchored proteins diffuse in the membrane while cav1 complexes remain stable. Shortly after, cavins, produced in the cytosol, interact with proteins and lipids such as PS and PIP2, in the caveolar domains. Kirkham et al., proposed that caveolins cause membrane deformations of the cytoplasmic leaflet through a combination of amphipathic helix insertion and interaction with cholesterol. The membrane deformation is then stabilized and concentrated through oligomerization of caveolins and their interaction with cholesterol (**Fig. 23**) (Parton, Hanzal-Bayer, et Hancock 2006) (Parton, McMahon, et Wu 2020) (Kirkham et al. 2008).

Two alternative models coexist for the role of cavin1 in caveolae assembly. In model 1 invaginated caveolae are stabilized by cavin1, while in the second hypothesis cavin1/PTRF associates with flat cav1 domains to induce membrane curvature. It is still unclear if cavins monomers or cavins complexes preassembled in the cytoplasm before to associate with cav1 complexes (**Fig. 23**) (Hayer et al. 2010).

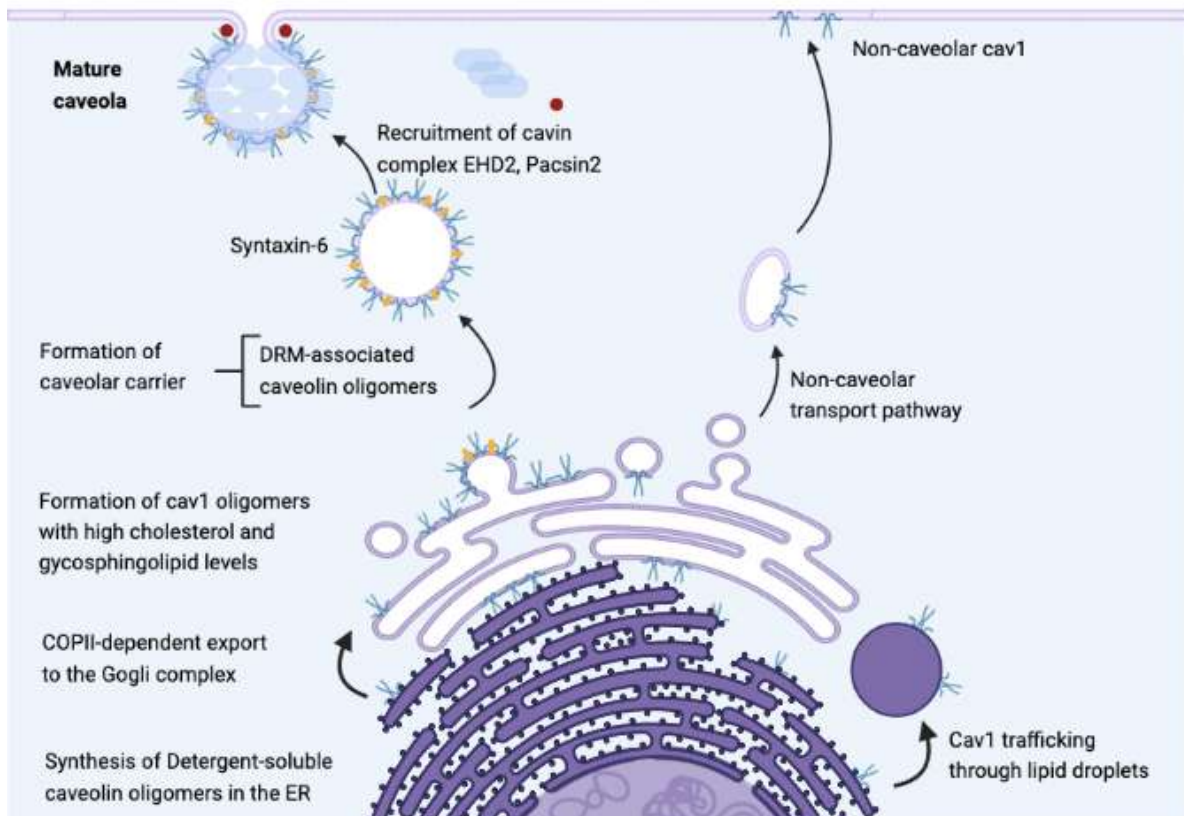


Figure 23. Schematic model of caveolin biogenesis

Cav1 is synthesized in the endoplasmic reticulum (ER) and is then transported to the Golgi apparatus as detergent-soluble oligomers in a COP-II dependent fashion. Oligomers associate with detergent-resistant membranes. Caveolar carriers composed of cav1, cholesterol (yellow), GM1 and GPI-anchored protein fuse with the plasma membrane through the control of syntaxin-6. Cav1 can also be transported to the plasma membrane by other carriers. After fusion with the PM, cavins (light blue) and accessory proteins such as EHD2 (red) interact with cav1 and specific lipid nano-domains to promote or to stabilize the invagination of the caveolar structure (adapted from (Parton et Simons 2007)).

The fate of caveolae at the PM varies, as they can be involved in endocytosis and trafficking, as well as in PM deployment in order to buffer mechanical stress applied to the PM. This will be developed in the next chapter: "role and functions of caveolae".

2.3. ROLE AND FUNCTION OF CAVEOLAE

2.3.1. Caveolae in lipid trafficking

Caveolae regulate trafficking and lipid accumulation into cells (Pilch et al. 2007). Indeed, they act as an entry door for the uptake of fatty acid FA from the extracellular environment. Fatty acids are then stored in cav1-containing lipid droplets (Öst et al. 2005). In adipocytes, which contain high levels of caveolae, association of cav1 with lipid droplets is stimulated by cholesterol and dependent on the dynamin-dependent budding of caveolae (Le Lay et al. 2006). Cav1 binds to FA and can relocate from the PM to lipid droplets in response to free FA (Trigatti, Anderson, et Gerber 1999) (Ostermeyer et al. 2001) (Pol et al.

2004). Moreover, cav1 C-terminal region is enriched in positively charged amino acids, which enhance the sequestration of FA in the inner leaflet of the PM and increase lipid storage in lipid droplets. These effects are accompanied by a significant protection against lipotoxicity in caveolin-expressing cells (Simard et al. 2010). Cells devoid of endogenous cav1 present impaired FA uptake, low levels of free cholesterol and low cholesterol export (Fielding et Fielding 2001) (Fu et al. 2004) (Meshulam et al. 2006). Interestingly, in human embryonic kidney (HEK) 293 cells, FA metabolism is not enhanced by cav1 expression. However, cav1, through its association to cholesterol, regulates oleic acid translocation across the lipid bilayer by a flip-flop mechanism, following its rapid binding to the extracellular side of the PM (Meshulam et al. 2006). These results suggest that caveolae can coordinate FA uptake and storage in lipid droplets, and raise the possibility that lipodystrophy associated with loss of Cav1 in patients reflects the increased sensitivity of adipose tissue to FA (Cao et al. 2008; Kim et al. 2008).

Very recently, Zhou et al., showed that cav1 associates with PS, PIP3, and cholesterol, mainly through its CSD domain, while cavin1 co-clusters with PIP2, PIP3 and PA *via* its HR domains. In addition, when cav1 and cavin1 are co-expressed, they trigger a quantitatively distinct lipid association profile as compared to the association profile of cav1 alone. Indeed, PIP3 association decreases, together with a significant increase of PIP2 and PA (Zhou et al. 2021).

Interestingly, in blood-brain barrier cells, caveolae are in low density and vesicular transport is low. Mfsd2a is thought to regulate transcytosis in brain endothelial cells by directly or indirectly affecting the mechanism of transcytosis. Recently, Mfsd2a, responsible for polyunsaturated fatty acids transport from the outer cytoplasmic leaflet to the inner cytoplasmic leaflet of the PM endothelial cell, has been shown to inhibit caveolae transcytosis to maintain a proper blood-brain barrier function (Andreone et al. 2017).

Therefore, caveolae and caveolins may act as lipid sensors, organizers, transporters and suppliers (Scheel et al. 1999). Cavin1 and EHD2 also regulate lipolysis and thus, the pool of intracellular lipids that can potentially follow these pathways (Ding et al. 2014; Morén et al. 2012). Together, these caveolar proteins generate a unique lipid environment specific to caveolae, where cav1 and cavin1 individually sort distinct plasma membrane lipids.

2.3.2. Caveolae as mechanoprotectors

The PM of cells facing high and repeated mechanical stress is covered with caveolar structures. For instance, epithelial cells located at the internal layer of the gall bladder are submitted to mechanical contraction during the release of bile fluids into the intestine. The endothelial cells lining the inside of the blood vessels, are subjected to permanent shear stress induced by the blood flow. Intensification of shear stress at the endothelial cell surface *in vitro* promote caveolae invagination (Rizzo et al. 2003). Caveolae are also abundant in adipocytes submitted to swelling and in muscle cells which experience high stretching upon contraction. This suggests that caveolae may play a critical function in the mechanoprotection of these cells.

Caveolae flatten following mechanical stresses

The first idea of caveolae as mechanoprotectors come from Dulhunty and colleagues in 1975, who demonstrated that caveolae from frog skeletal muscle cells can flatten in and out upon cell stretching. Thereby, unfolding of caveolae increase PM area and prevent PM rupture (Dulhunty et Franzini-Armstrong 1975). Forty years later, Sinha, Koster and colleagues confirmed the role of caveolae as PM reservoirs. Indeed, following osmotic shock or unilateral stretching, caveolae disappear, consistently with their unfolding (**Fig. 24A, B**). Upon flattening, caveolae provide an excess of membrane to the cell surface, which buffer an increase in PM tension (**Fig. 24C**). Using tether pulling experiment on both cells and plasma membrane spheres, the group highlighted that this buffering phenomenon is an actin- and ATP-independent cell response to membrane tension variation induced by mechanical stress. They observed that this process is reversible as caveolae can reform in an actin- and ATP-dependent manner. The absence of a functional caveolae in *cav3* deficient muscles cells isolated from patients presenting muscle dystrophies enhanced membrane fragility under mechanical stress. In addition, flattening of caveolae following mechanical stress has been described in different cell types such as epithelial cells, lung endothelial cells and fibroblasts (Sinha and Koester et al. 2011) together with various endothelial cells (Lee et Schmid-Schönbein 1995).

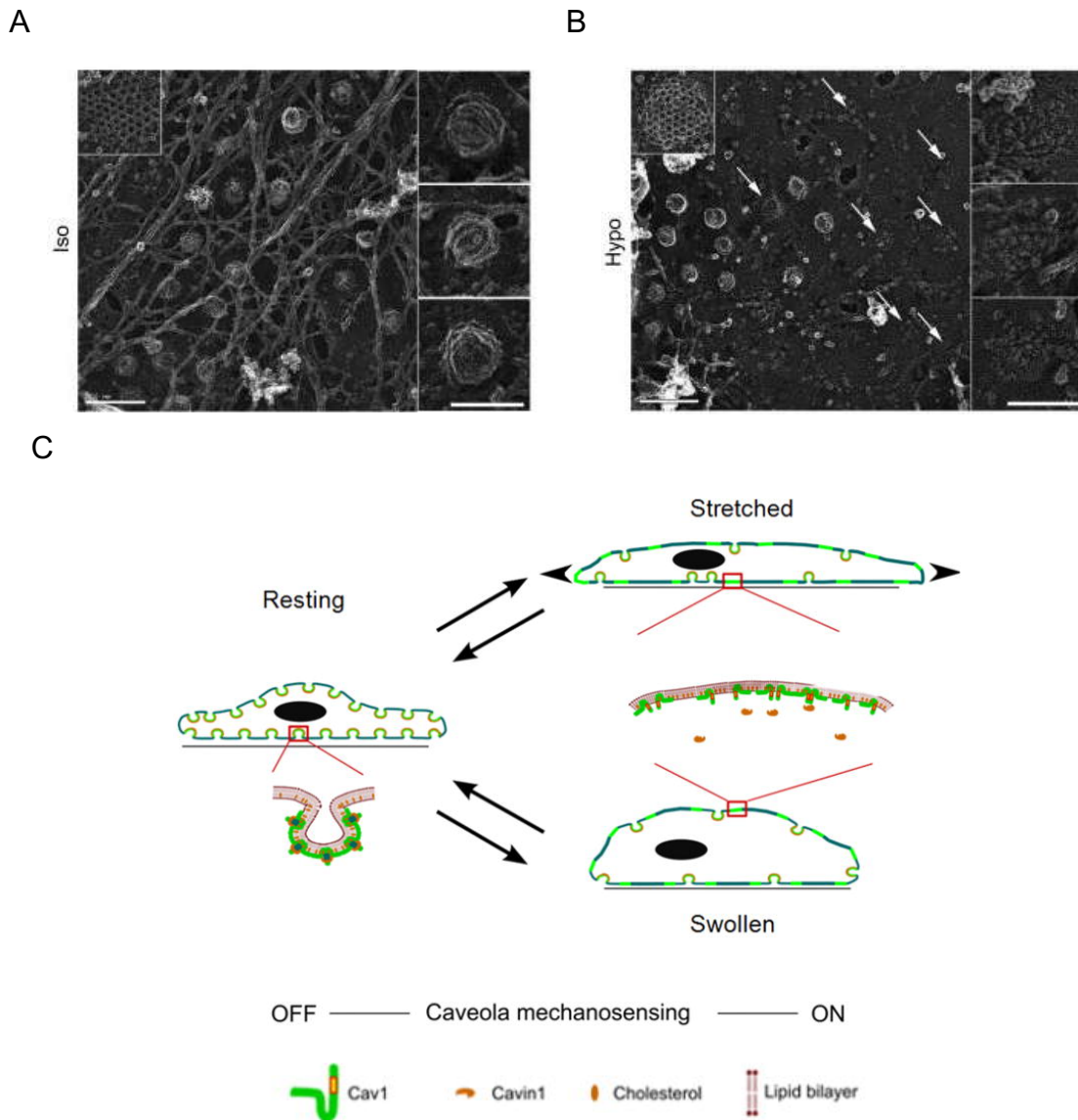


Figure 24. Caveolae flattening induced by osmotic shock.

Visualization of the caveolar coat at the ventral plasma membrane by transmission electron microscopy in (A) isotonic condition or (B) under hypotonic shock. Different types of caveolae structures are apparent, ranging from flat (A) to fully budded (B). (C) Schematic model of caveolae flattening following either cell stretching or osmotic shock (from (Sinha et al. 2011)).

Mechanical stress has also an impact on caveolar dynamics and signalling in myoblasts. Gervesio and colleagues observed cav1-positive caveolae-like structures that colocalize with highly packed glycosphingolipids GM1. Upon a brief cell stretching, GM1 packing dropped, reinforcing the idea of caveolae flattening in response to an increase of membrane tension. Interestingly, using repeated stretches, the authors observed an enhancement of caveolins and GM1 turnover together with a trafficking and remodeling of cav3-rich membrane domains. This indicates that cells likely adapt to mechanical stress via a reorganisation of caveolin-rich domains (Gervásio et al. 2011).

Caveolar structures disassemble upon mechanical stress

Caveolae and rosettes are abundantly found in cells submitted to chronic mechanical constraints. Muscle cells facing an increase of membrane tension show a disassembly of rosettes and caveolae structures at the sarcolemmal PM (Lo et al. 2015). The formation and stabilization of these caveolar structures depend on EHDs proteins. As a result, cells KO for EHDs submitted to prolonged cycles of stretching are more sensitive to PM rupture (Yeow et al. 2017). Similarly, deficiency in cavin1 impairs the sarcolemmal organization and leads to the formation of aberrant transverse tubules, which are extensions of the cell membrane that penetrate into the centre of skeletal and cardiac muscle cells. As a consequence, these cells are also highly sensitive to an increase of membrane tension. *In vivo* loss of cavin1/PTRF or mutation in cav3 induce sarcolemmal damages in response to a strong muscle activity (Lo et al. 2015) .

Flattening of caveolae drives their disassembly and therefore, the release of caveolar proteins are release into the cytosol, where they interact with and regulate intracellular proteins (**Fig. 25**) (Hayer et al. 2010) (Sinha et al. 2011) (Gambin et al. 2014). Indeed, mechanical stress reduces the interaction between the 2 major proteins cav1 and cavin1/PTRF. Consequently, cav1 increases as free molecule at the PM while cavin1/PTRF is found in the cytoplasm as caveolae disassemble (Sinha et al. 2011). Once in the cytoplasm, cavins interact with proteins involved in metabolism and stress signalling. Notably, cavin3 interacts with and inhibits the PP1 α phosphatase catalytic activity, which increases the phosphorylation level of histone H2AX, leading to apoptosis (McMahon et al. 2019).

Caveolae disassembly also releases accessory proteins such as EHD2, which is then SUMOylated to translocate to the nucleus (**Fig. 25**). From there, EHD2 regulates the expression of genes encoding caveolar components, involved in the cell cycle, in signalling pathways such as TNF- α , K-Ras, and receptors of the ECM. As an example, under mechanical stress, breast cancer cells deficient for EHD2 become unable to regulate the transcription of these target genes, as well as other genes involved in cell cycle. In addition, invaginated caveolae could not be observed at the ventral part of the PM when EDH2 was depleted (Torrino et al. 2018).

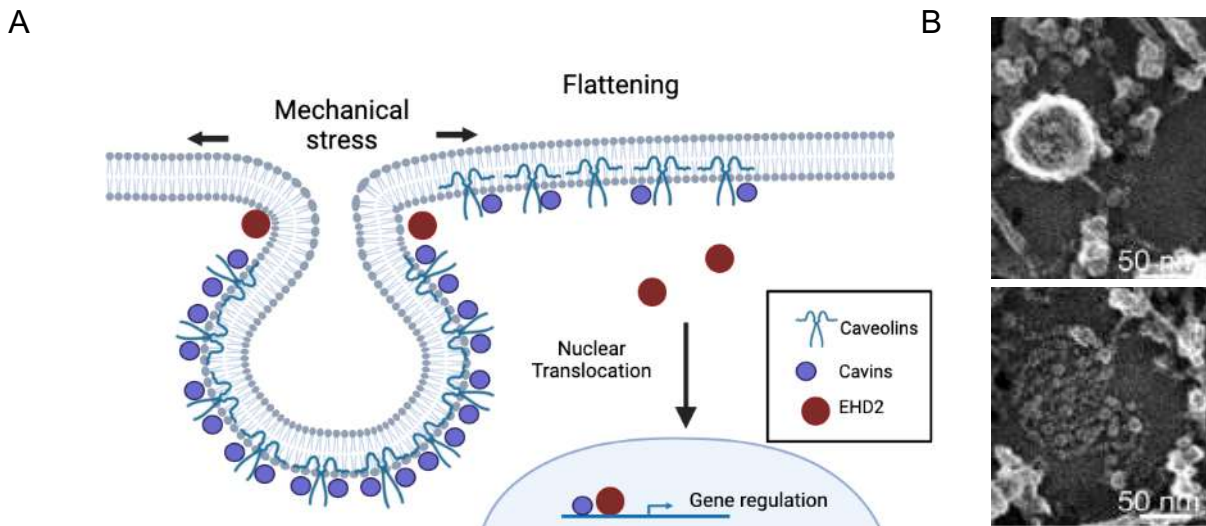


Figure 25. Schematic model of the flattening of the caveolae.

(A) It occurs during a mechanical stress on the membrane. The caveolae then flatten, releasing components such as EHD2 and cavins, which translocate to the nucleus where they regulate gene expression. (B) Visualization of invaginated or flat caveolae at the ventral plasma membrane by transmission electron microscopy. Scale bar 50 nm (from (Vassilopoulos 2020)).

In vivo, endothelial caveolae also play a key role in the protection of the PM against rupture upon shear stress induced by the blood flow. Artificial augmentation of the heart contractility and blood flow decrease the density of caveolae at the PM and increase the cytoplasmic pool of cavin1/PTRF. Therefore, high cardiac output drives caveolae disassembly. Consequently, mice lacking cav1 are more sensitive to an acute increase of cardiac output. Indeed, endothelial cells were ruptured and discontinuities in the endothelial layer was observed compared to wild type mice (Cheng et al. 2015).

Caveolae and cytoskeleton interactions

Importantly, caveolae can interact and regulate the actin cytoskeleton. Various studies suggest that this interaction enable the coupling and communication between these two mechanoactors, which is needed to maintain the integrity of the PM and to ensure a signalling response to mechanical stress. Observation of the alignment of caveolae structures on actin stress fibers have been made possible with the first immunostaining of cav1 and described for many cells type then (Rothberg et al. 1992). Interestingly, RhoA silencing reduces the alignment of cav1 given the absence of stress fibers (Muriel et al. 2011). Depolymerization of F-actin increases cav1 mobility reinforcing the idea that cav1 interacts with actin. This interaction may not be direct and a number of actin-binding proteins have been linked to caveolae. It has been proposed that filamin A, an actin cross linker, can regulate this interaction as it colocalizes with caveolae, cav1 and stress fibers (Stahlhut, Sandvig, et van Deurs 2000). Depletion of filamin A promotes caveolar dynamics and

impairs caveolae stability (Sverdlov et al. 2009) (Muriel et al. 2011). Similarly, cavin1/PTRF and EHD2 have been proposed to link caveolae to actin stress fibers (Morén et al. 2012) (Liu et Pilch 2008).

Upon cell migration, the leading edge protrudes, enhancing PM tension, while the rear edge retracts, resulting in lowering PM tension. When guided by ECM cues, cells control the retraction of the rear edge by PM tension sensing. The retraction process is controlled by caveolae that invaginate as a result of a PM tension reduction on a rigid substrate. Caveolae then recruit the GEF epithelial cell transforming 2 (Ect2) protein, which activates RhoA, thereby driving actomyosin polymerization to allow membrane retraction and cell migration (Hetmanski et al. 2019). Recently, Shi et al., proposed a model of negative feedback-driven regulation between actin and phosphorylated cav1 in migrating cells. Cytoplasmic cav1-positive vesicles show actin-associated motilities along actin filaments and bundles. Inhibition of contractile stress fibers diminishes the phosphorylation level of cav1, resulting in less motile larger vesicle. Impaired cav1 phosphorylation or KO CAV1 results in a reduced active level of RhoA-myosin II and increased active level of Rac1-PAK1-Cofilin leading to disordered contractile stress fibers compromising lamellipodia formation and cell migration (Shi et al. 2021).

In addition, inactivation of formin mDia1 and Abl kinases, triggers actin stress fibers disruption and cav1 clustering similarly to actin depolymerization, resulting in the formation of rosettes (Echarri et al. 2012). These structures have also been observed upon loss of cell adhesion, that induces a severe cytoskeleton remodeling. Reciprocally, an increase in stress fiber reduces the numbers of caveolar rosettes and induces caveolae flattening, which correlates with an augmentation of the membrane tension, suggesting a bidirectional interplay between caveolae and actin (Fujimoto s. d.; Mundy et al. 2002; Echarri et al. 2012).

Interestingly, cav1 regulates focal adhesion turnover and increases the stability of nascent adhesions at the cell edges. It has been proposed that this occurs following cav1 regulation of RhoA, which is involved in the maturation of nascent adhesions into focal adhesions (Grande-García et al. 2007) (Urra et al. 2012). Cav1 was also shown to be required for the force-induced cytoskeletal reorganization mediated by RhoA (Peng et al. 2007). For more information of caveolae and RhoA signalling regulation, please refer to “2.3.3.4 Caveolae and cell signalling”.

Together, these studies show an increase of caveolae flattening at the PM and subsequent disassembly, whereas a lowering of PM tension promotes caveolae formation.

This suggests that caveolae act as mechanoprotectors that protect the cells from PM rupturing following stretching.

2.3.3. Caveolae as endocytic carrier

The ability of caveolae to act as endocytic carriers has been extensively studied in recent years but is still a matter of debate. Caveolae can detach from the PM. Although some caveolae attempt to go back to the PM, others can fuse with early endosomes in a RAB5-dependent mode, before being recycled back to the PM. Moreover, a pool of caveolae budding from the PM can also fuse with structures called caveosomes and vice et versa. Caveosomes contain multiple caveolar domains and serve as an intermediate during internalization of the simian virus 40 (SV40) (Nichols 2002) (Pelkmans et al. 2004). However, the nature of these structures is still discussed as they could be late endosomes overexpressing cav1 (Hayer et al. 2010).

Although a majority of cav1 pool is very stable at the PM (Thomsen et al. 2002), a proportion is involved in a fast kiss-and-run process where transient fusion of the vesicle is observed (Pelkmans et Zerial 2005). The formation of rosettes appears before the trafficking of cav1 from the PM to the cytosol, suggesting that rosettes might be an intermediate stage of caveolae endocytosis (Echarri et al. 2012). Endocytosis of rosettes-like structures has been implicated in the removal of PM wounds, suggesting that rosettes could represent a way to endocytose relatively big areas of the PM in order to regulate its integrity (Corrotte et al. 2013).

Eventually, the budding of caveolae is mediated by dynamin 2, which inhibition leads to caveolae accumulation in epithelial cells (Henley et al. 1998). Dynamin2 also interacts with cav1 in endothelial cells (Yao et al. 2005). Conversely, EHD2 is a negative regulator of caveolar endocytosis as the budding of caveolae is increased upon EHD2 depletion (Pelkmans, Püntener, et Helenius 2002) (Morén et al. 2012) (Stoeber et al. 2012).

Caveolar endocytosis has been implicated in the uptake of cargos such as integrins and glycosphingolipids, as well as albumin and folic acid (Cheng et al. 2006) (Parton et Simons 2007). In epithelial cells, inhibition of dynamin II results in the accumulation of clathrin-coated pits and caveolae at the PM in good agreement with a recorded decrease of cholera toxin endocytosis (Henley et al. 1998). However, it should be noted that this toxin can still enter the cells by binding to the GM1 ganglioside (Kirkham et al. 2005). Although SV40 has long been thought to exploit caveolae to induce its internalization, it has been

shown that SV40 can also use a caveolae-independent mechanism to promote its endocytosis in cells lacking caveola (Pelkmans et al. 2001) (Damm et al. 2005).

Regardless of the cargo, caveolar endocytosis induces a reorganization of the actin cytoskeleton. This is mediated by dynamin, Src kinases and PKC (Mayor et Pagano 2007). Furthermore, it has been shown that activation of integrins inhibits caveolar internalization (Echarri, Muriel, et Del Pozo 2007).

Similarly, caveolae have been described in transcytosis of ligand from the bloodstream through the endothelium into lung tissue. Dynamic intravital fluorescence microscopy provided insight on the capacity of caveolae to act as pumps to mediate rapid transendothelial transport in the lung. Transport of cargos was impaired upon depletion of cav1. The kinetics of the transport were consistent with very rapid endocytosis via caveolae in endothelial cells (Oh et al. 2007).

2.3.4. Caveolae in cell signalling

Caveolae also act as signalling platforms, where many signalling proteins are enriched. As an example, calcium (Ca^{2+}) pumps are 25 times more numerous in caveolae nanodomains than at the PM (Fujimoto 1993). Disruption of caveolae triggers both Ca^{2+} releases and the subsequent activation of calcium/potassium currents, suggesting a role for caveolae in calcium signalling (Cheng et Jaggar 2006). In cardiac muscle, caveolar domains contain many calcium/calmodulin-dependent kinase II (CaMKII) targets and serves as a signalling platform. Here, caveolae, mainly *via* cav3, activate CaMKII signalling involved in cardiac hypertrophy (Tonegawa et al. 2017).

Phosphorylation of cav1 on its Tyr14 residue is involved in many signalling processes. Indeed, cav1, through its CSD, interacts with signalling proteins such as Src kinases (Li, Couet, et Lisanti 1996) although it was later suggested to be indirect. Indeed, free cytosolic cav1, phosphorylated at Tyr 14, may in fact interact with the Src inhibitory protein C-terminal Src Kinase CSK (Place et al. 2011). Cav1 CSD has also been suggested to interact with the inactive conformations of Src tyrosine kinases and of H-Ras (Li et al. 1996). In addition, cell detachment from the ECM triggers lipid rafts internalization in a cav1 phosphorylation-dependent manner (del Pozo et al. 2004) (del Pozo et al. 2005).

Few articles show that cav1 can interact with Rho GTPases, such as RhoC, which favors the development of metastasis by stimulating $\alpha 5$ -integrin expression and Src kinase-dependent activation of the p130Cas/Rac1, FAK/Pyk2, and Ras/Erk1/2 pathways (Arpaia et

al. 2012). Interestingly, one paper show that Rac1 physically associates with cav1 (Duncan et al. 2004). Similarly, phosphorylation of cav1 also activates Rho/ROCK signalling which then stabilizes the focal adhesion kinase (FAK) association with focal adhesions and promotes cell migration (Joshi et al. 2008). Indeed, cav1 activates RhoA in several cell types, supposedly through the negative regulation of the Src-p190RhoGAP pathway (Grande-García et al. 2007; Ogata et al. 2008; Goetz et al. 2011).

Interestingly, cav1 and RhoA physically interact into the same membrane nanodomains. Indeed, activation of RhoA upon stretching requires their proper localization within caveolae. Disruption of caveolae prevents RhoA activation and impairs stretch-induced actin cytoskeletal rearrangement suggesting that RhoA localization and activity could be regulated by cav1 (Kawamura, Miyamoto, et Brown 2003; Gingras et al. 1998).

Integrin-mediated cell adhesion is involved in many signalling pathways, including Erk, PI3k and Rac. These pathways play a role in cell growth, which is an anchorage-dependent process, as cells must first detach from the extracellular matrix to divide. Components of these pathways localize to lipid rafts and integrin-mediated adhesion regulates lipid rafts trafficking. Indeed, cell detachment triggers lipid rafts internalization and clearance from the PM. This internalization is mediated by cav1 phosphorylation on Tyr 14. A relocalization of phospho-cav1 from FA to caveolae induces lipid rafts internalization upon cell detachment, which mediates inhibition of Erk, PI 3-kinase and Rac (del Pozo et al. 2005).

Mitosis or cell detachment induce an internalization of caveolae. Filamin A, through its interaction with actin stress fibers, is required for the stabilization of cav1-positive vesicles to the PM. In addition, a cycling phosphorylation of FLNa is also required for cell-detachment-induced inward trafficking of caveolae. Thus, filamin A phosphorylation regulates inwards trafficking of a pool of the caveolae pool linked to actin filaments in an filamin A-dependent manner (Muriel et al. 2011). During the mammalian cell cycle, the density of the caveolae drops during metaphase and increases during cytokinesis to restore caveolar density to interphase levels. Depletion of cav1 increases membrane order and Rac1 targeting to the PM. Consequently, cells lacking cav1 progress through the cell cycle more rapidly (Cerezo et al. 2009 ; Boucrot et al. 2011).

Another example that has been extensively studied, is the association between cav1 and the endothelial nitric oxide synthase (eNOS). This will be detailed in the section “ 2.3.5. Caveolae and endothelium” of this thesis.

Taken together, these data show that caveolae and notably cav1, and their components are involved in various cell signalling pathways and therefore control different cellular processes. However, it is important to note that cav1 CSD forms an in-plane amphipathic helix buried within the membrane in mature caveolae. Thus, the role of this domain seems to be more compatible with a role for non-caveolar caveolin regulating signalling caveolae rather than mature caveolae (Hill et al. 2008).

2.4. PATHOLOGIES RELATED TO CAVEOLAE

Although caveolins KO mice are viable, the loss of caveolins has been related to a plethora of pathologies associated with adipose tissue, muscular tissue and endothelium. Mutations in caveolar genes are responsible for an arsenal of phenotypes both in humans and in animal models. Animal models were shown to develop glucose metabolism-related pathologies and lipodystrophies (Kim et al. 2008) (Cohen et al. 2004:20) (Briand et al. 2014). As an example, cav1-null mice are resistant to diet-induced obesity and show a decreased in (i) adiposity, (ii) levels of free cholesterol in adipocytes (iii) the formation of lipid droplets during liver regeneration (iv) survival after partial hepatectomy (Le Lay et al. 2006) (Park et al. 2002) (Fernández et al. 2006). Similarly, in both mouse model and human, deletion or mutation of cavin1/PTRF is associated with a loss of caveolae linked to lipodystrophies and muscle dystrophies (Liu et al. 2008) (Rajab et al. 2010) (Hayashi et al. 2009) (Ardissone et al. 2013).

Caveolins, mainly cav3 because of its specific localization in muscle cells, are also associated with muscle-related pathologies (Minetti et al. 2002; Pradhan et Prószyński 2020). More than 30 gene loci related to muscular dystrophies have been identified. Among them, cav3 heterozygous mutations, such as point mutations or small deletions, can be found in transmembrane and CSD domains leading to a dominant negative effect on cav3 cellular levels and formation of caveolae at the sarcolemma (Minetti et al. 2002; Pradhan et Prószyński 2020). Moreover, the absence of a functional caveola in myotubes from muscular dystrophic patients enhanced PM sensitivity to mechanical stress (Sinha et al. 2011).

Furthermore, *in vivo* experiment highlighted the role of cav1 in cell proliferation where it could act both as a tumor suppressor and promotor in various cancer and vascular abnormalities. In the next part we will focus on pathologies associated to the endothelium, mainly cause by cav1 mutation (Williams et Lisanti 2005) (Gupta, Toufaily, et Annabi 2014).

2.4.1. Cav1 and vascular pathologies

Cav1 KO mice present some vascular defects. Indeed, arterial vasodilation and vasorelaxation have been shown to be impaired seemingly due to an increase in the activity of eNOS, which is usually inhibited by cav1 (Razani et al. 2001). Conversely, cav1 inhibition of eNOS activity and subsequent drop in NO production can also induce vascular dysfunctions such as atherosclerosis (Kuhlencordt et al. 2001).

For more information of eNOS, refer to “2.3.5. Caveolae and endothelium”. Cav1 KO mice also present a decreased angiogenesis, induced by a deregulation of the VEGF (vascular endothelial growth factor) pathway, which is usually associated with cav1 (Frank et al. 2003). In lungs, depletion of cav1 induces the hyperproliferation of cells and triggers a thickening of alveolar septum responsible for lung defects (Razani et al. 2001). This also induces the initiation of pulmonary fibrosis (Drab 2001) and patients harboring CAV1 mutation also demonstrate pulmonary hypertension (Austin et al. 2012; Schrauwen et al. 2015; Han et al. 2016).

2.4.2. Caveolae and microbial pathogenesis

Caveolae have been extensively studied since their discovery 70 years ago. Many studies have shown that caveolae display various roles in microbial pathogenesis. They have been linked to parasite infection, as cholesterol-containing macrophage membrane domains, likely caveolae, colocalize with *Leishmania chagasi* and target parasites to a pathway that promotes delay of lysosome fusion and intracellular survival (Rodríguez, Gaur, et Wilson 2006). They also play a role in the regulation of *Typanosoma cruzi* infection (Adesse et al. 2010). However, it is still unclear if it is caveolae, caveolar proteins or caveole specific lipid composition that regulate pathogens infection, although it has been strongly suggested that cholesterol plays a central role in this regulation (Machado et al. 2012:20).

Viruses also exploit caveolae nano-domains to infect cells. The best example is the simian virus 40 (SV40) that recruits cav1, as discussed above, at its entry site, promoting its caveolae-dependent endocytosis. The virus is then transported to the ER through cav1-positive organelle called caveosome (Pelkmans 2001). Other viruses such as the human immunodeficiency virus (HIV) have been shown to influence cav1 regulation and cholesterol regulation. Cav1 inhibits the expression of HIV pro-viral DNA and restricts HIV infection through lysosomal degradation pathway (Mergia 2017).

Caveolae and their components are also involved in the uptake of several pathogenic bacteria. In 2004, Duncan et al described a role for lipid-rafts associated to caveolae in the entry *Escherichia coli* (*E. coli*). Indeed, caveolae formation imposes a specific lipid composition to the PM, thus inducing lipid-rafts like domains (Chapter 2.1.1.2). They demonstrate that in the mouse bladder, the *E. coli* type 1 fimbrial receptor, uroplakin Ia, localizes in lipid-rafts and associates with cav1. Consequently, intracellular *E. coli* associates with caveolae and lipid raft components. Disruption of lipid rafts by M β CD, or caveolae by small interfering RNA (siRNA) treatment, inhibits bacterial invasion. In addition, they observe that the small GTPase Rac1, required for *E. coli* invasion, physically associates with cav1 (Duncan et al. 2004). Of note, it should be taken into account that M β CD by depleting cholesterol from membrane affects both rafts and caveolae.

In epithelial and endothelial cells, cav1-positive PM invaginations have been detected in proximity to cell-associated *Streptococcus pyogenes*. Upon invasion, *S. pyogenes* is enclosed in caveosomes, thereby protected from fusion with lysosomes. The invasion process is dependent on the streptococcal invasin SfbI which activates the caveolae-mediated endocytic pathway, and it has been shown that the disruption of caveolae with M β CD abolished this process (Rohde et al. 2003). Similarly, in 2010, Hoffmann et al. described a crucial role for cav1 in negative regulation of membrane microdomain mobility, thereby affecting endocytosis of fibronectin-binding pathogens. Indeed, *S. aureus* attachment to β 1 integrins recruits cav1 and triggers the redistribution of caveolar specific detergent resistant domains components such as GM1 and GPI-linked proteins. Concomitantly, the disruption of membrane microdomains in cav1 deficient fibroblasts blocked *S. aureus* internalization (Hoffmann et al. 2010). In lung epithelial cells, *Pseudomonas* induces its internalization by a lipid-raft mediated endocytosis dependent on Src-phosphorylated cav2 but not cav1. In WT mice, intratracheal *Pseudomonas* infection triggers pneumonia leading to death whereas cav1-deficient mice are resistant to *Pseudomonas* (Zaas et al. 2009).

Recently, the dissemination of *Listeria monocytogenes* (*L. monocytogenes*) was associated to cav1. Depletion of cav1 impairs the formation of membrane protrusion formed during the cell-to-cell spreading of the bacteria. Isolated *L. monocytogenes* actin-based membrane protrusions trigger the recruitment of caveolar proteins in neighboring cells. The infectious model suggests that caveolae remain intact upon initial contact of *L. monocytogenes* with the recipient cell and next flatten during formation of actin-based protrusion format. Caveolae components, such as cavin2, EDH2 and cav1, remain within the inner leaflet of the PM, and filamentous actin surrounds the forming invagination,

whereas lipids such as PS, enriched in caveolae, diffuse across the forming protrusion (**Fig. 26**) (Dhanda et al. 2020).

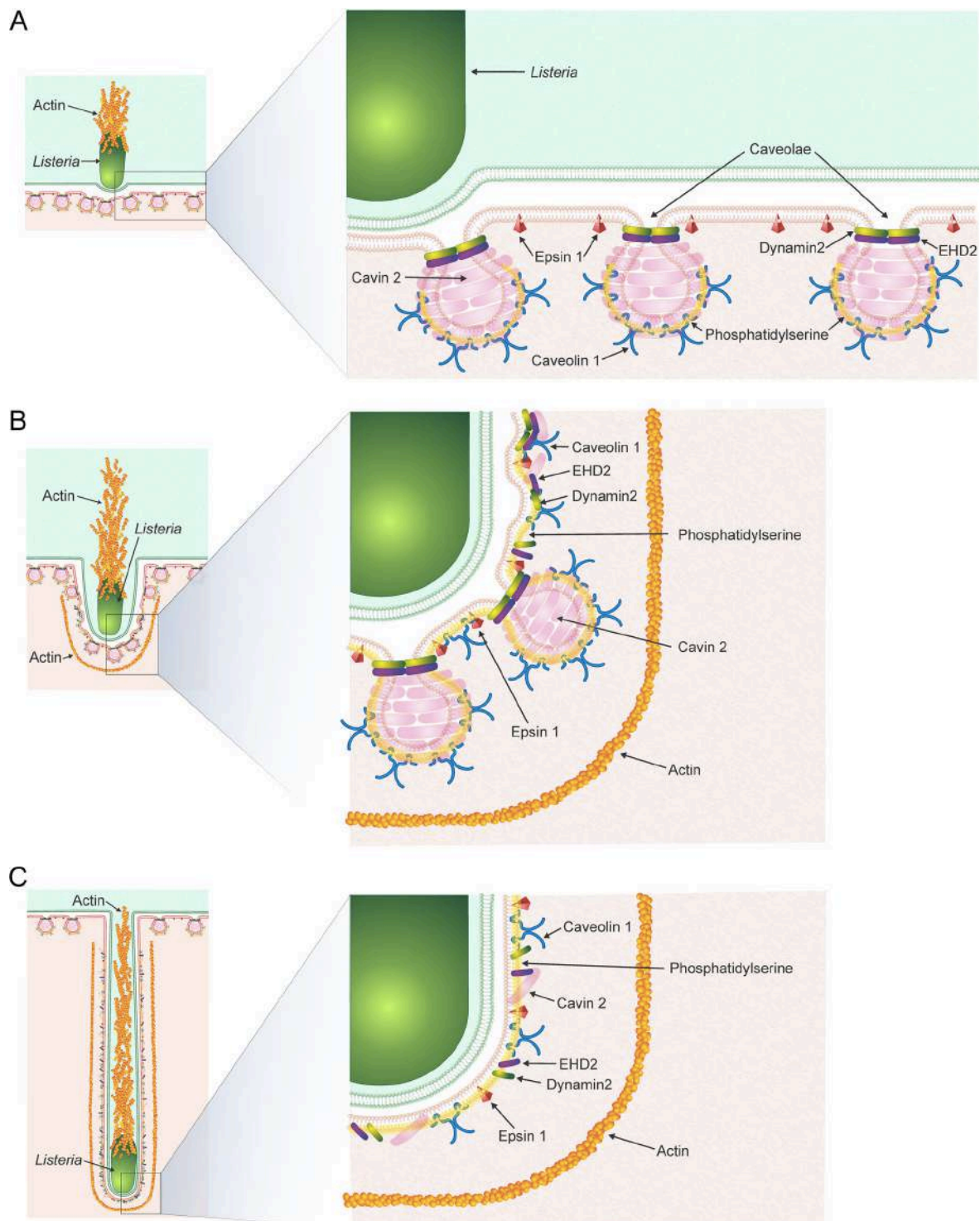


Figure 26. Proposed model for the caveolin-mediated uptake of *L. monocytogenes* membrane protrusions.

Scheme depicting (A) the Initial contact of *L. monocytogenes* with the neighboring cell. Caveolae and their protein components remain intact. Epsin-1 is positioned in the membrane, but not at caveolae. (B) Upon protrusion, caveolae begin to flatten along the entire length of the invagination. Their protein components remain within the inner leaflet of the invaginating cell plasma membrane, and filamentous actin surrounds the forming invagination. Phosphatidylserine that was initially at the caveolae now spreads across the forming protrusion. (C) Once invaginations fully elongate, caveolae flatten, but caveolar proteins and epsin1 remain associated with the invagination. Dynamin2 remains associated at regions surrounding the bacterium. Filamentous actin also elongates with the invagination.

2.5. CAVEOLAE AND ENDOTHELIUM

Endothelial caveolae display multiple functions, including the transport of ligands and solutes across the endothelial cell, during which caveolae act as transcytosis vesicles (Oh et al. 2007) (Predescu, Predescu, et Malik 2007) ; mechanotransduction (Albinsson et al. 2008) (Joshi et al. 2012); and diverse signalling processes that have been detailed previously in this thesis (Parton et Simons 2007) (Collins et al. 2012).

Another interesting aspect of endothelial caveolae is their possible involvement in transcellular migration of lymphocytes across the endothelium. Indeed, it was proposed that, after clustering, intercellular adhesion molecule-1 (ICAM-1) translocates to caveola- and F-actin-rich domains. From there, ICAM1 is internalized and transcytosed from apical to basal PM of the endothelial cells, which facilitates lymphocyte transmigration. In addition, CAV1 downregulation partially inhibits lymphocyte transmigration (Millán et al. 2006).

The control of the endothelial nitric oxide synthase has also been associated with caveolae (García-Cardena et al. 1997) (Siddiqui et al. 2011). Indeed, cav1 regulates the eNOS, which is responsible for the regulation of NO secreted by cells submitted to shear stress, in the vascular endothelium. In sinusoidal endothelial cells, the NO release is enhanced when cells are exposed to increase blood flow (Shah et al. 2014). The eNOS can be found in PM caveolar nanodomains as well as in the cytoplasm. It has been shown that eNOS is enzymatically active in caveolae whereas its interaction with cav1 provokes its inhibition. Under shear stress, eNOS interaction with cav1 is abolished, but eNOS remains concentrated into caveolae. This results in eNOS activation (Rizzo et al. 1998:199) (Rizzo et al. 2003). eNOS is targeted to caveolae by palmitoylation and is negatively regulated by its association with caveolin. Cav1 interacts with eNOS through its CSD. *In vivo*, this interaction is sufficient to inhibit eNOS enzymatic activity (Bernatchez et al. 2005) (Bucci et al. 2000) (Garcia-Cardena et al. 1996:199) (Sowa, Pypaert, et Sessa 2001).

Interestingly, both lymphocyte transmigration and sinusoidal endothelium share a spectacular structural feature, which is the formation of tunnel-like structures that will be reviewed in the next chapter.

3. TRANSCELLULAR TUNNELS AND THE ENDOTHELIUM

The lumen of the circulatory system is lined with endothelial cells that form a semi permeable barrier between the blood and organs and to foster exchanges. This involves a control of cell-to-cell junction integrity. In addition, it is formed with various discontinuities, including vesiculo-vacuolar organelles (formed by the coalescence of caveolin1-containing vesicles and vacuoles), transendothelial pores, tunnels and channels, fenestrae and large gaps, which differ in tissue location and composition. These tunnel-like structures have been described in the endothelium of various organs with a function that largely remains to be defined.

Defining cellular components controlling the width of this transcellular structures will allow better defining their function in physiology and physiopathology.

3.1. IN PHYSIOLOGY

An example of transient formation of transendothelial tunnel is described during transmigration of leucocytes through vasculature (Schimmel, Heemskerk, et van Buul 2016) (Nourshargh, Hordijk, et Sixt 2010). Although it has been controversial for a long time, the first evidence of transcytosis of leucocytes in endothelial cells has been demonstrated *in vivo* (Marchesi et Gowans 1964) and confirmed for monocytes, neutrophils, lymphocytes *in vitro* by Carman and Springer in 2004, using high resolution confocal imaging (Carman et Springer 2004). This high-resolution microscopy approach allowed the authors to define that the transcytosis occurred without disrupting the cell-cell junctions (**Fig. 27**).

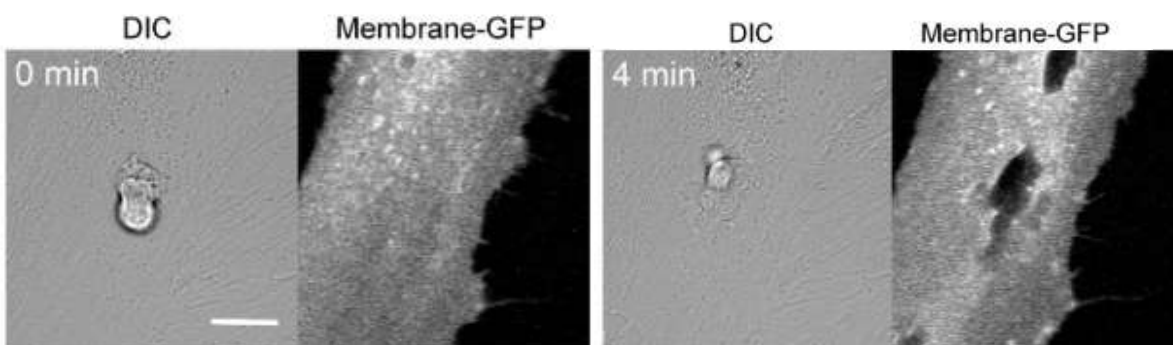


Figure 27. Formation of transcellular tunnels in endothelial cells during transcytosis. DIC images show a lymphocyte undergoing transcellular transmigration through an ENDOTHELIAL CELLS. Expressing membrane-tagged GFP in endothelial cells allow to visualize the transendothelial tunnel. Scale bar, 10 μ m (from (Mooren et al. 2014)).

After rolling and adhesion, leucocytes crawl along the endothelial cell surface and trigger their extravasation (Schwartz et al. 2021). Transcellular diapedesis of leucocytes

occurs through a so called “path of least resistance” in which leucocytes must identify extravasation sites on endothelial cells (Martinelli et al. 2014). This involves a crosstalk between integrins from leukocytes and their receptor ICAM-1, whose expression is up-regulated at the surface of endothelial cells in inflamed tissues. Leucocytes develop ventral protrusions, called podosomes, which scan the surface of endothelial cells seeking for permissive site with the lowest mechanical resistance. This process triggers the formation of invaginations, called podoprints, at the endothelial cell surface, which are believed to assist the leukocyte transmigration. Next, podosomes switch to an invasive state. They extend to the basal membrane of endothelial cells thereby promoting the formation of a transendothelial pore (**Fig. 28**) (Martinelli et al. 2014).

Mechanical and microscopy analyses have a softer region at the level of the transmigratory cup, caused by the disappearance of actin fibers underlying the invading site (Isaac et al. 2016; Riethmuller, Nasdala, et Vestweber 2008). From the endothelial side, podoprints are enriched in vesiculo-vacuolar organelles, in caveolae and in fusogenic proteins, such as SNAREs and VAMPs. These vesicles are involved in decreasing the local surface tension thanks to the supply of additional PM at the site of leukocyte diapedesis and associated formation of the transcellular pore. After binding to integrins, ICAM-1 is internalized in regions rich in caveolae and actin-rich membrane projections. When the leucocytes protrude inside the endothelial cells, ICAM-1 is translocated via caveolae towards the area of the transmigratory pore (Millán et al. 2006) (Carman et al. 2007).

The integrity of the endothelium barrier is maintained during leukocyte diapedesis thanks to the formation of an actin-myosin ring in endothelial cells, that is tightly adjusted to the size of leukocytes. This ring stabilizes the pore during the passage of leucocytes preventing from plasma leakage and associated formation of edema. Thus, the control of the size of transcellular tunnel is essential to prevent induction of pathophysiological manifestations. Formation of the actomyosin ring also involves the GEFs proteins Ect2 and LARG, that are recruited to ICAM-1 receptor for RhoA activation. This signalling axis controls the width of the ring. Indeed, RhoA phosphorylates the MLC in the actomyosin ring, driving its contraction around the pore, to avoid the plasma leakage upon leucocyte exit (Mooren et al. 2014) (Heemskerk et al. 2016).

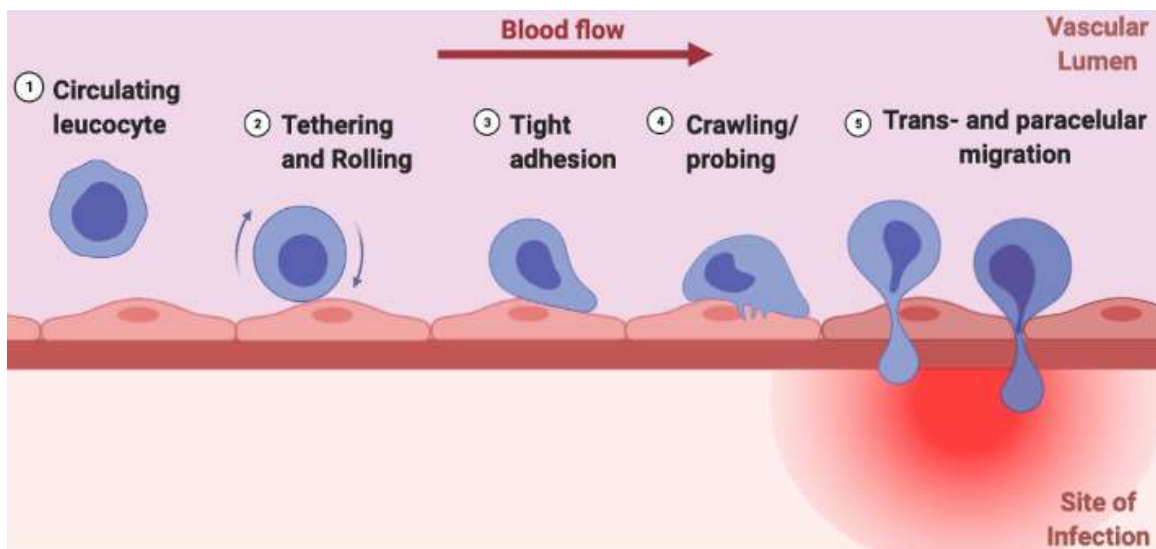


Figure 28. Diapedesis process of leucocytes.

A range of cell adhesion receptors on endothelial cells mediates the capture of a circulating leucocyte. Next, the leucocyte rolls, adheres and probes on the luminal endothelial cell surface. Eventually, leucocyte diapedesis occurs by transcellular or paracellular migration through the endothelium (adapted from (Schwartz et al. 2021)).

The last step of the transcellular route involves pore resealing, thought to prevent edema. This involves a burst of actin polymerization at the ventral side of lamellipodia of endothelial cells (**Fig. 29**). The formation of these actin-rich protrusions depends on the interaction between endothelial cells integrins and the extracellular matrix. This has been unveiled by an approach using fusion-blocking antibodies directed towards integrins with a blockage of pore closure. Ventral lamellipodia mainly emerge from a preexisting actin filament within 5 μm of the pore or gap. From this formation site, they move to reach the nearest edge of the pore (**Fig. 29**). Next, they move to the distal edge of the pore to complete the closure. In few cases, the ventral lamellipodia is initiated precisely at the first edge of the pore and moves to the opposite border, where it disappeared. It has been shown that the small Rho GTPase Rac1 and its effector WAVE and Arp2/3 control ventral lamellipodia formation, *via* induction of branched actin polymerization through the activity of the Arp2/3 complex. The pore forms subcellular regions of retraction where the tension is weaker (Martinelli et al. 2013). This favors ventral lamellipodia formation. In this model, the ventral lamellipodia extend towards areas of low tension whereas high tension zone is not permissive for the ventral lamellipodia propagation (**Fig. 29**).

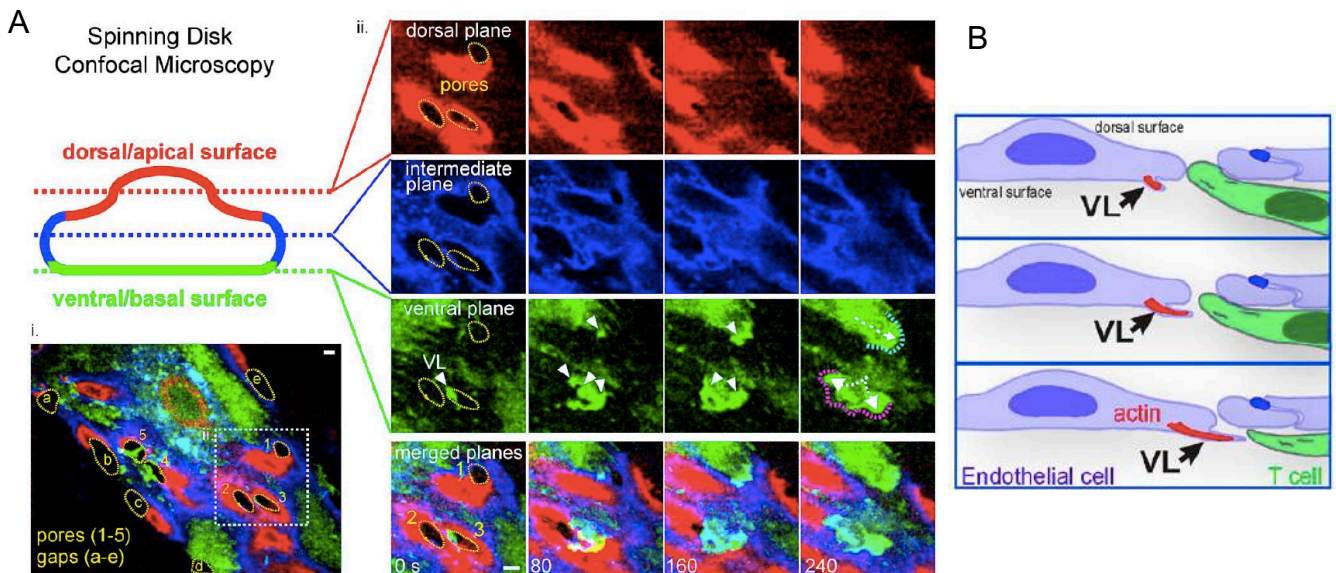


Figure 29. Transcellular pore closure is initiated by novel ventral lamellipodia

(A) Combined epifluorescence of the dorsal plane (red) and TIRF of the ventral plane (green) imaging of diapedesis pore (yellow line) being closed by a ventral lamellipodium (white arrowhead) in a MVEC expressing mDsRed. (i) Dynamic serial-section spinning disk confocal imaging of a mYFP-expressing endothelial cell during T cell diapedesis. Sections of dorsal/apical (red), intermediate (blue), and ventral/basal (green) planes were differentially pseudo-colored and overlaid. Dashed yellow lines indicate transcellular pores (1–5) and paracellular gaps (a–e) where individual T cells are transmigrating. (ii) Expanded view of the boxed region in panel i shows ventral lamellipodium (white arrowhead) formed in the ventral plane spreading under three pores (1,2,3). (B) Schematic model of ventral lamellipodia (red) pore closure during late stages of T cell (green) diapedesis across the endothelium (blue) (Martinelli et al., 2013).

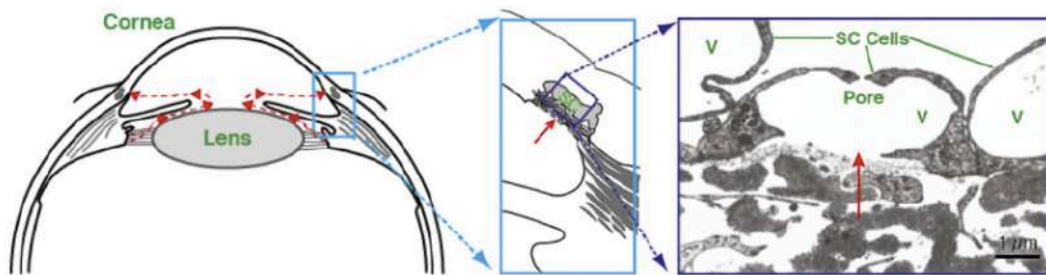
It exists various endothelial cell adhesion receptors involved in the diapedesis process. E- and P-selectins, together with I-CAM and V-CAM are involved in rolling and adhesion respectively. Interestingly, the vascular endothelial cadherin (VE-cadherin) is exclusively involved in the paracellular route, functioning as a barrier to transmigration. The only candidate for a cell surface protein that might be exclusively involved in transcellular diapedesis is plasmalemma vesicle protein 1 (PV1), which is an essential component of fenestral and stomatal diaphragms (for information, see the next paragraph in this chapter).

The treatment of endothelial cells with agents that reduce endothelia barrier function shifts the main route of transmigration from trans- to paracellular (Martinelli et al. 2014). Instead, treating heart endothelial cells with agents that enhance the barrier function, induce a significant reduction of paracellular route and increase of transcellular route. Moreover, *in vitro* exposure of endothelial cells to shear stress enriched cortical actin and reduce stress fibers, leading to an augmentation of transcellular migration. After the transmigration phase, the leucocytes pass the pericyte layer through gap and breach the basal membrane of endothelial cells in an enzymatic way and migrate towards the inflammation site by chemotaxis.

Another example of transendothelial pore can be found in the eye. Aqueous humor is drained through the trabecular meshwork into the juxtacanalicular connective tissue surrounding Schlemm's canal (SC), and ultimately into the aqueous veins. Because of their location, endothelial cells in the SC are chronically subjected to aqueous humor flow from the juxtacanalicular connective tissue (Mäepea et Bill 1992) (Johnson 2006).

Micro-sized pores have been observed in the endothelial cells lining SC, although they are nonuniformly distributed along the inner wall of the endothelium (**Fig. 30**) (Allingham et al. 1992). Proper formation of these transendothelial pores is essential to allow aqueous humor outflow. Dysfunction of these tunnel-like structures affects outflow resistance and increases intraocular pressure, thus causing glaucoma (Johnson et al. 2002). Transendothelial pores formed within the cell can be distinguished from paracellular pores formed between cells (Allingham et al. 1992) (Ethier et al. 1998).

A



B

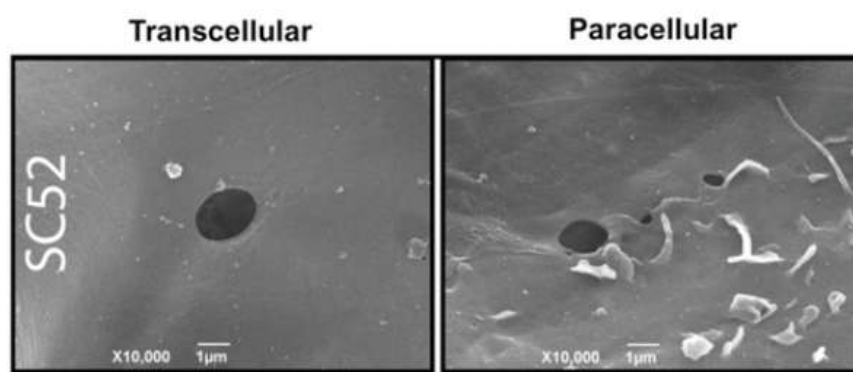


Figure 30. Schlemm's canal endothelium present pores.

(A) In the eye, the Schlemm's canal allow the evacuation of aqueous humor. Pore are located in the endothelial cells lining the Schlemm's canal. (B) Two types of pores can be observe in this endothelium: a transcellular pore inside the cells whereas paracellular pores are found between cells (from (Overby et al. 2014)).

Transendothelial pores formation process is still unclear, but it has been proposed that they form on the abluminal cell surface and develop into giant vacuoles, allowing them

to contact the luminal surface of the cells to discharge their content into the canal (Ethier et al. 1998). Braakman et al. described a mechanosensitive process of transendothelial pores formation. They show an increase of transendothelial pores, without affecting their diameter, in endothelial cells submitted to biaxial stretching (Braakman et al. 2014). Using correlative microscopy on enucleated human eyes, they visualized the outflow through the juxtacanalicular connective tissue.

They have shown that regions where the flow is strong, colocalize with regions of high pore density, suggesting that aqueous humor actually passes through pores in the inner wall endothelium of SC-bearing endothelium (Braakman et al. 2015).

In addition, SC cells are subject to large mechanical deformations as the intraocular pressure changes, but little is known about their mechanical properties (Ethier 2002). Using magnetic cytometry and tensile forces applied by beads adherents to SC cells, Zeng et al. estimated the elastic modulus of SC cells (between 1 and 3 Pa) and highlighted that it increases when the intraocular pressure is elevated (Zeng et al. 2010). Indeed, glaucomatous SC cells show a higher subcortical cytoskeleton stiffness than healthy cells which responsible for the increase in elastic modulus. This correlates with a decrease in the proportion of transendothelial pores in glaucomatous SC cells. In addition, it has been shown that the expression of glaucoma-related genes is dependent on ECM stiffness and is exaggerated in glaucomatous cells (Overby et al. 2014).

Finally, fenestrae structures have also been described in the endothelium of other tissues (**Fig. 31**). Two types of endothelium can be distinguished. The first, called fenestrae endothelium, is mainly found in the kidneys and digestive mucosa, whereas sinusoidal endothelium is found in the liver.

The fenestrae endothelium consists of a few caveolae, referred to here as plasmalemmal vesicles, and a transendothelial channel consisting of a stomatal diaphragm connected to the continuous endothelium (Bearer et Orci 1985). These diaphragms have been shown to share a vesicular protein, PV1, encoded by the plasmalemmal vesicle associated protein (PVLAP) gene, which is the major component essential for diaphragm formation (Stan, Kubitz, et Palade 1999). PVLAP KO mice, when viable, do not have diaphragms in caveolae or transendothelial ducts, and have a low number of endothelial fenestrae (Herrnberger et al. 2012). In addition, endothelial fenestrae consist of vesiculo-vacuolar organelles, that consist in assemblies of interconnected vesicles connecting the two sides of the cell. Thus, all these tunnel-like vesicular structures promote the transport of solutes and molecules across the endothelium (Feng et al. 1999).

Sinusoidal endothelium is a unique capillary structure. Indeed, it is a discontinuous tissue with very few caveolae and with large fenestrae of 100 to 150nm in diameter, which are not associated with a diaphragm and a basal lamina (Simionescu, Simionescu, et Palade 1974) (Milici, Peters, et Palade 1986). Fenestrae were first discovered by scanning electron microscopy in 1970 in liver endothelium, where they occupy up to 8% of the endothelial surface (**Fig. 31**) (Wisse 1970) (Wisse et al. 2008).

This structure acts as a filter for fluids, solutes, and particles that are exchanged between the sinusoidal lumen and the space of Disse (Wisse et al. 2008). In addition, they regulate the passage of vectors of gene transfer, such as adenoviruses, in a pore size-dependent manner (Wisse et al. 2008).

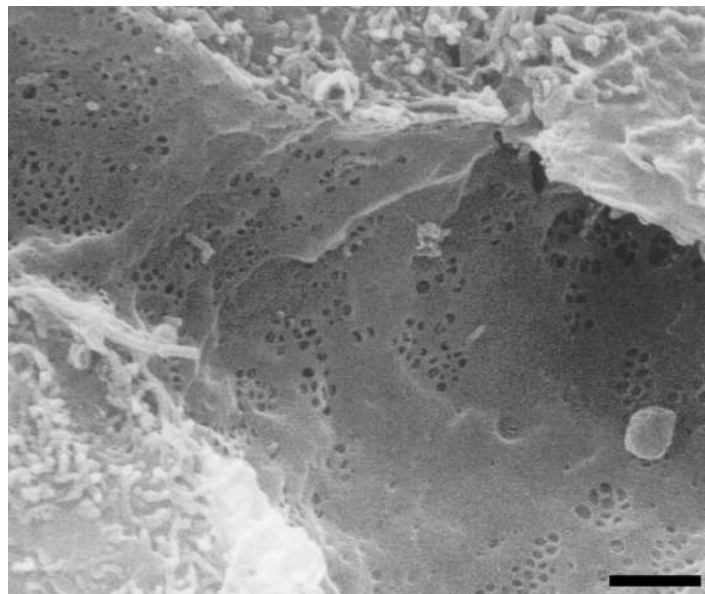


Figure 31. Fenestrae of rat liver sinusoidal endothelium.

Low magnification scanning electron micrograph showing the fenestrated wall. Scale bar, 1 μ m from ((Wisse et al. 2008)).

Fenestrae are dynamic structures, varying in diameter and number in response to multiple molecules and cues. Indeed, during cirrhosis, ethanol, as well as other hepatotoxins, have been shown to increase defenestration (Fraser, Dobbs, et Rogers 1995) (Wang et al. 2005). Formation of these tunnel-like structures they have been related to actin cytoskeleton as treatment with cytochalasin B increase fenestrae number and the percentage of the cellular surface opened by the fenestrae up to 300% compared control cells, without affecting fenestrae diameter (Steffan, Gendrault, et Kirn 1987). Similarly, it has been shown that RhoA modulate the formation of fenestrae via its role on cytoskeleton regulation. Indeed, cell treatment with a Rho stimulator lysophosphatidic acid increases actin stress fibers and phosphorylation of MLCK, leading to a contraction of the fenestrae.

Conversely, ExoC3 treatment induce a loss of stress fibers thereby triggering the dilatation and fusion of fenestrae (Yokomori et al. 2004). Using 4D-AFM and super-resolution fluorescence nanoscopy, it has been shown that spectrin, and actin lines the inner cell membrane of liver cells, therefore providing a structural support to the fenestrae. In addition, they highlighted that this actin-spectrin scaffold can be perturbed by iodoacetic acid (IAA), known to interrupt F-actin polymerization, that decrease fenestrae number. (Zapotoczny et al. 2019).

Interestingly, these structures are sensitive to the mechanical cues applied to the endothelium, such as shear stress induced by the blood flow, mechanical stretching and variation of ECM stiffness. Indeed, application of high or very low shear stress enlarge the fenestrae and induce a rapid loss of liver-specific function (Torii, Miyazawa, et Koyama 2005). In addition, when cultured on 6 kPa gels for 24 hours, cells exhibit well-defined fenestrae. In contrast, cells plated on 36 kPa gels lose fenestrae structures. Similarly, fenestrae diameter is also affected by stiffness variations (Ford, Jain, et Rajagopalan 2015). Altogether these astonishing pore-like structures are a hallmark of a high permeability tightly regulated. Much remains to be learned on their dynamics and how to manipulate them to control pathophysiological manifestations.

3.2. IN PATHOLOGIES

A common feature of pathogen infections is their ability to cross the host's natural barriers. To successfully invade their hosts, bacteria deploy an arsenal of virulence factors to colonize, multiply and disseminate across the host body. As an example, several bacterial pathogens can compromise the endothelial barrier function *via* the production of toxins, accessing the bloodstream and consequently the deep tissues and organs. *Pseudomonas aeruginosa* is a common colonizer of environment often associated to nosocomial infections. *P. aeruginosa* has the ability to produced various toxins disrupting the endothelium integrity. ExoS and ExoT toxins trigger an increase of RhoA/ α v β 5 integrin signalling while inhibiting Rac1 activity. Consequently, cell retraction increases by the means of actin cytoskeleton contractility, leading to pulmonary endothelial permeability (Ganter et al. 2008). In addition, Huber et al. show that sequential inactivation of RhoGTPases lead to dephosphorylation of Lim kinase, inducing actin filament severing activity of the cofilin. As a result, a dramatic retraction of endothelial cell occurs, eventually leading to a rupture of the endothelial monolayer (Huber et al. 2014).

Recently, the laboratory of Emmanuel Lemichez has identified a new process of endothelium breaching shared by several bacteria that are able to trigger the opening of transendothelial macroaperture (TEM) tunnels in cells up to 20 μm wide (**Fig. 29**) (Boyer et al. 2006). The formation of TEMs will be detailed in this chapter.

3.2.1. Transendothelial macroapertures tunnels induction

Over the past few years, Emmanuel Lemichez's lab has demonstrated that TEMs can be triggered by various bacteria through the production of toxins *Staphylococcus aureus*, *Clostridium botulinum* and *Bacillus anthracis*, through the secretion of epidermal differentiation inhibitor factor (EDIN), the ExoC3 and the oedematogenic toxin (ET), respectively (**Fig. 32**) (Boyer et al. 2006) Maddugoda et al., 2011).

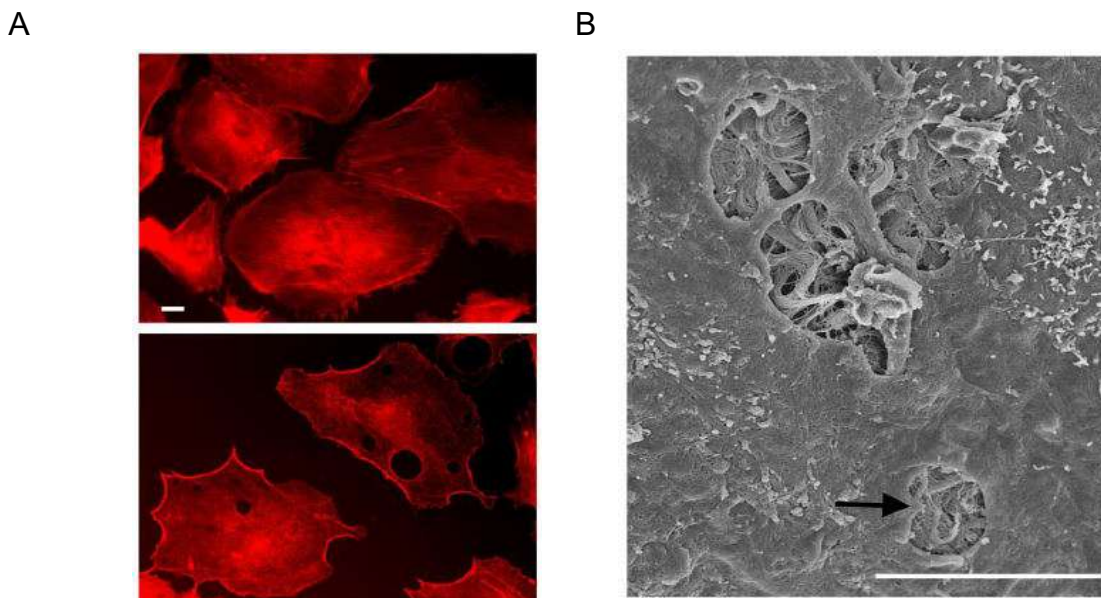


Figure 32. Formation of transendothelial macroapertures.

(A) Naïve HUVECs show strong actin cytoskeleton labelling whereas EDIN intoxicated HUVECs (bottom) showed the disruption of the actin stress fibers and TEMs formation. (B) Electron micrograph showing fibrous structures of the matrix underneath the endothelial cells after TEMs opening. Scale bars, 10 μm (from(Boyer et al. 2006)).

Bacillus anthracis is a well-known Gram-positive rod-shaped bacterium responsible for the anthrax disease, that has been extensively studied because of its bioterrorism potential. *B. anthracis* produces a three component AB-like toxin where we distinguish the lethal toxin (LT) and the ET. They are composed of the protective antigen that recognizes and interacts with the host cell receptor, and the lethal factor (LF) or the edema factor (EF), respectively (Collier et Young 2003) (Moayeri et Leppla 2004). LF disrupts MAPK Kinase

signalling (Duesbery et al. 1998) (Vitale, Bernardi, et Napolitani 2000) whereas EF is a calcium- and calmodulin-dependent adenylate cyclase, which catalyzes the production of cAMP (Tang et Guo 2009) (Dal Molin et al. 2006) (Leppla 1982). Increase of cAMP leads to the activation of the protein Kinase A (PKA) involved in a wide range of cellular processes. Many cytoskeleton regulators require PKA activity such as the activation of Rac/Cdc42 while others are inhibited including Rho GTPases and actin polymerization (Howe 2004). Indeed, PKA can phosphorylate RhoA at Ser188 increasing its interaction with RhoGDI in the cytoplasm (Lang et al. 1996). This has not been observed in human umbilical vein endothelial cells (HUVEC) (Maddugoda et al., 2011). Instead HUVECs, cAMP inhibits actomyosin contraction via the dephosphorylation of MLC. The cAMP can signal through the activation of the exchange protein directly activated by cAMP (Epac), a guanine nucleotide exchange factor (GEF) of the Ras GTPase Rap1 and Rap2 (de Rooij et al. 1998). Ras proximate (Rap) is converted from its inactive GDP- to its active GTP-bound form by this GEF. Further Rap activation has been implicated in RhoA inactivation (Krugmann et al. 2004).

In HUVECs, it has been demonstrated that ET from *B. anthracis* is able to activate Epac via increasing cAMP, that subsequently leads to the disassembly of stress fibers and the opening of a few TEMs of small size (Maddugoda et al. 2011). *In vivo*, intravascular injection of ET rapidly triggers prominent edema along the gastro-intestinal tract, hypotension, and organ failure (Firoved et al. 2007; Maddugoda et al. 2011). The reduction of actomyosin contractility by cAMP-induced PKA and EPAC/RAP pathways provokes dysfunction of the endothelial barrier that lines vessels leading to gelatinous edema and bacterial dissemination (Maddugoda et al. 2011).

S. aureus is a skin and mucosa colonizer of 30 to 50% of the human population. It is a Gram-positive bacterium regularly associated with nosocomial infections. Its multiresistance to antibiotics makes it a public health issue. It is also the most frequently isolated pathogen in diabetes foot infection commonly leading to lower-limb amputation (Boulton et al. 2005; Edwards et al. 2010). *S. aureus* is able to secrete various membrane damaging toxins, the best known being the alpha-toxin, a beta-barrel forming toxin responsible for leucocytes lysis (Valeva et al. 1997).

In addition, a few strains of *S. aureus* are also able to secrete a toxin belonging to the C3 exoenzyme family called EDIN (Aktories, Wilde, et Vogelsgesang 2005). The C3 exoenzyme family comprises seven exoenzymes with toxic activity that are produced by *S. aureus*, *C. botulinum*, *C. linosum*, and *Bacillus cereus*. One distinguishes three isoforms of

EDIN exoenzymes. EDIN-A and EDIN-C are encoded by a gene-borne plasmid, while EDIN-B is chromosomally encoded (Wild et al. 2004). In 2010, Munro et al. demonstrated in a model of metastatic infection using a bioluminescent clinically-derived strain of *S. aureus* that EDIN increases the number of disseminated infectious foci. They also showed that catalytically active form of the EDIN specifically promotes the dissemination of the bacterium from the bloodstream to tissues (Munro et al. 2010). Moreover, in 2015, Courjon et al. highlighted an increase capability of EDIN B-positive *S. aureus* to translocate from lung tissue to the bloodstream in a model of pneumonia. In this infectious model, the deletion of *edinB*, dramatically reduced the frequency and magnitude of mice displaying bacteremia without affecting the bacterial virulence in the blood stream and in lung tissues (Courjon et al. 2015). Furthermore, analysis of *S. aureus* strains retrieved from diabetes foot infections, indicated that edin-positive strains might be more associated with moderate-to-severe infections rather than low-grade infections (Messad et al. 2013:201). These *in vivo* and clinical studies support the idea that EDIN promotes the crossing of endothelia by *S. aureus* in support of the observation that EDIN triggers the formation of large transcellular tunnels in endothelial cells. In 2006, Boyer et al. highlighted the formation of large transendothelial tunnels induced by both recombinantly purified EDIN and EDIN-producing *S. aureus*. These openings were observed by scanning electron microscopy both *in vitro* in HUVEC monolayers and *ex vivo* in arterial endothelium (Boyer et al. 2006). These transcellular tunnels open transiently. Closure occurs thanks to the formation of F-actin rich membrane waves that expand over the tunnel up to their resealing. EDIN-induced TEMs are formed due to the mono-ADP-ribosylation of the GTPases RhoA on Asn 41, as well as RhoB and C to a lesser extent (Wild et al. 2004). The mono-ADP-ribosylation of Asn 41 of RhoA leads to its tight association with RhoGDI and relocation in the cytosol (Aktories et al. 2005). Inactivation of RhoA by mono-ADP-ribosylation provokes a disruption of actin stress fibers and consequently a loss of the endothelial barrier function via formation of these large transcellular tunnels (**Fig. 33**) (Chardin et al. 1989) (Aktories et al. 2005), providing to *S. aureus* a direct access to the endothelium basement membrane. Further in support of the importance of inhibition of RhoA for TEM formation, treatment of cells with the RhoA kinase (ROCK) inhibitor Y27632 also induces TEMs (Boyer et al. 2006).

Several strains of *C. botulinum* produce a EDIN-like exoenzyme (ExoC3), which also catalyzes the mono-ADP-ribosylation RhoA and opening of TEMs (**Fig. 33**). The next chapter will detail the processes of TEM formation. Incubation with high concentration of C3 (μM) for long period of time (24 hours) is required to induced morphological changes. The ExoC3 lacks known ligand recognition domain/motifs, thus little is known about how it enters

cells except it is through a clathrin-, actin-, cholesterol-independent but dynamin dependent pathway (Rohrbeck et Just 2017).

3.2.1.1. Transendothelial cell tunnels macroapertures opening

As discussed above, the formation of TEMs occurs as a consequence of a global relaxation of actomyosin cytoskeleton triggered either by an increase of cAMP or by inhibition of RhoA. Disruption of cytoskeleton cohesion upon RhoA inhibition release centripetal forces inducing a spreading of cells to about 1.5-fold (Maddugoda et al. 2011) (Cai et al. 2010). Both cell thinning and the traction forces that may generate cell spreading likely increase membrane tension, which has been shown to be the driving force for pore extension in vesicles (Sandre, Moreaux, et Brochard-Wyart 1999). In good agreement with the idea that membrane tension drives the opening of TEMs, treatment with the detergent deoxycholic acid reduces the mean area of TEMs (Stefani et al. 2017). Cell spreading and softening in response to inhibition of RhoA likely promotes the opening of TEMs (**Fig. 33**). Indeed, C3 intoxicated cells are 1.5-fold larger, 1.4-fold thinner, and 30-fold softer than control cells, likely making them prone to PM fusion events for TEMs openings (Ng et al. 2017).

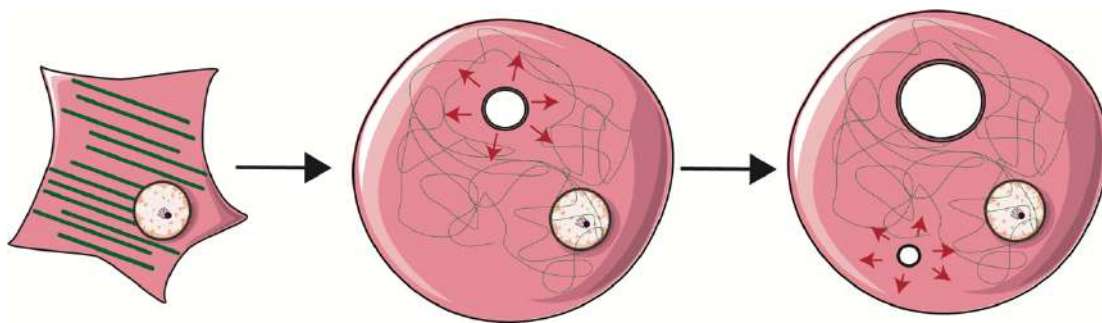


Figure 33. Inhibition of RhoA triggers transendothelial macroapertures formation.

HUVEC treated with ExoC3 exhibits a loss a stress fiber which correlates with RhoA inhibition. This leads to an increase of cell spreading and the formation of TEMs.

By using an AFM cantilever with a ~ 100 nm pyramidal tip diameter, Ng et al. applied mechanical forces of increasing strength on the apical membrane thereby provoking the formation of tunnels. This can be detected by a deflection of the cantilever of 10 nm (**Fig. 34A,C**). The authors were able to trigger TEMs of small diameters is non-intoxicated cells, indicating that the physical proximity of the two membranes is sufficient to promote their fusion for opening of TEMs (**Fig. 34B**) (Ng et al. 2017). This also shows that RhoA inhibition can promote the widening of TEMs likely through a decrease of

cytoskeletal resistance to cell spreading, which leads to a membrane tension increase. In addition, Braakman *et al.* (2014) showed that endothelial cells from the Schlemm's canal can modulate local pore formation, and that this mechanosensitive process is triggered by equibiaxial stretch. In this study they show that pores form either in cells or at cell-cell junctions (Braakman *et al.* 2014).

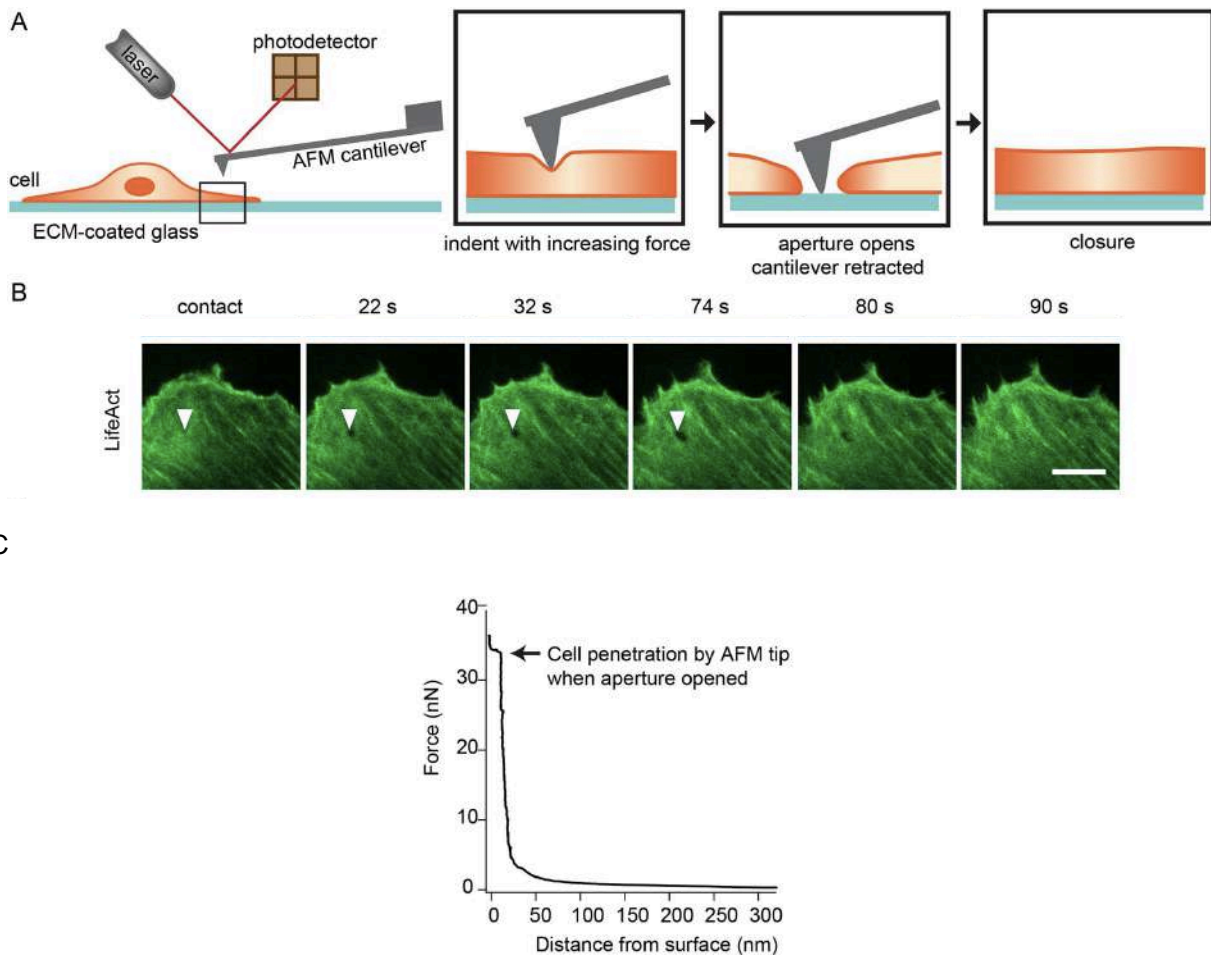


Figure 34. Local force application by the tip of an atomic force microscope cantilever is sufficient to induce transcellular tunnels in endothelial cells.

(A) Schematic diagram of the experimental setup. Using the AFM, a tipped cantilever is extended toward a spread HUVEC until the tip is in contact with the cell at 5 nN force. Then the applied force is slowly increased at a rate of 1 nN/s until a tunnel is observed by TIRF imaging of the cell membrane or the tip has been extended by 3–5 μm . The cantilever is retracted while the progression of the opening and closing of the tunnel is tracked by time-lapse imaging. (B) Time-lapse TIRF images of a HUVEC forming a tunnel when indented by the tip of an AFM cantilever. The cell was expressing GFP-MIM-I-BAR and LifeAct-mCherry and labeled with the CellMask far red membrane dye. Opening of the tunnel was followed by localization of MIM around the aperture and actin-rich wave formation to close the aperture. The arrowheads indicate location of the AFM cantilever tip. The time points of each image relative to tip contact ($t = 0$ s) are displayed above the image. Scale bar: 10 μm . (C) Example force vs. tip-substrate distance trace from a different cell, showing a gradual increase in force at the beginning of indentation, followed by a steeper increase in force as a function of deformation. A step displacement of the tip occurred at constant force due to full penetration of the cell when a tunnel opens (from (Ng *et al.* 2017)).

In 2011, Maddugoda *et al.* showed that TEM formation presents a phenomenological similarity with the dewetting phenomenon of viscous liquids forced to spread on a non-

wettable surface (**Fig. 35**). Indeed, this physical phenomenon is the process by which, when forced to spread, a viscous liquid withdraws from a non-wettable surface by nucleation and growth of dry patches (**Fig. 35 upper panel**) (de Gennes, Brochard-Wyart, et Quéré 2004). Thus, the theoretical analogy with cellular dewetting postulates that the increase of surface tension forces are responsible for the opening and enlargement of TEM tunnels (**Fig. 35 lower panel**). In the cell dewetting phenomenon, these driving forces integrate both membrane and cortical tension, this is why here they are referred to as effective membrane tension. The increase of effective membrane tension is postulated to correlate to the spreading of the intoxicated cell, an assumption that remains to be demonstrated.

In addition, using AFM, Maddugoda et al. highlighted the formation of a rim at the edge of TEMs, where cytosolic mater is collected from the dry patch. This rim formation is a hallmark of the dewetting phenomenon. In 2012, Gonzalez-Rodriguez et al. proposed the cellular dewetting as a physical model to explain TEM formation, with the difference that this phenomenon is transient, *i.e.* leading of a transient opening of TEM, and controlled by the cell, whereas liquid dewetting leads to an irreversible formation of droplets (**Fig. 35**). In this model, similarly to a pore opening in membranes, the driving force for a TEM to open is given by :

$$F_d = 2\sigma - \frac{T}{R'} \quad \text{Eq (1).}$$

where σ is the effective PM tension, with the factor of 2 reflecting the existence of upper and lower membranes, that increases as a function of the spreading of cells. T is the line tension arising from the energetic cost of forming the rim, which depends both on membrane bending rigidity and on the formation as a function of time of an actin ring encircling the TEM thereby blocking its enlargement (**Fig. 35**) (see 1.1.1.2. Stabilization). The initiation of dewetting is due to nucleation of a small TEM that can be triggered by membrane fluctuations leading to membrane fusion. R' is the radius of the TEM that needs to be larger than a certain nucleation radius, whose value is estimated as $R_n = 100$ nm for typical values of the experimental parameters. The surface tension in liquid dewetting remains constant through the whole process of hole enlargement up to the formation of droplets. In contrast, when a cell dewets, as the TEM opens, the excess membrane area increases and the effective PM σ declines as established by Helfrich law, considering all possible wavelengths of membrane fluctuations, from the smallest (lipid molecule) to the biggest (cell size) :

$$\sigma = \sigma_0 \exp \left\{ -\frac{R^2}{R_c^2} \right\}, \quad \text{Eq (2).}$$

Where σ_0 is the initial PM tension in the absence of TEM. Here, $R_c^2 = R_t^2(k_B T)/(8\pi\kappa)$ where R_t is cell size, $k_B T$ is the thermal agitation energy, and κ is the membrane's bending rigidity. The physical model of cell dewetting showed that combination of the dewetting equation with Helfrich's law can explain spontaneous TEM opening and the existence of a maximum TEM radius.

The widening of a TEM is constrained by the time to get encircled by an actomyosin cable stiff enough to counteract the driving force of opening (Stefani et al., 2017). The maximum TEM size is reached due to a decrease in PM tension as the pore opens, so that effective PM tension is balanced by the line tension. Nevertheless, the driving force never becomes null. This is supported by the fact that rupture of the cable leads to TEM resume growth.

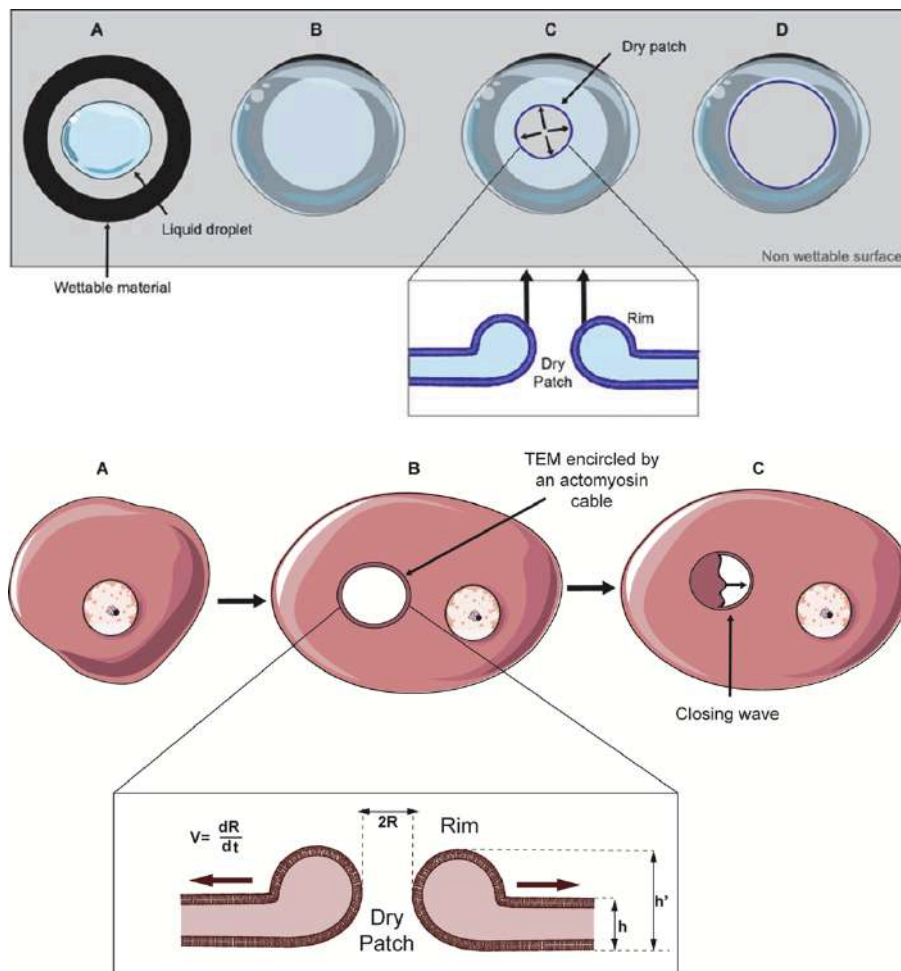


Figure 35. Physical process of liquid dewetting compared to biological cellular dewetting.

Upper panel: dewetting phenomenon. (A) A liquid droplet is deposited at the center of a non-wettable surface, surrounded by a black region that has been rendered wettable. (B) The droplet is mechanically forced to spread and gets pinned by the wettable region, created by a localized substrat treatment. Thus, a metastable state is reached. (C) Nucleation of a dry patch destabilizes the system. The dry patch opens up spontaneously so that free energy is minimized. (D) The dry patch grows until it fully withdraws from the non-wettable zone. The liquid removed from the dry zone accumulates in a rim. Lower panel: cellular dewetting phenomenon. (A) An untreated cell with its nucleus (in blue). (B) Upon RhoA inhibiting exoenzyme treatment, the cell spreads thereby increasing membrane tension. A TEM forms and enlarges up to a maximal size, also displaying the formation of a rim along the TEM. The formation of a rigid actin cable encircling the TEM allows its stabilization. (C) TEMs open transiently owing to the formation of membrane waves invading the dry patch up to complete resealing of the TEM. (D) Schematic side-view showing characteristic dimensions ($h = 50$ nm, $h' = 100$ nm, t : time, R : radius, V : opening speed).

3.2.1.2. Stabilization

The second step of TEM formation is its stabilization. Indeed, after its opening triggered by bacterial toxins as discussed previously, TEM widening is sensed by the host cells that counteracts its enlargement. In 2017, Stefani et al., unveiled by electronic microscopy, the presence of dense actin bundle concomitant with a high stiffness scaffold surrounding the TEM (**Fig. 36**). Laser ablation of this cable highlighted that it is responsible for the control of TEM enlargement. Indeed, the authors highlighted the stiff and inextensible nature of the cable encircling the TEMs, since it maintained the same length before and just after laser ablation. They have also shown that the cable is under tension as its severing causes excessive enlargements of pre-existing TEMs.

Supplemental laser ablation experiments of the actin cable in cells depleted for non-muscular myosin IIa (NMIIa), an actin binding protein that has actin cross-linking and contractile properties, revealed that it is critical in TEM stabilization by contributing to the line tension at the TEM edges. In a complementary manner, depletion of ezrin, a linker of PM and actin cytoskeleton belonging to the ERM family, impair NMIIa accumulation at TEM borders, suggesting that ezrin display an upstream role in stabilization of actin at the TEM border. Eventually, fluorescence-recovery-after-photobleaching (FRAP) experiments in cells KD for ezrin show an increase of F-actin recovery rate, confirming the upstream role of ezrin in stabilizing actin filaments at the edges of TEMs, thereby favoring their crosslinking by NMIIa (Stefani et al. 2017).

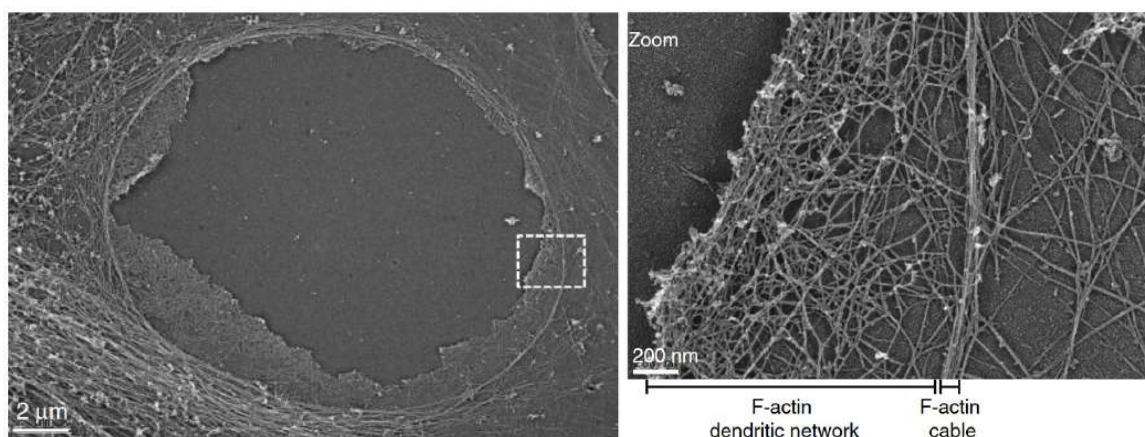


Figure 36. Organization of the actomyosin cytoskeleton along transendothelial macroapertures edges. Platinum replica electron micrograph of TEMs in HUVECs after exoC3 treatment for 24 h. Zoom shows enlarged boxed region. This displays at higher magnification the organization of F-actin into a dendritic meshwork protruding into membrane waves and into an actin bundle at the rear.

Based on the cellular dewetting theory, the authors established that the structural integrity of the actomyosin cable is essential to implement a line tension T at the TEM borders, which prevents an excessive enlargement of TEM that could lead to PM rupture (Eq. 1).

Of note, complete inhibition of Rho leads to TEMs opening that do not stop until they reach the entire cell surface. The actomyosin cable is not present when the TEM nucleates, but it is recruited over time, leading to a time-dependent contribution to line tension, $T = T(t)$ (Stefani et al., 2017). By comparison to liquid dewetting, the line tension is the force arising from the energetic cost needed to form a highly curved edge and that limits the widening of a hole (Stefani et al. 2017) (Gonzalez-Rodriguez et al. 2012). Consequently, in addition to cable assembly, the membrane-bending rigidity could explain the implementation of a line tension around the TEM. Indeed, in 1999, Sandre et al., showed that when a pore opens in a stretched vesicle, the lipid molecules along the edge of the pore must curve with a very small radius of curvature that scales as the membrane thickness.

This mechanism is responsible for a line tension that induces the closure of transient pores (Sandre et al. 1999). In the case of TEMs, the contribution of membrane bending to line tension is : $T = \frac{2\kappa}{h}$, where h is the cell thickness, which is around 50nm in intoxicated cells due to cytoskeleton disruption and κ the bending rigidity, approximately $\sim 40 \kappa_B T$. Taken together and with respect to the cellular dewetting model assumptions, the membrane bending contribution to line tension is of the order of $T_{mb} \sim 5$ pN (Stefani et al. 2017)/

3.2.1.3. Closure

Similarly, to liquid dewetting, TEM nucleation and growth induced the formation of a rim triggering *de novo* positive and negative membrane curvatures, where the membrane is curved away from or toward the cytoplasm. However, positive membrane curvature ease as a function of TEM opening. In 2011 Maddugoda et al., reported the rapid accumulation of MIM proteins, thanks to their I-BAR domain, at the edge of TEMs. TEMs were unable to close in cells deleted for MIM, establishing its critical role for closure. The closure occurs by 2 distinct mechanisms. First, the formation of an F-actin rich wave that extends from one edge of the TEM to the other, and second, a purse-string mechanism where the actomyosin cable tightens, contracts and closes the TEMs (**Fig. 37**).

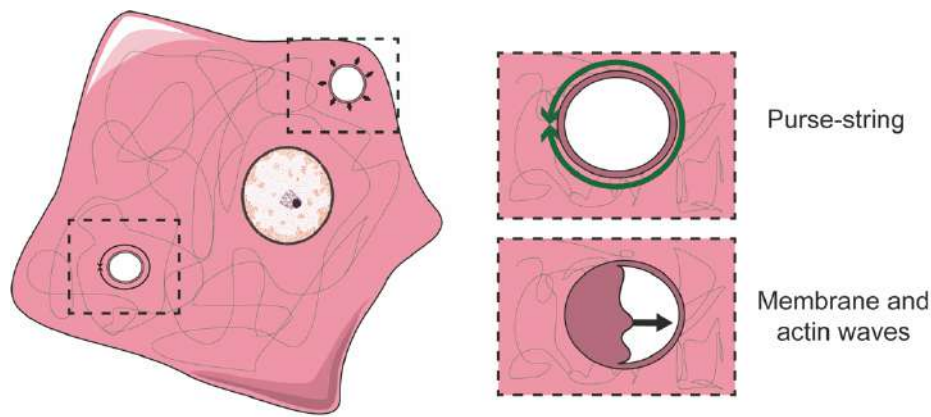


Figure 37. Transendothelial macroaperture closure mechanisms.

After reaching their maximal size, TEMs close back, by two distinct mechanisms. On one hand, the actomyosin cable tightens and contracts promoting the closure by a purse-string mechanism. On the other hand, the formation of an F-actin rich wave that extends from one edge of the TEM to the other leading to TEM closure in an Arp2/3-dependent fashion.

The actin wave is built of branched actin filaments, triggered by an Arp2/3-dependent polymerization that drives the formation of protrusion at the edge of the TEM. By its C-terminal WH2 domains and protein interaction, the MIM protein recruits the Arp2/3 complex at the edge of TEM (Lemichiez et Aktories 2013) (Maddugoda et al. 2011)

Of note, I-BAR- containing proteins may also enhance line tension (Saarikangas et al. 2009) (Gonzalez-Rodriguez et al. 2012). Association of these proteins to the TEM edge may increase the energetic cost of forming a border. Indeed, these proteins have a preferred spontaneous curvature that may deviate from the actual radius. An increase of the radius may thus force them to an unfavorable configuration, which would translate into a line tension. Interestingly, high-rate video acquisition showed that the I-BAR domain of MIM starts to accumulate along TEM edges a few hundred milliseconds after opening. The size of TEMs increases upon depletion of the MIM, which can be explained by a decrease of line tension (Maddugoda et al. 2011) (Gonzalez-Rodriguez et al. 2012).

3.2.2. Analogies of the cellular dewetting model

During my thesis, I participated in the writing of a review describing the different biophysical analogies of liquid dewetting in living systems. The first analogy accounts for multicellular systems, such as biofilms and multi-aggregates, here compared with the molecules of a liquid. Indeed, intercellular adhesions promote the attraction of bacteria, similarly to molecular interactions in a liquid. When the bacteria are not completely surrounded by neighbors, as is the case at the edge of the aggregate, an energetic

imbalance of forces is created, leading to a tendency of bacteria to spontaneously reorganize in order to maximize attractive interactions by minimizing the surface of the interface. The surface tension describes both the behavior of a liquid drop and a multicellular system. These physical similarities have led to the study of the collective dynamics of multicellular systems through analogies with wetting and dewetting (Douezan et al. 2011) (Gonzalez-Rodriguez et al. 2012).

Another analogy has been established between liquid surface tension and membrane tension of a single cell, modeled as a viscous liquid drop (Evans et Yeung 1989). The effective membrane tension in the cell is the sum of plasma membrane and cortical tension imposed by the underlying cortex (Sheetz et Dai 1996) (Diz-Muñoz, Fletcher, et Weiner 2013). The analogy with surface tension participates to the understanding of cell shape (Fischer-Friedrich et al. 2014), cell adhesion (Sackmann et Bruinsma s. d.), or cell dewetting. Dewetting is the process by which, when a liquid film is forced to spread on a non-wettable substrate, it withdraws from the substrate, leading to the formation of dry patches. Here the forces at stake are the tension, exerted in the plane of the film as a result of spreading, and a resisting force called the line tension. The imbalance between these two forces favors the nucleation and opening of dry patches. The theory predicts that a rim forms upon dry patch nucleation and its existence in cell dewetting has been experimentally demonstrated by a cell surface scanning approach using the AFM (Maddugoda et al. 2011). The opening of the patch is accompanied by the appearance of a line tension at the edge which tends to limit the opening. In addition, in the case of cellular dewetting, the law of membrane tension relaxation related to the enlargement of the patch can be described by Helfrich's law. Balance between membrane tension, line tension and viscous dissipation yields a dynamic equation that defines the opening speed. The viscosity term in the cell dewetting model is attributed to the friction between the receding rim and the substrate, which is expected to be the dominant viscous contribution, whereas the viscous contributions due to substrate friction outside the rim as well as to cytosolic flows are neglected.

To sum up, the cell dewetting in our model is induced by an increase of the effective membrane tension. TEM opening is then resisted by a line tension force at the edge of the TEM.



II. Materials and methods

1. CELL CULTURE

In this thesis, all experiments have been performed on Human umbilical vein endothelial cells (HUVECs), which were purchased from Promocell and cultured in human endothelial serum free medium (SFM, Gibco) supplemented with 20% foetal bovine serum (FBS), epidermal growth factor (EGF, Peprotech) at 10ng/mL, fibroblast growth factor (FGF, Peprotech) at 20ng/mL and heparin (Sigma-Aldrich) at 1ng/mL at 37°C 5% CO₂ up to six passages. For the rest of the thesis this medium will be called SFMc for Serum Free Medium, complete.

1.1. siRNA TRANSFECTION

Knock-down (KD) of proteins of interest, mainly caveolin1, cavin1/PTRF, EHD2 and FLNA, has been obtained by magnetofection. Briefly, HUVECs were seeded at sub confluence on the eve of the experiment. siRNAs (10µM) were prepared in a mix of serum-free OptiMEM (Gibco), PolyMag reagent (OZ Biosciences). The mix was incubated at room temperature (RT) for 20 min and then added to the cells. The dishes were then placed on a magnetic plate for 15 min at 37°C. After incubation time, the cells were left in the incubator for 1 hour, then the medium was exchanged for SFM complete and cells incubated at 37°C during 48 hours. Knock-down efficiency was verified by western-blot using the indicated antibodies. For the list of the siRNA used in this study, please see Table X.

1.2. DNA ELECTROPORATION

Electroporation was used for DNA transfection as described (Boyer et al., 2006). In brief, HUVECs were trypsinized and resuspended in Ingenio Solution (Mirus) containing the Lifeact-GFP DNA (10µg per 10⁶ cells) in a 4-mm cuvette (CellProjects). Cells were then electroporated at 300 V, 450 µF, one pulse by GenePulser electroporator (BioRad). Cells were incubated to recover and medium was changed 3hrs post-electroporation for SFMc. Cells were then incubated for 3 additional hours prior intoxication (see below).

1.3. CELL INTOXICATION

ExoC3 from *Clostridium botulinum* and EDIN from *Staphylococcus aureus* were produced and purified in the lab as described previously (Boyer et al. 2006). Briefly, toxins were purified by His-tag affinity chromatography. They were further dialyzed against 1X phosphate-buffered saline (PBS) overnight at 4°C and concentrated using centrifugal filter devices providing fast ultrafiltration (using Amicon® Ultra 15; Millipore). Cells have been treated with either the exoC3 or EDIN toxin at a final concentration of 100 µM in SFM complete filtered on a 22 µm pore filter and incubate for 24hrs at 37°C 5% CO₂.

2. MORPHOLOGICAL ANALYSIS

2.1. IMMUNOFLUORESCENCE

Cells were seeded on gelatin-coated polymer 35mm coverslip dish (Ibidi) and let adhere for 6hrs. Cells were then intoxicated as described above. After incubation time, cells were washed with PBS and fixed by a 4% PFA solution (Biorad) for 15 minutes at 37°C. Immunostaining was done using a permeabilization step (TritonX100, 0.5%) and a blocking step (bovine serum albumin (BSA) 0.1%). A list of antibodies at the dilutions used can be found in table XXX. Mainly, the actin cytoskeleton was labeled using 1 µg/ml fluorescein isothiocyanate (FITC)- or tetramethylrhodamine (TRITC)-conjugated phalloidin (Sigma-Aldrich). Immunosignals were analyzed with a spinning-disk microscope (Nikon T_i inverted, Ultraview spinning disk confocal system (Perkin Elmer)) with a 63× magnification lens. Images were processed using ImageJ and/or Icy software.

2.2. VIDEO MICROSCOPY

HUVECs were electroporated with LifeAct-GFP-pCMV as described above and seeded on gelatin coated polymer coverslip dish (Ibidi). After intoxication, cells were supplemented with 25 mM 4-(2-hydroxyethyl)-1-piperazineethanesulfonic acid (HEPES) (pH 7.4) and recorded on a 37°C heated stage of Nikon T_i inverted microscope using Ultraview spinning disk confocal system (Perkin Elmer). For the TEM opening, images were taken every 10 seconds for 1 hr. For determination of the opening speed (S_o) images were taken every second for 30 min. Acquired videos were analyzed by an ICY based semi-automatic protocol.

2.3. CELL VOLUME MEASUREMENT

All experiments have been done in collaboration with Matthieu Piel at Institut Pierre-Gilles de Gennes and Nishit Srivastava (post-doctoral fellow). After siRNA treatment and intoxication (see above) cells were cultured in a poly(dimethylsiloxan) (PDMS) chamber of controlled height with regular culture media supplemented with Alexa Fluor 488-dextran ($2 \cdot 10^6$ cells/mL). PDMS chambers were coated with $10 \mu\text{g/ml}$ fibronectin in PBS (Life Technologies) for 1 hr at RT. Chambers were washed with medium before cell seeding. Cells were resuspended in medium supplemented with 1 mg/ml Alexa Fluor 488 Dextran (molecular weight MW 10 kD; Life Technologies) and then injected in the chamber. Dextran is a polysaccharide preventing the Alexa Fluor 488-fluorescent dye from passively entering the cells. Cells thus exclude fluorescence and appear dark on a classic fluorescence image. The fluorescence displaced by a cell is linearly proportional to the cell volume (Bottier et al. 2011) (Zlotek-Zlotkiewicz et al. 2015) Finally, the chamber was immersed in medium to prevent evaporation. HUVECs were let to adhere for 4 to 6hrs in SFMc medium at 37°C , 5% CO_2 prior acquisition.

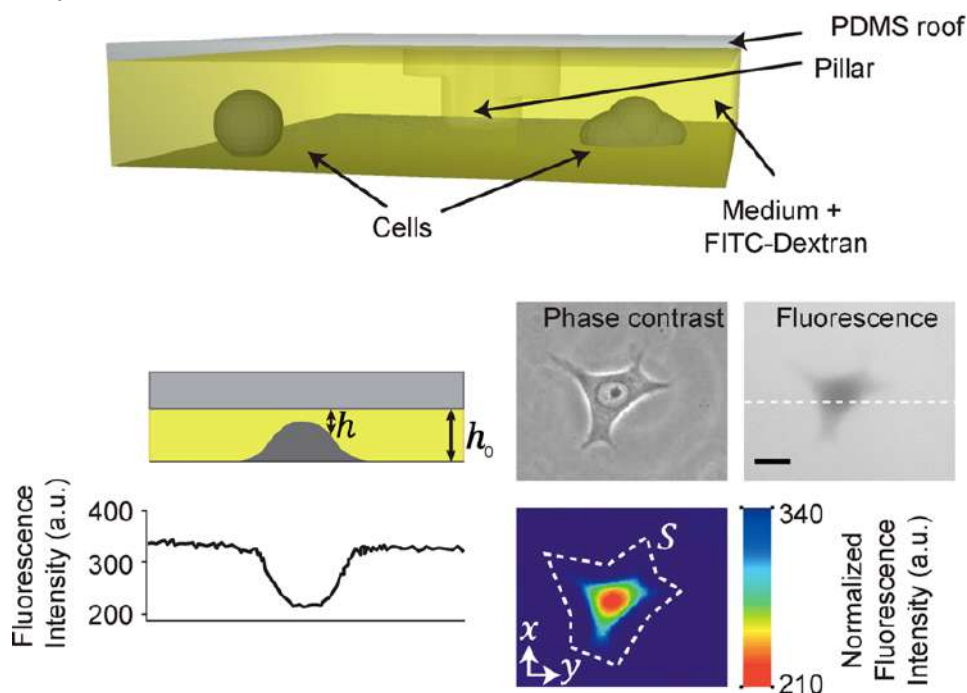


Figure 38. Principle of cell volume measurement.

Scheme depicting the thin PDMS chamber filled with fluorescent dextran for volume measurements, cross section of the chamber with the corresponding profile of fluorescence, and images of a cell in phase contrast and fluorescence in gray levels and false colors. Dashed lines on the grayscale image correspond to the sketch and profile on the left and on the color scale image show the integration area for calculation of cell volume (Zlotek-Zlotkiewicz et al. 2015).

2.4. VARIATION OF SUBSTRATE COMPLIANCE USING HYDROGELS

For monitoring the impact of substrate compliance variation of cell spreading, HUVECS were seeded on 35mm Matrigen Hydrogels of different stiffness after fibronectin coating for 2.5 hours at 37°C. These polyacrylamide hydrogels were commercially populated with quinone groups, which form covalent bonds with molecules containing a primary amine, thiol, or strong nucleophile – essentially any protein. Hydrogels varying elasticity range from 0.5 kPa to 50 kPa compliance, which correspond to physiologically observed stiffness of tissue. HUVECs where they submitted to immunofluorescence (see above) and imaged using a 40X long working distance objective (Nikon).

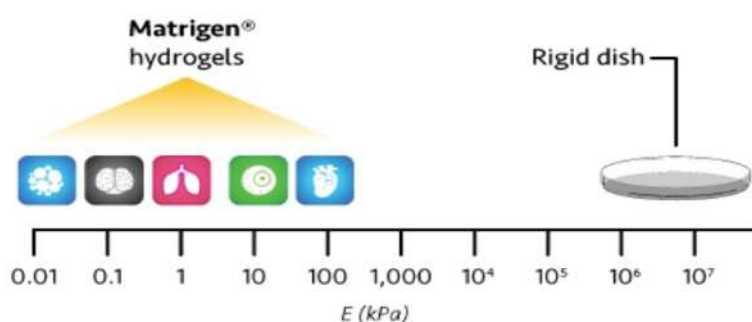


Figure 39. Variation of tissue stiffness in physiology.

As compared to a classical plastic petri dish, hydrogels are much softer and their range of stiffness, from 0.01 kPa to few hundreds of kilo pascals, match the physiological stiffness of tissue.

2.5. TRANSMISSION ELECTRON MICROSCOPY

These set of experiments have been done in collaboration with Eline Lemerle (PhD student) and Stéphane Vassilopoulos (Institut de Myologie). Metal replicate of ventral PM of HUVECs cultured on glass coverslips were obtained by sonication according to a protocol published (Heuser 2000) and adapted by S. Vassilopoulos, our collaborator. Briefly, cells were rinsed three times with Ringer's buffer with Ca^{2+} and then briefly subjected to a concentration of 0.5 mg/mL of poly-L-lysine diluted in Ca^{2+} -free Ringer's buffer (Sigma-Alrich). The poly-L-lysine is removed by washing with Ca^{2+} -free Ringer's buffer. The coverslips are immersed in a KHMgE buffer at 37°C before sonication (Vibra-Cell VCX130 ultrasonic processor, Sonics) at 20% amplitude. The unroofed cells were then immediately fixed for 30 minutes with 2% glutaraldehyde / 2% paraformaldehyde. The cells are treated sequentially with 1% OsO_4 , 1.5% tannic acid and 1% uranyl acetate before being dehydrated by successive ethanol successive ethanol baths finally substituted by hexamethyldisilazane (HMDS) (#C16700-250; LFG Distribution).

For Immuno-gold, sonicated PM are fixed only with 4% paraformaldehyde prior to incubation with primary and secondary antibodies coupled to gold beads (see table XX), the

membranes are incubated with a NaBH₄ solution to inactivate aldehydes. The membranes are finally fixed with 2% glutaraldehyde and subjected to the same treatment as for as for the morphology studies.

The dehydrated samples were then metallized by rotary metallization. The coverslips are placed in the chamber of a metallizer (ACE600, Leica Microsystems). Once under high vacuum (10⁻⁵ to 10⁻⁶ mBar) the membranes are covered with 2 nm of platinum that is stabilized by 4 to 6 nm of braided carbon. The resulting platinum replicas are separated from the glass by flotation on acid, washed several times by distilled water baths containing 0.1% detergent (one drop in 10ml, Photo-Flo, Kodak) and recovered on electron microscopy electron microscopy grids covered with a carbon film (200 mesh formvar/carbon, LFG Distribution). The grids are mounted in the goniometer with eucentric side entry of a transmission electron microscope transmission electron microscope operating at 80 kV (CM120, Philips) and the images are recorded with the Morada digital camera (Olympus). The images are processed by ImageJ software to adjust brightness and contrast and contrast and are presented in reverse contrast.

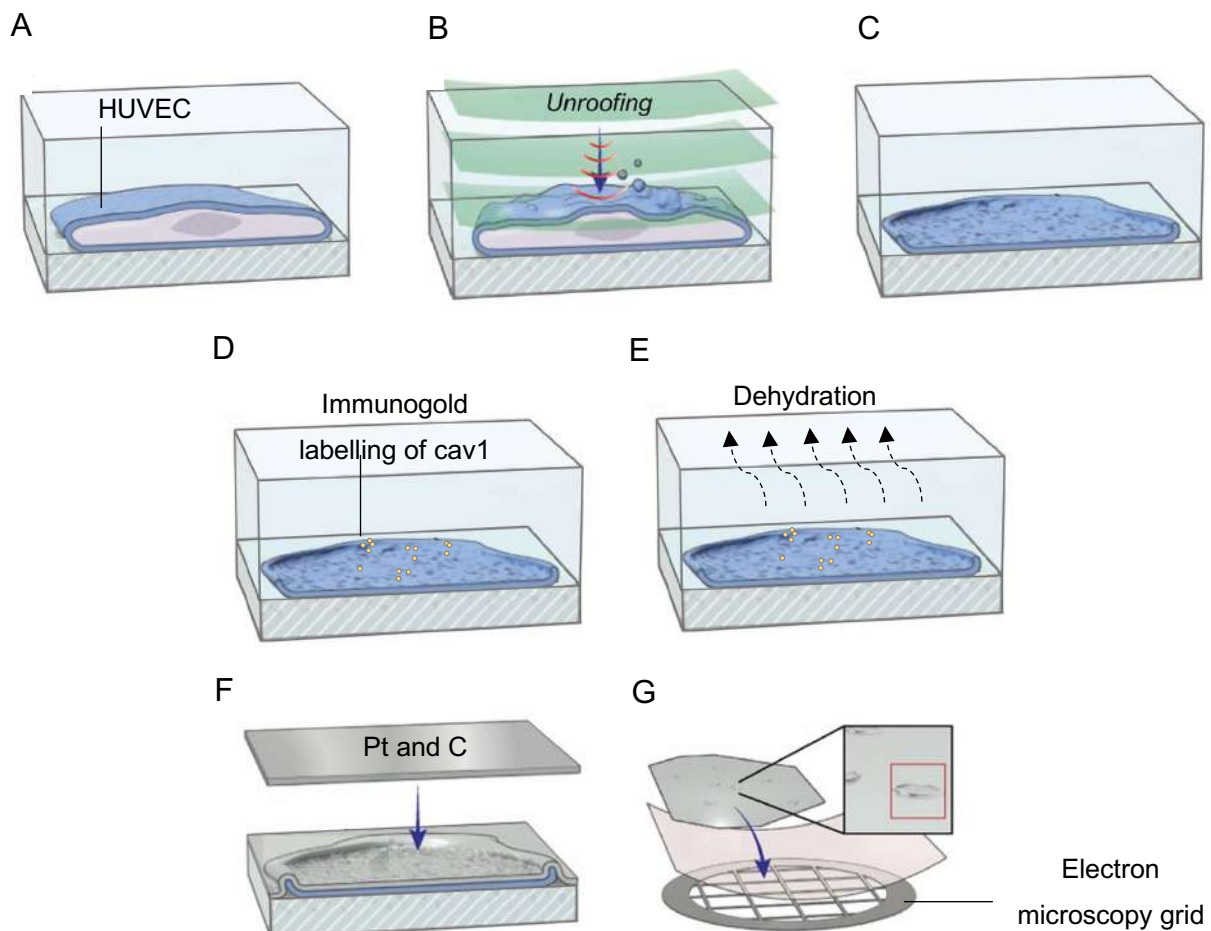


Figure 40. Unroofing of cells for transmission electron microscopy.

(A) HUVEC are grown on glass culture plates. (b) Cells are sonicated in order to unroof and expose the ventral side of the plasma membrane. (C) The cells are then chemically fixed. (D) The proteins of interest, here cav1, are labeled with primary and then secondary immunogold antibodies. (E) The samples are dehydrated and dried. (F) The samples are coated with a thin layer of platinum and carbon to create a replica of the membrane. (g) The replicas are separated from the box, rinsed, and transferred to transmission ME grids (Adapted from (Sochacki et al. 2014)).

3. BIOCHEMISTRY ANALYSIS

3.1. WESTERN BLOT ANALYSIS

Cell lysates from HUVECs cells were collected in a mix of PBS and Laemmli buffer (1X) and boiled for 5 minutes at 100°C. Twenty-five microliters of sample were resolved on a 12% SDS-polyacrylamide gel and transferred to nitrocellulose membrane (GE Healthcare). The proteins were colored with ponceau S (Biorad) and the membrane blocked 1hr with 5% milk in Tris-buffer saline supplemented with Tween 20 at 0.005% (TBS-T) (Euromedex). After blocking, membranes were incubated 2hrs with the primary antibody. Membranes were washed with TBS-T and incubated with horseradish peroxidase (HRP)-conjugated secondary antibodies for 1h. Signals were revealed using Immobion Western Chemiluminescent HRP Substrate (Merck). A list of antibodies is available in Table XX.

4. BENDING RIGIDITY MEASUREMENTS

4.1. PMS FORMATION

Plasma membrane spheres (PMS) were generated by a protocol adapted from (Lingwood et al. 2008). PMS are composed of plasma membrane, including proteins, and cytosol while the subcellular compartments and filamentous actin (Figure S6C) are excluded (Lingwood et al. 2008). Briefly, cells were grown on glass cover slips and incubated for 6–8hrs in PBS⁺⁺ supplemented with 10 μ M MG132. Individual PMS were selected for micropipette aspiration experiments as described previously for lipid vesicles (Sorre et al. 2009). In brief, PMS were held with a micropipette (diameter \sim 3 μ m) under slight aspiration. By partially entering the pipette, the membrane is strained. Tether forces were measured as explained above while the aspiration of the PMS was gradually increased.

4.2. TETHER EXTRACTION, MICROPIPETTE ASPIRATION AND FORCE MEASUREMENT

For the extraction of tethers, has been performed in collaboration with Feng-Chen Tsai and Patricia Bassereau (Institut Curie). We used confocal microscope (Nikon TE2000 inverted microscope) equipped with an optical tweezers consisting of a single fixed laser beam focused by a 100X objective was used for experiments with PMS, including micropipette aspiration and membrane tension measurement (Sorre et al. 2009) (Cuvelier et al. 2005). In order to pull tethers with trapped fibronectin-coated beads (3µm diameter) using an homemade optical tweezer set up, PMS were linearly displaced using a piezo-stage (PI, Karlsruhe, Germany). PMS were trapped using a casein-passivated micropipette connected to the piezo-stage and to an aspiration control system was inserted to manipulate single vesicles or cells. Micropipettes were home-made as described previously rec(Sinha et al. 2011). Briefly, borosilicate capillaries were pulled into fine cones using a laser pipette puller (P-2000, Sutter Instrument Co.) and microforged at the desired inside diameter (3-4µm). The microforge consisted of a glass bead heated by a titanium filament. The pipette was pushed into the melted bead and its cooling resulted in a sharp break of the pipette. After extraction, the tether was held at a constant length between 5 and 150 µm, and tether forces were measured from the detected position of the bead after calibration of the optical trap.

5. STATISTICAL ANALYSIS

Statistical tests were performed using R Software. All experiments were repeated at least three times to ensure reproducibility. P-values were calculated as indicated in the respective figure legends. P-values were considered statistically significant at $P \leq 0.05$. Significance levels are indicated as follows: ns: not significant: $P > 0.05$; $P \leq 0.05$: *; $P \leq 0.01$: **; $P \leq 0.001$: ***; $P \leq 0.001$: ****. We collaborated with Thomas Obadia, from the bioinformatics and biostatistics hub at Institut Pasteur, to perform all the statistical analysis.

Table 1. List of siRNA

Name	Provider	Reference
siCTRL	Eurogentec	SR-CL000-005
siCAV1	Dharmacon	L-003467-00-0005
siPTRF	Dharmacon	L-012807-02-0005
siEHD2	Dharmacon	L-016660-00-0005
siFLNA	Dharmacon	L-012579-02-0005

Table 2. list of primary and secondary antibodies

Name	Provider	Reference	Source	Working dilution
Cav1	CST	3238S	Rabbit	1/1000
PTRF	ProteinTech	18892-1-AP	Rabbit	1/2000
EHD2	Santa Cruz	Sc-100724	Mouse	1/100
FLNA	Merck	MAB1678	Mouse	1/2000
RhoA	Gift from Bertoglio's lab		Mouse	1/1000
GAPDH	Santa Cruz	sc-47724	Mouse	1/5000
Mouse-HRP	Dako	P0447	Goat	1/5000
Rabbit-HRP	Dako	P0399	Swine	1/5000
Cav1	Santa Cruz	sc-894	Rabbit	1/10
GFP	Thermo Fisher	A11122	Rabbit	1/20
Cavin 1	Thermo Fisher	A301.269A	Rabbit	1/20
Rabbit Mouse	Aurion	815.022	Goat	1/25
Rabbit gold	Aurion	815.011	Goat	1/25

6. PHYSICAL MODELING

TEM dynamics are theoretically interpreted by a generalization of our earlier model for a single TEM (Gonzalez-Rodriguez et al. 2012; Stefani et al. 2017) to account for the case of several TEMs opening simultaneously. This generalization has also been used to interpret the data in Annex 1: Tsai et al., 2021 (under revision), and we recall it here for completeness. The hypotheses underlying the model as well as its limitations will be carefully made explicit in the following discussion. In the model for TEM opening proposed by (Gonzalez-Rodriguez et al. 2012), the driving force for opening is given by:

$$F_d = 2\sigma - \frac{T}{R}, \quad (1)$$

where σ is the membrane tension, T is the line tension and R is the TEM radius. The line tension term corresponds to the effective mechanical resistance to TEM opening associated to the formation of the TEM border. This term encompasses contributions from membrane bending due to the local mean and Gaussian curvature, from border-associated and curvature-sensing proteins that are recruited around the TEM, and from actomyosin cable formation. For a model lipid membrane in the entropic regime, membrane tension σ depends on R through Helfrich's law, which here we write in a generalized form to account for the coexistence of N simultaneous TEMs in the same cell:

$$\sigma = \sigma_0 \exp \left[-\frac{\sum_{i=1}^N R_i^2}{R_c^2} \right], \quad (2)$$

where $R_c^2 = (R_{cell}^2 k_B \hat{T}) / (8\pi\kappa)$ is the so-called critical radius, with R_{cell} the total cell radius, k_B the Boltzmann constant, \hat{T} the temperature, and κ the effective membrane bending rigidity. While rigorously derived for a pure lipid membrane, we assume that Helfrich's law remains applicable to describe the relationship between the effective membrane tension σ acting on the TEMs and the observed projected surface in our cells. Thus, the parameter κ in Eq. 2 is an *effective* bending rigidity that accounts for the role of protein inclusions and for the mechanical contribution of the remaining cytoskeletal elements after cell intoxication. Moreover, because intoxicated cells are significantly spread, we suppose that membrane tension is relaxed as described by Helfrich's law from the onset of TEM opening, thus assuming that an eventual buffering role of the remaining caveolae does not modify the mathematical dependence in Helfrich's law. Rather, the presence of remaining caveolae only enters the equation through a modification of the parameters σ_0 and κ . We also note that the cell dewetting model describes TEM opening up to stabilization at its maximum size, but it does neither describe TEM closure, nor TEM nucleation, a very interesting phenomenon that we expect to highly depend on local cell thickness.

As discussed by (Stefani et al. 2017), the effective line tension is not a constant but rather it increases with time, due to the formation of an actomyosin cable around the TEM. Stefani et al. supposed a linear increase, $T \sim \alpha t$. This expression assumes that line tension is dominated by actomyosin cable dynamics rather than by membrane curvature effects, an assumption based on a comparison between the orders of magnitude of the two components (Stefani et al. 2017). The dynamics of TEM opening is governed by a balance between the net driving force (which combines membrane tension and line tension) and cell-substrate friction, characterized by a friction coefficient μ . For the case of N identical TEMs, this balance results in the following differential equation:

$$2\sigma_0 R \exp \left(-\frac{NR^2}{R_c^2} \right) - \alpha t = \mu R^2 \frac{dR}{dt}. \quad (3)$$

This equation can be naively interpreted as if it assumed that all TEMs open simultaneously, which is not the case. Rather, the equation must be interpreted as a simple mathematical description of the existence of domains of membrane tension heterogeneity. We expect that the presence of a first TEM will not significantly affect the opening of a second TEM at a different region of the cell, due to local heterogeneity of the membrane tension. However, when the second TEM increases in size, it will sense the membrane tension over a larger

region of the plasma membrane, which will make its opening to become affected by coexisting TEMs, an effect described by Equation (3).

While Equation (3) can be solved numerically, physical insight is better gained by analytical approximations. First, in the limit of short time, when R is small, the equation can be approximated by

$$v_i = \frac{dA}{dt} = \frac{4\pi\sigma_0}{\mu}, \quad (4)$$

where $A=\pi R^2$ is the TEM area. Therefore, initial TEM opening speed at short time, v_i , is proportional to the undisturbed, effective cell membrane tension σ_0 . Using our experimental data, we predict the values of the undisturbed membrane tension σ_0 shown in Table 3.

Second, the dependence of the maximum TEM area $A_{max}=\pi R_{max}^2$ on the model parameters σ_0 and κ can be estimated by the following approximation. Let us suppose that the initial opening speed v_i is an acceptable estimate of the average opening speed. Then, the opening time t_{max} is related to the maximum TEM area by

$$t_{max} \approx \frac{\mu A_{max}}{4\pi\sigma_0}. \quad (5)$$

Moreover, at $t = t_{max}$, the opening stops and $dR/dt=0$. Replacing Eqs. 4 and 5 into Eq. 3, we obtain the following relationship:

$$x \exp x^2 = \frac{8 \sigma_0^2 \sqrt{N}}{\mu \alpha R_c}, \quad (6)$$

where we have defined $x = N^{1/2} R_{max}/R_c$. The nondimensional parameter on the right-hand side of this expression typically somewhat larger than 1, which requires x to be of the order of or slightly larger than 1. In this range of values, small changes in x yield large changes of the exponential function, implying that x is weakly dependent on the right-hand side. Therefore, x will remain approximately constant for moderate changes of σ_0 and N , implying that, as a first approximation, $N^{1/2}R_{max} \sim R_c \sim 1/\kappa^{1/2}$. This result shows that the maximum TEM size is very sensitive to κ but rather insensitive to σ_0 . We thus obtain the following rough estimate of the effective membrane bending rigidity:

$$\kappa \approx \frac{k_B \hat{T}}{8\pi} \frac{A_{cell}}{N A_{max}}. \quad (7)$$

Based on the experimental results shown in Table 3, and using the estimate $\kappa \sim (N \cdot A_{max})^{-1}$ based on Eq. 7 we deduce an effective bending rigidity upon silencing cavin1/PTRF that is about 1.7 times smaller than under control conditions, whereas it is 5.9 times smaller upon silencing CAV1. These rough estimates can be refined using Eq. 6, which also takes into account variations in membrane tension. Eq. 6 yields a reduction in effective bending rigidity by a factor of about 1.4 for siPTRF and by a factor of about 3.1 for siCAV1.

Fit of the initial opening speed

At short time, the differential equation for opening dynamics can be simplified to

$$\mu R^2 \frac{dR}{dt} = 2\sigma_0 \left(1 - \frac{R_n}{R}\right), \quad (8)$$

here $R_n = T/(2\sigma_0)$ is the minimal nucleation radius. This equation can be integrated to obtain

$$R_n^2 \ln\left(\frac{R}{R_n} - 1\right) + R_n R + \frac{R^2}{2} - C = \frac{2\sigma_0}{\mu} t, \quad (9)$$

where C is an integration constant, whose value is such that $R = R_0$ for $t = 0$, with R_0 the unknown nucleated TEM radius, which is larger than the minimal nucleation radius R_n , $R_0 > R_n$. Because all TEM measurements are made for $R \gg R_0 > R_n$, the dominant term on the left-hand side is the term proportional to $R^2 = A/\pi$, where A is the TEM area. These considerations yield the following estimate of σ_0 :


$$\frac{\sigma_0}{\mu} = \frac{A_2 - A_1}{4\pi\Delta t} \quad (10)$$

where $\Delta t = 1$ s is the time interval between two acquisitions, A_1 the TEM area on the first image after opening (taken on average at a time $\Delta t/2$) and A_2 the TEM area on the second image.

Condition	σ_0 ($\mu\text{N/m}$)	A_{max} (μm^2)	N (average)	$(N \cdot A_{\text{max}})^{-1}$ (μm^{-2})
Control	25 ± 10	8.1 ± 0.5	0.90 ± 0.09	0.137 ± 0.022
siCAV1	50 ± 7	23 ± 4	1.92 ± 0.15	0.023 ± 0.006
siPTRF	29 ± 7	9.3 ± 0.7	1.34 ± 0.11	0.080 ± 0.012

Table 3. Estimate of the variation of the mechanical cell parameters between different experimental conditions. The value of the effective membrane tension σ_0 for the control case is taken from earlier estimates (Stefani et al. 2017).

The increase of σ_0 in siCAV1 and siPTRF conditions are deduced from our experimental data using Eq. 10. The TEM maximum area A_{max} is taken as its median rather than its average value, because the median is a more robust estimator in the presence of a few extremely large values. As discussed in the text, the variations of effective bending rigidity are roughly proportional to variations of $(N \cdot A_{\text{max}})^{-1}$, where N is the average number of simultaneous TEMs and A_{max} is the TEM maximum area.



III. Context and aim of the study

Major progress has been made in the last few years by my host laboratory in the understanding of the cellular components that regulate the size of TEMs. This comprises the role of ezrin to built an actomyosin cable surrounding the tunnels and block the enlargement of these tunnels (Stefani et al. 2017) as well as the role of two I- BAR domain containing proteins ABBA and MIM for the closure of tunnels. My thesis work consisted in better defining the molecular basis of the forces acting on the cell and the molecular actors governing the dynamics of these tunnels. I focused on the impact of caveolin1 and caveolae in the opening phase of TEMs and their speed of opening. This is of general interest as it allows us to hypothesize that caveolin1 and cavin1 have to different roles. Caveolin1 controls membrane stiffness whereas cavin1/PTRF, which is directly involved in the formation of caveolae pits, has a major role in regulating the cell volume of endothelial cells.

I also participated in a work that consisted in varying the level of unsaturation of the acyl chains of phospholipids, knowing that this implied a regulation of the membrane bending rigidity. We show that enrichment of PM with docosahexaenoic acid-containing PLs promotes an increase of TEM nucleation while reducing TEM size and cycle. The details of this study are described in chapter III of this work and essentially allow us to define that polyunsaturated fatty acids, essentially found in human diet, impact the regulation of the size and density of TEMs.

1. CONTEXT

Large transcellular pores are still poorly defined in term of regulation and function. Transcellular pores are typically found in the endothelium lining the Schlemm's canal. Evidence indicate that they fulfill an essential function in regulating the transfer of aqueous humor from the eye chamber to the bloodstream (Braakman et al. 2014; Overby et al. 2014). Moreover, leucocytes must cross the endothelium directly through cells or inter-endothelial junctions, to reach the site of infection (Carman et al. 2007). Leucocytes achieve this migration by triggering the opening of para- and trans-cellular pores of fitted size to avoid otherwise plasma leakage and edema (Barzilai et al. 2017; Heemskerk et al. 2016). Host-cell membrane reshaping by pathogens is a requirement for a successful infection (Charles-Orszag et al. 2016). As an example, through the secretion of toxins, bacteria can carve transendothelial cell macroaperture (TEMs) tunnels without inducing membrane-leakage and cell death (Rolando et al. 2009). However, the formation of TEMs in vessels can be associated with induction of vascular leakage and gelatinous edema, and correlate with an enhanced capacity of *S. aureus* to disseminate *via* the hematogenous route (Boyer et al.

2006; Maddugoda et al. 2011; Munro et al. 2010). Nevertheless, little is known on cell-intrinsic mechanical regulators that control TEM tunnels opening and widening.

Cells submitted to intense mechanical stresses, such as endothelial cells, are particularly rich in caveolae. Caveolae are unconventionally coated pits of spherical shape, with a typical diameter of 60-80 nm, connected to the membrane via a funnel-like membrane neck (Ludwig, Nichols, et Sandin 2016). The caveolar structure is composed of a complex comprising caveolin1 and cavin1 family proteins (Parton et Simons 2007). Caveolins are integral membrane proteins inserted in the inner layer of the PM thanks to a putative hairpin domain (Parton et al. 2006). The peripheral polymerization of cavins around caveolin oligomers consolidates the caveolin-cavin coat (Ludwig et al. 2016). The ATPase and Eps15 homology-domain containing protein EHD2 is recruited at the caveolar neck where it self-assembles into ring-like oligomers to stabilize the constricted neck and subsequently, the caveolar structure (Daumke et al. 2007; Yeow et al. 2017). Caveolae align along stress fibers suggesting the important coupling and communication between these two mechanosensors to maintain the integrity of the plasma membrane (Echarri et Del Pozo 2015; Sharma, Yu, et Bernatchez 2010). Functional analyses indicate that caveolin1 (cav1) interacting factor Filamin A, likely bridges caveolae with actin stress fibers (Muriel et al. 2011). Actin depolymerization (cytochalasin D/ drivers of actin stress fiber assembly) engages a rapid motility and clustering of caveolins, as well as the formation of rosettes. This precedes the inward transport of cav1 from the plasma membrane to the cytoplasm.

Caveolae structures fulfill several essential functions comprising mechano-protection of cells against tension-induced plasma membrane rupturing (Sinha et al. 2011). Indeed, in endothelial cells submitted to mechanical stretch, caveolae can flatten, thereby acting as a membrane reservoir, deploying immediately upon acute mechanical stresses to compensate for an increase of membrane tension (Lee et Schmid-Schönbein 1995; Prescott et Brightman 1976; Sinha et al. 2011).

Much remains to be learned on the role of caveolae structural components, mainly cavin1/PTRF and cav1, in the regulation of the effective membrane tension impose by various environmental stresses and in the regulation of the effective membrane bending rigidity; i.e. integrating membrane in interaction with the cortex.

2. AIM OF THE THESIS

The aim of this work was to investigate the physical processes involved in the formation of the TEMs that are still poorly understood, and to give a lead to their study in animal models. Here we have investigated the interplay between caveolar-coat and the membrane intrinsic capacity to control TEM formation. We uncover a specific function of cav1 in the regulation of effective membrane bending rigidity and tension that is independent from cavin1/PTRF and how it controls transcellular tunnel nucleation and widening. My thesis work is in direct continuity to the research conducted in the laboratory on cellular dewetting theory (Gonzalez-Rodriguez et al. 2012), which draws a parallel between TEMs formation and the physical phenomenon of viscous liquid dewetting. It is a well-known phenomenon that has been extensively studied by Pr Françoise Brochard-Wyart and Pierre-Gilles de Gennes.



IV. Results

1. ENDOTHELIAL CELL TREATMENT WITH RHOA INHIBITING TOXIN ALTERS CAVEOLAE DENSITY AT THE PLASMA MEMBRANE.

Caveolae flatten to buffer an acute increase of PM tension, thereby protecting the cell from PM rupture (Sinha et al. 2011). Under RhoA inhibition by ExoC3, endothelial cells are submitted to a chronic increase of their surface area due to spreading. Key questions are whether this mechanical stress of spreading analyzed within the cellular dewetting theory might offer an analytical framework to better define roles of caveolae in the control of plasma membrane mechanical properties. The cellular dewetting, as discussed below, presents phenomenological analogies with viscous liquid dewetting phenomenon. Indeed, it reports that the mechanical forces of tension at play on the PM, taken as a whole together with the underlying cytoskeleton cortex, account for nucleation and widening of TEMs in response to an inhibition of RhoA (Gonzalez-Rodriguez et al. 2012). These mechanical forces are the effective membrane tension and bending rigidity, which act at different stages of cellular dewetting (Gonzalez-Rodriguez, Morel, et Lemichez 2020). After nucleation, TEMs reach a maximal area and undergo a phase of closure, either by a purse-string mechanism or by extension of actin-rich membrane wave. Therefore, the iterative nature of TEM formation in a cell, and concomitant opening of several TEMs, both suggest a conservation over time of the driving force of TEM opening and widening.

We first assessed whether RhoA inhibition by ExoC3 treatment affects the density of omega-shaped caveolae pits at the ventral side of the plasma membrane of endothelial cells. To this aim, we used a defined unroofing approach of the PM followed by platinum replica analysis by transmission electron microscopy to visualize caveolae. We collaborated with Stephane Vassiloupoulos at Institut de Myologie and his PhD student Eline Lemerle to perform these experiments. Transmission electron microscopy consists of a beam of electrons transmitted through ultra-thin sections of the sample, to form an image reflecting the electron density. The preparation of the samples can be very complex, from the fixation process to the inclusion in the staining or contrast with heavy metals. These sequential steps can all introduce artifacts and structural degradation. In addition, thin sections are intrinsically limited as they only provide a two-dimensional view of the sectioned structures. In our set of experiments, we performed a cell unroofing method allowing us to strip the dorsal part of HUVECs to gain access to the cytoplasmic side of the ventral PM. The ventral PM and associated proteins are thin enough for electrons to pass through and provide

excellent contrast while maintaining their three-dimensional structure. In the original version of this experiment the cells or tissues are fixed by rapid freezing to avoid ice crystal formation in the sample. The biological structures are then opened by a technique called "freeze-fracture" or directly dried in the cold by water sublimation (Heuser et Kirschner 1980). The removal of water by sublimation allows the removal of water on the surface of the sample without damaging the underlying structures. Next, an extremely thin layer of metal (usually platinum) is deposited on the surface of the sample, followed by a layer of carbon to stabilize the platinum grains. Heuser would later introduce cell unroofing to adapt this technique to the visualization of the cytoplasmic faces of biological membranes and membrane proteins (Heuser 2000). S. Vassilopoulos adapted this protocol to adherent PM of cells, grown on glass coverslips. Cell unroofing is here obtained by sonication according to a protocol published (See section Material and Method "transmission electron microscopy").

First, we observed in both control and ExoC3-treated HUVECs the presence of a network of membrane-associated actin filaments (F-actin). We also observe the presence of membrane invaginations such as the honeycomb structure of clathrin rafts and coated pits, together with pits with a rough aspect indicative of the presence of invaginated caveolae surrounded by coat proteins, likely cavin1/PTRF (**Fig. 41 B, D**). As expected, TEMs can be observed in cells treated with ExoC3 (**Fig. 41 A, C**, white stars). However, this method does not allow to conclude on the action of the ExoC3 on actin stress fibers, since unroofing provokes a detachment of the cytoskeleton from the PM, together with the nucleus, mitochondria and large organelles.

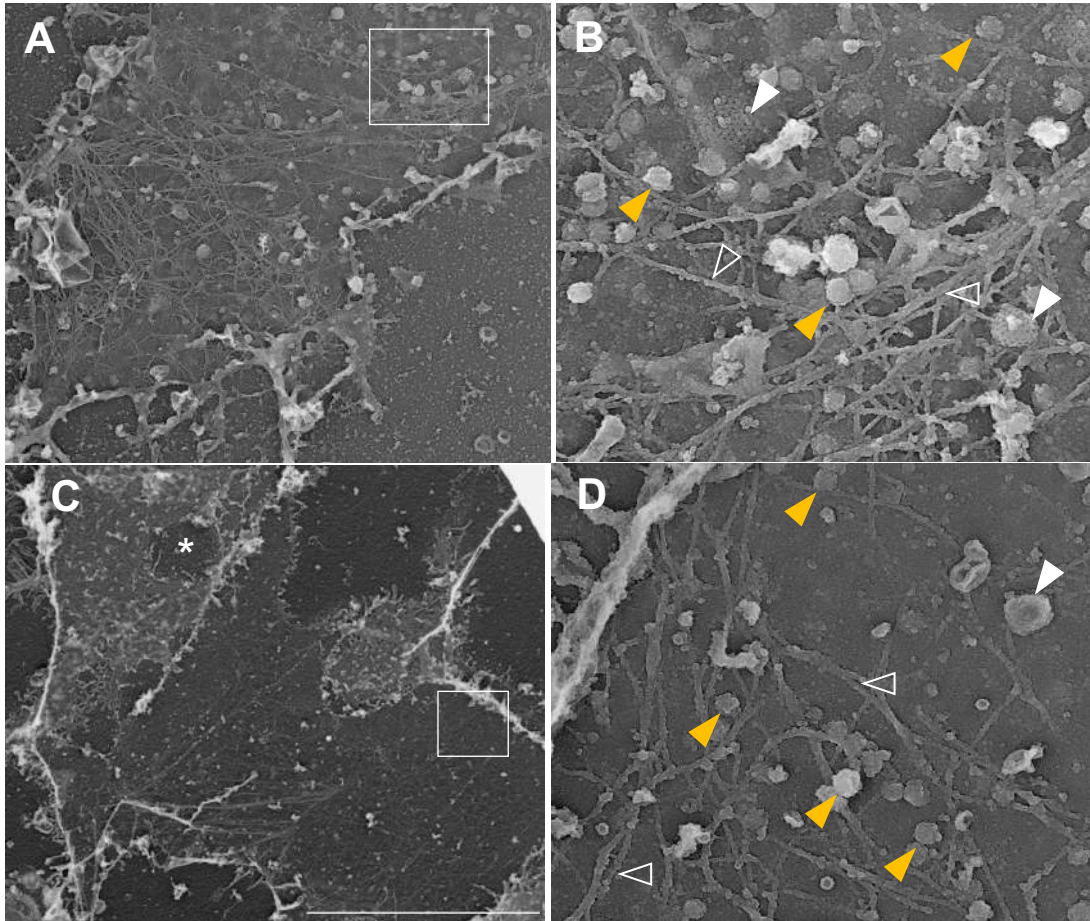


Figure 41. Density of caveolae at plasma membrane decreases upon RhoA inhibition by ExoC3 from *C. botulinum*.

Transmission electron micrographs of unroofed HUVECs control (**A and B**) or intoxicated with ExoC3 (**C and D**). Left panel (**B and D**) show high magnification areas from right panels. This shows i) caveolae (plain yellow arrowhead); ii) clathrin coated pits and patches (plain white arrowhead); iii) stress fibers (empty white arrowhead).

We investigated whether these PM invaginations of similar size than caveolae were indeed caveolar pits. Cells were transfected with a plasmid expressing GFP-cav1. Gold immunolabelling of the GFP-tag cav1 allowed us to identify these invaginations as cav1-positive pits at the ventral side of the plasma membrane of both control and ExoC3-intoxicated HUVECs (**Fig. 42**).

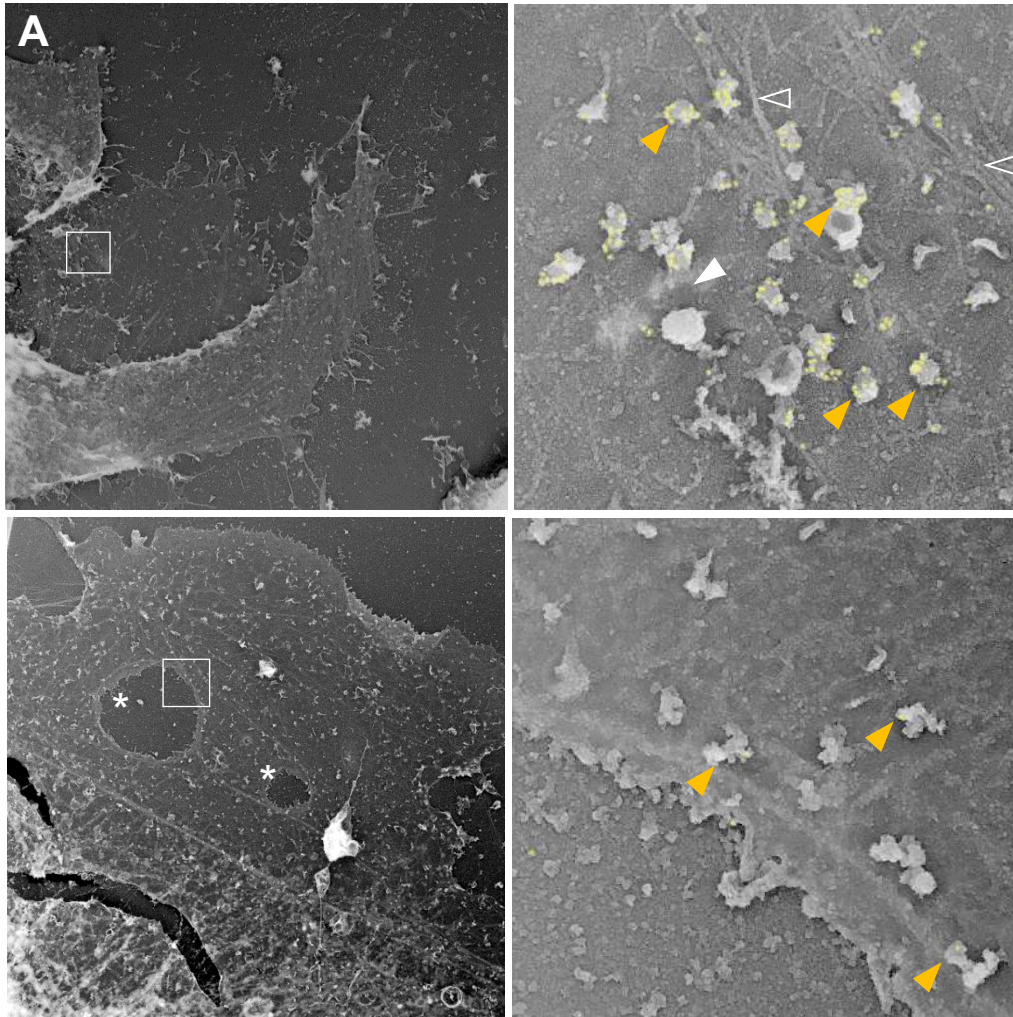


Figure 42. Immunogold labelling of GFP-Cav1.

Transmission electron micrographes of unroofed HUVECs control (**A and B**) or intoxicated with ExoC3 (**C and D**). Left panels (**B and C**) show high magnification areas depicted in right panels. This shows i) caveolae (plain yellow arrowhead); ii) clathrin coated pits and patches (plain white arrowhead); iii) stress fibers (empty white arrowhead). Gold beads (25 nm) are represented by yellow circles.

We then performed a quantitative analysis of the density of caveolae at the ventral PM of both control and ExoC3-treated HUVECs (**Fig. 43**). We quantified the total number of caveolae at the PM surface in each condition. In total, we analyzed 175 μm^2 of PM in naïve HUVECs cells and 214 μm^2 of ExoC3-treated cells from $n \geq 16$ and 19 areas of independent cells, respectively. Graph of Figure 32 shows a 1.6-fold decrease of the mean density of caveolae/ plasma membrane surface in ExoC3-treated cells up to 3.4 caveolae/ μm^2 , compared with 5.4 caveolae/ μm^2 in control cells.

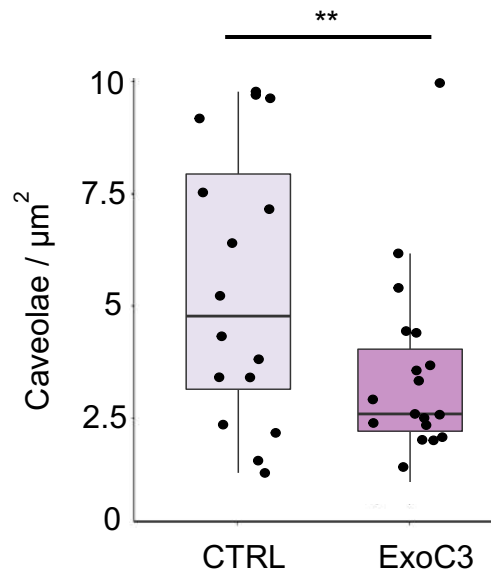


Figure 43. Density of caveolae at the plasma membrane of HUVEC control or treated 24h with ExoC3, quantified on transmission electron micrographs

Data show mean of the density of caveolae/ \pm s.d. Mean-CTRL = 5.4 ± 3.1 caveolae/ μm^2 and mean-ExoC3 = 3.4 ± 2.1 caveolae/ μm^2 . * $P=0,027$ by unpaired t-test. $n>16$ cells, three technical replicates.

Collectively, our quantitative and qualitative structural analyses show that HUVECs intoxicated with ExoC3 exhibit invaginated caveolae pits at the plasma membrane, although with a lower density compared with naïve HUVECs, document a yet unknown aspect of the cross-talk between RhoA and caveolae.

2. CAVEOLAE COMPONENTS LIMIT THE FORMATION OF TEMS

Next, we evaluated whether caveolae structural components, mainly cav1 and cavin1/PTRF, interfere with TEM formation. To this aim, we transfected HUVECs with siRNA targeting either cav1 (siCAV1) or cavin1/PTRF (siPTRF) during 48h.

First, we verified that siRNA treatments were effective (**Fig. 44**). Depletion of cav1 and cavin1/PTRF was monitored after all independent experiments by western blotting. Immunoblots were analyzed with the ImageJ software. Both siCAV1 and siPTRF were effective at decreasing the amount of caveolin1 or cavin1 by about 80% of the total amount of the target protein, as compared to siCTRL condition. As previously described, we also observed a decrease in the amount of cavin1/PTRF (about 40%) when cells were treated by siCAV1 (Hill et al. 2008; Ravid et al. 2008). In addition, we noted a cross-depletion effect between siPTRF and cav1 although to a lesser extent (**Fig. 44**).

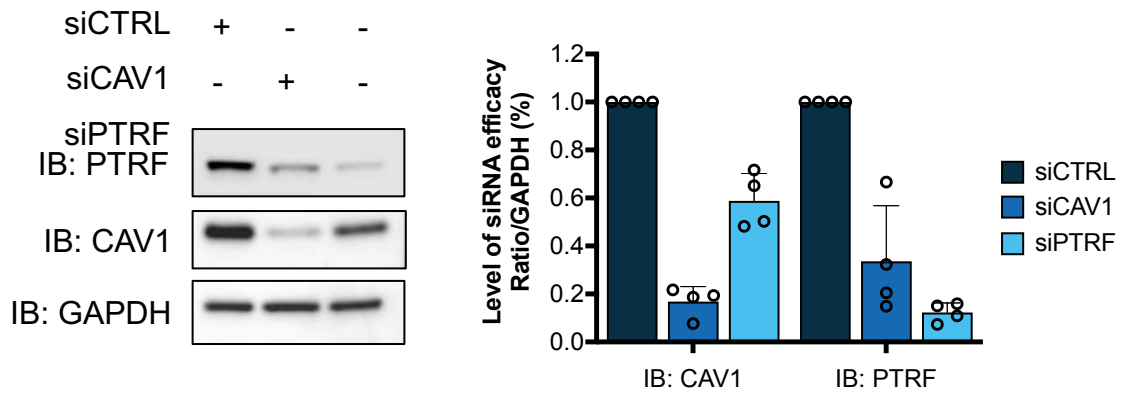


Figure 44. Depletion of structural components of caveolae by siRNA effectively reduces the level of targeted proteins.

HUVECs were treated 48h with siRNA targeting either caveolin1 (siCAV1) or cavin1/PTRF (siPTRF) prior ExoC3 intoxication. Caveolin1 and cavin1/PTRF depletion efficiency was monitored by westernblot analysis. GAPDH was used as a loading control. Images show one representative experiments. Quantification was performed on 4 biological replicates.

The inactivation of RhoA by ExoC3 is a consequence of its sequestration in the cytosol by its inhibitor RhoGDI. This is the result of mono-ADPribosylation of RhoA on its asparagine N41 residue. In a second step, we therefore monitored the efficiency of ExoC3 treatment of HUVECs by western blotting. To do so, we performed *in vitro* sequential mono-ADP-ribosylation experiments. We confirmed that under all siRNA conditions, mono-ADP-ribosylated RhoA in intoxicated cells is no longer mono-ADP-ribosylated *in vitro* by ExoC3. This result reflects the efficacy of ExoC3 treatment of cells, which is independent of siRNA treatment targeting caveolae components (Fig. 45).

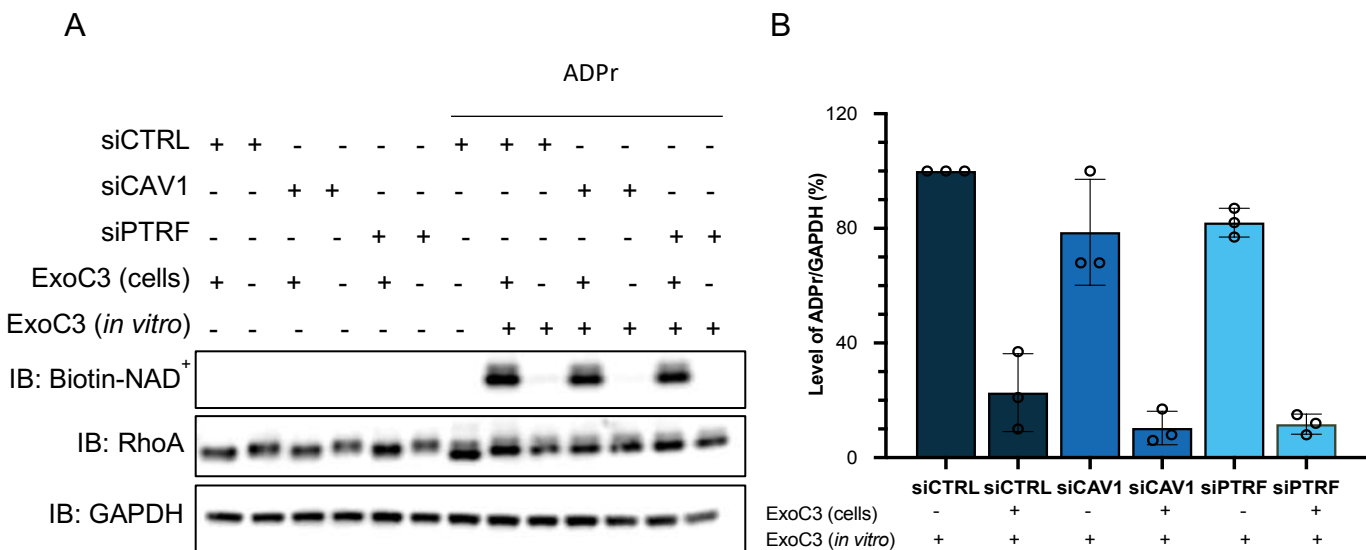


Figure 45. Controls of RhoA mono-ADP ribosylation.

(A) Detection of biotin-labeled mono-ADP-ribosylated RhoA (ADPr) by Western blotting using streptavidin-peroxidase shows the extent of RhoA mono-ADPribosylation in ExoC3-treated HUVEC transfected with siCTRL, siCAV1 or siPTRF. IB anti-RhoA and antiGAPDH show controls. One representative experiment, 3 biological replicates. (B) Quantification of 3 biological replicates as observed in (A).

In this set of experiments, we also confirmed that the cell treatment by siCAV1 or siPTRF were efficient (**Fig. 46**). We therefore conducted western blot analysis to detect the level of proteins targeted by siRNA treatment. In all siRNA conditions, the level of target protein decreased by at least 80 %. Here again, we noticed a cross-depletion effect of siCAV1 on cavin1/PTRF level (decrease of 80%) and of siPTRF on cav1 level (40 %) although to a lesser extent (**Fig. 46**).

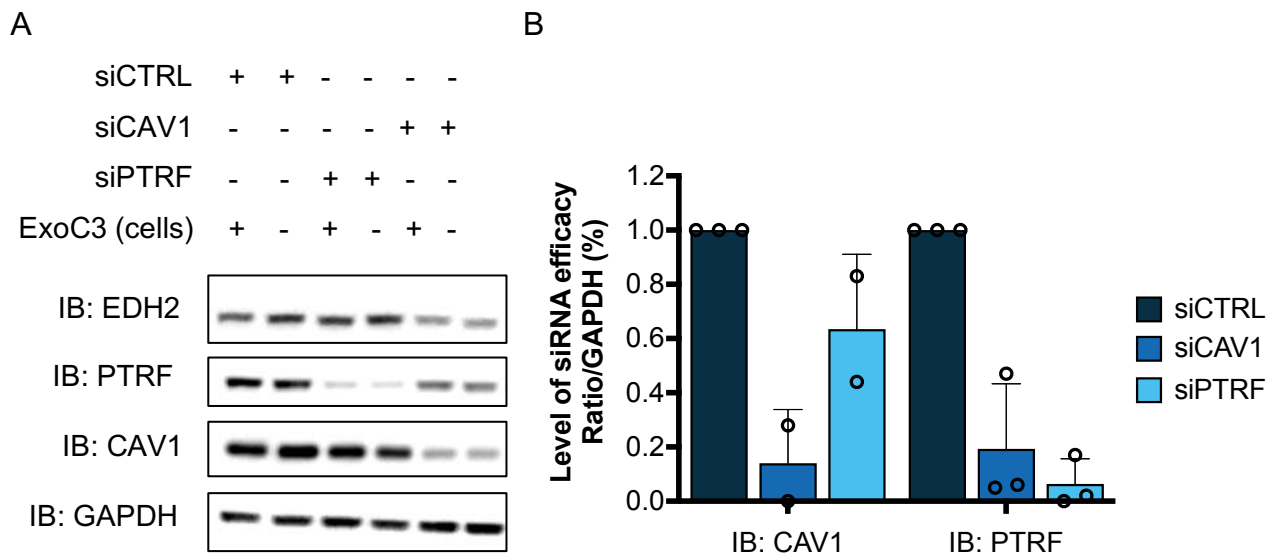


Figure 46. Control of siRNA efficacy in RhoA mono-ADP ribosylation experiments.

(A) HUVECs were treated 48h with siRNA targeting either caveolin1 (siCAV1) or cavin1/PTRF (siPTRF) and next treated 24h with ExoC3. Caveolin1 and cavin1/PTRF depletion efficiency was monitored by westernblot analysis. GAPDH was used as a loading control. Images show one representative experiments. (B) Quantification of level of proteins from 3 biological replicates as observed in (A).

Next, HUVEC treated with siRNA targeting either cav1 (siCAV1) or cavin1/PTRF (siPTRF) were intoxicated for 24h with ExoC3 and fixed by PFA prior to FITC-phalloidin treatment, to visualize the actin cytoskeleton (**Fig. 47**). This enabled us first to observed by immunofluorescence a proper disruption of actin stress fibers following RhoA inhibition by the ExoC3, in all siRNA conditions. Then, the actin labelling allowed us to visualize both the edge of cells and TEMs, surrounded by F-actin (**Fig. 47**).

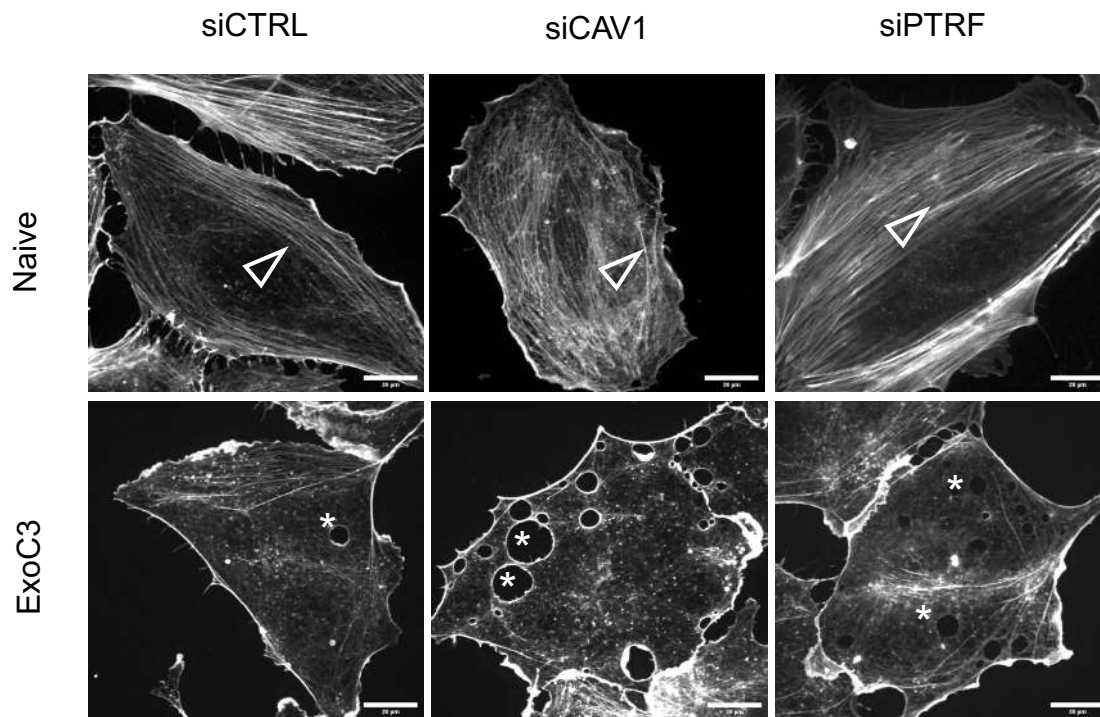


Figure 47. TEM density increases in CAV1 or cavin1/PTRF siRNA-treated cells.

Confocal images of HUVEC showing lifeAct-GFP signal. Prior to ExoC3 treatment HUVEC were transfected with control siRNA (siCTRL) or siRNA targeting either CAV1 (siCAV1) or cavin1/PTRF (siPTRF). Stars show several TEMs in each condition. White arrow head show stress fibers. Scale bar 20 μ m.

From these confocal images (**Fig. 48**), we then manually assessed the percentage of cells displaying TEMs. This quantitative analysis allowed us to uncover a significant increase of the percentage of cells presenting at least one TEM in HUVEC treated with siCAV1 ($37.6 \pm 1.29\%$) or with siPTRF ($36.4 \pm 1.29\%$), as compared to $28.8\% \pm 1.21$ in siControl (siCTRL) conditions (**Fig. 48**).

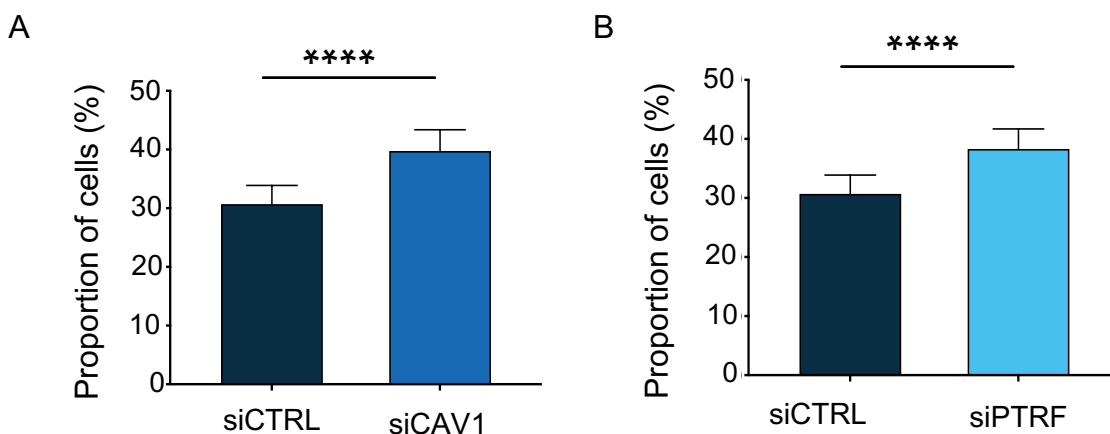


Figure 48. TEM density increases in CAV1 or cavin1/PTRF siRNA-treated cells.

Histograms show percentages of cells with TEMs after 24 hours of ExoC3 treatment of HUVEC were transfected with siCTRL, siCAV1 (**A**) or siPTRF (**B**) ($n=1,400$ cells per condition, 8 biological replicates). Error bars represent 95% confidence intervals. Logistic regression with pairwise comparisons after adjustment using a Tukey's HSD test. **** $P < 0.0001$, siCTRL vs siCAV1 and siCTRL vs siPTRF.

We also monitored the distribution of TEMs in cells depleted for cav1 or cavin1/PTRF before treatment with ExoC3 (**Fig. 49**). We recorded a significant increase in the density of TEMs per cell in HUVECs knocked down for cav1 or cavin1/PTRF. We also calculated the average density of TEMs per cell, including cells that did not show any TEM. Here again, we observed a significant increase of TEMs per cell in both siCAV1 and siPTRF conditions (inset, **Fig. 49**).

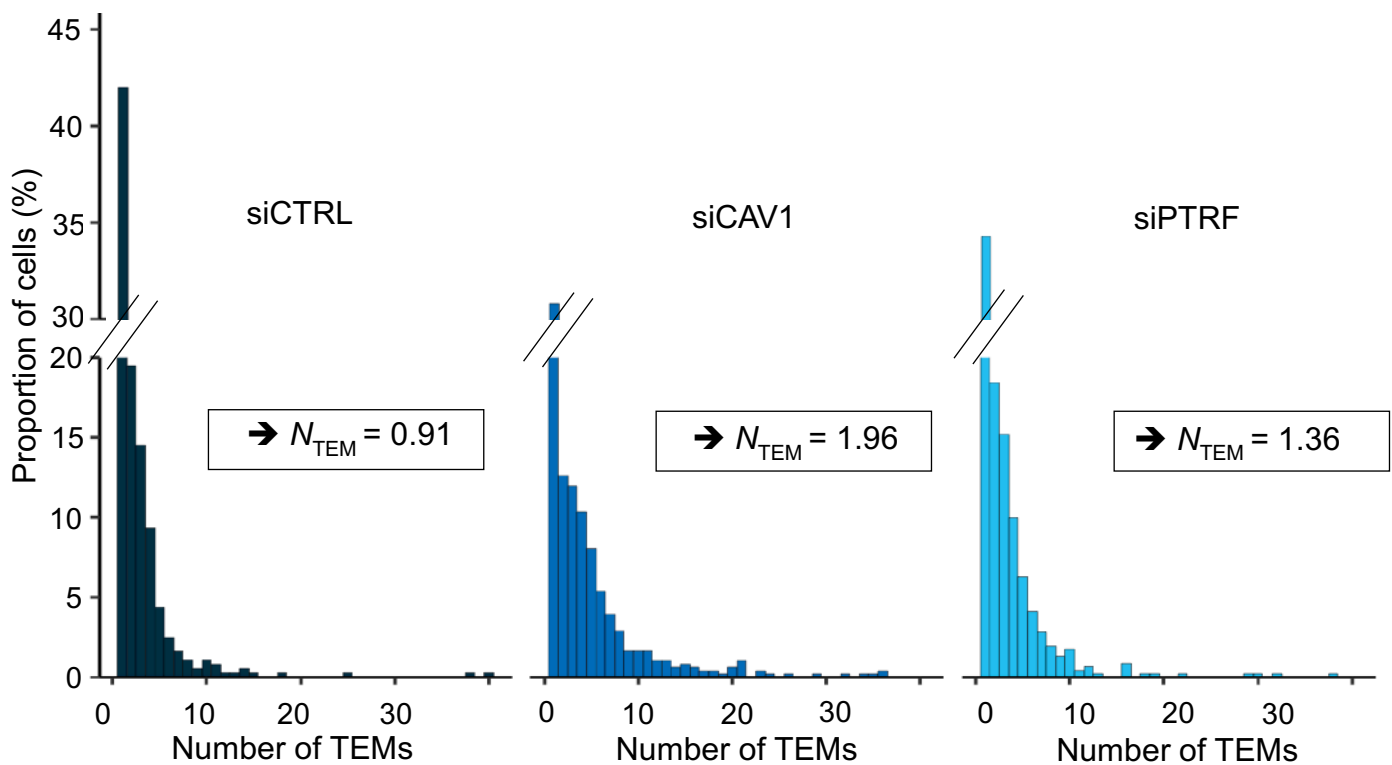
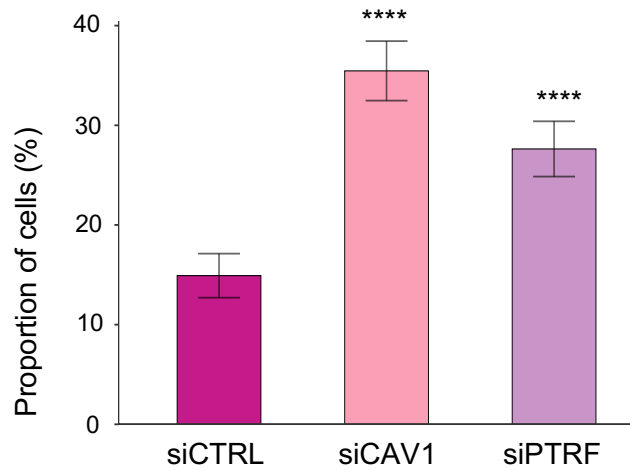


Figure 49. TEM density increases in CAV1 or cavin1/PTRF siRNA-treated cells.

Graphs show the distribution of the number of cells (y-axis) displaying 1 or more TEMs (x-axis) in HUVEC transfected with control siRNA (siCTRL) or siRNA targeting either CAV1 or cavin1/PTRF prior to ExoC3 treatment. This shows a distribution of cells with 1 and more TEMs skewed to the right in siCAV1 or siPTRF conditions. The y-axis is cut between 18 and 30%. Insets show the mean of the density of TEMs per cell within the whole cell population/ \pm s.d. siCTRL = 0.91 ± 0.08 TEMs/ cells; mean-siCAV1 = 1.96 ± 0.16 TEMs/ cells; mean-siPTRF = 1.36 ± 0.11 TEMs/ cells. **** $P < 0.0001$ by a linear mixed model (Poisson regression), with random intercept accounting for technical replicates and fixed effects, $n = 1400$ cells per conditions, 7 biological replicates.

Above findings were broadened by showing that cav1 and cavin1/PTRF also control the formation of TEMs induced by the ExoC3-homologous toxin EDIN from *S. aureus* (**Fig. 50**). Indeed, we noted an increase of the percentage of EDIN-intoxicated cells displaying TEMs once transfected with siCAV1 ($35.3 \pm 2.9\%$) or with siPTRF ($27.4 \pm 2.6\%$), as compared to $14.7\% \pm 1.8$ in siCTRL conditions. We also observed a significant increase of the density of TEMs per cell in HUVEC knocked-down for cav1 or cavin1/PTRF (**Fig. 50**).

A



B

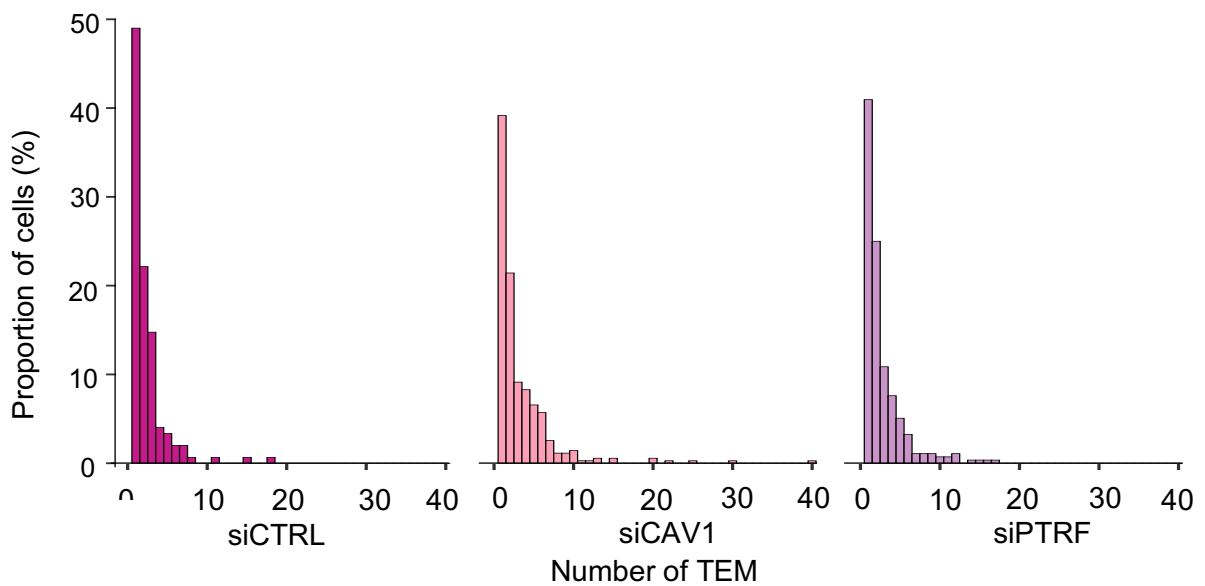


Figure 50. In HUVEC intoxicated with the EDIN from *S. aureus*, TEM density increases in CAV1 or cavin1/PTRF siRNA-treated cells.

(A) Histograms show percentages (%) of cells with TEMs after 24 hours of EDIN treatment of HUVEC transfected with siCTRL, siCAV1 or siPTRF (n= 980 cells per condition, 5 biological replicates). Error bars represent 95% confidence intervals. Logistic regression with pairwise comparisons after adjustment using a Tukey's HSD test. **** $P < 0.0001$ for all comparisons (Mean \pm siCTRL = 14.7 ± 1.8 %; siCAV1 = 35.3 ± 2.9 % or siPTRF = 27.4 ± 2.6 %). (B) Graphs show the distribution of the number of cells (y-axis) displaying 1 or more TEMs (x-axis) in HUVEC transfected with control siRNA (siCTRL) or siRNA targeting either CAV1 or cavin1/PTRF prior to EDIN treatment. This shows a distribution of cells with 2 and more TEMs skewed to the right in siCAV1 or siPTRF conditions. Mean of the density of TEMs per cells in the whole cell population/ \pm s.d.: siCTRL = 0.32 ± 6.0 TEMs/ cells; siCAV1 = 1.09 ± 19.6 TEMs/ cells; mean-siPTRF = 0.71 ± 12.3 TEMs/ cells. **** $P < 0.0001$ by a linear mixed model (Poisson regression), with random intercept accounting for technical replicates and fixed effects, n=980 cells per conditions, 5 biological replicates.

Complementary to these findings, we analyzed roles of caveolae accessory proteins known to stabilize the omega-shaped caveolae pits and their distribution at the plasma membrane (**Fig. 51**) (Muriel et al., 2011; Parton et al., 2020). Here, we investigated the effect of the ATPase EHD2, localized at the neck of the caveolae and of the linker protein filamin A (FLNA), which interacts with both cav1 and F-actin network underneath the plasma membrane. These proteins are not essential for the formation of caveolae, but they both

stabilize the structure. We found that siRNA-targeted depletion of EHD2 in HUVECs treated with ExoC3 also significantly increased the percentage of cells displaying TEMs and their density per cell, as compared to siCTRL. Similar results were obtained with siFLNA, although to a lesser extent. This suggests that a proper caveola structure is required to limit TEM formation. However, the involvement of EHD2 or FLNA seems to be weaker than that of the essential proteins cav1 and cavin1/PTRF as their effect on TEM density is lower (**Fig. 51**).

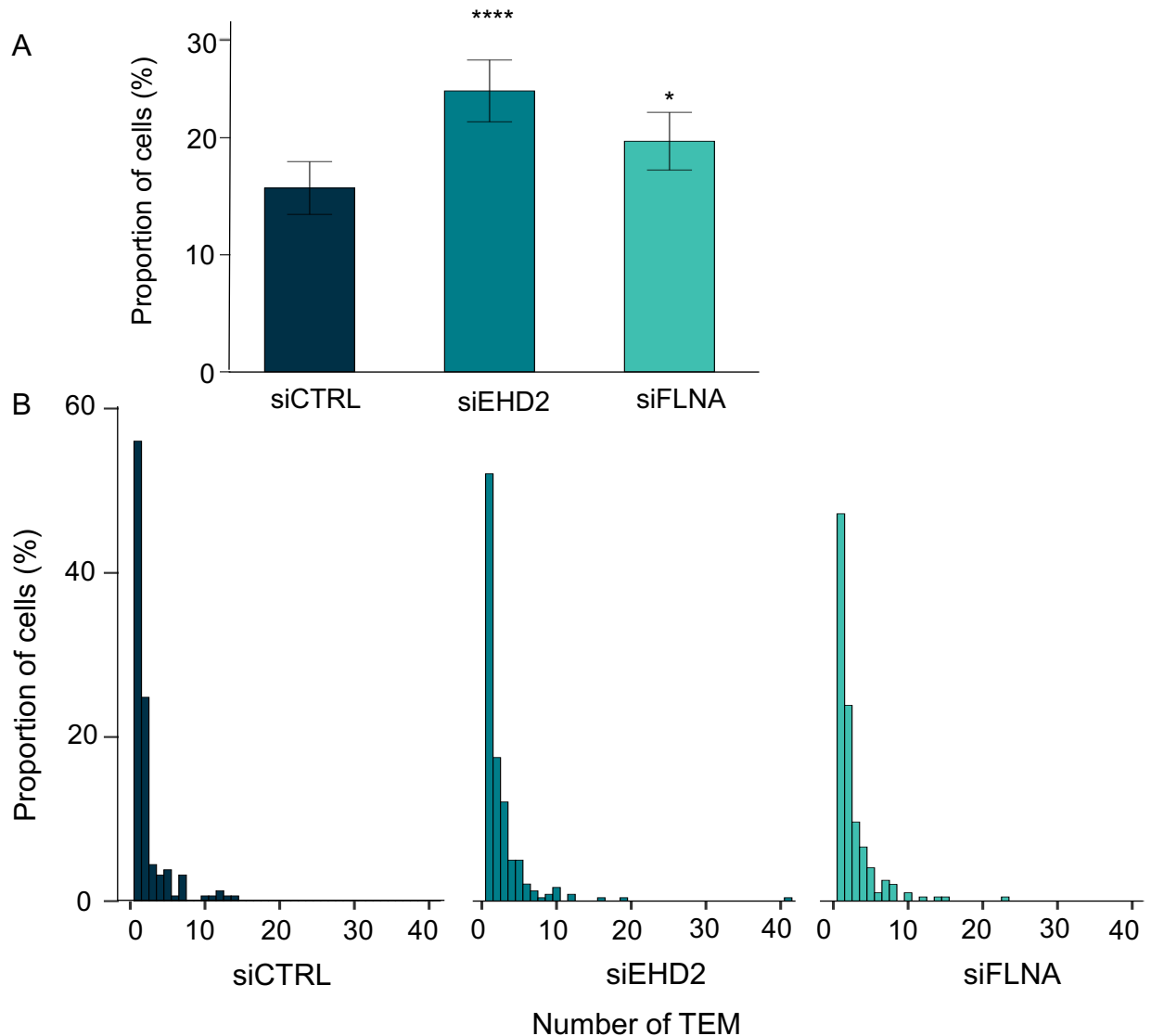


Figure 51. TEM density increases in siEHD2 or siFLNA treated cells.

(A) Histograms show percentages of cells with TEMs after 24 hours of ExoC3 treatment of HUVEC transfected with siCTRL, siEHD2 or siFLNA (n=1000 cells, 5 biological replicates). Error bars represent 95% confidence intervals. Logistic regression with pairwise comparisons after adjustment using a Tukey's HSD test. **** $P < 0.0001$ for all comparisons: (Mean \pm s.d: siCTRL = 15.4 ± 1.9 %; siEHD2 = 23.7 ± 2.5 % or siFLNA = 19.4 ± 2.2 %). (B) Graphs show the distribution of the number of cells (y-axis) displaying 1 or more TEMs (x-axis) in HUVEC transfected with control siRNA (siCTRL) or siRNA targeting either EHD2 or FLNA prior to ExoC3 treatment. This shows a distribution of cells with 2 and more TEMs skewed to the right in siEHD2 or siFLNA conditions. Mean of the density of TEMs per cells in the whole cell population: siCTRL = 0.33 ± 0.06 TEMs/ cells ; siEHD2 = 0.58 ± 0.09 TEMs/ cells; siFLNA = 0.47 ± 0.08 TEMs/ cells.

**** $P < 0.0001$ by a linear mixed model (Poisson regression), with random intercept accounting for technical replicates and fixed effects, n=1000 cells per conditions, 5 biological replicates.

Overall, these results are consistent with a role of cav1 and cavin1/PTRF in limiting TEM formation. This is also observed with accessory proteins such as EHD2 and FLNA, although these latter are involved to a lesser extent. Therefore, these data suggest that proper caveolae formation is necessary to limit the formation of TEMs, induced by both ExoC3 or EDIN treatment.

3. RELATIONSHIP BETWEEN CELL SPREADING AND TEM FORMATION AS FUNCTION OF CELLULAR MATRIX STIFFNESS

ECM compliance is perceived by cells to adapt their behavior. Notably, variations of the stiffness of the extracellular matrix has a great impact on the spreading and migration of cells. Here, we have tested whether variations matrix compliance, using acrylamide hydrogels of different stiffness coated with fibronectin, might modulate the efficacy of TEM formation. HUVECs were plated on fibronectin-coated hydrogels ranging from 0.5 to 50 kPa. Cells were left untreated or intoxicated with ExoC3 prior to actin cytoskeleton staining with FITC-phalloidin (**Fig. 52A**) and we quantified the percentage of TEM-displaying cells (**Fig. 52B**) and the number of TEMs per cell (**Fig. 52C**). We have determined that in the whole cell population, the proportion of cells displaying TEMs increases as a function of the increase of matrix compliance. Indeed, 3.4% of the cells displayed TEMs when plated on 0.5 kPa hydrogels, while we recorded an increase up to 20% of cells with TEMs on the 50 kPa condition. Moreover, we measured a 8-fold increase of the density of TEMs per cell in the whole cell population plated on matrix of high compliance (0.57 TEM/cell at 50 kPa condition), compared with low substrate stiffness hydrogels (0.07 TEMs/cell at 0.5 kPa) (**Fig. 52**).

We hypothesized that the striking difference of TEM formation efficiency might correlate with variation cell spreading. Therefore, we measured the area of untreated or intoxicated HUVECs, plated on hydrogels whose substrate compliance range from 0.5 to 50 kPa conditions. First, we observed that ExoC3 induces a spreading of HUVECs in all conditions ($****P \leq 0.0001$) except at high stiffness (50 kPa), although a tendency of spreading was recorded (11,520 μm^2 in non-treated condition vs 14,700 μm^2 in cell treated with ExoC3). Considering that spreading du ExoC3-treated cells is significant when cells are plated on plastic the result obtained at the condition 50 kPa requires more measurements. We also observed that cells display larger areas when plated on high substrate stiffness, in

both untreated or intoxicated conditions (**** $P \leq 0.0001$). Of note, no difference was recorded for the percentage of cells with TEMs in the conditions 25 and 50 kPa. We interpret this as a maximal value of TEM formation reached around 25 kPa for HUVEC treated with ExoC3 which a value in good agreement with our data is obtained with cells plated on plastic dishes.

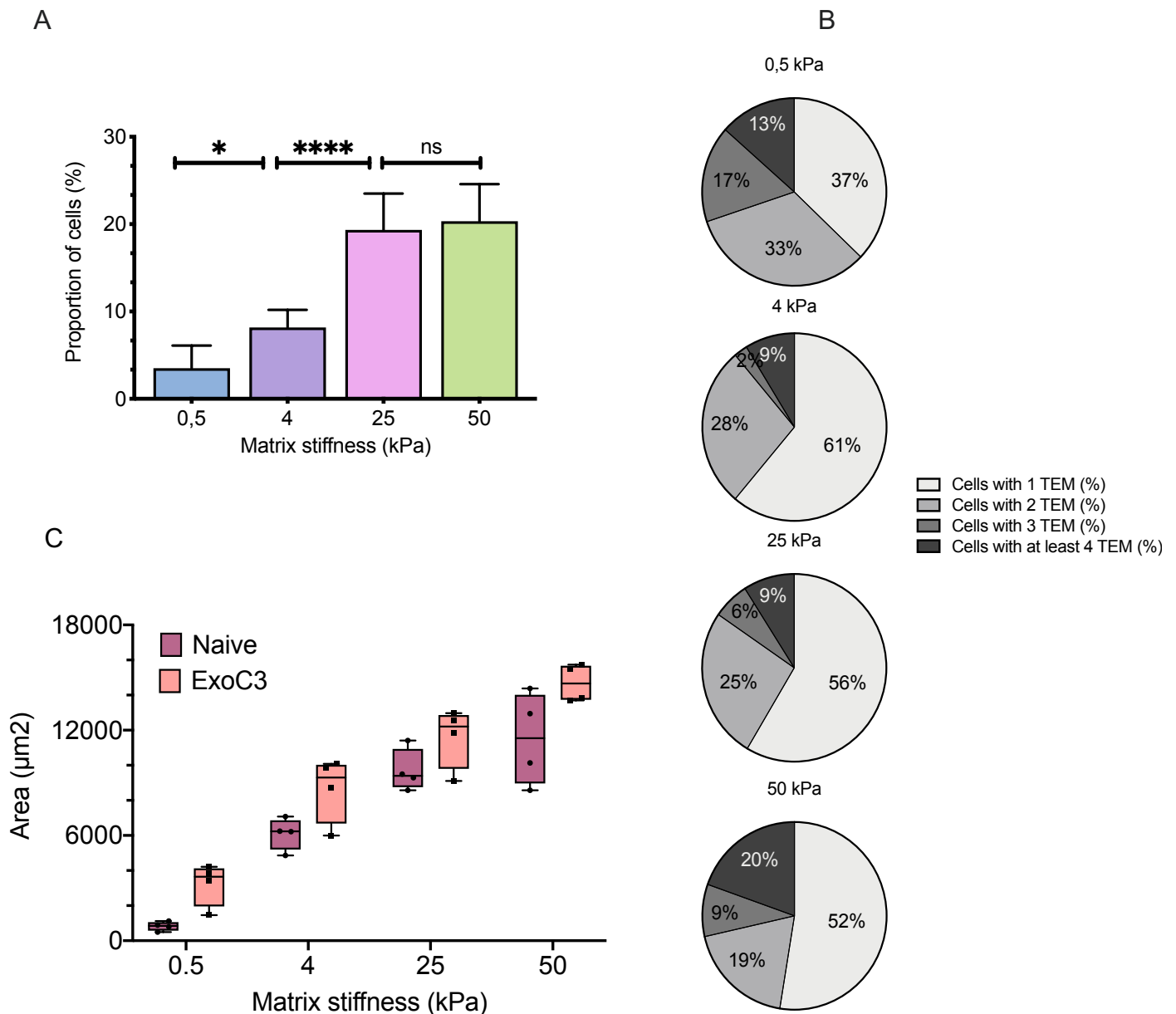


Figure 52. Variations of cell spreading and percentage of TEM formation in HUVEC plated on matrix of different compliance.

(A) Boxplot shows the percentage of cells with TEMs as a function of substrate compliance: 3.5 ± 0.008 % SD of cells present TEM when plated on 0.5 kPa hydrogels against 8 ± 0.012 % SD in the 4kPa condition, 19.2 ± 0.019 % SD in the 25 kPa condition and 10.3 ± 0.019 % in 50 kPa condition (mixed-effect model with multiple comparisons). (B) The number of TEMs per cell is shown as percentages. (C) Boxplot shows measures of the areas of HUVEC treated with ExoC3 for 24h or left untreated ($n=800$ cells per condition, 4 biological replicates). $P=0.5$ between 50 kPa and 50 kPa + ExoC3. $P=0.6$ between 25 kPa + ExoC3 and 50 kPa + ExoC3. Comparison of other conditions show highly significant differences **** $P < 0.0001$. Linear mixed model with random intercept accounting for technical replicates and fixed effects applied on a log10 scale of the cell surface areas.

These results suggest that increase of cell spreading correlates with an increase of both frequency and density of TEMs.

4. CAVEOLIN1 AND CAVIN1/PTRF IN THE CONTROL OF CELL SPREADING

TEMs can be mechanically induced in both control and ExoC3-treated cells by pushing forces applied onto the dorsal plasma membrane (Ng et al. 2017). This is consistent with the idea that a thinning of cells favors the nucleation of TEMs by promoting the apposition of dorsal and ventral plasma membranes for fusion.

Next, we monitored variations of the volume and spreading of HUVEC following siRNA-targeted depletion of CAV1 or cavin1/PTRF before and after ExoC3 treatment. Variations of cell area were determined by measure of the actin-rich perimeter of FITC-phalloidin treated cells. The perimeter of the cell was defined using the polygon tool from ImageJ software (**Fig. 53**). We randomly selected cells of various sizes, in both non-treated and in ExoC3-treated conditions. In this last case, we selected cells displaying an effect of the toxin, *i.e.* without stress fibers and with or without TEMs. As expected, in all conditions, inhibition of RhoA by the ExoC3 triggers a significant spreading of cells (**Fig. 53**)

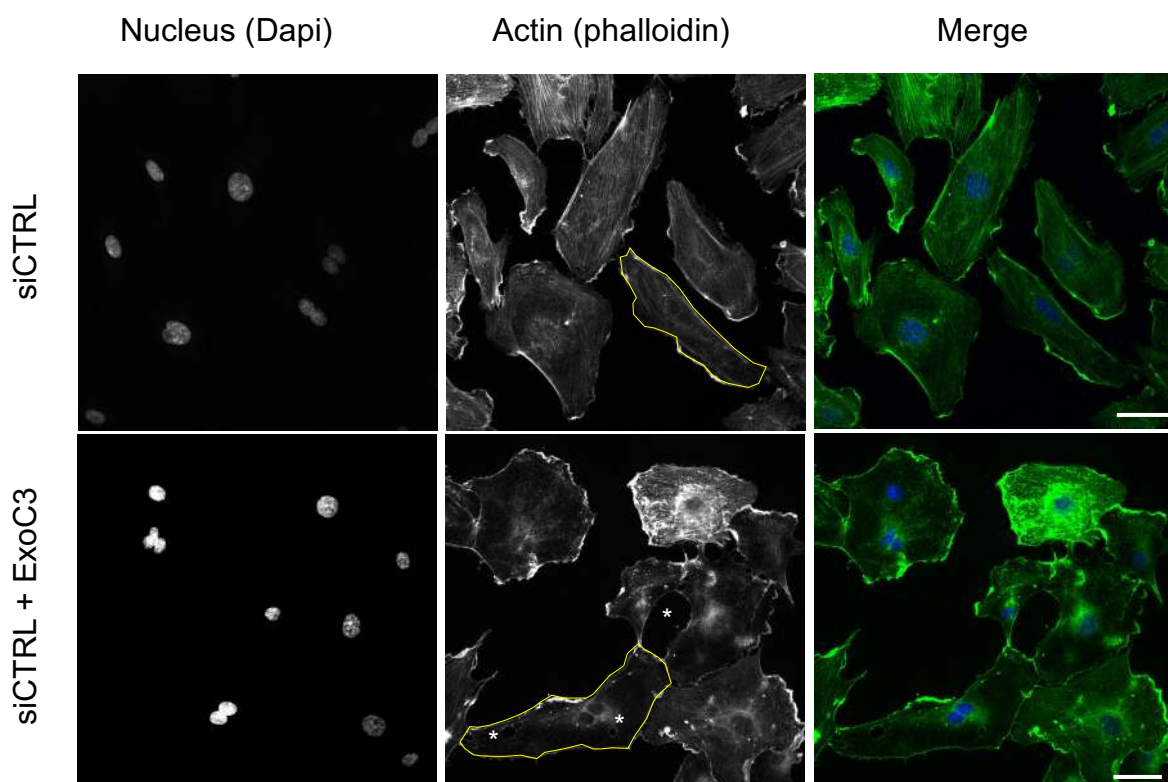


Figure 53. Example of a confocal micrographs of cells show the spreading determination process. Confocal images of HUVEC control (high panel) or intoxicated with ExoC3 (low panel). A cell perimeter is depicted in yellow as an example in each condition. Stars show TEMs.

Interestingly, while depletion of cav1 had no significant effect, the knock down of cavin1/PTRF led to a significant increase of the area of non-intoxicated cell, as compared to siCTRL treated cells. Nevertheless, we recorded a slight increase of the spreading of cells in siCAV1-treated cells, and no difference was recorded between siCAV1 and siPTRF transfected cells (Fig. 54).

When cells were intoxicated with ExoC3, we measured a 1.4-fold increase of the area of cells compared with non-intoxicated cells. Despite the induction of spreading due to ExoC3 treatment, we measured in both siCAV1 and siPTRF KD cells a spread area mark-up that was significant in both conditions (Fig. 54).

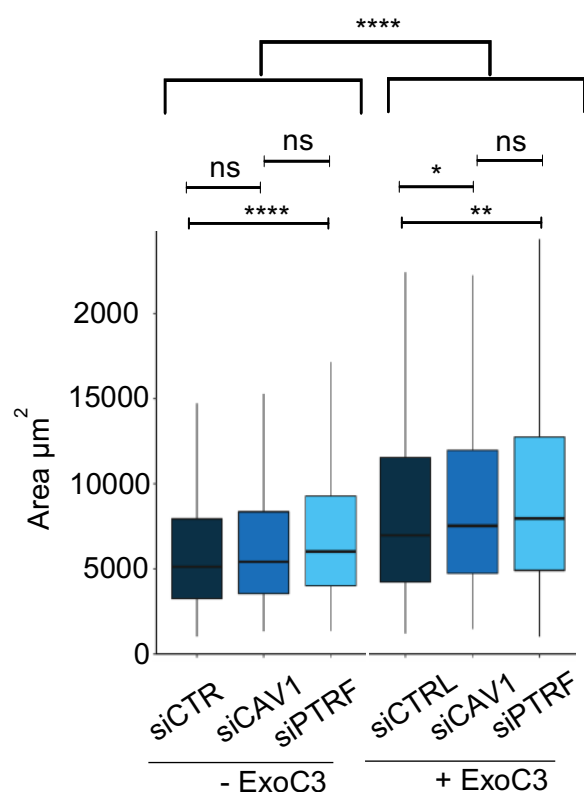


Figure 54. Cavin1/PTRF plays key role in the control of the spreading of HUVEC.

Boxplot shows distributions of areas of HUVEC treated with siCTRL, siCAV1 or siPTRF prior to ExoC3 treatment for 24h ($n > 698$ cells, 5 biological replicates). Linear mixed model with random intercept accounting for technical replicates and fixed effects applied on a log₁₀ scale of the cell surface areas. **** $P < 0.0001$, pair conditions between control (-ExoC3) and +ExoC3 condition, siCTRL and siPTRF; * $P < 0.05$ (siCTRL and siCAV1) +ExoC3, ** $P < 0.01$ (siCTRL and siPTRF) +ExoC3. Comparisons of other conditions show no significant difference (Mean \pm s.d.: siCTRL = $6,582.9 \pm 5,168 \mu\text{m}^2$, siCAV1 = $7,048.1 \pm 5,583 \mu\text{m}^2$ or siPTRF = $7,539.1 \pm 5,450 \mu\text{m}^2$ vs siCTRL+ExoC3 = $9,024.6 \pm 7,258 \mu\text{m}^2$, siCAV1+ExoC3 = $9,831.3 \pm 7,984 \mu\text{m}^2$ or siPTRF+ExoC3 = $10,139.1 \pm 7,873 \mu\text{m}^2$).

We concluded from these experiments that RhoA together with cavin1/PTRF work against spreading of HUVECs in both control and ExoC3-treated cells with cav1 displaying a significant effect limited to the ExoC3 condition.

5. CAVEOLIN1 AND CAVIN1/PTRF IN THE CONTROL OF CELL VOLUME

Previous studies have determined that cells decrease their volume as they spread in order to minimize the otherwise increase of membrane tension (Xie, Yang, et Jiang 2018). Cell height is directly proportional to the volume divided by the surface and is therefore expected to be a key parameter in the rate of membrane fusion for nucleation of TEMs (Ng et al. 2017).

We went on to assess the function of cav1 and cavin1/PTRF in the regulation of the cell volume. Variations of cell volume was monitored by the FITC-dextran-exclusion fluorescence method in cells depleted for cav1 or cavin 1, with or without treatment by the ExoC3 (**Fig. 55**) (Zlotek-Zlotkiewicz et al. 2015). We collaborated with Matthieu Piel (Institut PierreGilles de Gennes) and Nnshit Srivastava (post-doctoral fellow), to perform these experiments. In ExoC3-treated cells, we recorded an increase of the volume of cells in all conditions as compared to non-intoxicated cells, indicating that RhoA inhibition triggers an increase of the volume of cells. For example, upon inhibition of RhoA by ExoC3 HUVECs significantly displayed a significant increase of volume from 2,384 μm^3 to 2,727 μm^3 . Interestingly, we measured that siCAV1 and siPTRF treatments induced a decrease of the volume of ExoC3-treated cells, compared with siCTRL-treated cells. In cells that were not intoxicated, we only recorded a decrease of volume due to cavin1/PTRF depletion. We concluded that cavin1/PTRF works against adjustment of cell volume during cell spreading as well as cav1 in ExoC3-treated cells (**Fig. 55**).

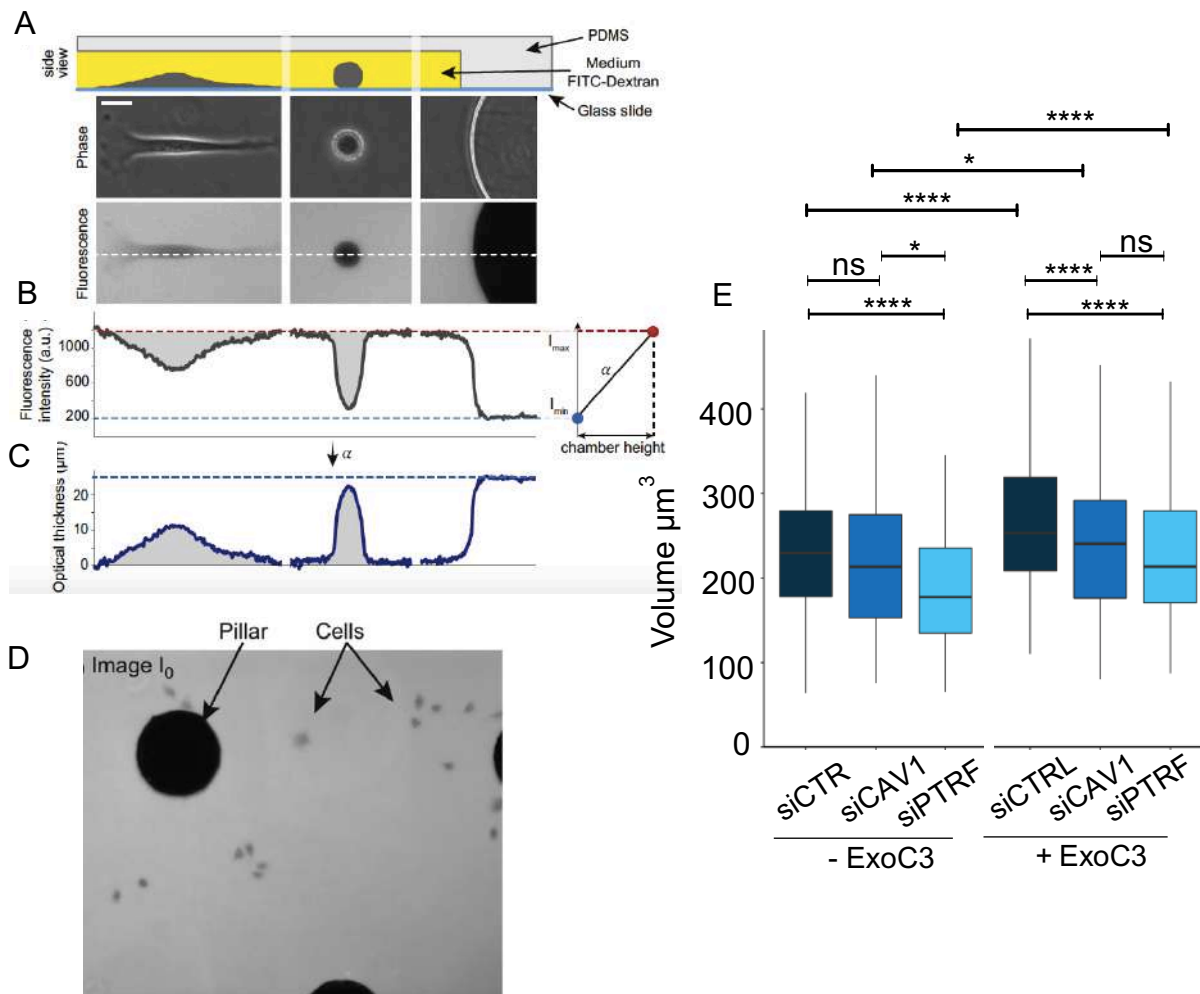


Figure 55. Cavin1/PTRF plays key role in the control of the volume of HUVEC.

(A) Cells placed in PDMS chambers of calibrated height set by pillars. SFMc is supplemented with FITC-Dextran. Bottom panel: cells exclude fluorescence on epifluorescence images (Scale bar 20 mm). (B) The fluorescence profile corresponding to the dotted line in (A): maximum and minimum of fluorescence intensity correspond to chamber maximal height (background) and zero height (pillar), respectively. Right: these values are used to calibrate the signal and calculate the optical thickness of the cells. (C) Finally, cell volume is obtained by integrating the total fluorescence intensity over the cell area (Cadart et al. 2017).

(D) Raw image of a typical field observed with a 10x objective NA0.3. A pillar sustaining the ceiling is on the left and parts of two other pillars can be observed on the edges of the field. HeLa cells appear in grey (E) Boxplot shows distributions of volume of HUVEC treated with siCTRL, siCAV1 or siPTRF prior to ExoC3 treatment for 24h ($n > 152$ cells per conditions, 3 biological replicates). Linear mixed model with a gamma link function. * $P < 0.05$, pair conditions between control (-ExoC3) and +ExoC3 treatment, **** $P < 0.0001$ between siCTRL and siPTRF; * $P < 0.05$ between siCAV1 and siPTRF **** $P < 0.0001$, (siCTRL and siCAV1) +ExoC3 and (siCTRL and siPTRF) +ExoC3. Comparisons of other conditions show no significant difference (Mean \pm s.d.: siCTRL = $2,320.4 \pm 214.1 \mu\text{m}^3$, siCAV1 = $2,146.3 \pm 197.1 \mu\text{m}^3$ or siPTRF = $1,914.3 \pm 178.3 \mu\text{m}^3$ vs siCTRL+ExoC3 = $2,710.0 \pm 246.5 \mu\text{m}^3$, siCAV1+ExoC3 = $2,357.9 \pm 214.4 \mu\text{m}^3$ or siPTRF+ExoC3 = $2,282.3 \pm 213.2 \mu\text{m}^3$).

Altogether, these data suggest that upon RhoA inactivation, siCAV1 and siPTRF treatments decrease cell volume concomitantly to the spreading of cells, which are expected to work together to reduce the cell height. Thinner cells then ease TEMs nucleation, likely by favoring the fusion of dorsal and basal membranes.

6. DIFFERENTIAL IMPACT OF CAVIN1/PTRF AND CAVEOLIN1 ON TEM DYNAMICS

We set a high-throughput analytical pipeline of live cell video imaging to define TEM dynamics parameters of speed and maximal area. This relies on the visualization of Lifeact-GFP signal accumulation at the edge of TEMs (Stefani et al. 2017). Post-processing analysis of the confocal video micrographs allowed us to define each Lifeact-GFP TEM-periphery as regions of interest (ROI) using a refined version of custom-made Icy-based analytical program, described previously and developed by Stephane Dallongeville in the group of JC Olivo-Marin at the Pasteur Institute (See annexe: Tsai et al., under revision). We identified each TEM as ROI and we analyzed the distribution and the extent of all initial area of TEM tunnels recorded during 1 hour at an acquisition rate of 1 second per image, in cells depleted for cav1 or cavin1/PTRF and treated by the ExoC3. We first established a heat-map of TEM opening, allowing us to observe that TEMs are evenly distributed along the periphery of cells with a low level of overlap of initial opening area (**Fig. 56**). Consistent with our analysis of fixed cells, we observed a higher density of TEMs in siCAV1 and siPTRF conditions, as compared to siCTRL (**Fig. 56**).

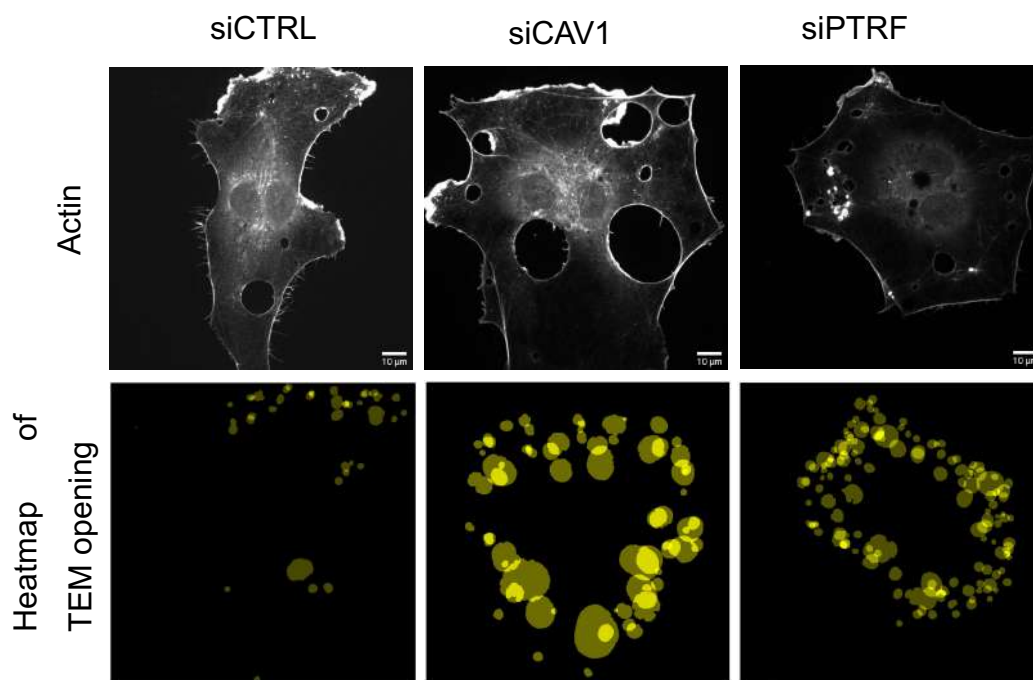


Figure 56. Heatmap of TEMs opening in HUVEC

Heat maps show cumulative initial TEM areas in cells (yellow patch) recorded by time-lapse microscopy during 1 hour with an image acquisition rate of 10 seconds. HUVEC treated with siCTRL, siCAV1 or siPTRF prior to 24h of treatment with ExoC3. Scale bar represent 10 µm.

Furthermore, this semi-automated protocol allowed us to draw the kinetics of TEM area variations as a function of time (**Fig. 57**). TEM cycle takes about 10 to 15 minutes. Kinetics allowed us to extract the mean area of TEM for each time point, here ten seconds.

Strikingly, we observed wider TEMs in siCAV1 treated cells. Indeed, this method established that the mean maximal area of TEMs expand by 5.4-folds in siCAV1 cells as compared to siCTRL condition. In addition, no specific variation of TEM size was recorded between siPTRF and siCTRL conditions (Fig. 57A). This was suggestive of a specific effect of caveolin1 with regards to cavin1/PTRF function.

To thoroughly analyze parameters of speed of opening, we performed a second set of time-lapse video recording at a 10-fold higher speed *i.e.* ten seconds (Fig. 57B). This established a high resolution of TEM kinetics and allowed us to extract the t_{max} *i.e.* the value of time for which TEM reach their maximal size. In all conditions, most TEMs stop their widening after about 1 minute (values are shown in figure 44B, inset) despite variations of maximal size. Refined analysis of TEM opening speed allowed us to capture with high resolution the parameters of TEM opening phase. We measured no significant variation of the opening speed of TEMs between the conditions siCTRL and siPTRF (Velocity of opening from the opening of TEM until it reaches its maximal size : V_o : $V_{o_siCTRL} = 66.8 \mu m^2/ min$ versus $V_{o_siPTRF} = 102 \mu m^2/ min$, $P=0.4$). In contrast, we recorded a higher speed of TEM opening in CAV1-depleted cells $V_{o_siCav1} = 146.5 \mu m^2/ min$, that was significant compared to siPTRF or siCTRL conditions ($P \leq 0.02$). This established that cav1 specifically controls the TEM opening speed (Fig. 57B).

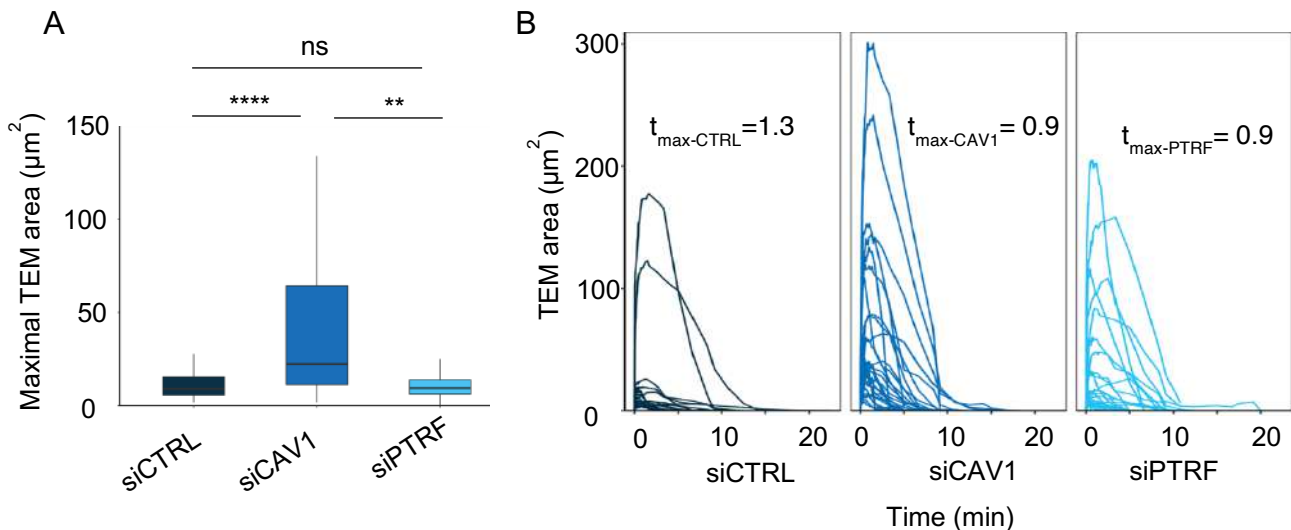


Figure 57. Caveolin1 controls parameters of speed of TEM opening and maximal size.

(A) Boxplot shows values of TEM maximal area in HUVECs transfected with siCTRL, siCAV1 or siPTRF prior to 24h of treatment with ExoC3. TEM maximal area were determined from the kinetics shown in b. Means \pm s.d.: siCTRL= $6.21 \pm 1.7 \mu m^2$, siCAV1= $33.8 \pm 9.16 \mu m^2$ and siPTRF= $10.6 \pm 3.77 \mu m^2$ ($n > 107$ TEMs per condition and $N = 7$ cells per conditions, biological replicates > 3 ; biological replicates were pooled). Acquisition rate: one image every ten seconds. Significant differences, means were estimated by a linear mixed model, with random intercept accounting for technical replicates: **** $P < 0.0001$, siCAV1 vs siCTRL or siPTRF. No significant difference between siCTRL and siPTRF. (B) Graph shows variations of TEM areas as a function of time expressed in minute (min). HUVECs transfected by siCTRL, siCAV1 or siPTRF were treated 24h with ExoC3 ($n > 107$ TEMs per condition and $N = 7$ cells per conditions, biological replicates > 3). Acquisition rate: one image per second. In all conditions, most TEMs stop their widening after about 1 minute (value t_{max} siCTRL= 1.33 ± 1.5 min; t_{max} siCAV1= 0.9 ± 0.6 min; t_{max} siPTRF= 0.9 ± 1.1 min). No significant difference, Kruskal-Wallis test: $P = 0.25$.

Using theoretical modeling, we analyzed the impact of key membrane parameters on TEM dynamics. We generalized our previously published model of TEM dynamics (Gonzalez-Rodriguez et al. 2012; Stefani et al. 2017) to account for the presence of several TEMs opening simultaneously. The model relies on the strong hypothesis that plasma membrane can be described by two effective parameters: the effective plasma tension and bending rigidity, which considers the adhesion of the actin cortex. As detailed in the Materials and Methods section, the model predicts that the initial TEM opening speed (v_i), few seconds after TEM opening, is proportional to the effective membrane tension, including both in plane membrane tension and membrane adhesion to cortical components (Sens et Plastino 2015). This defines TEM nucleation and its extent of growth.

Starting from values extracted from the literature in control conditions ($\sigma_0 = 2.5 \cdot 10^{-5}$ N/m, (Raucher Sheetz 2000) and $\kappa = 40 K_B T$ (Gonzalez-Rodriguez et al. 2012; Lipowsky et Sackmann 1995), the model predicts a significant 2-fold increase of effective membrane tension upon cav1 depletion, but no significant effect in siPTRF condition as compared to siCTRL. It also predicts an effective bending rigidity that is ~ 1.5 -fold smaller upon silencing cavin1/PTRF, whereas it is 3-fold smaller upon silencing CAV1 than under control conditions. These predictions are in good agreement with numerical fits of average opening curves by the full model, shown in **figure 59**.

In conclusion, Altogether, acknowledging the approximate nature of the model estimates due to the simplifying physical hypotheses, the model suggests that a moderate decrease of effective bending rigidity accounts for variation of TEM opening in siPTRF conditions and that cav1 controls both effective membranes bending rigidity and tension in opposite directions to concur to limit the widening of TEMs (**Table 4, Fig. 58**).

Conditions	σ_0 ($\mu\text{N/m}$)	A_{max} (μm^2)	N (average)	$(N \cdot A_{\text{max}})^{-1}$ (μm^{-2})
siCTRL	25 ± 10	8.1 ± 0.5	0.90 ± 0.09	0.137 ± 0.02
siCAV1	50 ± 7	23 ± 4	1.92 ± 0.15	0.023 ± 0.006
siPTRF	29 ± 7	9.3 ± 0.7	1.34 ± 0.11	0.08 ± 0.012

Table 4. Caveolin1 controls effective membrane bending rigidity and tension. Table shows estimate of the variation of the mechanical cell parameters between different experimental conditions. The value of the effective membrane tension σ_0 for the control case is taken from earlier estimates (Stefani et al., 2017). The increase of σ_0 in siCAV1 and siPTRF conditions were deduced from our experimental data using Eq. 10. Each TEM maximum area A_{max} is taken as its median and calculated from the experimental data. As discussed in the text, the variations of effective membrane bending rigidity are roughly proportional to variations of $(N \cdot A_{\text{max}})^{-1}$, where N is the average number of simultaneous TEMs and A_{max} is the TEM maximum area, which are deduced from the experimental data.

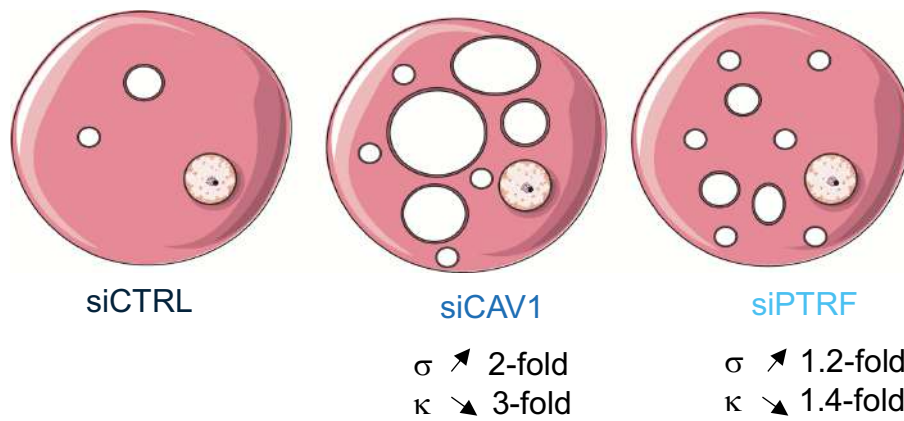


Figure 58. Caveolin1 controls effective membrane bending rigidity and tension.

Scheme depicting key findings of our results, framed in the cellular dewetting model. It describes the major forces at play in transendothelial macroaperture tunnel opening in HUVECs transfected with siCTRL, siCAV1 or siPTRF prior to intoxication with ExoC3 for 24h. siPTRF and siCAV1 both controls TEM nucleation by reducing cell volume and increasing cell spreading. siCAV1 controls physical parameters: it increases effective membrane tension (σ) and decrease effective bending rigidity (κ).

These predictions are in good agreement with numerical fits of average opening curves by the full model, as shown in **Fig. 59**. Therefore, the good fit between the theoretical model and the raw data allow us to make the hypothesis that cav1 controls both the effective membrane bending rigidity and tension in opposite directions thereby cooperating in limiting the widening of TEMs.

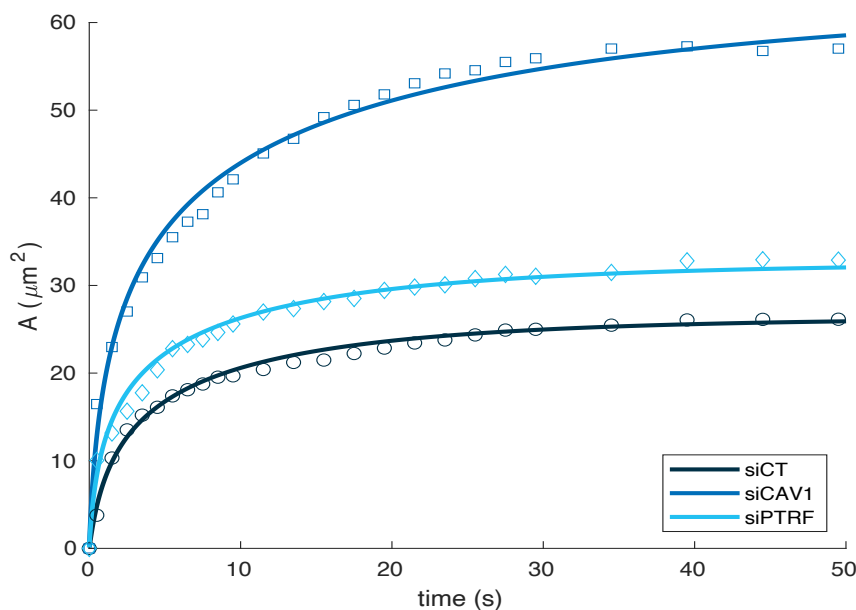


Figure 59. Caveolin1 controls effective membrane bending rigidity and tension.

Graph shows variations of initial TEM areas as a function of time expressed in second. Data recorded from time-lapse video set with an image acquisition rate of 1 second for 30 minutes. HUVEC were treated with siCTRL, siCAV1 or siPTRF prior to intoxication with ExoC3 for 24h. Fit based on the theoretical dewetting model (plain curve) of the experimental data (markers) under experimental conditions siCTRL (dark blue), siCAV1 (medium blue) and siPTRF (light blue) ($n > 22$ TEMs per condition, 4 biological replicates).

7. DIFFERENTIAL IMPACT OF CAVEOLIN AND CAVIN ON MEMBRANE RIGIDITY

Our theoretical description of TEM dynamics suggests that cav1 regulate the effective membrane bending rigidity as well as membrane tension. We tested this hypothesis by directly measuring the physical properties of membrane using a tether pulling experiment (Bo et Waugh 1989) from plasma membrane spheres (PMS) (Lingwood et al. 2008) following a previous study that focused only on the role of cav1 in membrane tension regulation (Sinha et al., 2011). We collaborated with Patricia Bassereau and Fen-Chin Tsai (Institut Curie) to perform these experiments. Briefly, PMS, prepared from control or CAV1 KD or cavin1/PTRF KD HUVECs, were aspirated in a micropipette to control membrane tension and membrane tethers were pulled using optical tweezers (**Fig. 60B**).

The pulling forces were then modulated as a function of aspiration pressure increase in the micropipette, which set the membrane tension of the spheres (Bo et Waugh 1989). As the force scales with the square root of the bending rigidity and the plasma membrane $f = 2\pi\sqrt{(2\cdot\kappa\cdot\sigma)}$, analysis of the slope of the force vs square root of membrane tension curve gave access to the bending rigidity (**Fig. 60A**). We quantified the bending rigidity in different conditions from preliminary experiments (**Fig. 60A,B,C**). We observed that it was significantly decreased in siCav1 conditions ($\kappa \sim 9 \pm 2 \text{ k}_B\text{T}$, $p=0.03$) compared with control ($\kappa \sim 18.4 \pm 6 \text{ k}_B\text{T}$), and moderately decreased in the case of siPTRF condition ($\kappa \sim 12.5 \pm 2 \text{ k}_B\text{T}$, n.s. $p=0.1$). At least three tubes were pulled by conditions, but the experiments were performed twice for siCav1 and siPTRF and only once for siCTRL. Our preliminary measurements are in qualitative agreement with the predictions from the theoretical models and reinforce our hypothesis that cav1 controls the TEM dynamics by regulating the membrane mechanical properties. However, the lack of repeats and the low statistics presented here make us be very careful with the interpretation of the results. Besides, we need to make sure, as in the Sinha, Koster et al., paper (2011), that there is a tongue present in the micropipette in order to validate the calculations of the bending rigidity, which remains, for the moment only estimations.

More work will be necessary after this thesis to perform the repeats and to validate the accuracy of the experimental conditions.

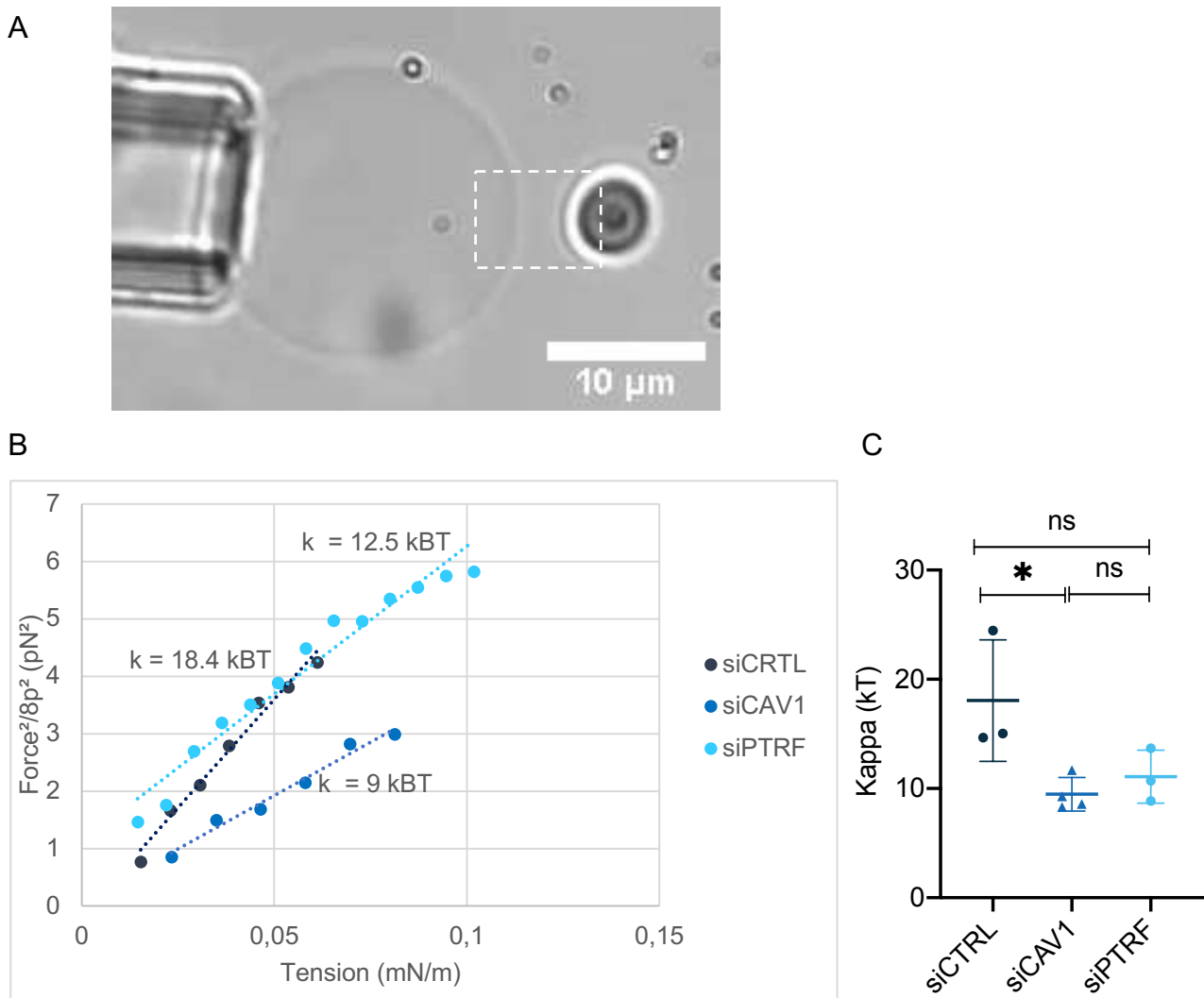


Figure 60. Caveolin1 controls effective membrane rigidity and tension

Measure of bending rigidity by tether pulling experiments. **(A)** Confocal DIC image of a classical tube pulling experiment on a plasma membrane spheres (PMS) produced by HUVECs treated by ExoC3 during 24h. Dotted square shows were the tube forms between the PMS and the bead **(B)** Representative force-extension curve at different tensions, fixed by micropipette aspiration. Curves were established with one representative tube by condition. The slope of the curve gives the bending rigidity **(C)** Boxplot of the quantification of the bending rigidity in HUVECs transfected with siCTRL, siCAV1 or siPTRF prior to intoxication with ExoC3 for 24h. Geometric means \pm SD, siCTRL $\sim 18 \pm 6$ k_BT, siCAV1 $\sim 9 \pm 2$ k_BT, siPTRF $\sim 11 \pm 2$ k_BT. Significant differences, t-test: siCAV1 conditions $\sim 9 \pm 2$ k_BT (SD, n=4, p=0.03) compared with control $\sim 18 \pm 6$ k_BT (, n=3), and moderately decreased in the case of siPTRF $\sim 11 \pm 2$ k_BT (SD, n=3, n.s. p=0.1).



V. Discussion

Our data unveil key findings on the control of plasma membrane mechanical properties and cell shape by caveolin1 and cavin1/PTRF. First, our data framed in our cell dewetting model (Gonzalez-Rodriguez et al. 2012; Stefani et al. 2017) show that cav1 controls parameters of effective membrane bending rigidity and likely effective membrane tension that concur to limit the widening of TEMs. Second, we show that cavin1/PTRF controls cell parameters of spreading and volume, *i.e.* cell height, as well as interferes with membrane bending rigidity but to a lower extent compared to cav1. We propose that together this reflects a difference in intrinsic function of caveolin1, a protein anchored in the PM inner leaflet, compared to that of cavin1/PTRF, which controls organization of cavin1 oligomers into the flask-shaped caveolae. Difference of functions highlighted here between caveolin1 and cavin1/PTRF point for the control of effective membrane bending rigidity by caveolin1 as a dominant regulation of TEM opening speed and width, as predicted by the model.

Analysis of TEM dynamics assigns a specific function to caveolin1 for the control of TEMs opening size. Importantly, we provide compelling evidence that cav1 controls the effective bending rigidity. This is supported by direct assessment of membrane mechanical properties on PMS-derived from CAV1 knocked down endothelial cells. As the cortical actin is strongly disrupted by the RhoA inhibition induced by the exoC3 treatment, we assume here that the contribution of the membrane to the effective bending rigidity is prevailing over the contribution of the cortical actin. Therefore, the effective bending rigidity, which sets the TEM dynamics of opening, is dominated by the membrane contribution. This also justifies, why the Helfrich model, originally established for lipidic membrane, could still be applied in our cell dewetting model and applied to plasma membrane (Gonzalez-Rodriguez et al. 2012; Stefani et al. 2017).

Strikingly, our findings show that the effect of cav1 depletion is not phenocopied by the knocking down of cavin1/PTRF. This is in favor of a function of cav1 independent from that of cavin1/PTRF scaffolding function of cav1 pits. Interestingly, it has been shown that cav1 is inserted into the inner leaflet of the plasma membrane and oligomerizes to form higher order caveolae pits and plates (Kurzchalia et al. 1992; Schlegel et Lisanti 2000). Thus, one likely hypothesis is that caveolin oligomers anchored in the inner leaflet of plasma membrane fulfil a scaffolding function in interaction with the cytoskeleton cortex to rigidify membranes. A none exclusive hypothesis is that this may also involve a partitioning of cholesterol and sphingolipids in caveolin domains.

We attribute to cavin1/PTRF a major function in regulating cell shape, *i.e.* cell spreading and volume, and therefore on TEM nucleation. This function is shared by caveolin1 in the context of RhoA inhibition. The concomitant spreading of cells associated with a decrease of their volume in ExoC3-treated cells affects cell height. To that respect, depletion of cav1 and cavin1/PTRF has an impact on the height that we link to the increase of nucleation rate of TEMs in ExoC3-treated cells. This is in good agreement with previous data on mechanically-induced TEMs showing that force-induced contact between apical and ventral plasma membranes is sufficient to trigger the nucleation of transcellular tunnels (Ng et al. 2017): the smaller the distance between apical and basal membrane is and the easier it is to induce fusion between them. In addition, we show here that cavin1/PTRF depletion has a moderate impact on the regulation of membrane properties. However, this could be a consequence of cross depletion of caveolin1 upon siPTRF, shown in Fig. 41, and previously reported (Kim et al. 2008). Similarly, regulatory function of cav1 on cell shape likely could reflect cavin1/PTRF depletion due to cross reaction upon siCAV1 treatment. Thus, careful conclusions should be made relative to weak effects of siPTRF. Hence, our major conclusion on cavin1/PTRF function is its broad role in the control of cell shape, *i.e.* spreading and volume.

An analogy was previously drawn between the phenomenon of adhesion of cells to the extracellular matrix and compression of cells by external forces, considering that both phenomena force cells to contact their adhesive substrate (Stewart et al. 2011). Moreover, compressive forces applied to a cell, whether they have intact or blunted RhoA/ROCK signaling, promote the opening of TEMs (Ng et al. 2017). It has been reported that the volume of cells decreases proportionally to the extent of cell spreading over the adhesive substrate, unless Rho kinase signaling is abrogated (Xie et al. 2018). Here, we confirm that inhibition of RhoA by ExoC3 intoxication leads to a default of volume adjustment during spreading, *i.e.* default in the so-called mechanism of adhesion-induced compression of cells (Xie et al. 2018). This absence of adjustment is expected to modulate membrane tension, which is involved in the force-induced TEM nucleation and opening, as described in the cellular dewetting theory (Gonzalez-Rodriguez et al. 2012). In the absence of volume regulation, we expect membrane tension to increase, thus promoting TEM opening. In contrast, volume regulation will compensate the spreading effect and thus lead towards conservation of membrane tension. Our experiments show a reduction of cell height in siPTRF and siCAV1, which further increases TEM nucleation while decreasing cell volume.

Together, this indicates that siPTRF and siCAV1 induce TEM nucleation by a decrease of cell height, which is most likely a dominant effect over their modulation of membrane tension.



VI. Conclusion, perspectives

I report here the study of the role of two major proteins of omega-shaped caveolae, namely caveolin1 and cavin1, in the formation and the of transendothelial cell macroaperture (TEM) tunnels that are induced by RhoA-targeting bacterial ADP-ribosyltransferases of the ExoC3 family. This work uncovers two specific functions for these proteins in the regulation of 1) membrane mechanical properties and 2) cell shape. This also opens important perspectives, as discussed below, 3) in cell biology with regards to caveolin1 versus caveolae-dependent processes as well as 4) physiology or pathophysiological processes.

8. CAVEOLINS VS CAVEOLAE IN SIGNALLING PROCESSES

Our data point here for independent roles of caveolin1 and cavin1/PTRF on the regulation of cell shape and membrane mechanics. This points for a role of caveolin that is independent from caveolae pit regulation. In line with this idea, caveolae could not be detected in the liver and brain, whereas cav1 is present and cavin1 is absent (Bastiani et al. 2009; Echarri et Del Pozo 2015). A specific role of caveolin1 has been already hypothesized (Pol et al. 2020). Our data point for a role on cavin1 in the stiffening of these cellular membranes, such as in scaffolding domains where cav1 exhibits an increased lateral mobility (Kim et al. 2008).

Much remains to be learned on the distinct function of caveolin1 independent from structuration of caveolae pits. Our data are in good agreement with these findings. Indeed, our results point towards a distinct non-caveolar role of cav1 in the control of TEM dynamic, through the modulation of mechanical properties of the PM. However, we still lack the underlying signalization events explaining this phenotype.

A relevant hint that should be investigated is the involvement of the Hippo pathway in TEM regulation. The Hippo pathway consists of a series of kinases that control the localization and stability of the Yes-associated protein (YAP) and transcriptional coactivator with PDZ-binding motif (TAZ), which are homologous transcriptional co-factors that relocate to the nucleus to regulates genes, including CAV1 and CAVIN1/PTRF (Rausch et al. 2019). YAP is also controlled by mechanical signals, such as ECM stiffness, shear stress, and stretching (Codelia, Sun, et Irvine 2014; Dupont et al. 2011; Zhong et al. 2013). Furthermore, caveolar-mediated shear stress response activates YAP/TAZ signalling (Rausch et al. 2019). In addition, CAV1 positively modulates the YAP mechano-responses to ECM stiffening through actin cytoskeleton-dependent mechanisms.

Constitutive YAP activation rescued phenotypes associated with CAV1 loss, including defective ECM remodeling. Therefore, it would be interesting to investigate the involvement of YAP/TAZ signalling in the regulation of TEMs involving caveolae and cav1. A first approach would be to disrupt YAP/TAZ signalling in cells prior to intoxication, and to monitor the effect of such treatment of TEM dynamics. Next, it would be pertinent to observe the localization of YAP/TAZ in both siCAV1 and siCAVIN/PTRF condition. This would be accompanied by the location of YAP/TAZ in cells treated by the ExoC3.

Another possible aspect is the implication of mTORC2, that acts through PM tension to control of actin cytoskeleton assembly and endocytosis (Diz-Muñoz et al. 2016; Riggi et al. 2019). The coupling between tension and volume was shown to be regulated by the actin cytoskeleton, ion channels and mTOR signalling to maintain a quantitative relation between volume and tension well described by passive physical mechanisms (Roffay et al. 2021). Our data suggest that cav1 depletion increases the PM tension, promoting TEM formation. Therefore, it would be interesting to investigate the involvement of mTORC2 signalling in the regulation of TEMs. A first approach would be to monitor the activation of mTORC2 in intoxicated cells and in cells depleted for cav1 and cavin1. Next, it would be pertinent to investigate the effect of the disruption of mTORC2 signalling in cells submitted or not to intoxication, and to monitor the effect of such treatment of TEM dynamics.

Flattening of caveolae triggers a release of accessory proteins together with Cavin1/PTRF, into the cytoplasm. Numerous proteins have been identified as targets of cavin/PTRF (McMahon et al. 2019), which was originally described as a transcription factor (Jansa et al. 1998). Interestingly, caveolae flattening triggers a release of cavin1/PTRF in the cytoplasm. Free molecules of cavin1/PTRF act as transcription factors (Jansa et al. 1998). In adipocytes, indicating a caveolae-independent rDNA transcriptional role of cavin1/PTRF has been described in response to metabolic challenges (Liu et Pilch 2016). This suggest that in our case, disruption of caveolae by cav1 silencing could trigger cavin1/PTRF release, which could interact with various target genes to regulate their transcription. Such genes could be involved in the cell response to mechanical constrains, as in the case of YAP/TAZ and mTORC2 signalling. The idea would be to perform genomic analysis including chromatin immunoprecipitation combined with microarray screening and bioinformatic approaches. This would first be done in cells depleted for cav1, in order to observe how cavin1 targeted genes are regulated as compared to control, when the cells

face PM tension increase and a PM bending rigidity decrease induced by caveolae disruption coupled to ExoC3 treatment.

9. MEMBRANE MECHANICAL PROPERTIES

9.1. IMPACT OF CHOLESTEROL DEPLETION AND PERTURBATION OF PM LIPID COMPOSITION

First, we elucidate a new role of caveolin1 in the regulation of effective membrane bending rigidity and tension. We make the hypothesis that caveolin1 forms rafts or cups inserted in the membrane leaflet that have a scaffolding function in connection with the underneath cortical cytoskeleton. This important question calls for further analysis of the structural function of caveolin and other membrane associated proteins or lipids.

However, one cannot exclude that cav1 phenotype may also involves the partitioning of cholesterol, PS and PIP3 to the PM in caveolae or non-caveolar domains (Zhou et al. 2021). Therefore, as a perspective, an interesting approach would be to investigate whether depletion of cholesterol could mimic the effect of cav1 depletion, and impact TEM formation. Methyl- β -cyclodextrin (M β CD) is a cyclic hepta-saccharide presenting affinity to cholesterol due to the presence of hydrophobic core. The molecule forms a torus-like shape with a hydrophobic interior, scavenging cholesterol molecules. Therefore, M β CD is commonly used as a complexing agent to deplete cholesterol from the PM, or to enriched cholesterol by exposing the cells to M β CD saturated with cholesterol. Multiple studies suggest that cholesterol stiffen PM (Chakraborty et al. 2020). Upon cav1 depletion we showed that bending rigidity decrease, therefore the presence of inserted cav1 stiffen the PM. Assuming that the specific phenotype of cav1 depends solely on cholesterol trafficking to the PM, we would expect a similar effect between cav1 depletion and cholesterol depletion.

Interestingly, PS depletion reduces EM-detectable caveolae, suggesting that PS is involved in caveolae stability and formation (Hirama et al. 2017). It would be interesting to perturb the amount of PS (depletion/insertion) on TEM dynamics in order to verify to what extent the phenotypes observed in cav1 and cavin1 depletion could be reproduced and to investigate possible rescue experiments.

Of note, we showed that cavin1/PTRF depletion slightly affect the bending rigidity compared with cav1 depletion. Yet, we cannot rule out that the effect of cavin1/PTRF on bending rigidity may be a cross-depletion effect of siCAV1 on cavin1/PTRF level (Hill et al. 2008). This absence of important effect of cavin1/PTRF in membrane with regard to a potential effect of cholesterol is consistent with an absence of impact of cavin1/PTRF on cholesterol trafficking to the PM (Zhou et al. 2021). We showed that TEM nucleation is higher in both KD conditions. Therefore, the disturbance of cholesterol trafficking by cav1 depletion could explain the role of cav1 in regulating TEM dynamics via the control of membrane bending rigidity. Nevertheless, this cannot explain the increase in TEM nucleation observed in cells depleted by cav1 or cavin1/PTRF.

9.2. LIPIDOMIC ANALYSIS

In a collaborative work with the group of H el ene Barelli and Bruno Antony (Tsai et al., under revision, Annexe 1; Laboratoire Institut de Pharmacologie Mol culaire et Cellulaire, Nice) we performed lipidomics analysis on cells enriched with polyunsaturated docosahexaenoic acid (22:6, DHA)-containing phospholipids (PLs) compared to oleic acid (OA). We observed that an increase in DHA-PLs induces a perturbation of PM homeostasis leading to an increase of the nucleation rate of TEM compared to OA diet. In view of our work on cav1 and cavin1, it would be interesting to perform similar lipidomics analysis on cells depleted for cav1 or cavin1. The idea would be to quantify their impact on the nature and the level of phospholipids at the PM, which could give us insights on their role in the control of membrane physical properties.

9.3. PROBING MEMBRANE MECHANICAL PROPERTIES OF THE PLASMA MEMBRANE

Caveolae are enriched at the retraction rear and leading edges of migration cells (Hetmanski et al. 2019). Whether membrane tension is a local or a global effect is still unclear, and studies reinforce both possibilities (Shi et al. 2018). To investigate this aspect, it would be interesting to use the Flipter probe developed by Colomb et al. in 2018, coupled to FILM imaging to visualize PM tension in cells depleted with cav1 and cavin1.

10. CELL SHAPE

In our study we demonstrated that *cav1* and *cavin1* depletion impact cell spreading and volume. To reinforce the hypothesis that the modification of cell shape is important for TEM nucleation and dynamics, it would be interesting to experimentally manipulate the cell height, whose decrease would favor the proximity of the ventral and dorsal membranes, and thereby promoting membrane fusion events and TEM nucleation. The idea would be to control cell area using micropatterned substrates. By limiting cell spreading, we expect to increase cell height and therefore decrease TEM nucleation. The impact on TEM dynamics and its regulation by *cav1* and *cavin1* would depend on how the physical properties of the membrane are modified. In the same line of thoughts, it would be interesting to investigate the impact of substrate rigidity. In our study we show that HUVECs spread more on substrates with high compliance which is concomitant to TEM nucleation. Yet, the impact on membrane properties is much less understood. Studying TEM dynamics in these conditions could reveal new mechanisms involved in mechanosensing.

11. PHYSIOLOGY AND PATHOPHYSIOLOGY PROCESSES

11.1. OTHER TOXINS

Another perspective of this work would be to challenge our findings on the role of *cav1* and *cavin1* on membrane physical properties, using other TEM-inducing toxins such as cyclic-AMP producing adenylate cyclase toxins from *Bacillus anthracis* and *Bordetella pertussis*. These toxins promote TEM formation through cAMP signalling (Maddugoda et al. 2011). Therefore, monitoring TEM formation in cells intoxicated with other TEM-inducing toxins and depleted for *cav1* and *cavin1*/PTRF would give us insight on the implication of caveolae and caveolar proteins at a broader spectrum.

11.2. *IN VITRO* SYNTHETIC BLOOD VESSELS

The lumen of the circulatory system is lined with endothelial cells that are submitted to intense mechanical stresses, such as shear stress induced by the blood flow, stretching due to vaso-constriction and dilation and ECM stiffness variation. In addition, caveolae are particularly rich at the PM of cells submitted to high mechanical stress, such as endothelial cells. Traditionally, endothelial cells are cultured in the absence of flow on stiff substrates

such as plastic. Therefore, the mechanics of cells is strongly biased. To overcome these limitations and to investigate if our results could be reproducible in more physiological conditions, we could use an *in vitro* microfluidic coextrusion device used to produce mature functional blood vessels. This device consists of an alginate hydrogel tube internally coated with extracellular matrix (Andrique et al. 2019). This would allow us to test how relevant physiological mechanical stress, such as cells curvature in tubular vessel and shear stress affects TEM formation. It would be also interesting to see how caveolae respond to these stresses. To do so, we would culture cells, with and without siRNA depletion of caveolar component, in this synthetic vessel perfused with medium contain ExoC3 toxins.

11.3. *IN VIVO* ANIMAL MODELS

Caveolins, mainly cav3 has been associated in multiple genetic human diseases such as lipodystrophies and muscles dystrophies (Pradhan et Prószyński 2020). Cav1 was also described in pathogenic infection although it was strongly suggested that it was because of its role in cholesterol trafficking (Duncan et al. 2004). In mouse, the EDIN toxin promotes the dissemination of the EDIN-producing *S. aureus* strain which then form disseminate foci across the mouse body. We hypothesize that caveolin1, through the control of TEM dynamics, could favor the dissemination of the bacteria. Indeed, our results show that cav1 governs the size and speeds of the TEM. To test this hypothesis, we would infect mice KO for cav1 with *S. aureus* bioluminescent strains producing the EDIN toxin. Similarly, to what has been performed by our lab collaborators, the formation of disseminated foci by the bacteria would then be monitored by imaging using an IVIS100 imaging system (Caliper Life Sciences Inc.) (Munro et al. 2010). We would expect a higher rate of disseminated foci in cav1 KO mice as compared to wild type mice. In addition, one would expect that increase rate and width of TEMs would promote animal death during infection, suggesting that cav1 could act as a susceptibility gene to infection.



VII. Bibliography

- Aboulaich, Nabila, Julia P. Vainonen, Peter Strålfors, et Alexander V. Vener. 2004. « Vectorial proteomics reveal targeting, phosphorylation and specific fragmentation of polymerase I and transcript release factor (PTRF) at the surface of caveolae in human adipocytes ». *Biochemical Journal* 383(Pt 2):237-48. doi: 10.1042/BJ20040647.
- Adamson, P., H. F. Paterson, et A. Hall. 1992. « Intracellular localization of the P21rho proteins. » *Journal of Cell Biology* 119(3):617-27. doi: 10.1083/jcb.119.3.617.
- Adesse, Daniel, Michael P. Lisanti, David C. Spray, Fabiana S. Machado, Maria de Nazareth Meirelles, Herbert B. Tanowitz, et Luciana Ribeiro Garzoni. 2010. « Trypanosoma cruzi infection results in the reduced expression of caveolin-3 in the heart ». *Cell cycle (Georgetown, Tex.)* 9(8):1639-46.
- Aimon, Sophie, Andrew Callan-Jones, Alice Berthaud, Mathieu Pinot, Gilman E. S. Toombes, et Patricia Bassereau. 2014. « Membrane Shape Modulates Transmembrane Protein Distribution ». *Developmental Cell* 28(2):212-18. doi: 10.1016/j.devcel.2013.12.012.
- Aktories, K., C. Wilde, et M. Vogelsang. 2005. « Rho-Modifying C3-like ADP-Ribosyltransferases ». P. 1-22 in *Reviews of Physiology, Biochemistry and Pharmacology*. Vol. 152, *Reviews of Physiology, Biochemistry and Pharmacology*. Berlin, Heidelberg: Springer Berlin Heidelberg.
- Albert, Henrik, Emily C. Dale, Elsa Lee, et David W. Ow. 1995. « Site-Specific Integration of DNA into Wild-Type and Mutant Lox Sites Placed in the Plant Genome ». *The Plant Journal* 7(4):649-59. doi: 10.1046/j.1365-3113X.1995.7040649.x.
- Albinsson, Sebastian, Ina Nordström, Karl Swärd, et Per Hellstrand. 2008. « Differential Dependence of Stretch and Shear Stress Signaling on Caveolin-1 in the Vascular Wall ». *American Journal of Physiology-Cell Physiology* 294(1):C271-79. doi: 10.1152/ajpcell.00297.2007.
- Alekhina, Olga, Ezra Burstein, et Daniel D. Billadeau. 2017. « Cellular Functions of WASP Family Proteins at a Glance ». *Journal of Cell Science jcs*.199570. doi: 10.1242/jcs.199570.
- Allingham, R. Rand, Annelies W. de Kater, C. Ross Ethier, P. John Anderson, Ellen Hertzmark, et David L. Epstein. 1992. « The Relationship Between Pore Density and Outflow Facility in Human Eyes ». *INVESTIGATIVE OPHTHALMOLOGY* 33(5):9.
- Anderson, Richard G. W. 1998. « The caveolae membrane system ». *Annual Review of Biochemistry* 67(1):199-225. doi: 10.1146/annurev.biochem.67.1.199.
- Andreone, Benjamin J., Brian Wai Chow, Aleksandra Tata, Baptiste Lacoste, Ayal Ben-Zvi, Kevin Bullock, Amy A. Deik, David D. Ginty, Clary B. Clish, et Chenghua Gu. 2017. « Blood-brain barrier permeability is regulated by lipid transport-dependent suppression of caveolae-mediated transcytosis ». *Neuron* 94(3):581-594.e5. doi: 10.1016/j.neuron.2017.03.043.
- Andrique, L., G. Recher, K. Alessandri, N. Pujol, M. Feyeux, P. Bon, L. Cognet, P. Nassoy, et A. Bikfalvi. 2019. « A Model of Guided Cell Self-Organization for Rapid and Spontaneous Formation of Functional Vessels ». *Science Advances* 5(6):eaau6562. doi: 10.1126/sciadv.aau6562.
- Antonny, Bruno, Stefano Vanni, Hideo Shindou, et Thierry Ferreira. 2015. « From Zero to Six Double Bonds: Phospholipid Unsaturation and Organelle Function ». *Trends in Cell Biology* 25(7):427-36. doi: 10.1016/j.tcb.2015.03.004.
- Ardissone, Anna, Cinzia Bragato, Lorella Caffi, Flavia Blasevich, Sabrina Maestrini, Maria Luisa Bianchi, Lucia Morandi, Isabella Moroni, et Marina Mora. 2013. « Novel PTRF Mutation in a Child with Mild Myopathy and Very Mild Congenital Lipodystrophy ». *BMC Medical Genetics* 14(1):89. doi: 10.1186/1471-2350-14-89.
- Ariotti, Nicholas, Manuel A. Fernández-Rojo, Yong Zhou, Michelle M. Hill, Travis L. Rodkey, Kerry L. Inder, Lukas B. Tanner, Markus R. Wenk, John F. Hancock, et Robert G. Parton. 2014. « Caveolae regulate the nanoscale organization of the plasma membrane to remotely control Ras signaling ». *Journal of Cell Biology* 204(5):777-92. doi: 10.1083/jcb.201307055.
- Arpaia, E., H. Blaser, M. Quintela-Fandino, G. Duncan, H. S. Leong, A. Ablack, S. C. Nambiar, E. F. Lind, J. Silvester, C. K. Fleming, A. Rufini, M. W. Tusche, A. Brüstle, P. S. Ohashi, J. D. Lewis, et T. W. Mak. 2012. « The Interaction between Caveolin-1 and Rho-GTPases Promotes Metastasis by Controlling the Expression of Alpha5-Integrin and the Activation of Src, Ras and Erk ». *Oncogene* 31(7):884-96. doi: 10.1038/onc.2011.288.

- Aspenström, Pontus, Åsa Fransson, et Jan Saras. 2004. « Rho GTPases Have Diverse Effects on the Organization of the Actin Filament System ». *Biochemical Journal* 377(2):327-37. doi: 10.1042/bj20031041.
- Austin, Eric D., Lijiang Ma, Charles LeDuc, Erika Berman Rosenzweig, Alain Borczuk, John A. Phillips, Teresa Palomero, Pavel Sumazin, Hyunjae R. Kim, Megha H. Talati, James West, James E. Loyd, et Wendy K. Chung. 2012. « Whole Exome Sequencing to Identify a Novel Gene (Caveolin-1) Associated with Human Pulmonary Arterial Hypertension ». *Circulation. Cardiovascular Genetics* 5(3):336-43. doi: 10.1161/CIRCGENETICS.111.961888.
- Barzilai, Sagi, Sandeep Kumar Yadav, Steven Morrell, Francesco Roncato, Eugenia Klein, Liat Stoler-Barak, Ofra Golani, Sara W. Feigelson, Assaf Zemel, Sussan Nourshargh, et Ronen Alon. 2017. « Leukocytes Breach Endothelial Barriers by Insertion of Nuclear Lobes and Disassembly of Endothelial Actin Filaments ». *Cell Reports* 18(3):685-99. doi: 10.1016/j.celrep.2016.12.076.
- Bastiani, Michele, Libin Liu, Michelle M. Hill, Mark P. Jedrychowski, Susan J. Nixon, Harriet P. Lo, Daniel Abankwa, Robert Luetterforst, Manuel Fernandez-Rojo, Michael R. Breen, Steven P. Gygi, Jorgen Vinten, Piers J. Walser, Kathryn N. North, John F. Hancock, Paul F. Pilch, et Robert G. Parton. 2009. « MURC/Cavin-4 and cavin family members form tissue-specific caveolar complexes ». *The Journal of Cell Biology* 185(7):1259-73. doi: 10.1083/jcb.200903053.
- Batchelder, E. L., G. Hollopeter, C. Campillo, X. Mezanges, E. M. Jorgensen, P. Nassoy, P. Sens, et J. Plastino. 2011. « Membrane Tension Regulates Motility by Controlling Lamellipodium Organization ». *Proceedings of the National Academy of Sciences* 108(28):11429-34. doi: 10.1073/pnas.1010481108.
- Bear, James E., Tatyana M. Svitkina, Matthias Krause, Dorothy A. Schafer, Joseph J. Loureiro, Geraldine A. Strasser, Ivan V. Maly, Oleg Y. Chaga, John A. Cooper, Gary G. Borisy, et Frank B. Gertler. 2002. « Antagonism between Ena/VASP Proteins and Actin Filament Capping Regulates Fibroblast Motility ». *Cell* 109(4):509-21. doi: 10.1016/s0092-8674(02)00731-6.
- Bearer, E. L., et L. Orci. 1985. « Endothelial fenestral diaphragms: a quick-freeze, deep-etch study. » *Journal of Cell Biology* 100(2):418-28. doi: 10.1083/jcb.100.2.418.
- Bergdahl, Andreas, et Karl Swärd. 2004. « Caveolae-associated signalling in smooth muscle ». *Canadian Journal of Physiology and Pharmacology* 82(5):289-99. doi: 10.1139/y04-033.
- Bergert, Martin, Sergio Lembo, Sumana Sharma, Luigi Russo, Danica Milovanović, Kristjan H. Gretarsson, Mandy Börmel, Pierre A. Neveu, Jamie A. Hackett, Evangelia Petsalaki, et Alba Diz-Muñoz. 2021. « Cell Surface Mechanics Gate Embryonic Stem Cell Differentiation ». *Cell Stem Cell* 28(2):209-216.e4. doi: 10.1016/j.stem.2020.10.017.
- Bernards, André. 2003. « GAPs Galore! A Survey of Putative Ras Superfamily GTPase Activating Proteins in Man and Drosophila ». *Biochimica Et Biophysica Acta* 1603(2):47-82. doi: 10.1016/s0304-419x(02)00082-3.
- Bernatchez, Pascal N., Philip M. Bauer, Jun Yu, Jay S. Prendergast, Pingnian He, et William C. Sessa. 2005. « Dissecting the molecular control of endothelial NO synthase by caveolin-1 using cell-permeable peptides ». *Proceedings of the National Academy of Sciences of the United States of America* 102(3):761-66. doi: 10.1073/pnas.0407224102.
- Biswas, Arikta, Purba Kashyap, Sanchari Datta, Titas Sengupta, et Bidisha Sinha. 2019. « Cholesterol Depletion by M β CD Enhances Cell Membrane Tension and Its Variations-Reducing Integrity ». *Biophysical Journal* 116(8):1456-68. doi: 10.1016/j.bpj.2019.03.016.
- Bitsikas, Vassilis, Ivan R. Corrêa Jr, et Benjamin J. Nichols. 2014. « Clathrin-independent pathways do not contribute significantly to endocytic flux » édité par S. R. Pfeffer. *eLife* 3:e03970. doi: 10.7554/eLife.03970.
- Bo, L., et R. E. Waugh. 1989. « Determination of Bilayer Membrane Bending Stiffness by Tether Formation from Giant, Thin-Walled Vesicles ». *Biophysical Journal* 55(3):509-17. doi: 10.1016/S0006-3495(89)82844-9.
- Bosch, Marta, Montserrat Marí, Albert Herms, Ana Fernández, Alba Fajardo, Adam Kassar, Albert Giral, Anna Colell, David Balgoma, Elisabet Barbero, Elena González-Moreno, Nuria Matias, Francesc Tebar, Jesús Balsinde, Marta Camps, Carlos Enrich, Steven P. Gross, Carmen García-Ruiz, Esther Pérez-Navarro, José C. Fernández-Checa, et Albert Pol. 2011. « Caveolin-1 Deficiency Causes Cholesterol-Dependent Mitochondrial Dysfunction and Apoptotic Susceptibility ». *Current Biology: CB* 21(8):681-86. doi: 10.1016/j.cub.2011.03.030.

- Botos, E., J. Klumperman, V. Oorschot, B. Ígyártó, A. Magyar, M. Oláh, et A. L. Kiss. 2008. « Caveolin-1 is transported to multi-vesicular bodies after albumin-induced endocytosis of caveolae in HepG2 cells ». *Journal of Cellular and Molecular Medicine* 12(5a):1632-39. doi: 10.1111/j.1582-4934.2007.00167.x.
- Bottier, Céline, Chiara Gabella, Benoît Vianay, Lara Buscemi, Ivo F. Sbalzarini, Jean-Jacques Meister, et Alexander B. Verkhovsky. 2011. « Dynamic Measurement of the Height and Volume of Migrating Cells by a Novel Fluorescence Microscopy Technique ». *Lab on a Chip* 11(22):3855-63. doi: 10.1039/c1lc20807a.
- Boucrot, Emmanuel, Mark T. Howes, Tomas Kirchhausen, et Robert G. Parton. 2011. « Redistribution of caveolae during mitosis ». *Journal of Cell Science* 124(12):1965-72. doi: 10.1242/jcs.076570.
- Boulant, Steeve, Comert Kural, Jean-Christophe Zeeh, Florent Ubelmann, et Tom Kirchhausen. 2011. « Actin dynamics counteract membrane tension during clathrin-mediated endocytosis ». *Nature cell biology* 13(9):1124-31. doi: 10.1038/ncb2307.
- Boulton, Andrew J. M., Loretta Vileikyte, Gunnel Ragnarson-Tennvall, et Jan Apelqvist. 2005. « The Global Burden of Diabetic Foot Disease ». *Lancet (London, England)* 366(9498):1719-24. doi: 10.1016/S0140-6736(05)67698-2.
- Boyer, Laurent, Anne Doye, Monica Rolando, Gilles Flatau, Patrick Munro, Pierre Gounon, René Clément, Céline Pulcini, Michel R. Popoff, Amel Mettouchi, Luce Landraud, Olivier Dussurget, et Emmanuel Lemichez. 2006. « Induction of Transient Macroapertures in Endothelial Cells through RhoA Inhibition by Staphylococcus Aureus Factors ». *J Cell Biol* 173(5):809-19. doi: 10.1083/jcb.200509009.
- Braakman, Sietse T., Ryan M. Pedrigi, A. Thomas Read, James A. E. Smith, W. Daniel Stamer, C. Ross Ethier, et Darryl R. Overby. 2014. « Biomechanical Strain as a Trigger for Pore Formation in Schlemm's Canal Endothelial Cells ». *Experimental eye research* 127:224-35. doi: 10.1016/j.exer.2014.08.003.
- Braakman, Sietse T., A. Thomas Read, Darren W. H. Chan, C. Ross Ethier, et Darryl R. Overby. 2015. « Colocalization of Outflow Segmentation and Pores along the Inner Wall of Schlemm's Canal ». *Experimental Eye Research* 130:87-96. doi: 10.1016/j.exer.2014.11.008.
- Brakebusch, Cord, et Reinhard Fässler. 2003. « The Integrin-Actin Connection, an Eternal Love Affair ». *The EMBO Journal* 22(10):2324-33. doi: 10.1093/emboj/cdg245.
- Braunger, Julia A., Bastian R. Brückner, Stefan Nehls, Anna Pietuch, Volker Gerke, Ingo Mey, Andreas Janshoff, et Claudia Steinem. 2014. « Phosphatidylinositol 4,5-Bisphosphate Alters the Number of Attachment Sites between Ezrin and Actin Filaments ». *Journal of Biological Chemistry* 289(14):9833-43. doi: 10.1074/jbc.M113.530659.
- Breen, Michael R., Marta Camps, Francisco Carvalho-Simoes, Antonio Zorzano, et Paul F. Pilch. 2012. « Cholesterol Depletion in Adipocytes Causes Caveolae Collapse Concomitant with Proteosomal Degradation of Cavin-2 in a Switch-Like Fashion ». *PLOS ONE* 7(4):e34516. doi: 10.1371/journal.pone.0034516.
- Briand, Nolwenn, Cécilia Prado, Guillaume Mabilieu, Françoise Lasnier, Xavier Le Lièpvre, Jeffrey D. Covington, Eric Ravussin, Soazig Le Lay, et Isabelle Dugail. 2014. « Caveolin-1 Expression and Cavin Stability Regulate Caveolae Dynamics in Adipocyte Lipid Store Fluctuation ». *Diabetes* 63(12):4032-44. doi: 10.2337/db13-1961.
- Bryan, J., et M. Kurth. 1984. « Actin-gelsolin interactions. Evidence for two actin-binding sites. » *The Journal of biological chemistry*. doi: 10.1016/s0021-9258(17)42816-x.
- Bucci, Mariarosaria, Jean-Philippe Gratton, Radu Daniel Rudic, Lisette Acevedo, Fiorentina Roviezzo, Giuseppe Cirino, et William C. Sessa. 2000. « In Vivo Delivery of the Caveolin-1 Scaffolding Domain Inhibits Nitric Oxide Synthesis and Reduces Inflammation ». *Nature Medicine* 6(12):1362-67. doi: 10.1038/82176.
- Burgener, R., M. Wolf, T. Ganz, et M. Baggiolini. 1990. « Purification and Characterization of a Major Phosphatidylserine-Binding Phosphoprotein from Human Platelets ». *Biochemical Journal* 269(3):729-34. doi: 10.1042/bj2690729.
- Burridge, Keith, et Magdalena Chrzanowska-Wodnicka. 1996. « FOCAL ADHESIONS, CONTRACTILITY, AND SIGNALING ». *Annual Review of Cell and Developmental Biology* 12(1):463-519. doi: 10.1146/annurev.cellbio.12.1.463.

- Byfield, Fitzroy J., Helim Aranda-Espinoza, Victor G. Romanenko, George H. Rothblat, et Irena Levitan. 2004. « Cholesterol Depletion Increases Membrane Stiffness of Aortic Endothelial Cells ». *Biophysical Journal* 87(5):3336-43. doi: 10.1529/biophysj.104.040634.
- Cadart, C., E. Zlotek-Zlotkiewicz, L. Venkova, O. Thouvenin, V. Racine, M. Le Berre, S. Monnier, et M. Piel. 2017. « Chapter 6 - Fluorescence EXclusion Measurement of Volume in Live Cells ». P. 103-20 in *Methods in Cell Biology*. Vol. 139, *Cell Polarity and Morphogenesis*, édité par T. Lecuit. Academic Press.
- Cai, Y., O. Rossier, N. C. Gauthier, N. Biais, M. A. Fardin, X. Zhang, L. W. Miller, B. Ladoux, V. W. Cornish, et M. P. Sheetz. 2010. « Cytoskeletal Coherence Requires Myosin-IIA Contractility ». *Journal of Cell Science* 123(3):413-23. doi: 10.1242/jcs.058297.
- Campelo, Felix, Harvey T. McMahon, et Michael M. Kozlov. 2008. « The Hydrophobic Insertion Mechanism of Membrane Curvature Generation by Proteins ». *Biophysical Journal* 95(5):2325-39. doi: 10.1529/biophysj.108.133173.
- Cao, Henian, Lindsay Alston, Jennifer Ruschman, et Robert A. Hegele. 2008. « Heterozygous CAV1 frameshift mutations (MIM 601047) in patients with atypical partial lipodystrophy and hypertriglyceridemia ». *Lipids in Health and Disease* 7:3. doi: 10.1186/1476-511X-7-3.
- Capozza, Franco, Alex W. Cohen, Michelle W. C. Cheung, Federica Sotgia, William Schubert, Michela Battista, Hyangkyu Lee, Philippe G. Frank, et Michael P. Lisanti. 2005. « Muscle-specific interaction of caveolin isoforms: differential complex formation between caveolins in fibroblastic vs. muscle cells ». *American Journal of Physiology-Cell Physiology* 288(3):C677-91. doi: 10.1152/ajpcell.00232.2004.
- Carlier, Marie-France, Valérie Laurent, Jérôme Santolini, Ronald Melki, Dominique Didry, Gui-Xian Xia, Yan Hong, Nam-Hai Chua, et Dominique Pantaloni. 1997. « Actin Depolymerizing Factor (ADF/Cofilin) Enhances the Rate of Filament Turnover: Implication in Actin-based Motility ». *The Journal of Cell Biology* 136(6):1307-22.
- Carman, Christopher V., Peter T. Sage, Tracey E. Sciuto, Miguel A. de la Fuente, Raif S. Geha, Hans D. Ochs, Harold F. Dvorak, Ann M. Dvorak, et Timothy A. Springer. 2007. « Transcellular Diapedesis Is Initiated by Invasive Podosomes ». *Immunity* 26(6):784-97. doi: 10.1016/j.immuni.2007.04.015.
- Carman, Christopher V., et Timothy A. Springer. 2004. « A transmigratory cup in leukocyte diapedesis both through individual vascular endothelial cells and between them ». *The Journal of Cell Biology* 167(2):377-88. doi: 10.1083/jcb.200404129.
- Casares, Doralicia, Pablo V. Escribá, et Catalina Ana Rosselló. 2019. « Membrane Lipid Composition: Effect on Membrane and Organelle Structure, Function and Compartmentalization and Therapeutic Avenues ». *International Journal of Molecular Sciences* 20(9):2167. doi: 10.3390/ijms20092167.
- Cerezo, Ana, Marta C. Guadamillas, Jacky G. Goetz, Sara Sánchez-Perales, Eric Klein, Richard K. Assoian, et Miguel A. del Pozo. 2009. « The Absence of Caveolin-1 Increases Proliferation and Anchorage-Independent Growth by a Rac-Dependent, Erk-Independent Mechanism ». *Molecular and Cellular Biology* 29(18):5046-59. doi: 10.1128/MCB.00315-09.
- Chakraborty, Saptarshi, Milka Doktorova, Trivikram R. Molugu, Frederick A. Heberle, Haden L. Scott, Boris Dzikovski, Michihiro Nagao, Laura-Roxana Stingaciu, Robert F. Standaert, Francisco N. Barrera, John Katsaras, George Khelashvili, Michael F. Brown, et Rana Ashkar. 2020. « How Cholesterol Stiffens Unsaturated Lipid Membranes ». *Proceedings of the National Academy of Sciences* 117(36):21896-905. doi: 10.1073/pnas.2004807117.
- Chardin, P., P. Boquet, P. Madaule, M. R. Popoff, E. J. Rubin, et D. M. Gill. 1989. « The Mammalian G Protein RhoC Is ADP-Ribosylated by Clostridium Botulinum Exoenzyme C3 and Affects Actin Microfilaments in Vero Cells ». *The EMBO Journal* 8(4):1087-92.
- Charles-Orszag, Arthur, Emmanuel Lemichez, Guy Tran Van Nhieu, et Guillaume Duménil. 2016. « Microbial pathogenesis meets biomechanics ». *Current Opinion in Cell Biology* 38:31-37. doi: 10.1016/j.ceb.2016.01.005.
- Charras, Guillaume, et Ewa Paluch. 2008. « Blebs Lead the Way: How to Migrate without Lamellipodia ». *Nature Reviews. Molecular Cell Biology* 9(9):730-36. doi: 10.1038/nrm2453.
- Cheng, Jade P. X., Carolina Mendoza-Topaz, Gillian Howard, Jessica Chadwick, Elena Shvets, Andrew S. Cowburn, Benjamin J. Dunmore, Alexi Crosby, Nicholas W. Morrell, et Benjamin J. Nichols. 2015.

- « Caveolae protect endothelial cells from membrane rupture during increased cardiac output ». *Journal of Cell Biology* 211(1):53-61. doi: 10.1083/jcb.201504042.
- Cheng, Xiaoyang, et Jonathan H. Jaggar. 2006. « Genetic ablation of caveolin-1 modifies Ca²⁺ spark coupling in murine arterial smooth muscle cells ». *American Journal of Physiology-Heart and Circulatory Physiology* 290(6):H2309-19. doi: 10.1152/ajpheart.01226.2005.
- Cheng, Zhi-Jie, Raman Deep Singh, David L. Marks, et Richard E. Pagano. 2006. « Membrane Microdomains, Caveolae, and Caveolar Endocytosis of Sphingolipids (Review) ». *Molecular Membrane Biology* 23(1):101-10. doi: 10.1080/09687860500460041.
- Chesarone, Melissa A., Amy Grace DuPage, et Bruce L. Goode. 2010. « Unleashing Formins to Remodel the Actin and Microtubule Cytoskeletons ». *Nature Reviews Molecular Cell Biology* 11(1):62-74. doi: 10.1038/nrm2816.
- Choudhury, Amit, David L. Marks, Kirsty M. Proctor, Gwyn W. Gould, et Richard E. Pagano. 2006. « Regulation of Caveolar Endocytosis by Syntaxin 6-Dependent Delivery of Membrane Components to the Cell Surface ». *Nature Cell Biology* 8(4):317-28. doi: 10.1038/ncb1380.
- Codelia, Verónica A., Gongping Sun, et K. Irvine. 2014. « Regulation of YAP by Mechanical Strain through Jnk and Hippo Signaling ». *Current Biology*. doi: 10.1016/j.cub.2014.07.034.
- Cohen, Alex W., Robert Hnasko, William Schubert, et Michael P. Lisanti. 2004. « Role of Caveolae and Caveolins in Health and Disease ». *Physiological Reviews* 84(4):1341-79. doi: 10.1152/physrev.00046.2003.
- Collier, R. John, et John A. T. Young. 2003. « Anthrax Toxin ». *Annual Review of Cell and Developmental Biology* 19:45-70. doi: 10.1146/annurev.cellbio.19.111301.140655.
- Collins, Brett M., Melissa J. Davis, John F. Hancock, et Robert G. Parton. 2012. « Structure-Based Reassessment of the Caveolin Signaling Model: Do Caveolae Regulate Signaling through Caveolin-Protein Interactions? ». *Developmental Cell* 23(1):11-20. doi: 10.1016/j.devcel.2012.06.012.
- Colom, Adai, Emmanuel Derivery, Saeideh Soleimanpour, Caterina Tomba, Marta Dal Molin, Naomi Sakai, Marcos González-Gaitán, Stefan Matile, et Aurélien Roux. 2018. « A Fluorescent Membrane Tension Probe ». *Nature Chemistry* 10(11):1118-25. doi: 10.1038/s41557-018-0127-3.
- Čopič, Alenka, Catherine F. Latham, Max A. Horlbeck, Jennifer G. D'Arcangelo, et Elizabeth A. Miller. 2012. « ER Cargo Properties Specify A Requirement For COPII Coat Rigidity Mediated By Sec13p ». *Science (New York, N.y.)* 335(6074):1359-62. doi: 10.1126/science.1215909.
- Corrotte, Matthias, Patricia E. Almeida, Christina Tam, Thiago Castro-Gomes, Maria Cecilia Fernandes, Bryan A. Millis, Mauro Cortez, Heather Miller, Wenxia Song, Timothy K. Maugel, et Norma W. Andrews. 2013. « Caveolae Internalization Repairs Wounded Cells and Muscle Fibers ». *ELife* 2:e00926. doi: 10.7554/eLife.00926.
- Courjon, Johan, Patrick Munro, Yvonne Benito, Orane Visvikis, Coralie Bouchiat, Laurent Boyer, Anne Doye, Hubert Lepidi, Eric Ghigo, Jean-Philippe Lavigne, François Vandenesch, et Emmanuel Lemichez. 2015. « EDIN-B Promotes the Translocation of Staphylococcus aureus to the Bloodstream in the Course of Pneumonia ». *Toxins* 7(10):4131-42. doi: 10.3390/toxins7104131.
- Cramer, Louise P., Margaret Siebert, et Timothy J. Mitchison. 1997. « Identification of Novel Graded Polarity Actin Filament Bundles in Locomoting Heart Fibroblasts: Implications for the Generation of Motile Force ». *The Journal of Cell Biology* 136(6):1287-1305.
- Cullen, Peter J., et Hendrik C. Korswagen. 2011. « Sorting Nexins Provide Diversity for Retromer-Dependent Trafficking Events ». *Nature Cell Biology* 14(1):29-37. doi: 10.1038/ncb2374.
- Cuvelier, D., N. Chiaruttini, P. Bassereau, et P. Nassoy. 2005. « Pulling Long Tubes from Firmly Adhered Vesicles ». *EPL (Europhysics Letters)* 71(6):1015. doi: 10.1209/epl/i2005-10173-4.
- Dai, Jianwu, et Michael P. Sheetz. 1999. « Membrane Tether Formation from Blebbing Cells ». *Biophysical Journal* 77(6):3363-70. doi: 10.1016/S0006-3495(99)77168-7.
- Dai, Jianwu, Michael P. Sheetz, Xiaodong Wan, et Catherine E. Morris. 1998. « Membrane Tension in Swelling and Shrinking Molluscan Neurons ». *The Journal of Neuroscience* 18(17):6681-92. doi: 10.1523/JNEUROSCI.18-17-06681.1998.

- Dal Molin, Federica, Fiorella Tonello, Daniel Ladant, Irene Zorretta, Ilaria Zamparo, Giulietta Di Benedetto, Manuela Zaccolo, et Cesare Montecucco. 2006. « Cell entry and cAMP imaging of anthrax edema toxin ». *The EMBO Journal* 25(22):5405-13. doi: 10.1038/sj.emboj.7601408.
- Dalkilic, Isin, et Louis M. Kunkel. 2003. « Muscular Dystrophies: Genes to Pathogenesis ». *Current Opinion in Genetics & Development* 13(3):231-38. doi: 10.1016/S0959-437X(03)00048-0.
- Damm, Eva-Maria, Lucas Pelkmans, Jürgen Kartenbeck, Anna Mezzacasa, Teymuraz Kurzchalia, et Ari Helenius. 2005. « Clathrin- and caveolin-1-independent endocytosis ». *The Journal of Cell Biology* 168(3):477-88. doi: 10.1083/jcb.200407113.
- Daniel, E. E., A. El-Yazbi, et W. J. Cho. 2006. « Caveolae and Calcium Handling, a Review and a Hypothesis ». *Journal of Cellular and Molecular Medicine* 10(2):529-44. doi: 10.1111/j.1582-4934.2006.tb00418.x.
- Daumke, Oliver, Richard Lundmark, Yvonne Vallis, Sascha Martens, P. Jonathan G. Butler, et Harvey T. McMahon. 2007. « Architectural and Mechanistic Insights into an EHD ATPase Involved in Membrane Remodelling ». *Nature* 449(7164):923-27. doi: 10.1038/nature06173.
- De Belly, Henry, Aki Stubb, Ayaka Yanagida, Céline Labouesse, Philip H. Jones, Ewa K. Paluch, et Kevin J. Chalut. 2021. « Membrane Tension Gates ERK-Mediated Regulation of Pluripotent Cell Fate ». *Cell Stem Cell* 28(2):273-284.e6. doi: 10.1016/j.stem.2020.10.018.
- Dent, Erik W., Adam V. Kwiatkowski, Leslie M. Mebane, Ulrike Philippar, Melanie Barzik, Douglas A. Rubinson, Stephanie Gupton, J. Edward Van Veen, Craig Furman, Jianguang Zhang, Arthur S. Alberts, Susumu Mori, et Frank B. Gertler. 2007. « Filopodia Are Required for Cortical Neurite Initiation ». *Nature Cell Biology* 9(12):1347-59. doi: 10.1038/ncb1654.
- Derenyi, Imre, Frank Julicher, et Jacques Prost. 2002. « Formation and Interaction of Membrane Tubes ». *Physical Review Letters* 88(23):238101. doi: 10.1103/PhysRevLett.88.238101.
- Dhanda, Aaron S., Connie Yu, Katarina T. Lulic, A. Wayne Vogl, Valentina Rausch, Diana Yang, Benjamin J. Nichols, Sung Hyun Kim, Simona Polo, Carsten G. Hansen, et Julian A. Guttman. 2020. « *Listeria Monocytogenes* Exploits Host Caveolin for Cell-to-Cell Spreading » édité par S. I. Miller. *MBio* 11(1). doi: 10.1128/mBio.02857-19.
- Dietzen, Dennis J., W. Randall Hastings, et Douglas M. Lublin. 1995. « Caveolin Is Palmitoylated on Multiple Cysteine Residues: PALMITOYLATION IS NOT NECESSARY FOR LOCALIZATION OF CAVEOLIN TO CAVEOLAE (*) ». *Journal of Biological Chemistry* 270(12):6838-42. doi: 10.1074/jbc.270.12.6838.
- Ding, Shi-Ying, Mi-Jeong Lee, Ross Summer, Libin Liu, Susan K. Fried, et Paul F. Pilch. 2014. « Pleiotropic Effects of Cavin-1 Deficiency on Lipid Metabolism ». *The Journal of Biological Chemistry* 289(12):8473-83. doi: 10.1074/jbc.M113.546242.
- Diz-Muñoz, Alba, Daniel A. Fletcher, et Orion D. Weiner. 2013. « Use the Force: Membrane Tension as an Organizer of Cell Shape and Motility ». *Trends in Cell Biology* 23(2):47-53. doi: 10.1016/j.tcb.2012.09.006.
- Diz-Muñoz, Alba, Michael Krieg, Martin Bergert, Itziar Ibarlucea-Benitez, Daniel J. Muller, Ewa Paluch, et Carl-Philipp Heisenberg. 2010. « Control of Directed Cell Migration In Vivo by Membrane-to-Cortex Attachment ». *PLoS Biology* 8(11):e1000544. doi: 10.1371/journal.pbio.1000544.
- Diz-Muñoz, Alba, Kevin Thurley, Sana Chintamen, Steven J. Altschuler, Lani F. Wu, Daniel A. Fletcher, et Orion D. Weiner. 2016. « Membrane Tension Acts Through PLD2 and MTORC2 to Limit Actin Network Assembly During Neutrophil Migration ». *PLoS Biology* 14(6):e1002474. doi: 10.1371/journal.pbio.1002474.
- Diz-Muñoz, Alba, Orion D. Weiner, et Daniel A. Fletcher. 2018. « In Pursuit of the Mechanics That Shape Cell Surfaces ». *Nature Physics* 14(7):648-52. doi: 10.1038/s41567-018-0187-8.
- Doherty, Gary J., et Harvey T. McMahon. 2008. « Mediation, Modulation, and Consequences of Membrane-Cytoskeleton Interactions ». *Annual Review of Biophysics* 37:65-95. doi: 10.1146/annurev.biophys.37.032807.125912.
- Douezan, Stéphane, Karine Guevorkian, Randa Naouar, Sylvie Dufour, Damien Cuvelier, et Françoise Brochard-Wyart. 2011. « Spreading Dynamics and Wetting Transition of Cellular Aggregates ». *Proceedings of the National Academy of Sciences of the United States of America* 108(18):7315-20. doi: 10.1073/pnas.1018057108.

- Drab, M. 2001. « Loss of Caveolae, Vascular Dysfunction, and Pulmonary Defects in Caveolin-1 Gene-Disrupted Mice ». *Science* 293(5539):2449-52. doi: 10.1126/science.1062688.
- Duesbery, N. S., C. P. Webb, S. H. Leppla, V. M. Gordon, K. R. Klimpel, T. D. Copeland, N. G. Ahn, M. K. Oskarsson, K. Fukasawa, K. D. Paull, et G. F. Vande Woude. 1998. « Proteolytic Inactivation of MAP-Kinase-Kinase by Anthrax Lethal Factor ». *Science (New York, N.Y.)* 280(5364):734-37. doi: 10.1126/science.280.5364.734.
- Dulhunty, A. F., et C. Franzini-Armstrong. 1975. « The relative contributions of the folds and caveolae to the surface membrane of frog skeletal muscle fibres at different sarcomere lengths. » *The Journal of Physiology* 250(3):513-39.
- Duncan, Matthew J., Guojie Li, Jeoung-Sook Shin, Johnny L. Carson, et Soman N. Abraham. 2004. « Bacterial Penetration of Bladder Epithelium through Lipid Rafts* ». *Journal of Biological Chemistry* 279(18):18944-51. doi: 10.1074/jbc.M400769200.
- Dupont, Sirio, Leonardo Morsut, Mariaceleste Aragona, Elena Enzo, Stefano Giullitti, Michelangelo Cordenonsi, Francesca Zanconato, Jimmy Le Digabel, Mattia Forcato, Silvio Bicciato, Nicola Elvassore, et Stefano Piccolo. 2011. « Role of YAP/TAZ in Mechanotransduction ». *Nature* 474(7350):179-83. doi: 10.1038/nature10137.
- Echarri, A., et M. A. Del Pozo. 2015. « Caveolae - Mechanosensitive Membrane Invaginations Linked to Actin Filaments ». *Journal of Cell Science* 128(15):2747-58. doi: 10.1242/jcs.153940.
- Echarri, Asier, Olivia Muriel, et Miguel A. Del Pozo. 2007. « Intracellular Trafficking of Raft/Caveolae Domains: Insights from Integrin Signaling ». *Seminars in Cell & Developmental Biology* 18(5):627-37. doi: 10.1016/j.semcd.2007.08.004.
- Echarri, Asier, Olivia Muriel, Dácil M. Pavón, Hind Azegrouz, Fernando Escolar, María C. Terrón, Fátima Sanchez-Cabo, Fernando Martínez, María C. Montoya, Oscar Llorca, et Miguel A. Del Pozo. 2012. « Caveolar Domain Organization and Trafficking Is Regulated by Abl Kinases and MDia1 ». *Journal of Cell Science* 125(Pt 13):3097-3113. doi: 10.1242/jcs.090134.
- Eden, Sharon, Rajat Rohatgi, Alexandre V. Podtelejnikov, Matthias Mann, et Marc W. Kirschner. 2002. « Mechanism of Regulation of WAVE1-Induced Actin Nucleation by Rac1 and Nck ». *Nature* 418(6899):790-93. doi: 10.1038/nature00859.
- Edwards, Andrew M., Jennifer R. Potts, Elisabet Josefsson, et Ruth C. Massey. 2010. « Staphylococcus Aureus Host Cell Invasion and Virulence in Sepsis Is Facilitated by the Multiple Repeats within FnBPA ». *PLOS Pathogens* 6(6):e1000964. doi: 10.1371/journal.ppat.1000964.
- Eeman, Marc, et Magali Deleu. 2010. « From Biological Membranes to Biomimetic Model Membranes ». *Biotechnol. Agron. Soc. Environ.* 18.
- Epand, Richard M., Brian G. Sayer, et Raquel F. Epand. 2005. « Caveolin Scaffolding Region and Cholesterol-Rich Domains in Membranes ». *Journal of Molecular Biology* 345(2):339-50. doi: 10.1016/j.jmb.2004.10.064.
- Ethier, C. Ross. 2002. « The Inner Wall of Schlemm's Canal ». *Experimental Eye Research* 74(2):161-72. doi: 10.1006/exer.2002.1144.
- Ethier, C. Ross, Fides M. Coloma, Arthur J. Sit, et Mark Johnson. 1998. « Two Pore Types in the Inner-Wall Endothelium of Schlemm's Canal ». 39(11):8.
- Etienne-Manneville, Sandrine, et Alan Hall. 2002. « Rho GTPases in Cell Biology ». *Nature* 420(6916):629-35. doi: 10.1038/nature01148.
- Evans, E., et A. Yeung. 1989. « Apparent Viscosity and Cortical Tension of Blood Granulocytes Determined by Micropipet Aspiration ». *Biophysical Journal* 56(1):151-60. doi: 10.1016/S0006-3495(89)82660-8.
- Fairn, Gregory D., Nicole L. Schieber, Nicholas Ariotti, Samantha Murphy, Lars Kuerschner, Richard I. Webb, Sergio Grinstein, et Robert G. Parton. 2011. « High-Resolution Mapping Reveals Topologically Distinct Cellular Pools of Phosphatidylserine ». *The Journal of Cell Biology* 194(2):257-75. doi: 10.1083/jcb.201012028.
- Fehon, Richard G., Andrea I. McClatchey, et Anthony Bretscher. 2010. « Organizing the Cell Cortex: The Role of ERM Proteins ». *Nature Reviews. Molecular Cell Biology* 11(4):276-87. doi: 10.1038/nrm2866.

- Feng, Xiaodong, Richard A. F. Clark, Dennis Galanakis, et Marcia G. Tonnesen. 1999. « Fibrin and Collagen Differentially Regulate Human Dermal Microvascular Endothelial Cell Integrins: Stabilization of Av/B3 MRNA by Fibrin1 ». *Journal of Investigative Dermatology* 113(6):913-19. doi: 10.1046/j.1523-1747.1999.00786.x.
- Ferguson, Joshua P., Scott D. Huber, Nathan M. Willy, Esra Aygün, Sevde Goker, Tugba Atabey, et Comert Kural. 2017. « Mechanoregulation of clathrin-mediated endocytosis ». *Journal of Cell Science* 130(21):3631-36. doi: 10.1242/jcs.205930.
- Fernández, Manuel A., Cecilia Albor, Mercedes Ingelmo-Torres, Susan J. Nixon, Charles Ferguson, Teymuraz Kurzchalia, Francesc Tebar, Carlos Enrich, Robert G. Parton, et Albert Pol. 2006. « Caveolin-1 Is Essential for Liver Regeneration ». *Science* 313(5793):1628-32. doi: 10.1126/science.1130773.
- Fielding, C. J., et P. E. Fielding. 2001. « Caveolae and Intracellular Trafficking of Cholesterol ». *Advanced Drug Delivery Reviews* 49(3):251-64. doi: 10.1016/s0169-409x(01)00140-5.
- Firoved, Aaron M., Mahtab Moayeri, Jason F. Wiggins, Yuequan Shen, Wei-Jen Tang, et Stephen H. Leppla. 2007. « Anthrax Edema Toxin Sensitizes DBA/2J Mice to Lethal Toxin ». *Infection and Immunity* 75(5):2120-25. doi: 10.1128/IAI.01781-06.
- Fischer-Friedrich, Elisabeth, Anthony A. Hyman, Frank Jülicher, Daniel J. Müller, et Jonne Helenius. 2014. « Quantification of Surface Tension and Internal Pressure Generated by Single Mitotic Cells ». *Scientific Reports* 4:6213. doi: 10.1038/srep06213.
- Ford, Andrew J., Gaurav Jain, et Padmavathy Rajagopalan. 2015. « Designing a Fibrotic Microenvironment to Investigate Changes in Human Liver Sinusoidal Endothelial Cell Function ». *Acta Biomaterialia* 24:220-27. doi: 10.1016/j.actbio.2015.06.028.
- Ford, Marijn G. J., Ian G. Mills, Brian J. Peter, Yvonne Vallis, Gerrit J. K. Praefcke, Philip R. Evans, et Harvey T. McMahon. 2002. « Curvature of Clathrin-Coated Pits Driven by Epsin ». *Nature* 419(6905):361-66. doi: 10.1038/nature01020.
- Fra, A. M., E. Williamson, K. Simons, et R. G. Parton. 1995. « De Novo Formation of Caveolae in Lymphocytes by Expression of VIP21-Caveolin ». *Proceedings of the National Academy of Sciences* 92(19):8655-59. doi: 10.1073/pnas.92.19.8655.
- Frank, Philippe G., Scott E. Woodman, David S. Park, et Michael P. Lisanti. 2003. « Caveolin, Caveolae, and Endothelial Cell Function ». *Arteriosclerosis, Thrombosis, and Vascular Biology* 23(7):1161-68. doi: 10.1161/01.ATV.0000070546.16946.3A.
- Fraser, Robin, Bruce R. Dobbs, et George W. T. Rogers. 1995. « Lipoproteins and the Liver Sieve: The Role of the Fenestrated Sinusoidal Endothelium in Lipoprotein Metabolism, Atherosclerosis, and Cirrhosis ». *Hepatology* 21(3):863-74. doi: 10.1002/hep.1840210337.
- Fridolfsson, Heidi N., Yoshitaka Kawaraguchi, Sameh S. Ali, Mathivadhani Panneerselvam, Ingrid R. Niesman, J. Cameron Finley, Sarah E. Kellerhals, Michael Y. Migita, Hideshi Okada, Ana L. Moreno, Michelle Jennings, Michael W. Kidd, Jacqueline A. Bonds, Ravi C. Balijepalli, Robert S. Ross, Piyush M. Patel, Atsushi Miyanochara, Qun Chen, Edward J. Lesnefsky, Brian P. Head, David M. Roth, Paul A. Insel, et Hemal H. Patel. 2012. « Mitochondria-Localized Caveolin in Adaptation to Cellular Stress and Injury ». *FASEB Journal: Official Publication of the Federation of American Societies for Experimental Biology* 26(11):4637-49. doi: 10.1096/fj.12-215798.
- Fu, Ying, Anh Hoang, Genevieve Escher, Robert G. Parton, Zygmunt Krozowski, et Dmitri Sviridov. 2004. « Expression of Caveolin-1 Enhances Cholesterol Efflux in Hepatic Cells * ». *Journal of Biological Chemistry* 279(14):14140-46. doi: 10.1074/jbc.M311061200.
- Fujimoto, T. 1993. « Calcium Pump of the Plasma Membrane Is Localized in Caveolae ». *The Journal of Cell Biology* 120(5):1147-57. doi: 10.1083/jcb.120.5.1147.
- Fujimoto, T. s. d. « Caveolin-1 Isoforms and Caveola Structure ». 9.
- Fujita, Akikazu, Jinglei Cheng, Kumi Tauchi-Sato, Tadaomi Takenawa, et Toyoshi Fujimoto. 2009. « A distinct pool of phosphatidylinositol 4,5-bisphosphate in caveolae revealed by a nanoscale labeling technique ». *Proceedings of the National Academy of Sciences of the United States of America* 106(23):9256-61. doi: 10.1073/pnas.0900216106.
- Gambin, Yann, Nicholas Ariotti, Kerrie-Ann McMahon, Michele Bastiani, Emma Sierecki, Oleksiy Kovtun, Mark E. Polinkovsky, Astrid Magenau, WooRam Jung, Satomi Okano, Yong Zhou, Natalya Leneva, Sergey

- Mureev, Wayne Johnston, Katharina Gaus, John F. Hancock, Brett M. Collins, Kirill Alexandrov, et Robert G. Parton. 2014. « Single-molecule analysis reveals self assembly and nanoscale segregation of two distinct cavin subcomplexes on caveolae » édité par S. R. Pfeffer. *eLife* 3:e01434. doi: 10.7554/eLife.01434.
- Ganter, Michael T., Mitchell J. Cohen, Karim Brohi, Brian B. Chesebro, Kristan L. Staudenmayer, Pamela Rahn, Sarah C. Christiaans, Natasha D. Bir, et Jean-François Pittet. 2008. « Angiopoietin-2, Marker and Mediator of Endothelial Activation with Prognostic Significance Early after Trauma? » *Annals of Surgery* 247(2):320-26. doi: 10.1097/SLA.0b013e318162d616.
- García-Cardena, G., P. Martasek, B. S. Masters, P. M. Skidd, J. Couet, S. Li, M. P. Lisanti, et W. C. Sessa. 1997. « Dissecting the Interaction between Nitric Oxide Synthase (NOS) and Caveolin. Functional Significance of the Nos Caveolin Binding Domain in Vivo ». *The Journal of Biological Chemistry* 272(41):25437-40. doi: 10.1074/jbc.272.41.25437.
- Garcia-Cardena, G., P. Oh, J. Liu, J. E. Schnitzer, et W. C. Sessa. 1996. « Targeting of Nitric Oxide Synthase to Endothelial Cell Caveolae via Palmitoylation: Implications for Nitric Oxide Signaling. » *Proceedings of the National Academy of Sciences* 93(13):6448-53. doi: 10.1073/pnas.93.13.6448.
- Geiger, Benjamin, Joachim P. Spatz, et Alexander D. Bershadsky. 2009. « Environmental Sensing through Focal Adhesions ». *Nature Reviews. Molecular Cell Biology* 10(1):21-33. doi: 10.1038/nrm2593.
- de Gennes, Pierre-Gilles, Françoise Brochard-Wyart, et David Quéré. 2004. *Capillarity and Wetting Phenomena*. New York, NY: Springer New York.
- Gerl, Mathias J., Julio L. Sampaio, Severino Urban, Lucie Kalvodova, Jean-Marc Verbavatz, Beth Binnington, Dirk Lindemann, Clifford A. Lingwood, Andrej Shevchenko, Cornelia Schroeder, et Kai Simons. 2012. « Quantitative analysis of the lipidomes of the influenza virus envelope and MDCK cell apical membrane ». *The Journal of Cell Biology* 196(2):213-21. doi: 10.1083/jcb.201108175.
- Gervásio, Othon L., William D. Phillips, Louise Cole, et David G. Allen. 2011. « Caveolae Respond to Cell Stretch and Contribute to Stretch-Induced Signaling ». *Journal of Cell Science* 124(Pt 21):3581-90. doi: 10.1242/jcs.084376.
- Gingras, Denis, France Gauthier, Sylvie Lamy, Richard R. Desrosiers, et Richard Béliveau. 1998. « Localization of RhoA GTPase to Endothelial Caveolae-Enriched Membrane Domains ». *Biochemical and Biophysical Research Communications* 247(3):888-93. doi: 10.1006/bbrc.1998.8885.
- Girard, P., J. Prost, et P. Bassereau. 2005. « Passive or Active Fluctuations in Membranes Containing Proteins ». *Physical Review Letters* 94(8):088102. doi: 10.1103/PhysRevLett.94.088102.
- Glenney, J. R., et D. Soppet. 1992. « Sequence and Expression of Caveolin, a Protein Component of Caveolae Plasma Membrane Domains Phosphorylated on Tyrosine in Rous Sarcoma Virus-Transformed Fibroblasts ». *Proceedings of the National Academy of Sciences* 89(21):10517-21. doi: 10.1073/pnas.89.21.10517.
- Goetz, Jacky G., Patrick Lajoie, Sam M. Wiseman, et Ivan R. Nabi. 2008. « Caveolin-1 in Tumor Progression: The Good, the Bad and the Ugly ». *Cancer and Metastasis Reviews* 27(4):715-35. doi: 10.1007/s10555-008-9160-9.
- Goetz, Jacky G., Susana Minguet, Inmaculada Navarro-Lérida, Juan José Lazcano, Rafael Samaniego, Enrique Calvo, Marta Tello, Teresa Osteso-Ibáñez, Teijo Pellinen, Asier Echarri, Ana Cerezo, Andres J. P. Klein-Szanto, Ricardo Garcia, Patricia J. Keely, Paloma Sánchez-Mateos, Edna Cukierman, et Miguel A. Del Pozo. 2011. « Biomechanical remodeling of the microenvironment by stromal Caveolin-1 favors tumor invasion and metastasis ». *Cell* 146(1):148-63. doi: 10.1016/j.cell.2011.05.040.
- Gonzalez-Rodriguez, David, Madhavi P. Maddugoda, Caroline Stefani, Sebastien Janel, Frank Lafont, Damien Cuvelier, Emmanuel Lemichez, et Françoise Brochard-Wyart. 2012. « Cellular Dewetting: Opening of Macroapertures in Endothelial Cells ». *Physical Review Letters* 108(21):218105. doi: 10.1103/PhysRevLett.108.218105.
- Gonzalez-Rodriguez, David, Camille Morel, et Emmanuel Lemichez. 2020. « Dewetting: From Physics to the Biology of Intoxicated Cells ». *Advances in Experimental Medicine and Biology* 1267:101-15. doi: 10.1007/978-3-030-46886-6_6.
- Govek, Eve-Ellen, Sarah E. Newey, et Linda Van Aelst. 2005. « The Role of the Rho GTPases in Neuronal Development ». *Genes & Development* 19(1):1-49. doi: 10.1101/gad.1256405.

- Grande-García, Araceli, Asier Echarri, Johan de Rooij, Nazilla B. Alderson, Clare M. Waterman-Storer, José M. Valdivielso, et Miguel A. del Pozo. 2007. « Caveolin-1 regulates cell polarization and directional migration through Src kinase and Rho GTPases ». *Journal of Cell Biology* 177(4):683-94. doi: 10.1083/jcb.200701006.
- Grösch, Sabine, Susanne Schiffmann, et Gerd Geisslinger. 2012. « Chain Length-Specific Properties of Ceramides ». *Progress in Lipid Research* 51(1):50-62. doi: 10.1016/j.plipres.2011.11.001.
- Gumí-Audenis, Berta, Luca Costa, Lidia Ferrer-Tasies, Imma Ratera, Nora Ventosa, Fausto Sanz, et Marina I. Giannotti. 2018. « Pulling Lipid Tubes from Supported Bilayers Unveils the Underlying Substrate Contribution to the Membrane Mechanics ». *Nanoscale* 10(30):14763-70. doi: 10.1039/c8nr03249a.
- Guo, Shuohan, Xiaohan Zhang, Mei Zheng, Xiaowei Zhang, Chengchun Min, Zengtao Wang, Seung Hoon Cheon, Min-Ho Oak, Seung-Yeol Nah, et Kyeong-Man Kim. 2015. « Selectivity of Commonly Used Inhibitors of Clathrin-Mediated and Caveolae-Dependent Endocytosis of G Protein-Coupled Receptors ». *Biochimica Et Biophysica Acta* 1848(10 Pt A):2101-10. doi: 10.1016/j.bbamem.2015.05.024.
- Gupta, Reshu, Chirine Toufaily, et Borhane Annabi. 2014. « Caveolin and cavin family members: Dual roles in cancer ». *Biochimie* 107:188-202. doi: 10.1016/j.biochi.2014.09.010.
- Gustincich, S., et C. Schneider. 1993. « Serum deprivation response gene is induced by serum starvation but not by contact inhibition ». *Cell Growth & Differentiation* 4(9):753.
- Gustincich, Stefano, Paolo Vatta, Sandro Goruppi, Marlene Wolf, Salvatore Saccone, Giuliano Della Valle, Marco Baggiolini, et Claudio Schneider. 1999. « The Human Serum Deprivation Response Gene (SDPR) Maps to 2q32-Q33 and Codes for a Phosphatidylserine-Binding Protein ». *Genomics* 57(1):120-29. doi: 10.1006/geno.1998.5733.
- Han, Bing, Courtney A. Copeland, Ajit Tiwari, et Anne K. Kenworthy. 2016. « Assembly and Turnover of Caveolae: What Do We Really Know? ». *Frontiers in Cell and Developmental Biology* 4:68. doi: 10.3389/fcell.2016.00068.
- Hansen, Carsten G., Nicholas A. Bright, Gillian Howard, et Benjamin J. Nichols. 2009. « SDPR induces membrane curvature and functions in the formation of caveolae ». *Nature cell biology* 11(7):807-14. doi: 10.1038/ncb1887.
- Hansen, Carsten G., et Ben J. Nichols. 2010. « Exploring the caves: cavins, caveolins and caveolae ». *Trends in Cell Biology* 20(4):177-86. doi: 10.1016/j.tcb.2010.01.005.
- Hansen, Carsten Gram, Gillian Howard, et Benjamin J. Nichols. 2011. « Pacsin 2 is recruited to caveolae and functions in caveolar biogenesis ». *Journal of Cell Science* 124(16):2777-85. doi: 10.1242/jcs.084319.
- Hansen, Carsten Gram, Elena Shvets, Gillian Howard, Kirsi Riento, et Benjamin James Nichols. 2013. « Deletion of Cavin Genes Reveals Tissue-Specific Mechanisms for Morphogenesis of Endothelial Caveolae ». *Nature Communications* 4(1):1831. doi: 10.1038/ncomms2808.
- Harayama, Takeshi, et Howard Riezman. 2018. « Understanding the Diversity of Membrane Lipid Composition ». *Nature Reviews Molecular Cell Biology* 19(5):281-96. doi: 10.1038/nrm.2017.138.
- Hayashi, Yukiko K., Chie Matsuda, Megumu Ogawa, Kanako Goto, Kayo Tominaga, Satomi Mitsuhashi, Young-Eun Park, Ikuya Nonaka, Naomi Hino-Fukuyo, Kazuhiro Haginoya, Hisashi Sugano, et Ichizo Nishino. 2009. « Human PTRF mutations cause secondary deficiency of caveolins resulting in muscular dystrophy with generalized lipodystrophy ». *The Journal of Clinical Investigation* 119(9):2623-33. doi: 10.1172/JCI38660.
- Hayer, Arnold, Miriam Stoeber, Christin Bissig, et Ari Helenius. 2010. « Biogenesis of Caveolae: Stepwise Assembly of Large Caveolin and Cavin Complexes ». *Traffic* 11(3):361-82. doi: 10.1111/j.1600-0854.2009.01023.x.
- Heemskerk, Niels, Lilian Schimmel, Chantal Oort, Jos van Rijssel, Taofei Yin, Bin Ma, Jakobus van Unen, Bettina Pitter, Stephan Huveneers, Joachim Goedhart, Yi Wu, Eloi Montanez, Abigail Woodfin, et Jaap D. van Buul. 2016. « F-actin-rich contractile endothelial pores prevent vascular leakage during leukocyte diapedesis through local RhoA signalling ». *Nature Communications* 7. doi: 10.1038/ncomms10493.
- Helfrich, W. 1973. « Elastic Properties of Lipid Bilayers: Theory and Possible Experiments ». *Zeitschrift Fur Naturforschung. Teil C: Biochemie, Biophysik, Biologie, Virologie* 28(11):693-703. doi: 10.1515/znc-1973-11-1209.

- Helfrich, W. 1985. « Effect of Thermal Undulations on the Rigidity of Fluid Membranes and Interfaces ». *Journal de Physique* 46(7):1263-68. doi: 10.1051/jphys:019850046070126300.
- Helfrich, W., et R. M. Servuss. 1984. « Undulations, Steric Interaction and Cohesion of Fluid Membranes ». // *Nuovo Cimento D* 3(1):137-51. doi: 10.1007/BF02452208.
- Henley, John R., Eugene W. A. Krueger, Barbara J. Oswald, et Mark A. McNiven. 1998. « Dynamin-mediated Internalization of Caveolae ». *The Journal of Cell Biology* 141(1):85-99.
- Herrnberger, Leonie, Kathrin Ebner, Benjamin Junglas, et Ernst R. Tamm. 2012. « The Role of Plasmalemma Vesicle-Associated Protein (PLVAP) in Endothelial Cells of Schlemm's Canal and Ocular Capillaries ». *Experimental Eye Research* 105:27-33. doi: 10.1016/j.exer.2012.09.011.
- Hetmanski, Joseph H. R., Henry de Belly, Ignacio Busnelli, Thomas Waring, Roshna V. Nair, Vanesa Sokleva, Oana Dobre, Angus Cameron, Nils Gauthier, Christophe Lamaze, Joe Swift, Aránzazu del Campo, Tobias Starborg, Tobias Zech, Jacky G. Goetz, Ewa K. Paluch, Jean-Marc Schwartz, et Patrick T. Caswell. 2019. « Membrane Tension Orchestrates Rear Retraction in Matrix-Directed Cell Migration ». *Developmental Cell* 51(4):460-475.e10. doi: 10.1016/j.devcel.2019.09.006.
- Heuser, J. E., et M. W. Kirschner. 1980. « Filament Organization Revealed in Platinum Replicas of Freeze-Dried Cytoskeletons ». *The Journal of Cell Biology* 86(1):212-34. doi: 10.1083/jcb.86.1.212.
- Heuser, John. 2000. « The Production of 'Cell Cortices' for Light and Electron Microscopy ». *Traffic* 1(7):545-52. doi: 10.1034/j.1600-0854.2000.010704.x.
- Hill, Michelle M., Michele Bastiani, Robert Luetterforst, Matthew Kirkham, Annika Kirkham, Susan J. Nixon, Piers Walser, Daniel Abankwa, Viola M. J. Oorschot, Sally Martin, John F. Hancock, et Robert G. Parton. 2008. « PTRF-cavin, a conserved cytoplasmic protein required for caveola formation and function ». *Cell* 132(1):113-24. doi: 10.1016/j.cell.2007.11.042.
- Hirama, Takashi, Raibatak Das, Yanbo Yang, Charles Ferguson, Amy Won, Christopher M. Yip, Jason G. Kay, Sergio Grinstein, Robert G. Parton, et Gregory D. Fairn. 2017. « Phosphatidylserine Dictates the Assembly and Dynamics of Caveolae in the Plasma Membrane ». *Journal of Biological Chemistry* 292(34):14292-307. doi: 10.1074/jbc.M117.791400.
- Ho, Hsin-Yi Henry, Rajat Rohatgi, Andres M. Lebensohn, Le Ma, Jiaxu Li, Steven P. Gygi, et Marc W. Kirschner. 2004. « Toca-1 Mediates Cdc42-Dependent Actin Nucleation by Activating the N-WASP-WIP Complex ». *Cell* 118(2):203-16. doi: 10.1016/j.cell.2004.06.027.
- Hochmuth, R. M., N. Mohandas, et P. L. Blackshear. 1973. « Measurement of the Elastic Modulus for Red Cell Membrane Using a Fluid Mechanical Technique ». *Biophysical Journal* 13(8):747-62. doi: 10.1016/S0006-3495(73)86021-7.
- Hochmuth, Robert M. 2000. « Micropipette Aspiration of Living Cells ». *Journal of Biomechanics* 33(1):15-22. doi: 10.1016/S0021-9290(99)00175-X.
- Hoffmann, Christine, Anne Berking, Franziska Agerer, Alexander Buntru, Florian Neske, G. Singh Chhatwal, Knut Ohlsen, et Christof R. Hauck. 2010. « Caveolin Limits Membrane Microdomain Mobility and Integrin-Mediated Uptake of Fibronectin-Binding Pathogens ». *Journal of Cell Science* 123(24):4280-91. doi: 10.1242/jcs.064006.
- Hotulainen, Pirta, et Pekka Lappalainen. 2006. « Stress Fibers Are Generated by Two Distinct Actin Assembly Mechanisms in Motile Cells ». *The Journal of Cell Biology* 173(3):383-94. doi: 10.1083/jcb.200511093.
- Houk, Andrew R., Alexandra Jilkine, Cecile O. Mejean, Rostislav Boltyanskiy, Eric R. Dufresne, Sigurd B. Angenent, Steven J. Altschuler, Lani F. Wu, et Orion D. Weiner. 2012. « Membrane Tension Maintains Cell Polarity by Confining Signals to the Leading Edge during Neutrophil Migration ». *Cell* 148(1):175-88. doi: 10.1016/j.cell.2011.10.050.
- Howe, Alan K. 2004. « Regulation of Actin-Based Cell Migration by CAMP/PKA ». *Biochimica et Biophysica Acta (BBA) - Molecular Cell Research* 1692(2):159-74. doi: 10.1016/j.bbamcr.2004.03.005.
- Huber, P., S. Bouillot, S. Elsen, et I. Attrée. 2014. « Sequential Inactivation of Rho GTPases and Lim Kinase by Pseudomonas Aeruginosa Toxins ExoS and ExoT Leads to Endothelial Monolayer Breakdown ». *Cellular and Molecular Life Sciences* 71(10):1927-41. doi: 10.1007/s00018-013-1451-9.

- Innocenti, Metello, Adriana Zucconi, Andrea Disanza, Emanuela Frittoli, Liliana B. Areces, Anika Steffen, Theresia E. B. Stradal, Pier Paolo Di Fiore, Marie-France Carlier, et Giorgio Scita. 2004. « Abi1 Is Essential for the Formation and Activation of a WAVE2 Signalling Complex ». *Nature Cell Biology* 6(4):319-27. doi: 10.1038/ncb1105.
- Isaac, Vivian, Chia-Yi Wu, Chun-Ta Huang, Bernhard T. Baune, Chia-Lin Tseng, et Craig S. McLachlan. 2016. « Elevated neutrophil to lymphocyte ratio predicts mortality in medical inpatients with multiple chronic conditions ». *Medicine* 95(23):e3832. doi: 10.1097/MD.0000000000003832.
- Izumi, Yasushi, Syu-ichi Hirai, Yoko Tamai, Ariko Fujise-Matsuoka, Yoshifumi Nishimura, et Shigeo Ohno. 1997. « A Protein Kinase C δ -Binding Protein SRBC Whose Expression Is Induced by Serum Starvation * ». *Journal of Biological Chemistry* 272(11):7381-89. doi: 10.1074/jbc.272.11.7381.
- Jansa et al. 1998. « Cloning and functional characterization of PTRF, a novel protein which induces dissociation of paused ternary transcription complexes ». *The EMBO Journal* 17(10):2855-64. doi: 10.1093/emboj/17.10.2855.
- Jarin, Zack, Alexander J. Pak, Patricia Bassereau, et Gregory A. Voth. 2021. « Lipid-Composition-Mediated Forces Can Stabilize Tubular Assemblies of I-BAR Proteins ». *Biophysical Journal* 120(1):46-54. doi: 10.1016/j.bpj.2020.11.019.
- Johnson, Mark. 2006. « 'What Controls Aqueous Humour Outflow Resistance?' ». *Experimental Eye Research* 82(4):545-57. doi: 10.1016/j.exer.2005.10.011.
- Johnson, Mark, Darren Chan, A. Thomas Read, Cindy Christensen, Arthur Sit, et C. Ross Ethier. 2002. « The Pore Density in the Inner Wall Endothelium of Schlemm's Canal of Glaucomatous Eyes ». 43(9):6.
- Joshi, Bharat, Michele Bastiani, Scott S. Strugnell, Cecile Boscher, Robert G. Parton, et Ivan R. Nabi. 2012. « Phosphocaveolin-1 is a mechanotransducer that induces caveola biogenesis via Egr1 transcriptional regulation ». *The Journal of Cell Biology* 199(3):425-35. doi: 10.1083/jcb.201207089.
- Joshi, Bharat, Scott S. Strugnell, Jacky G. Goetz, Liliana D. Kojic, Michael E. Cox, Obi L. Griffith, Simon K. Chan, Steven J. Jones, Sher-Ping Leung, Hamid Masoudi, Samuel Leung, Sam M. Wiseman, et Ivan R. Nabi. 2008. « Phosphorylated Caveolin-1 Regulates Rho/ROCK-Dependent Focal Adhesion Dynamics and Tumor Cell Migration and Invasion ». *Cancer Research* 68(20):8210-20. doi: 10.1158/0008-5472.CAN-08-0343.
- Kawamura, Shuji, Shigeki Miyamoto, et Joan Heller Brown. 2003. « Initiation and Transduction of Stretch-Induced RhoA and Rac1 Activation through Caveolae: CYTOSKELETAL REGULATION OF ERK TRANSLOCATION* ». *Journal of Biological Chemistry* 278(33):31111-17. doi: 10.1074/jbc.M300725200.
- Khater, Ismail M., Qian Liu, Keng C. Chou, Ghassan Hamarneh, et Ivan Robert Nabi. 2019. « Super-Resolution Modularity Analysis Shows Polyhedral Caveolin-1 Oligomers Combine to Form Scaffolds and Caveolae ». *Scientific Reports* 9(1):9888. doi: 10.1038/s41598-019-46174-z.
- Kim, C. A., Marc Delépine, Emilie Boutet, Haquima El Mourabit, Soazig Le Lay, Muriel Meier, Mona Nemani, Etienne Bridel, Claudia C. Leite, Debora R. Bertola, Robert K. Semple, Stephen O'Rahilly, Isabelle Dugail, Jacqueline Capeau, Mark Lathrop, et Jocelyne Magré. 2008. « Association of a Homozygous Nonsense Caveolin-1 Mutation with Berardinelli-Seip Congenital Lipodystrophy ». *The Journal of Clinical Endocrinology & Metabolism* 93(4):1129-34. doi: 10.1210/jc.2007-1328.
- Kimura, Kazushi, Masaaki Ito, Mutsuki Amano, Kazuyasu Chihara, Yuko Fukata, Masato Nakafuku, Bunpei Yamamori, Jianhua Feng, Takeshi Nakano, Katsuya Okawa, Akihiro Iwamatsu, et Kozo Kaibuchi. 1996. « Regulation of Myosin Phosphatase by Rho and Rho-Associated Kinase (Rho-Kinase) ». *Science* 273(5272):245-48. doi: 10.1126/science.273.5272.245.
- Kirchhausen, Tomas. 2000. « Clathrin ». *Annual Review of Biochemistry* 69(1):699-727. doi: 10.1146/annurev.biochem.69.1.699.
- Kirkham, Matthew, Akikazu Fujita, Rahul Chadda, Susan J. Nixon, Teymuras V. Kurzchalia, Deepak K. Sharma, Richard E. Pagano, John F. Hancock, Satyajit Mayor, et Robert G. Parton. 2005. « Ultrastructural identification of uncoated caveolin-independent early endocytic vehicles ». *The Journal of Cell Biology* 168(3):465-76. doi: 10.1083/jcb.200407078.
- Kirkham, Matthew, Susan J. Nixon, Mark T. Howes, Laurent Abi-Rached, Diane E. Wakeham, Michael Hanzal-Bayer, Charles Ferguson, Michelle M. Hill, Manuel Fernandez-Rojo, Deborah A. Brown, John F.

- Hancock, Frances M. Brodsky, et Robert G. Parton. 2008. « Evolutionary analysis and molecular dissection of caveola biogenesis ». *Journal of Cell Science* 121(12):2075-86. doi: 10.1242/jcs.024588.
- Koster, Gerbrand, Angelo Cacciuto, Imre Derényi, Daan Frenkel, et Marileen Dogterom. 2005. « Force Barriers for Membrane Tube Formation ». *Physical Review Letters* 94(6):068101. doi: 10.1103/PhysRevLett.94.068101.
- Koster, Gerbrand, Martijn VanDuijn, Bas Hofs, et Marileen Dogterom. 2003. « Membrane Tube Formation from Giant Vesicles by Dynamic Association of Motor Proteins ». *Proceedings of the National Academy of Sciences of the United States of America* 100(26):15583-88. doi: 10.1073/pnas.2531786100.
- Kovtun, Oleksiy, Vikas A. Tillu, Nicholas Ariotti, Robert G. Parton, et Brett M. Collins. 2015. « Cavin family proteins and the assembly of caveolae ». *Journal of Cell Science* 128(7):1269-78. doi: 10.1242/jcs.167866.
- Kovtun, Oleksiy, Vikas A. Tillu, WooRam Jung, Natalya Leneva, Nicholas Ariotti, Natasha Chaudhary, Ramya A. Mandyam, Charles Ferguson, Garry P. Morgan, Wayne A. Johnston, Stephen J. Harrop, Kirill Alexandrov, Robert G. Parton, et Brett M. Collins. 2014. « Structural Insights into the Organization of the Cavin Membrane Coat Complex ». *Developmental Cell* 31(4):405-19. doi: 10.1016/j.devcel.2014.10.002.
- Kozlov, Michael M., Felix Campelo, Nicole Liska, Leonid V. Chernomordik, Siewert J. Marrink, et Harvey T. McMahon. 2014. « Mechanisms Shaping Cell Membranes ». *Current Opinion in Cell Biology* 29:53-60. doi: 10.1016/j.ceb.2014.03.006.
- Kozlov, Michael M., et Leonid V. Chernomordik. 2015. « Membrane Tension and Membrane Fusion ». *Current Opinion in Structural Biology* 33:61-67. doi: 10.1016/j.sbi.2015.07.010.
- Kristensen, Michael, Martin Krøyer Rasmussen, et Carsten Juel. 2008. « Na⁺-K⁺ Pump Location and Translocation during Muscle Contraction in Rat Skeletal Muscle ». *Pflügers Archiv - European Journal of Physiology* 456(5):979-89. doi: 10.1007/s00424-008-0449-x.
- Krugmann, Sonja, Roger Williams, Len Stephens, et Phillip T. Hawkins. 2004. « ARAP3 Is a PI3K- and Rap-Regulated GAP for RhoA ». *Current Biology* 14(15):1380-84. doi: 10.1016/j.cub.2004.07.058.
- Kuhlencordt, P. J., R. Gyurko, F. Han, M. Scherrer-Crosbie, T. H. Aretz, R. Hajjar, M. H. Picard, et P. L. Huang. 2001. « Accelerated Atherosclerosis, Aortic Aneurysm Formation, and Ischemic Heart Disease in Apolipoprotein E/Endothelial Nitric Oxide Synthase Double-Knockout Mice ». *Circulation* 104(4):448-54. doi: 10.1161/hc2901.091399.
- Kurzchalia, T. V., P. Dupree, R. G. Parton, R. Kellner, H. Virta, M. Lehnert, et K. Simons. 1992. « VIP21, a 21-KD Membrane Protein Is an Integral Component of Trans-Golgi-Network-Derived Transport Vesicles. » *Journal of Cell Biology* 118(5):1003-14. doi: 10.1083/jcb.118.5.1003.
- Kwon, Hayeong, Jaewoong Lee, Kyuho Jeong, Donghwan Jang, et Yunbae Pak. 2015. « Fatty Acylated Caveolin-2 Is a Substrate of Insulin Receptor Tyrosine Kinase for Insulin Receptor Substrate-1-Directed Signaling Activation ». *Biochimica et Biophysica Acta (BBA) - Molecular Cell Research* 1853(5):1022-34. doi: 10.1016/j.bbamcr.2015.02.002.
- Lang, P., F. Gesbert, M. Delespine-Carmagnat, R. Stancou, M. Pouchelet, et J. Bertoglio. 1996. « Protein Kinase A Phosphorylation of RhoA Mediates the Morphological and Functional Effects of Cyclic AMP in Cytotoxic Lymphocytes ». *The EMBO Journal* 15(3):510-19.
- Larson, Stephanie M., Hyo J. Lee, Pei-hsuan Hung, Lauren M. Matthews, Douglas N. Robinson, et Janice P. Evans. 2010. « Cortical Mechanics and Meiosis II Completion in Mammalian Oocytes Are Mediated by Myosin-II and Ezrin-Radixin-Moesin (ERM) Proteins ». *Molecular Biology of the Cell* 21(18):3182-92. doi: 10.1091/mbc.E10-01-0066.
- Lazarides, Elias, et Keith Burridge. 1975. « α -Actinin: Immunofluorescent Localization of a Muscle Structural Protein in Nonmuscle Cells ». *Cell* 6(3):289-98. doi: 10.1016/0092-8674(75)90180-4.
- Le Lay, Soazig, Eric Hajdуч, Margaret R. Lindsay, Xavier Le Lièvre, Christoph Thiele, Pascal Ferré, Robert G. Parton, Teymuras Kurzchalia, Kai Simons, et Isabelle Dugail. 2006. « Cholesterol-Induced Caveolin Targeting to Lipid Droplets in Adipocytes: A Role for Caveolar Endocytosis ». *Traffic* 7(5):549-61. doi: 10.1111/j.1600-0854.2006.00406.x.
- Leduc, C., O. Campas, K. B. Zeldovich, A. Roux, P. Jolimaitre, L. Bourel-Bonnet, B. Goud, J. F. Joanny, P. Bassereau, et J. Prost. 2004. « Cooperative Extraction of Membrane Nanotubes by Molecular Motors ». *Proceedings of the National Academy of Sciences* 101(49):17096-101. doi: 10.1073/pnas.0406598101.

- Leduc, Cécile, Otger Campàs, Jean-François Joanny, Jacques Prost, et Patricia Bassereau. 2010. « Mechanism of Membrane Nanotube Formation by Molecular Motors ». *Biochimica et Biophysica Acta (BBA) - Biomembranes* 1798(7):1418-26. doi: 10.1016/j.bbamem.2009.11.012.
- Lee, Jye, et Geert W. Schmid-Schönbein. 1995. « Biomechanics of Skeletal Muscle Capillaries: Hemodynamic Resistance, Endothelial Distensibility, and Pseudopod Formation ». *Annals of Biomedical Engineering* 23(3):226-46. doi: 10.1007/BF02584425.
- Lee, Stella Y., Jia-Shu Yang, Wanjin Hong, Richard T. Premont, et Victor W. Hsu. 2005. « ARFGAP1 plays a central role in coupling COPI cargo sorting with vesicle formation ». *The Journal of Cell Biology* 168(2):281-90. doi: 10.1083/jcb.200404008.
- Lehtimäki, Jaakko I., Eeva Kaisa Rajakylä, Sari Tojkander, et Pekka Lappalainen. 2021. « Generation of stress fibers through myosin-driven reorganization of the actin cortex » édité par R. Fässler, A. Akhmanova, R. Fässler, et F. Schnorrer. *eLife* 10:e60710. doi: 10.7554/eLife.60710.
- Lemichez, Emmanuel, et Klaus Aktories. 2013. « Hijacking of Rho GTPases during bacterial infection ». *Experimental Cell Research* 319(15):2329-36. doi: 10.1016/j.yexcr.2013.04.021.
- Leppla, S. H. 1982. « Anthrax Toxin Edema Factor: A Bacterial Adenylate Cyclase That Increases Cyclic AMP Concentrations of Eukaryotic Cells ». *Proceedings of the National Academy of Sciences of the United States of America* 79(10):3162-66. doi: 10.1073/pnas.79.10.3162.
- Li, Fang, et Henry N. Higgs. 2003. « The Mouse Formin MDia1 Is a Potent Actin Nucleation Factor Regulated by Autoinhibition ». *Current Biology: CB* 13(15):1335-40. doi: 10.1016/s0960-9822(03)00540-2.
- Li, Shengwen, Jacques Couet, et Michael P. Lisanti. 1996. « Src Tyrosine Kinases, G α Subunits, and H-Ras Share a Common Membrane-anchored Scaffolding Protein, Caveolin ». *The Journal of biological chemistry* 271(46):29182-90. doi: 10.1074/jbc.271.46.29182.
- Lieber, Arnon D., Shlomit Yehudai-Resheff, Erin L. Barnhart, Julie A. Theriot, et Kinneret Keren. 2013. « Membrane Tension in Rapidly Moving Cells Is Determined by Cytoskeletal Forces ». *Current Biology* 23(15):1409-17. doi: 10.1016/j.cub.2013.05.063.
- Lin, Jinxiu, Jiali Liu, Ying Wang, Jianwei Zhu, Kang Zhou, Nicole Smith, et Xi Zhan. 2005. « Differential Regulation of Cortactin and N-WASP-Mediated Actin Polymerization by Missing in Metastasis (MIM) Protein ». *Oncogene* 24(12):2059-66. doi: 10.1038/sj.onc.1208412.
- Lingwood, Daniel, Jonas Ries, Petra Schwille, et Kai Simons. 2008. « Plasma Membranes Are Poised for Activation of Raft Phase Coalescence at Physiological Temperature ». *Proceedings of the National Academy of Sciences of the United States of America* 105(29):10005-10. doi: 10.1073/pnas.0804374105.
- Lingwood, Daniel, et Kai Simons. 2010. « Lipid Rafts as a Membrane-Organizing Principle ». *Science (New York, N.Y.)* 327(5961):46-50. doi: 10.1126/science.1174621.
- Lipowsky, R., et E. Sackmann. 1995. *Structure and Dynamics of Membranes: I. From Cells to Vesicles / II. Generic and Specific Interactions*. Elsevier.
- Liu, Libin, Dennis Brown, Mary McKee, Nathan K. LeBrasseur, Dan Yang, Kenneth H. Albrecht, Katya Ravid, et Paul F. Pilch. 2008. « Deletion of Cavin/PTRF causes global loss of caveolae, dyslipidemia and glucose intolerance ». *Cell metabolism* 8(4):310-17. doi: 10.1016/j.cmet.2008.07.008.
- Liu, Libin, Carsten G. Hansen, Brian J. Honeyman, Benjamin J. Nichols, et Paul F. Pilch. 2014. « Cavin-3 Knockout Mice Show That Cavin-3 Is Not Essential for Caveolae Formation, for Maintenance of Body Composition, or for Glucose Tolerance ». *PLOS ONE* 9(7):e102935. doi: 10.1371/journal.pone.0102935.
- Liu, Libin, et Paul F. Pilch. 2008. « A Critical Role of Cavin (Polymerase I and Transcript Release Factor) in Caveolae Formation and Organization * ». *Journal of Biological Chemistry* 283(7):4314-22. doi: 10.1074/jbc.M707890200.
- Liu, Libin, et Paul F. Pilch. 2016. « PTRF/Cavin-1 Promotes Efficient Ribosomal RNA Transcription in Response to Metabolic Challenges ». *ELife* 5:e17508. doi: 10.7554/eLife.17508.
- Liu, Yin, Natalya V. Belkina, Chung Park, Raj Nambiar, Scott M. Loughhead, Genaro Patino-Lopez, Khadija Ben-Aissa, Jian-Jiang Hao, Michael J. Kruhlak, Hai Qi, Ulrich H. von Andrian, John H. Kehrl, Matthew J. Tyska, et Stephen Shaw. 2012. « Constitutively active ezrin increases membrane tension, slows migration, and impedes endothelial transmigration of lymphocytes in vivo in mice ». *Blood* 119(2):445-53. doi: 10.1182/blood-2011-07-368860.

- Lo, Harriet P., Susan J. Nixon, Thomas E. Hall, Belinda S. Cowling, Charles Ferguson, Garry P. Morgan, Nicole L. Schieber, Manuel A. Fernandez-Rojo, Michele Bastiani, Matthias Floetenmeyer, Nick Martel, Jocelyn Laporte, Paul F. Pilch, et Robert G. Parton. 2015. « The caveolin–cavin system plays a conserved and critical role in mechanoprotection of skeletal muscle ». *Journal of Cell Biology* 210(5):833-49. doi: 10.1083/jcb.201501046.
- Ludwig, Alexander, Gillian Howard, Carolina Mendoza-Topaz, Thomas Deerinck, Mason Mackey, Sara Sandin, Mark H. Ellisman, et Benjamin J. Nichols. 2013. « Molecular Composition and Ultrastructure of the Caveolar Coat Complex ». *PLoS Biology* 11(8):e1001640. doi: 10.1371/journal.pbio.1001640.
- Ludwig, Alexander, Benjamin James Nichols, et Sara Sandin. 2016. « Architecture of the caveolar coat complex ». *Journal of Cell Science* 129(16):3077-83. doi: 10.1242/jcs.191262.
- Machacek, Matthias, Louis Hodgson, Christopher Welch, Hunter Elliott, Olivier Pertz, Perihan Nalbant, Amy Abell, Gary L. Johnson, Klaus M. Hahn, et Gaudenz Danuser. 2009. « Coordination of Rho GTPase Activities during Cell Protrusion ». *Nature* 461(7260):99-103. doi: 10.1038/nature08242.
- Machado, Fabiana S., Nilda E. Rodriguez, Daniel Adesse, Luciana R. Garzoni, Lisia Esper, Michael P. Lisanti, Robert D. Burk, Chris Albanese, Koenraad Van Doorslaer, Louis M. Weiss, Fnu Nagajothi, Joshua D. Nosanchuk, Mary E. Wilson, et Herbert B. Tanowitz. 2012. « RECENT DEVELOPMENTS IN THE INTERACTIONS BETWEEN CAVEOLIN AND PATHOGENS ». *Advances in experimental medicine and biology* 729:65-82. doi: 10.1007/978-1-4614-1222-9_5.
- Madaule, P., et R. Axel. 1985. « A Novel Ras-Related Gene Family ». *Cell* 41(1):31-40. doi: 10.1016/0092-8674(85)90058-3.
- Maddugoda, Madhavi P., Caroline Stefani, David Gonzalez-Rodriguez, Juha Saarikangas, Stéphanie Torrino, Sebastien Janel, Patrick Munro, Anne Doye, François Prodon, Michel Aurrand-Lions, Pierre L. Goossens, Frank Lafont, Patricia Bassereau, Pekka Lappalainen, Françoise Brochard, et Emmanuel Lemichez. 2011. « CAMP Signaling by Anthrax Edema Toxin Induces Transendothelial Cell Tunnels, Which Are Resealed by MIM via Arp2/3-Driven Actin Polymerization ». *Cell Host & Microbe* 10(5):464-74. doi: 10.1016/j.chom.2011.09.014.
- Maekawa, M., T. Ishizaki, S. Boku, N. Watanabe, A. Fujita, A. Iwamatsu, T. Obinata, K. Ohashi, K. Mizuno, et S. Narumiya. 1999. « Signaling from Rho to the Actin Cytoskeleton through Protein Kinases ROCK and LIM-Kinase ». *Science (New York, N.Y.)* 285(5429):895-98. doi: 10.1126/science.285.5429.895.
- Mäepea, O., et A. Bill. 1992. « Pressures in the Juxtacanalicular Tissue and Schlemm's Canal in Monkeys ». *Experimental Eye Research* 54(6):879-83. doi: 10.1016/0014-4835(92)90151-h.
- Maguy, Ange, Terence E. Hebert, et Stanley Nattel. 2006. « Involvement of lipid rafts and caveolae in cardiac ion channel function ». *Cardiovascular Research* 69(4):798-807. doi: 10.1016/j.cardiores.2005.11.013.
- Marchesi, V. T., et J. L. Gowans. 1964. « THE MIGRATION OF LYMPHOCYTES THROUGH THE ENDOTHELIUM OF VENULES IN LYMPH NODES: AN ELECTRON MICROSCOPE STUDY ». *Proceedings of the Royal Society of London. Series B, Biological Sciences* 159:283-90. doi: 10.1098/rspb.1964.0002.
- Marsh, Derek. 2006. « Elastic Curvature Constants of Lipid Monolayers and Bilayers ». *Chemistry and Physics of Lipids* 144(2):146-59. doi: 10.1016/j.chemphyslip.2006.08.004.
- Martinelli, Roberta, Masataka Kamei, Peter T. Sage, Ramiro Massol, Laya Varghese, Tracey Sciuto, Mourad Toporsian, Ann M. Dvorak, Tomas Kirchhausen, Timothy A. Springer, et Christopher V. Carman. 2013. « Release of cellular tension signals self-restorative ventral lamellipodia to heal barrier micro-wounds ». *The Journal of Cell Biology* 201(3):449-65. doi: 10.1083/jcb.201209077.
- Martinelli, Roberta, Adam S. Zeiger, Matthew Whitfield, Tracey E. Sciuto, Ann Dvorak, Krystyn J. Van Vliet, John Greenwood, et Christopher V. Carman. 2014. « Probing the biomechanical contribution of the endothelium to lymphocyte migration: diapedesis by the path of least resistance ». *Journal of Cell Science* 127(17):3720-34. doi: 10.1242/jcs.148619.
- Masters, T. A., B. Pontes, V. Viasnoff, Y. Li, et N. C. Gauthier. 2013. « Plasma Membrane Tension Orchestrates Membrane Trafficking, Cytoskeletal Remodeling, and Biochemical Signaling during Phagocytosis ». *Proceedings of the National Academy of Sciences* 110(29):11875-80. doi: 10.1073/pnas.1301766110.

- Masuda, Michitaka, et Naoki Mochizuki. 2010. « Structural Characteristics of BAR Domain Superfamily to Sculpt the Membrane ». *Seminars in Cell & Developmental Biology* 21(4):391-98. doi: 10.1016/j.semcd.2010.01.010.
- Mattila, Pieta K., Anette Pykäläinen, Juha Saarikangas, Ville O. Paavilainen, Helena Vihinen, Eija Jokitalo, et Pekka Lappalainen. 2007. « Missing-in-metastasis and IRSp53 deform PI(4,5)P2-rich membranes by an inverse BAR domain-like mechanism ». *The Journal of Cell Biology* 176(7):953-64. doi: 10.1083/jcb.200609176.
- Mayor, Satyajit, et Richard E. Pagano. 2007. « Pathways of Clathrin-Independent Endocytosis ». *Nature Reviews Molecular Cell Biology* 8(8):603-12. doi: 10.1038/nrm2216.
- McMahon, H. T., et E. Boucrot. 2015. « Membrane Curvature at a Glance ». *Journal of Cell Science* 128(6):1065-70. doi: 10.1242/jcs.114454.
- McMahon, Harvey T., et Emmanuel Boucrot. 2011. « Molecular Mechanism and Physiological Functions of Clathrin-Mediated Endocytosis ». *Nature Reviews. Molecular Cell Biology* 12(8):517-33. doi: 10.1038/nrm3151.
- McMahon, Harvey T., et Jennifer L. Gallop. 2005. « Membrane Curvature and Mechanisms of Dynamic Cell Membrane Remodelling ». *Nature* 438(7068):590-96. doi: 10.1038/nature04396.
- McMahon, Harvey T., et Ian G. Mills. 2004. « COP and Clathrin-Coated Vesicle Budding: Different Pathways, Common Approaches ». *Current Opinion in Cell Biology* 16(4):379-91. doi: 10.1016/j.ceb.2004.06.009.
- McMahon, Kerrie-Ann, Yeping Wu, Yann Gambin, Emma Sierecki, Vikas A. Tillu, Thomas Hall, Nick Martel, Satomi Okano, Shayli Varasteh Moradi, Jayde E. Ruelcke, Charles Ferguson, Alpha S. Yap, Kirill Alexandrov, Michelle M. Hill, et Robert G. Parton. 2019. « Identification of Intracellular Cavin Target Proteins Reveals Cavin-PP1alpha Interactions Regulate Apoptosis ». *Nature Communications* 10(1):3279. doi: 10.1038/s41467-019-11111-1.
- McMahon, Kerrie-Ann, Hubert Zajicek, Wei-Ping Li, Michael J. Peyton, John D. Minna, V. James Hernandez, Katherine Luby-Phelps, et Richard G. W. Anderson. 2009. « SRBC/cavin-3 is a caveolin adapter protein that regulates caveolae function ». *The EMBO Journal* 28(8):1001-15. doi: 10.1038/emboj.2009.46.
- van Meer, Gerrit, Dennis R. Voelker, et Gerald W. Feigenson. 2008. « Membrane lipids: where they are and how they behave ». *Nature reviews. Molecular cell biology* 9(2):112-24. doi: 10.1038/nrm2330.
- Mejillano, Marisan R., Shin-ichiro Kojima, Derek Anthony Applewhite, Frank B. Gertler, Tatyana M. Svitkina, et Gary G. Borisy. 2004. « Lamellipodial Versus Filopodial Mode of the Actin Nanomachinery: Pivotal Role of the Filament Barbed End ». *Cell* 118(3):363-73. doi: 10.1016/j.cell.2004.07.019.
- Meng, Fanrui, Sandeep Saxena, Youtao Liu, Bharat Joshi, Timothy H. Wong, Jay Shankar, Leonard J. Foster, Pascal Bernatchez, et Ivan R. Nabi. 2017. « The Phospho-Caveolin-1 Scaffolding Domain Dampens Force Fluctuations in Focal Adhesions and Promotes Cancer Cell Migration ». *Molecular Biology of the Cell* 28(16):2190-2201. doi: 10.1091/mbc.E17-05-0278.
- Mergia, Ayalew. 2017. « The Role of Caveolin 1 in HIV Infection and Pathogenesis ». *Viruses* 9(6):129. doi: 10.3390/v9060129.
- Meshulam, Tova, Jeffrey R. Simard, Jonathan Wharton, James A. Hamilton, et Paul F. Pilch. 2006. « Role of Caveolin-1 and Cholesterol in Transmembrane Fatty Acid Movement ». *Biochemistry* 45(9):2882-93. doi: 10.1021/bi051999b.
- Messad, N., L. Landraud, B. Canivet, G. Lina, J. L. Richard, A. Sotto, J. P. Lavigne, E. Lemichez, et French Study Group on the Diabetic Foot. 2013. « Distribution of Edin in Staphylococcus Aureus Isolated from Diabetic Foot Ulcers ». *Clinical Microbiology and Infection: The Official Publication of the European Society of Clinical Microbiology and Infectious Diseases* 19(9):875-80. doi: 10.1111/1469-0691.12084.
- Milici, A. J., K. R. Peters, et G. E. Palade. 1986. « The Endothelial Pocket ». *Cell and Tissue Research* 244(3):493-99. doi: 10.1007/BF00212526.
- Millán, Jaime, Lindsay Hewlett, Matthew Glyn, Derek Toomre, Peter Clark, et Anne J. Ridley. 2006. « Lymphocyte Transcellular Migration Occurs through Recruitment of Endothelial ICAM-1 to Caveola- and F-Actin-Rich Domains ». *Nature Cell Biology* 8(2):113-23. doi: 10.1038/ncb1356.
- Minetti, Carlo, Massimo Bado, Paolo Broda, Federica Sotgia, Claudio Bruno, Ferruccio Galbiati, Daniela Volonte, Giuseppe Lucania, Antonio Pavan, Eduardo Bonilla, Michael P. Lisanti, et Giuseppe Cordone.

2002. « Impairment of Caveolae Formation and T-System Disorganization in Human Muscular Dystrophy with Caveolin-3 Deficiency ». *The American Journal of Pathology* 160(1):265-70.
- Minguet, Susana, Kathrin Kläsener, Anna-Maria Schaffer, Gina J. Fiala, Teresa Osteso-Ibáñez, Katrin Raute, Inmaculada Navarro-Lérida, Frederike A. Hartl, Maximilian Seidl, Michael Reth, et Miguel A. Del Pozo. 2017. « Caveolin-1-Dependent Nanoscale Organization of the BCR Regulates B Cell Tolerance ». *Nature Immunology* 18(10):1150-59. doi: 10.1038/ni.3813.
- Mizutani, Kosuke, Hernan Roca, Zachary Varsos, et Kenneth J. Pienta. 2009. « Possible Mechanism of CCL2-Induced Akt Activation in Prostate Cancer Cells ». *Anticancer Research* 29(8):3109-13.
- Moayeri, Mahtab, et Stephen H. Leppla. 2004. « The Roles of Anthrax Toxin in Pathogenesis ». *Current Opinion in Microbiology* 7(1):19-24. doi: 10.1016/j.mib.2003.12.001.
- Monier, S., R. G. Parton, F. Vogel, J. Behlke, A. Henske, et T. V. Kurzchalia. 1995. « VIP21-caveolin, a membrane protein constituent of the caveolar coat, oligomerizes in vivo and in vitro. » *Molecular Biology of the Cell* 6(7):911-27.
- Monier, Solange, Dennis J. Dietzen, W. Randall Hastings, Douglas M. Lublin, et Teymuraz V. Kurzchalia. 1996. « Oligomerization of VIP21-Caveolin in Vitro Is Stabilized by Long Chain Fatty Acylation or Cholesterol ». *FEBS Letters* 388(2-3):143-49. doi: 10.1016/0014-5793(96)00519-4.
- Mooren, Olivia L., Jinmei Li, Julie Nawas, et John A. Cooper. 2014. « Endothelial cells use dynamic actin to facilitate lymphocyte transendothelial migration and maintain the monolayer barrier ». *Molecular Biology of the Cell* 25(25):4115-29. doi: 10.1091/mbc.E14-05-0976.
- Mora, Rosalia, Vera L. Bonilha, Alan Marmorstein, Philipp E. Scherer, Dennis Brown, Michael P. Lisanti, et Enrique Rodriguez-Boulán. 1999. « Caveolin-2 Localizes to the Golgi Complex but Redistributes to Plasma Membrane, Caveolae, and Rafts When Co-Expressed with Caveolin-1 * ». *Journal of Biological Chemistry* 274(36):25708-17. doi: 10.1074/jbc.274.36.25708.
- Morén, Björn, Claudio Shah, Mark T. Howes, Nicole L. Schieber, Harvey T. McMahon, Robert G. Parton, Oliver Daumke, et Richard Lundmark. 2012. « EHD2 Regulates Caveolar Dynamics via ATP-Driven Targeting and Oligomerization ». *Molecular Biology of the Cell* 23(7):1316-29. doi: 10.1091/mbc.E11-09-0787.
- Mullins, R. D., J. A. Heuser, et T. D. Pollard. 1998. « The Interaction of Arp2/3 Complex with Actin: Nucleation, High Affinity Pointed End Capping, and Formation of Branching Networks of Filaments ». *Proceedings of the National Academy of Sciences* 95(11):6181-86. doi: 10.1073/pnas.95.11.6181.
- Mundy, Dorothy I., Thomas Machleidt, Yun-shu Ying, Richard G. W. Anderson, et George S. Bloom. 2002. « Dual Control of Caveolar Membrane Traffic by Microtubules and the Actin Cytoskeleton ». *Journal of Cell Science* 115(22):4327-39. doi: 10.1242/jcs.00117.
- Munro, Patrick, Maxime Benchetrit, Marie-Anne Nahori, Caroline Stefani, René Clément, Jean-François Michiels, Luce Landraud, Olivier Dussurget, et Emmanuel Lemichez. 2010. « The Staphylococcus Aureus Epidermal Cell Differentiation Inhibitor Toxin Promotes Formation of Infection Foci in a Mouse Model of Bacteremia ». *Infection and Immunity* 78(8):3404-11. doi: 10.1128/IAI.00319-10.
- Murata, M., J. Peränen, R. Schreiner, F. Wieland, T. V. Kurzchalia, et K. Simons. 1995. « VIP21/Caveolin Is a Cholesterol-Binding Protein ». *Proceedings of the National Academy of Sciences* 92(22):10339-43. doi: 10.1073/pnas.92.22.10339.
- Muriel, O., A. Echarri, C. Hellriegel, D. M. Pavon, L. Beccari, et M. A. Del Pozo. 2011. « Phosphorylated Filamin A Regulates Actin-Linked Caveolae Dynamics ». *Journal of Cell Science* 124(16):2763-76. doi: 10.1242/jcs.080804.
- Nassar, Zeyad D., et Marie-Odile Parat. 2015. « Chapter Six - Cavin Family: New Players in the Biology of Caveolae ». P. 235-305 in *International Review of Cell and Molecular Biology*. Vol. 320, édité par K. W. Jeon. Academic Press.
- Navale, Archana M., et Archana N. Paranjape. 2016. « Glucose Transporters: Physiological and Pathological Roles ». *Biophysical Reviews* 8(1):5-9. doi: 10.1007/s12551-015-0186-2.
- Nethe, Micha, Eloise C. Anthony, Mar Fernandez-Borja, Rob Dee, Dirk Geerts, Paul J. Hensbergen, André M. Deelder, Gudula Schmidt, et Peter L. Hordijk. 2010. « Focal-Adhesion Targeting Links Caveolin-1 to a Rac1-Degradation Pathway ». *Journal of Cell Science* 123(11):1948-58. doi: 10.1242/jcs.062919.

- Ng, Win Pin, Kevin D. Webster, Caroline Stefani, Eva M. Schmid, Emmanuel Lemichez, Patricia Bassereau, Daniel A. Fletcher, et Valerie Marie Weaver. 2017. « Force-induced transcellular tunnel formation in endothelial cells ». *Molecular Biology of the Cell* 28(20):2650-60. doi: 10.1091/mbc.e17-01-0080.
- Nguyen, Long N., Dongliang Ma, Guanghou Shui, Peiyan Wong, Amaury Cazenave-Gassiot, Xiaodong Zhang, Markus R. Wenk, Eyleen L. K. Goh, et David L. Silver. 2014. « Mfsd2a Is a Transporter for the Essential Omega-3 Fatty Acid Docosahexaenoic Acid ». *Nature* 509(7501):503-6. doi: 10.1038/nature13241.
- Nichols, Benjamin J. 2002. « A Distinct Class of Endosome Mediates Clathrin-Independent Endocytosis to the Golgi Complex ». *Nature Cell Biology* 4(5):374-78. doi: 10.1038/ncb787.
- Nobes, Catherine D., et Alan Hall. 1995. « Rho, Rac, and Cdc42 GTPases Regulate the Assembly of Multimolecular Focal Complexes Associated with Actin Stress Fibers, Lamellipodia, and Filopodia ». *Cell* 81(1):53-62. doi: 10.1016/0092-8674(95)90370-4.
- Nourshargh, Sussan, Peter L. Hordijk, et Michael Sixt. 2010. « Breaching Multiple Barriers: Leukocyte Motility through Venular Walls and the Interstitium ». *Nature Reviews Molecular Cell Biology* 11(5):366-78. doi: 10.1038/nrm2889.
- Ogata, Takehiro, Tomomi Ueyama, Koji Isodono, Masashi Tagawa, Naofumi Takehara, Tsuneaki Kawashima, Koichiro Harada, Tomosaburo Takahashi, Tetsuo Shioi, Hiroaki Matsubara, et Hidemasa Oh. 2008. « MURC, a Muscle-Restricted Coiled-Coil Protein That Modulates the Rho/ROCK Pathway, Induces Cardiac Dysfunction and Conduction Disturbance ». *Molecular and Cellular Biology* 28(10):3424-36. doi: 10.1128/MCB.02186-07.
- Oh, Phil, Per Borgström, Halina Witkiewicz, Yan Li, Bengt J. Borgström, Adrian Chrastina, Koji Iwata, Kurt R. Zinn, Richard Baldwin, Jacqueline E. Testa, et Jan E. Schnitzer. 2007. « Live dynamic imaging of caveolae pumping targeted antibody rapidly and specifically across endothelium in the lung ». *Nature biotechnology* 25(3):327-37. doi: 10.1038/nbt1292.
- Okamoto, Michiyo, Kazuo Kurokawa, Kumi Matsuura-Tokita, Chieko Saito, Ryogo Hirata, et Akihiko Nakano. 2012. « High-Curvature Domains of the ER Are Important for the Organization of ER Exit Sites in *Saccharomyces Cerevisiae* ». *Journal of Cell Science* jcs.100065. doi: 10.1242/jcs.100065.
- Olofsson, B. 1999. « Rho Guanine Dissociation Inhibitors: Pivotal Molecules in Cellular Signalling ». *Cellular Signalling* 11(8):545-54. doi: 10.1016/s0898-6568(98)00063-1.
- Olson, Michael F., et Erik Sahai. 2009. « The Actin Cytoskeleton in Cancer Cell Motility ». *Clinical & Experimental Metastasis* 26(4):273-87. doi: 10.1007/s10585-008-9174-2.
- Örtengren, Unn, Margareta Karlsson, Natascha Blazic, Maria Blomqvist, Fredrik H. Nystrom, Johanna Gustavsson, Pam Fredman, et Peter Strålfors. 2004. « Lipids and Glycosphingolipids in Caveolae and Surrounding Plasma Membrane of Primary Rat Adipocytes ». *European Journal of Biochemistry* 271(10):2028-36. doi: 10.1111/j.1432-1033.2004.04117.x.
- Öst, Anita, Unn Örtengren, Johanna Gustavsson, Fredrik H. Nystrom, et Peter Strålfors. 2005. « Triacylglycerol Is Synthesized in a Specific Subclass of Caveolae in Primary Adipocytes * ». *Journal of Biological Chemistry* 280(1):5-8. doi: 10.1074/jbc.C400429200.
- Ostermeyer, Anne G., James M. Paci, Youchun Zeng, Douglas M. Lublin, Sean Munro, et Deborah A. Brown. 2001. « Accumulation of Caveolin in the Endoplasmic Reticulum Redirects the Protein to Lipid Storage Droplets ». *The Journal of Cell Biology* 152(5):1071-78.
- Overby, D. R., E. H. Zhou, R. Vargas-Pinto, R. M. Pedrigi, R. Fuchshofer, S. T. Braakman, R. Gupta, K. M. Perkumas, J. M. Sherwood, A. Vahabikashi, Q. Dang, J. H. Kim, C. R. Ethier, W. D. Stamer, J. J. Fredberg, et M. Johnson. 2014. « Altered Mechanobiology of Schlemm's Canal Endothelial Cells in Glaucoma ». *Proceedings of the National Academy of Sciences* 111(38):13876-81. doi: 10.1073/pnas.1410602111.
- Palade, George E. 1953. « AN ELECTRON MICROSCOPE STUDY OF THE MITOCHONDRIAL STRUCTURE ». *Journal of Histochemistry & Cytochemistry* 1(4):188-211. doi: 10.1177/1.4.188.
- Pan, Jianjun, Stephanie Tristram-Nagle, et John F. Nagle. 2009. « Effect of Cholesterol on Structural and Mechanical Properties of Membranes Depends on Lipid Chain Saturation ». *Physical Review. E, Statistical, Nonlinear, and Soft Matter Physics* 80(2 Pt 1):021931. doi: 10.1103/PhysRevE.80.021931.
- Park, David S., Scott E. Woodman, William Schubert, Alex W. Cohen, Philippe G. Frank, Madhulika Chandra, Jamshid Shirani, Babak Razani, Baiyu Tang, Linda A. Jelicks, Stephen M. Factor, Louis M. Weiss,

- Herbert B. Tanowitz, et Michael P. Lisanti. 2002. « Caveolin-1/3 Double-Knockout Mice Are Viable, but Lack Both Muscle and Non-Muscle Caveolae, and Develop a Severe Cardiomyopathic Phenotype ». *The American Journal of Pathology* 160(6):2207-17. doi: 10.1016/S0002-9440(10)61168-6.
- Parton, Robert G., Michael Hanzal-Bayer, et John F. Hancock. 2006. « Biogenesis of caveolae: a structural model for caveolin-induced domain formation ». *Journal of Cell Science* 119(5):787-96. doi: 10.1242/jcs.02853.
- Parton, Robert G., Kerrie-Ann McMahon, et Yeping Wu. 2020. « Caveolae: Formation, Dynamics, and Function ». *Current Opinion in Cell Biology* 65:8-16. doi: 10.1016/j.ceb.2020.02.001.
- Parton, Robert G., et Miguel A. del Pozo. 2013. « Caveolae as Plasma Membrane Sensors, Protectors and Organizers ». *Nature Reviews Molecular Cell Biology* 14(2):98-112. doi: 10.1038/nrm3512.
- Parton, Robert G., et Kai Simons. 2007. « The Multiple Faces of Caveolae ». *Nature Reviews Molecular Cell Biology* 8(3):185-94. doi: 10.1038/nrm2122.
- Parton, Robert G., Vikas Tillu, Kerrie-Ann McMahon, et Brett M. Collins. 2021. « Key Phases in the Formation of Caveolae ». *Current Opinion in Cell Biology* 71:7-14. doi: 10.1016/j.ceb.2021.01.009.
- Paul, Aditya, et Thomas Pollard. 2008. « The Role of the FH1 Domain and Profilin in Formin-Mediated Actin-Filament Elongation and Nucleation ». *Current Biology* 18(1):9-19. doi: 10.1016/j.cub.2007.11.062.
- Peetla, Chiranjeevi, Sivakumar Vijayaraghavalu, et Vinod Labhasetwar. 2013. « Biophysics of Cell Membrane Lipids in Cancer Drug Resistance: Implications for Drug Transport and Drug Delivery with Nanoparticles ». *Advanced Drug Delivery Reviews* 65(13-14):1686-98. doi: 10.1016/j.addr.2013.09.004.
- Pelkmans, Lucas, Thomas Bürli, Marino Zerial, et Ari Helenius. 2004. « Caveolin-Stabilized Membrane Domains as Multifunctional Transport and Sorting Devices in Endocytic Membrane Traffic ». *Cell* 118(6):767-80. doi: 10.1016/j.cell.2004.09.003.
- Pelkmans, Lucas, Jürgen Kartenbeck, et Ari Helenius. 2001. « Caveolar Endocytosis of Simian Virus 40 Reveals a New Two-Step Vesicular-Transport Pathway to the ER ». *Nature Cell Biology* 3(5):473-83. doi: 10.1038/35074539.
- Pelkmans, Lucas, Daniel Püntener, et Ari Helenius. 2002. « Local Actin Polymerization and Dynamin Recruitment in SV40-Induced Internalization of Caveolae ». *Science* 296(5567):535-39. doi: 10.1126/science.1069784.
- Pelkmans, Lucas, et Marino Zerial. 2005. « Kinase-Regulated Quantal Assemblies and Kiss-and-Run Recycling of Caveolae ». *Nature* 436(7047):128-33. doi: 10.1038/nature03866.
- Pellegrin, Stéphanie, et Harry Mellor. 2005. « The Rho Family GTPase Rif Induces Filopodia through MDia2 ». *Current Biology* 15(2):129-33. doi: 10.1016/j.cub.2005.01.011.
- Peng, Fangfang, Dongcheng Wu, Alistair J. Ingram, Baifang Zhang, Bo Gao, et Joan C. Krepinsky. 2007. « RhoA Activation in Mesangial Cells by Mechanical Strain Depends on Caveolae and Caveolin-1 Interaction ». *Journal of the American Society of Nephrology* 18(1):189-98. doi: 10.1681/ASN.2006050498.
- Peter, Brian J., Helen M. Kent, Ian G. Mills, Yvonne Vallis, P. Jonathan G. Butler, Philip R. Evans, et Harvey T. McMahon. 2004. « BAR Domains as Sensors of Membrane Curvature: The Amphiphysin BAR Structure ». *Science* 303(5657):495-99. doi: 10.1126/science.1092586.
- Pietuch, Anna, Bastian R. Brückner, et Andreas Janshoff. 2013. « Membrane Tension Homeostasis of Epithelial Cells through Surface Area Regulation in Response to Osmotic Stress ». *Biochimica et Biophysica Acta (BBA) - Molecular Cell Research* 1833(3):712-22. doi: 10.1016/j.bbamcr.2012.11.006.
- Pilch, Paul F., Ricardo P. Souto, Libin Liu, Mark P. Jedrychowski, Eric A. Berg, Catherine E. Costello, et Steven P. Gygi. 2007. « Cellular Spelunking: Exploring Adipocyte Caveolae ». *Journal of Lipid Research* 48(10):2103-11. doi: 10.1194/jlr.R700009-JLR200.
- Pinot, Mathieu, Stefano Vanni, Sophie Pagnotta, Sandra Lacas-Gervais, Laurie-Anne Payet, Thierry Ferreira, Romain Gautier, Bruno Goud, Bruno Antonny, et Hélène Barelli. 2014. « Polyunsaturated Phospholipids Facilitate Membrane Deformation and Fission by Endocytic Proteins ». *Science*. doi: 10.1126/science.1255288.
- Place, Aaron T., Zhenlong Chen, Farnaz R. Bakhshi, Guoquan Liu, John P. O'Bryan, et Richard D. Minshall. 2011. « Cooperative Role of Caveolin-1 and C-Terminal Src Kinase Binding Protein in C-Terminal Src

- Kinase-Mediated Negative Regulation of c-Src ». *Molecular Pharmacology* 80(4):665-72. doi: 10.1124/mol.111.073957.
- Plomann, Markus, Rita Lange, Gaby Vopper, Harold Cremer, Uwe A. O. Heinlein, Stephen Scheff, Stanley A. Baldwin, Michael Leitges, Matthias Cramer, Mats Paulsson, et Dagmar Barthels. 1998. « PACSIN, a Brain Protein That Is Upregulated upon Differentiation into Neuronal Cells ». *European Journal of Biochemistry* 256(1):201-11. doi: 10.1046/j.1432-1327.1998.2560201.x.
- Plomann, Markus, Julia G. Wittmann, et Markus G. Rudolph. 2010. « A Hinge in the Distal End of the PACSIN 2 F-BAR Domain May Contribute to Membrane-Curvature Sensing ». *Journal of Molecular Biology* 400(2):129-36. doi: 10.1016/j.jmb.2010.05.008.
- Pol, Albert, Sally Martin, Manuel A. Fernandez, Charles Ferguson, Amanda Carozzi, Robert Luetterforst, Carlos Enrich, et Robert G. Parton. 2004. « Dynamic and Regulated Association of Caveolin with Lipid Bodies: Modulation of Lipid Body Motility and Function by a Dominant Negative Mutant ». *Molecular Biology of the Cell* 15(1):99-110. doi: 10.1091/mbc.E03-06-0368.
- Pol, Albert, Sally Martin, Manuel A. Fernández, Mercedes Ingelmo-Torres, Charles Ferguson, Carlos Enrich, et Robert G. Parton. 2005. « Cholesterol and Fatty Acids Regulate Dynamic Caveolin Trafficking through the Golgi Complex and between the Cell Surface and Lipid Bodies ». *Molecular Biology of the Cell* 16(4):2091-2105. doi: 10.1091/mbc.E04-08-0737.
- Pol, Albert, Frederic Morales-Paytuví, Marta Bosch, et Robert G. Parton. 2020. « Non-Caveolar Caveolins – Duties Outside the Caves ». *Journal of Cell Science* 133(9):jcs241562. doi: 10.1242/jcs.241562.
- Pontes, Bruno, Pascale Monzo, Laurent Gole, Anabel-Lise Le Roux, Anita Joanna Kosmalska, Zhi Yang Tam, Weiwei Luo, Sophie Kan, Virgile Viasnoff, Pere Roca-Cusachs, Lisa Tucker-Kellogg, et Nils C. Gauthier. 2017. « Membrane tension controls adhesion positioning at the leading edge of cells ». *The Journal of Cell Biology* 216(9):2959-77. doi: 10.1083/jcb.201611117.
- del Pozo, Miguel A., Nazilla B. Alderson, William B. Kiosses, Hui-Hsien Chiang, Richard G. W. Anderson, et Martin A. Schwartz. 2004. « Integrins Regulate Rac Targeting by Internalization of Membrane Domains ». *Science* 303(5659):839-42. doi: 10.1126/science.1092571.
- del Pozo, Miguel A., Nagaraj Balasubramanian, Nazilla B. Alderson, William B. Kiosses, Araceli Grande-García, Richard G. W. Anderson, et Martin A. Schwartz. 2005. « Phospho-Caveolin-1 Mediates Integrin-Regulated Membrane Domain Internalization ». *Nature Cell Biology* 7(9):901-8. doi: 10.1038/ncb1293.
- Pradhan, Bhola Shankar, et Tomasz J. Prószyński. 2020. « A Role for Caveolin-3 in the Pathogenesis of Muscular Dystrophies ». *International Journal of Molecular Sciences* 21(22):8736. doi: 10.3390/ijms21228736.
- Predescu, Sanda A., Dan N. Predescu, et Asrar B. Malik. 2007. « Molecular Determinants of Endothelial Transcytosis and Their Role in Endothelial Permeability ». *American Journal of Physiology-Lung Cellular and Molecular Physiology* 293(4):L823-42. doi: 10.1152/ajplung.00436.2006.
- Prescott, L., et M. W. Brightman. 1976. « The Sarcolemma of Aplysia Smooth Muscle in Freeze-Fracture Preparations ». *Tissue & Cell* 8(2):248-58.
- Pruyne, David, Marie Evangelista, Changsong Yang, Erfei Bi, Sally Zigmund, Anthony Bretscher, et Charles Boone. 2002. « Role of Formins in Actin Assembly: Nucleation and Barbed-End Association ». *Science*. doi: 10.1126/science.1072309.
- Rajab, Anna, Volker Straub, Liza J. McCann, Dominik Seelow, Raymonda Varon, Rita Barresi, Anne Schulze, Barbara Lucke, Susanne Lützkendorf, Mohsen Karbasiyan, Sebastian Bachmann, Simone Spuler, et Markus Schuelke. 2010. « Fatal Cardiac Arrhythmia and Long-QT Syndrome in a New Form of Congenital Generalized Lipodystrophy with Muscle Rippling (CGL4) Due to PTRF-CAVIN Mutations ». *PLOS Genetics* 6(3):e1000874. doi: 10.1371/journal.pgen.1000874.
- Raucher, D., et M. P. Sheetz. 1999. « Characteristics of a membrane reservoir buffering membrane tension. ». *Biophysical Journal* 77(4):1992-2002.
- Raucher, Drazen, et Michael P. Sheetz. 2000. « Cell Spreading and Lamellipodial Extension Rate Is Regulated by Membrane Tension ». *Journal of Cell Biology* 148(1):127-36. doi: 10.1083/jcb.148.1.127.

- Rausch, Valentina, Jonathan R. Bostrom, Jiwon Park, Isabel R. Bravo, Yi Feng, David C. Hay, Brian A. Link, et Carsten G. Hansen. 2019. « The Hippo Pathway Regulates Caveolae Expression and Mediates Flow Response via Caveolae ». *Current Biology* 29(2):242-255.e6. doi: 10.1016/j.cub.2018.11.066.
- Ravid, Dana, Dana Chuderland, Limor Landsman, Yaakov Lavie, Reuven Reich, et Mordechai Liscovitch. 2008. « Filamin A Is a Novel Caveolin-1-Dependent Target in IGF-I-Stimulated Cancer Cell Migration ». *Experimental Cell Research* 314(15):2762-73. doi: 10.1016/j.yexcr.2008.06.004.
- Razani, Babak, Jeffery A. Engelman, Xiao Bo Wang, William Schubert, Xiao Lan Zhang, Carolyn B. Marks, Frank Macaluso, Robert G. Russell, Maomi Li, Richard G. Pestell, Dolores Di Vizio, Harry Hou, Burkhard Kneitz, Guy Lagaud, George J. Christ, Winfried Edelmann, et Michael P. Lisanti. 2001. « Caveolin-1 Null Mice Are Viable but Show Evidence of Hyperproliferative and Vascular Abnormalities* ». *Journal of Biological Chemistry* 276(41):38121-38. doi: 10.1074/jbc.M105408200.
- dos Remedios, C. G., D. Chhabra, M. Kekic, I. V. Dedova, M. Tsubakihara, D. A. Berry, et N. J. Nosworthy. 2003. « Actin Binding Proteins: Regulation of Cytoskeletal Microfilaments ». *Physiological Reviews* 83(2):433-73. doi: 10.1152/physrev.00026.2002.
- Ressad, F., D. Didry, C. Egile, D. Pantaloni, et M. F. Carlier. 1999. « Control of Actin Filament Length and Turnover by Actin Depolymerizing Factor (ADF/Cofilin) in the Presence of Capping Proteins and ARP2/3 Complex ». *The Journal of Biological Chemistry* 274(30):20970-76. doi: 10.1074/jbc.274.30.20970.
- Ridley, Anne J., et Alan Hall. 1992. « The Small GTP-Binding Protein Rho Regulates the Assembly of Focal Adhesions and Actin Stress Fibers in Response to Growth Factors ». *Cell* 70(3):389-99. doi: 10.1016/0092-8674(92)90163-7.
- Ridley, Anne J., Hugh F. Paterson, Caroline L. Johnston, Dagmar Diekmann, et Alan Hall. 1992. « The Small GTP-Binding Protein Rac Regulates Growth Factor-Induced Membrane Ruffling ». *Cell* 70(3):401-10. doi: 10.1016/0092-8674(92)90164-8.
- Riento, Kirsi, et Anne J. Ridley. 2003. « Rocks: Multifunctional Kinases in Cell Behaviour ». *Nature Reviews. Molecular Cell Biology* 4(6):446-56. doi: 10.1038/nrm1128.
- Riethmuller, Christoph, Ines Nasdala, et Dietmar Vestweber. 2008. « Nano-surgery at the leukocyte–endothelial docking site ». *Pflugers Archiv* 456:71-81. doi: 10.1007/s00424-007-0412-2.
- Riggi, Margot, Clélia Bourgoing, Mariano Macchione, Stefan Matile, Robbie Loewith, et Aurélien Roux. 2019. « TORC2 Controls Endocytosis through Plasma Membrane Tension ». *Journal of Cell Biology* 218(7):2265-76. doi: 10.1083/jcb.201901096.
- Ritter et al. 1999. « PACSIN 2, a Novel Member of the PACSIN Family of Cytoplasmic Adapter Proteins1 ». *FEBS Letters* 454(3):356-62. doi: 10.1016/S0014-5793(99)00830-3.
- Ritz, Danilo, Maja Vuk, Philipp Kirchner, Monika Bug, Sabina Schütz, Arnold Hayer, Sebastian Bremer, Caleb Lusk, Robert H. Baloh, Houkeun Lee, Timo Glatter, Matthias Gstaiger, Ruedi Aebersold, Conrad C. Wehl, et Hemmo Meyer. 2011. « Endolysosomal Sorting of Ubiquitylated Caveolin-1 Is Regulated by VCP and UBXD1 and Impaired by VCP Disease Mutations ». *Nature Cell Biology* 13(9):1116-23. doi: 10.1038/ncb2301.
- Riveline, Daniel, Eli Zamir, Nathalie Q. Balaban, Ulrich S. Schwarz, Toshimasa Ishizaki, Shuh Narumiya, Zvi Kam, Benjamin Geiger, et Alexander D. Bershadsky. 2001. « Focal Contacts as Mechanosensors: Externally Applied Local Mechanical Force Induces Growth of Focal Contacts by an Mdia1-Dependent and Rock-Independent Mechanism ». *Journal of Cell Biology* 153(6):1175-86. doi: 10.1083/jcb.153.6.1175.
- Rizzo, Victor, Deirdre P. McIntosh, Phil Oh, et Jan E. Schnitzer. 1998. « In Situ Flow Activates Endothelial Nitric Oxide Synthase in Luminal Caveolae of Endothelium with Rapid Caveolin Dissociation and Calmodulin Association* ». *Journal of Biological Chemistry* 273(52):34724-29. doi: 10.1074/jbc.273.52.34724.
- Rizzo, Victor, Christine Morton, Natacha DePaola, Jan E. Schnitzer, et Peter F. Davies. 2003. « Recruitment of endothelial caveolae into mechanotransduction pathways by flow conditioning in vitro ». *American Journal of Physiology-Heart and Circulatory Physiology* 285(4):H1720-29. doi: 10.1152/ajpheart.00344.2002.
- Rodríguez, Nilda E., Upasna Gaur, et Mary E. Wilson. 2006. « Role of Caveolae in Leishmania Chagasi Phagocytosis and Intracellular Survival in Macrophages ». *Cellular Microbiology* 8(7):1106-20. doi: 10.1111/j.1462-5822.2006.00695.x.

- Roffay, Chloé, Guillaume Molinard, Kyoohyun Kim, Victoria Barbarassa, Marta Urbanska, Vincent Mercier, José García-Calvo, Stefan Matile, Jochen Guck, Martin Lenz, et Aurélien Roux. 2021. *Quantitative Coupling of Cell Volume and Membrane Tension during Osmotic Shocks*. doi: 10.1101/2021.01.22.427801.
- Rohde, Manfred, Ellruth Müller, Gursharan S. Chhatwal, et Susanne R. Talay. 2003. « Host Cell Caveolae Act as an Entry-Port for Group A Streptococci ». *Cellular Microbiology* 5(5):323-42. doi: 10.1046/j.1462-5822.2003.00279.x.
- Rohn, Jennifer L., et Buzz Baum. 2010. « Actin and Cellular Architecture at a Glance ». *Journal of Cell Science* 123(Pt 2):155-58. doi: 10.1242/jcs.049759.
- Rohrbeck, Astrid, et Ingo Just. 2017. « Cell Entry of C3 Exoenzyme from Clostridium Botulinum ». *Current Topics in Microbiology and Immunology* 406:97-118. doi: 10.1007/82_2016_44.
- Rolando, Monica, Patrick Munro, Caroline Stefani, Patrick Auberger, Gilles Flatau, et Emmanuel Lemichez. 2009. « Injection of Staphylococcus aureus EDIN by the Bacillus anthracis Protective Antigen Machinery Induces Vascular Permeability ». *Infection and Immunity* 77(9):3596-3601. doi: 10.1128/IAI.00186-09.
- Romero, Stéphane, Christophe Le Clairche, Dominique Didry, Coumaran Egile, Dominique Pantaloni, et Marie-France Carlier. 2004. « Formin Is a Processive Motor That Requires Profilin to Accelerate Actin Assembly and Associated ATP Hydrolysis ». *Cell* 119(3):419-29. doi: 10.1016/j.cell.2004.09.039.
- de Rooij, J., F. J. Zwartkruis, M. H. Verheijen, R. H. Cool, S. M. Nijman, A. Wittinghofer, et J. L. Bos. 1998. « Epac Is a Rap1 Guanine-Nucleotide-Exchange Factor Directly Activated by Cyclic AMP ». *Nature* 396(6710):474-77. doi: 10.1038/24884.
- Rothberg, Karen G., John E. Heuser, William C. Donzell, Yun-Shu Ying, John R. Glenney, et Richard G. W. Anderson. 1992. « Caveolin, a Protein Component of Caveolae Membrane Coats ». *Cell* 68(4):673-82. doi: 10.1016/0092-8674(92)90143-Z.
- Roux, A., G. Cappelletto, J. Cartaud, J. Prost, B. Goud, et P. Bassereau. 2002. « A Minimal System Allowing Tubulation with Molecular Motors Pulling on Giant Liposomes ». *Proceedings of the National Academy of Sciences* 99(8):5394-99. doi: 10.1073/pnas.082107299.
- Roux, A., G. Koster, M. Lenz, B. Sorre, J. B. Manneville, P. Nassoy, et P. Bassereau. 2010. « Membrane Curvature Controls Dynamin Polymerization ». *Proceedings of the National Academy of Sciences* 107(9):4141-46. doi: 10.1073/pnas.0913734107.
- Roux, Aurélien, Damien Cuvelier, Pierre Nassoy, Jacques Prost, Patricia Bassereau, et Bruno Goud. 2005. « Role of Curvature and Phase Transition in Lipid Sorting and Fission of Membrane Tubules ». *The EMBO Journal* 24(8):1537-45. doi: 10.1038/sj.emboj.7600631.
- Rueda-Contreras, Mara Denisse, Andreu F. Gallen, J. Roberto Romero-Arias, Aurora Hernandez-Machado, et Rafael A. Barrio. 2021. « On Gaussian Curvature and Membrane Fission ». *Scientific Reports* 11(1):9562. doi: 10.1038/s41598-021-88851-y.
- Saarikangas, Juha, Hongxia Zhao, Anette Pykäläinen, Pasi Laurinmäki, Pieta K. Mattila, Paavo K. J. Kinnunen, Sarah J. Butcher, et Pekka Lappalainen. 2009. « Molecular Mechanisms of Membrane Deformation by I-BAR Domain Proteins ». *Current Biology: CB* 19(2):95-107. doi: 10.1016/j.cub.2008.12.029.
- Sackmann, E., et R. Bruinsma. s. d. « CELL ADHESION AS WETTING TRANSITION? » 25.
- Sagot, Isabelle, Avital A. Rodal, James Moseley, Bruce L. Goode, et David Pellman. 2002. « An Actin Nucleation Mechanism Mediated by Bni1 and Profilin ». *Nature Cell Biology* 4(8):626-31. doi: 10.1038/ncb834.
- Sandre, Olivier, Laurent Moreaux, et Françoise Brochard-Wyart. 1999. « Dynamics of transient pores in stretched vesicles ». *Proceedings of the National Academy of Sciences of the United States of America* 96(19):10591-96.
- Sargiacomo, M., M. Sudol, Z. Tang, et MP Lisanti. 1993. « Signal transducing molecules and glycosylphosphatidylinositol-linked proteins form a caveolin-rich insoluble complex in MDCK cells ». *Journal of Cell Biology* 122(4):789-807. doi: 10.1083/jcb.122.4.789.
- Scheel, Jochen, Jagan Srinivasan, Ulrike Honnert, Annemarie Henske, et Teymuras V. Kurzchalia. 1999. « Involvement of Caveolin-1 in Meiotic Cell-Cycle Progression in Caenorhabditis Elegans ». *Nature Cell Biology* 1(2):127-29. doi: 10.1038/10100.

- Scherer, P. E., T. Okamoto, M. Chun, I. Nishimoto, H. F. Lodish, et M. P. Lisanti. 1996. « Identification, Sequence, and Expression of Caveolin-2 Defines a Caveolin Gene Family. » *Proceedings of the National Academy of Sciences* 93(1):131-35. doi: 10.1073/pnas.93.1.131.
- Schimmel, Lilian, Niels Heemskerk, et Jaap D. van Buul. 2016. « Leukocyte transendothelial migration: A local affair ». *Small GTPases* 8(1):1-15. doi: 10.1080/21541248.2016.1197872.
- Schirenbeck, Antje, Till Bretschneider, Rajesh Arasada, Michael Schleicher, et Jan Faix. 2005. « The Diaphanous-Related Formin DDi2 Is Required for the Formation and Maintenance of Filopodia ». *Nature Cell Biology* 7(6):619-25. doi: 10.1038/ncb1266.
- Schlegel, A., et M. P. Lisanti. 2000. « A Molecular Dissection of Caveolin-1 Membrane Attachment and Oligomerization. Two Separate Regions of the Caveolin-1 C-Terminal Domain Mediate Membrane Binding and Oligomer/Oligomer Interactions in Vivo ». *The Journal of Biological Chemistry* 275(28):21605-17. doi: 10.1074/jbc.M002558200.
- Schmidt, Anja, et Michael N. Hall. 1998. « SIGNALING TO THE ACTIN CYTOSKELETON ». *Annual Review of Cell and Developmental Biology* 14(1):305-38. doi: 10.1146/annurev.cellbio.14.1.305.
- Schroeder, R., E. London, et D. Brown. 1994. « Interactions between Saturated Acyl Chains Confer Detergent Resistance on Lipids and Glycosylphosphatidylinositol (GPI)-Anchored Proteins: GPI-Anchored Proteins in Liposomes and Cells Show Similar Behavior. » *Proceedings of the National Academy of Sciences* 91(25):12130-34. doi: 10.1073/pnas.91.25.12130.
- Schwartz, Amy B., Obed A. Campos, Ernesto Criado-Hidalgo, Shu Chien, Juan C. del Álamo, Juan C. Lasheras, et Yi-Ting Yeh. 2021. « Elucidating the Biomechanics of Leukocyte Transendothelial Migration by Quantitative Imaging ». *Frontiers in Cell and Developmental Biology* 9:704. doi: 10.3389/fcell.2021.635263.
- Senju, Yosuke, Yuzuru Itoh, Kazunori Takano, Sayaka Hamada, et Shiro Suetsugu. 2011. « Essential role of PACSIN2/syndapin-II in caveolae membrane sculpting ». *Journal of Cell Science* 124(12):2032-40. doi: 10.1242/jcs.086264.
- Sens, Pierre, et Julie Plastino. 2015. « Membrane Tension and Cytoskeleton Organization in Cell Motility ». *Journal of Physics. Condensed Matter: An Institute of Physics Journal* 27(27):273103. doi: 10.1088/0953-8984/27/27/273103.
- Shah, Claudio, Balachandra G. Hegde, Björn Morén, Elmar Behrmann, Thorsten Mielke, Gregor Moenke, Christian M. T. Spahn, Richard Lundmark, Oliver Daumke, et Ralf Langen. 2014. « Structural Insights into Membrane Interaction and Caveolar Targeting of Dynamin-like EHD2 ». *Structure* 22(3):409-20. doi: 10.1016/j.str.2013.12.015.
- Sharma, Arpeeta, Carol Yu, et Pascal N. Bernatchez. 2010. « New Insights into Caveolae, Caveolins and Endothelial Function ». *The Canadian Journal of Cardiology* 26 Suppl A:5A-8A. doi: 10.1016/s0828-282x(10)71053-9.
- Sheetz, M. P., et J. Dai. 1996. « Modulation of Membrane Dynamics and Cell Motility by Membrane Tension ». *Trends in Cell Biology* 6(3):85-89. doi: 10.1016/0962-8924(96)80993-7.
- Sheetz, Michael P. 2001. « Cell Control by Membrane–Cytoskeleton Adhesion ». *Nature Reviews Molecular Cell Biology* 2(5):392-96. doi: 10.1038/35073095.
- Shi, Xuemeng, Zeyu Wen, Yajun Wang, Yan-Jun Liu, Kun Shi, et Yaming Jiu. 2021. « Feedback-Driven Mechanisms Between Phosphorylated Caveolin-1 and Contractile Actin Assemblies Instruct Persistent Cell Migration ». *Frontiers in Cell and Developmental Biology* 9:665919. doi: 10.3389/fcell.2021.665919.
- Shi, Zheng, Zachary T. Graber, Tobias Baumgart, Howard A. Stone, et Adam E. Cohen. 2018. « Cell Membranes Resist Flow ». *Cell* 175(7):1769-1779.e13. doi: 10.1016/j.cell.2018.09.054.
- Siddiqui, M. Rizwan, Yulia A. Komarova, Stephen M. Vogel, Xiaopei Gao, Marcelo G. Bonini, Johnson Rajasingh, You-Yang Zhao, Viktor Brovkovich, et Asrar B. Malik. 2011. « Caveolin-1–eNOS signaling promotes p190RhoGAP-A nitration and endothelial permeability ». *Journal of Cell Biology* 193(5):841-50. doi: 10.1083/jcb.201012129.
- Simard, Jeffrey R., Tova Meshulam, Biju K. Pillai, Michael T. Kirber, Kellen Brunaldi, Su Xu, Paul F. Pilch, et James A. Hamilton. 2010. « Caveolins sequester FA on the cytoplasmic leaflet of the plasma membrane, augment triglyceride formation, and protect cells from lipotoxicity ». *Journal of Lipid Research* 51(5):914-22. doi: 10.1194/jlr.M900251.

- Simionescu, Maia, Nicolae Simionescu, et George E. Palade. 1974. « MORPHOMETRIC DATA ON THE ENDOTHELIUM OF BLOOD CAPILLARIES ». *Journal of Cell Biology* 60(1):128-52. doi: 10.1083/jcb.60.1.128.
- Simón, L., A. Campos, L. Leyton, et A. F. G. Quest. 2020. « Caveolin-1 Function at the Plasma Membrane and in Intracellular Compartments in Cancer ». *Cancer and Metastasis Reviews* 39(2):435-53. doi: 10.1007/s10555-020-09890-x.
- Simunovic, Mijo, Emma Evergren, Ivan Golushko, Coline Prévost, Henri-François Renard, Ludger Johannes, Harvey T. McMahon, Vladimir Lorman, Gregory A. Voth, et Patricia Bassereau. 2016. « How Curvature-Generating Proteins Build Scaffolds on Membrane Nanotubes ». *Proceedings of the National Academy of Sciences* 113(40):11226-31. doi: 10.1073/pnas.1606943113.
- Singer, S. J., et G. L. Nicolson. 1972. « The Fluid Mosaic Model of the Structure of Cell Membranes ». *Science (New York, N. Y.)* 175(4023):720-31. doi: 10.1126/science.175.4023.720.
- Sinha, Bidisha, Darius Köster, Richard Ruez, Pauline Gonnord, Michele Bastiani, Daniel Abankwa, Radu V. Stan, Gillian Butler-Browne, Benoit Védie, Ludger Johannes, Nobuhiro Morone, Robert G. Parton, Graça Raposo, Pierre Sens, Christophe Lamaze, et Pierre Nassoy. 2011. « Cells Respond to Mechanical Stress by Rapid Disassembly of Caveolae ». *Cell* 144(3):402-13. doi: 10.1016/j.cell.2010.12.031.
- Small, J. Victor, K. Rottner, I. Kaverina, et K. I. Anderson. 1998. « Assembling an Actin Cytoskeleton for Cell Attachment and Movement ». *Biochimica et Biophysica Acta (BBA) - Molecular Cell Research* 1404(3):271-81. doi: 10.1016/S0167-4889(98)00080-9.
- Sochacki, Kem A., Gleb Shtengel, Schuyler B. van Engelenburg, Harald F. Hess, et Justin W. Taraska. 2014. « Correlative super-resolution fluorescence and metal replica transmission electron microscopy ». *Nature methods* 11(3):305-8. doi: 10.1038/nmeth.2816.
- Sorre, Benoit, Andrew Callan-Jones, Jean-Baptiste Manneville, Pierre Nassoy, Jean-François Joanny, Jacques Prost, Bruno Goud, et Patricia Bassereau. 2009. « Curvature-Driven Lipid Sorting Needs Proximity to a Demixing Point and Is Aided by Proteins ». *Proceedings of the National Academy of Sciences* 106(14):5622-26. doi: 10.1073/pnas.0811243106.
- Sowa, Grzegorz, Marc Pypaert, et William C. Sessa. 2001. « Distinction between Signaling Mechanisms in Lipid Rafts vs. Caveolae ». *Proceedings of the National Academy of Sciences* 98(24):14072-77. doi: 10.1073/pnas.241409998.
- Stachowiak, Jeanne C., Eva M. Schmid, Christopher J. Ryan, Hyoung Sook Ann, Darryl Y. Sasaki, Michael B. Sherman, Phillip L. Geissler, Daniel A. Fletcher, et Carl C. Hayden. 2012. « Membrane Bending by Protein-Protein Crowding ». *Nature Cell Biology* 14(9):944-49. doi: 10.1038/ncb2561.
- Stahlhut, Martin, Kirsten Sandvig, et Bo van Deurs. 2000. « Caveolae: Uniform Structures with Multiple Functions in Signaling, Cell Growth, and Cancer ». *Experimental Cell Research* 261(1):111-18. doi: 10.1006/excr.2000.4960.
- Stan, Radu-Virgil, Marion Kubitzka, et George E. Palade. 1999. « PV-1 Is a Component of the Fenestral and Stomatal Diaphragms in Fenestrated Endothelia ». *Proceedings of the National Academy of Sciences* 96(23):13203-7. doi: 10.1073/pnas.96.23.13203.
- Stefani, Caroline, David Gonzalez-Rodriguez, Yosuke Senju, Anne Doye, Nadia Efimova, Sébastien Janel, Justine Lipuma, Meng Chen Tsai, Daniel Hamaoui, Madhavi P. Maddugoda, Olivier Cochet-Escartin, Coline Prévost, Frank Lafont, Tatyana Svitkina, Pekka Lappalainen, Patricia Bassereau, et Emmanuel Lemichez. 2017. « Ezrin Enhances Line Tension along Transcellular Tunnel Edges via NMIIa Driven Actomyosin Cable Formation ». *Nature Communications* 8:15839. doi: 10.1038/ncomms15839.
- Steffan, Anne-Marie, Jean-Louis Gendraut, et André Kirn. 1987. « Increase in the Number of Fenestrae in Mouse Endothelial Liver Cells by Altering the Cytoskeleton with Cytochalasin B ». *Hepatology* 7(6):1230-38. doi: 10.1002/hep.1840070610.
- Steffen, Anika, Jan Faix, Guenter P. Resch, Joern Linkner, Juergen Wehland, J. Victor Small, Klemens Rottner, et Theresia E. B. Stradal. 2006. « Filopodia Formation in the Absence of Functional WAVE- and Arp2/3-Complexes ». *Molecular Biology of the Cell* 17:11.
- Steffen, Kathrin, Carolyn A. Emery, Maria Romiti, Jian Kang, Mario Bizzini, Jiri Dvorak, Caroline F. Finch, et Willem H. Meeuwisse. 2013. « High Adherence to a Neuromuscular Injury Prevention Programme (FIFA 11+) Improves Functional Balance and Reduces Injury Risk in Canadian Youth Female Football Players: A

- Cluster Randomised Trial ». *British Journal of Sports Medicine* 47(12):794-802. doi: 10.1136/bjsports-2012-091886.
- Stewart, Martin P., Jonne Helenius, Yusuke Toyoda, Subramanian P. Ramanathan, Daniel J. Muller, et Anthony A. Hyman. 2011. « Hydrostatic Pressure and the Actomyosin Cortex Drive Mitotic Cell Rounding ». *Nature* 469(7329):226-30. doi: 10.1038/nature09642.
- Stoeber, Miriam, Ina Karen Stoeck, Christine Hänni, Christopher Karl Ernst Bleck, Giuseppe Balistreri, et Ari Helenius. 2012. « Oligomers of the ATPase EHD2 confine caveolae to the plasma membrane through association with actin ». *The EMBO Journal* 31(10):2350-64. doi: 10.1038/emboj.2012.98.
- Stone, Matthew B., Sarah A. Shelby, Marcos F. Núñez, Kathleen Wisser, et Sarah L. Veatch. 2017. « Protein Sorting by Lipid Phase-like Domains Supports Emergent Signaling Function in B Lymphocyte Plasma Membranes ». *ELife* 6:e19891. doi: 10.7554/eLife.19891.
- Straub, F. B., et G. Feuer. 1950. « Adenosinetriphosphate the Functional Group of Actin ». *Biochimica et Biophysica Acta* 4:455-70. doi: 10.1016/0006-3002(50)90052-7.
- Suetsugu, Shiro, Shusaku Kurisu, Tsukasa Oikawa, Daisuke Yamazaki, Atsushi Oda, et Tadaomi Takenawa. 2006. « Optimization of WAVE2 Complex-Induced Actin Polymerization by Membrane-Bound IRSp53, PIP(3), and Rac ». *The Journal of Cell Biology* 173(4):571-85. doi: 10.1083/jcb.200509067.
- Sverdlov, Maria, Vasily Shinin, Aaron T. Place, Maricela Castellon, et Richard D. Minshall. 2009. « Filamin A Regulates Caveolae Internalization and Trafficking in Endothelial Cells ». *Molecular Biology of the Cell* 20(21):4531-40. doi: 10.1091/mbc.E08-10-0997.
- Svitkina, Tatyana M., et Gary G. Borisy. 1999. « Arp2/3 Complex and Actin Depolymerizing Factor/Cofilin in Dendritic Organization and Treadmilling of Actin Filament Array in Lamellipodia ». *The Journal of Cell Biology* 145(5):1009-26.
- Svitkina, Tatyana M., Elena A. Bulanova, Oleg Y. Chaga, Danijela M. Vignjevic, Shin-ichiro Kojima, Jury M. Vasiliev, et Gary G. Borisy. 2003. « Mechanism of Filopodia Initiation by Reorganization of a Dendritic Network ». *The Journal of Cell Biology* 160(3):409-21. doi: 10.1083/jcb.200210174.
- Tagawa, Akiko, Anna Mezzacasa, Arnold Hayer, Andrea Longatti, Lucas Pelkmans, et Ari Helenius. 2005. « Assembly and trafficking of caveolar domains in the cell ». *The Journal of Cell Biology* 170(5):769-79. doi: 10.1083/jcb.200506103.
- Taggart, Michael J. 2001. « Smooth Muscle Excitation-Contraction Coupling: a Role for Caveolae and Caveolins? ». *Physiology* 16(2):61-65. doi: 10.1152/physiologyonline.2001.16.2.61.
- Tan, Andrew M., Severine Stamboulian, Yu-Wen Chang, Peng Zhao, Avis B. Hains, Stephen G. Waxman, et Bryan C. Hains. 2008. « Neuropathic Pain Memory Is Maintained by Rac1-Regulated Dendritic Spine Remodeling after Spinal Cord Injury ». *The Journal of Neuroscience* 28(49):13173-83. doi: 10.1523/JNEUROSCI.3142-08.2008.
- Tang, Wei-Jen, et Qing Guo. 2009. « The Adenylyl Cyclase Activity of Anthrax Edema Factor ». *Molecular aspects of medicine* 30(6):423-30. doi: 10.1016/j.mam.2009.06.001.
- Tang, ZhaoLan, Philipp E. Scherer, Takashi Okamoto, Kenneth Song, Caryn Chu, D. Stave Kohtz, Ikuo Nishimoto, Harvey F. Lodish, et Michael P. Lisanti. 1996. « Molecular Cloning of Caveolin-3, a Novel Member of the Caveolin Gene Family Expressed Predominantly in Muscle (*) ». *Journal of Biological Chemistry* 271(4):2255-61. doi: 10.1074/jbc.271.4.2255.
- Thomsen, Peter, Kirstine Roepstorff, Martin Stahlhut, et Bo van Deurs. 2002. « Caveolae Are Highly Immobile Plasma Membrane Microdomains, Which Are not Involved in Constitutive Endocytic Trafficking ». *Molecular Biology of the Cell* 13(1):238-50. doi: 10.1091/mbc.01-06-0317.
- Thorn, Hans, Karin G. Stenkula, Margareta Karlsson, Unn Örtengren, Fredrik H. Nystrom, Johanna Gustavsson, et Peter Strålfors. 2003. « Cell Surface Orifices of Caveolae and Localization of Caveolin to the Necks of Caveolae in Adipocytes ». *Molecular Biology of the Cell* 14(10):3967-76. doi: 10.1091/mbc.E03-01-0050.
- Tillu et al. 2018. « A variable undecad repeat domain in cavin1 regulates caveola formation and stability ». *EMBO reports* 19(9):e45775. doi: 10.15252/embr.201845775.
- Tonegawa, Kota, Wataru Otsuka, Shohei Kumagai, Sachi Matsunami, Nao Hayamizu, Shota Tanaka, Kazumasa Moriwaki, Masanori Obana, Makiko Maeda, Michio Asahi, Hiroshi Kiyonari, Yasushi Fujio, et

- Hiroiyuki Nakayama. 2017. « Caveolae-specific activation loop between CaMKII and L-type Ca²⁺ channel aggravates cardiac hypertrophy in α 1-adrenergic stimulation ». *American Journal of Physiology-Heart and Circulatory Physiology* 312(3):H501-14. doi: 10.1152/ajpheart.00601.2016.
- Torii, T., M. Miyazawa, et I. Koyama. 2005. « Effect of Continuous Application of Shear Stress on Liver Tissue: Continuous Application of Appropriate Shear Stress Has Advantage in Protection of Liver Tissue ». *Transplantation Proceedings* 37(10):4575-78. doi: 10.1016/j.transproceed.2005.10.118.
- Torrino, Stéphanie, Wei-Wei Shen, Cédric M. Blouin, Satish Kailasam Mani, Christine Viaris de Lesegno, Pierre Bost, Alexandre Grassart, Darius Köster, Cesar Augusto Valades-Cruz, Valérie Chambon, Ludger Johannes, Paolo Pierobon, Vassili Soumelis, Catherine Coirault, Stéphane Vassilopoulos, et Christophe Lamaze. 2018. « EHD2 is a mechanotransducer connecting caveolae dynamics with gene transcription ». *Journal of Cell Biology* 217(12):4092-4105. doi: 10.1083/jcb.201801122.
- Trigatti, B. L., R. G. Anderson, et G. E. Gerber. 1999. « Identification of Caveolin-1 as a Fatty Acid Binding Protein ». *Biochemical and Biophysical Research Communications* 255(1):34-39. doi: 10.1006/bbrc.1998.0123.
- Tsai, Feng-Ching, Aurelie Bertin, Hugo Bousquet, John Manzi, Yosuke Senju, Meng-Chen Tsai, Laura Picas, Stephanie Miserey-Lenkei, Pekka Lappalainen, Emmanuel Lemichez, Evelyne Coudrier, et Patricia Bassereau. s. d. « Ezrin enrichment on curved membranes requires a specific conformation or interaction with a curvature-sensitive partner ». *eLife* 7. doi: 10.7554/eLife.37262.
- Urra, Hery, Vicente A. Torres, Rina J. Ortiz, Lorena Lobos, María I. Díaz, Natalia Díaz, Steffen Härtel, Lisette Leyton, et Andrew F. G. Quest. 2012. « Caveolin-1-Enhanced Motility and Focal Adhesion Turnover Require Tyrosine-14 but Not Accumulation to the Rear in Metastatic Cancer Cells ». *PLOS ONE* 7(4):e33085. doi: 10.1371/journal.pone.0033085.
- Valeva, Angela, Iwan Walev, Matthias Pinkernell, Barbara Walker, Hagan Bayley, Michael Palmer, et Sucharit Bhakdi. 1997. « Transmembrane β -barrel of staphylococcal α -toxin forms in sensitive but not in resistant cells ». *Proceedings of the National Academy of Sciences of the United States of America* 94(21):11607-11.
- Vanni, Stefano, Hisaaki Hirose, Hélène Barelli, Bruno Antony, et Romain Gautier. 2014. « A Sub-Nanometre View of How Membrane Curvature and Composition Modulate Lipid Packing and Protein Recruitment ». *Nature Communications* 5(1):4916. doi: 10.1038/ncomms5916.
- Vassilopoulos, Stéphane. 2020. « Unconventional Roles for Membrane Traffic Proteins in Response to Muscle Membrane Stress ». *Current Opinion in Cell Biology* 65:42-49. doi: 10.1016/j.ceb.2020.02.007.
- Vignjevic, Danijela, Shin-ichiro Kojima, Yvonne Aratyn, Oana Danciu, Tatyana Svitkina, et Gary G. Borisy. 2006. « Role of fascin in filopodial protrusion ». *Journal of Cell Biology* 174(6):863-75. doi: 10.1083/jcb.200603013.
- Vinten, J., A. H. Johnsen, P. Roepstorff, J. Harpøth, et J. Tranum-Jensen. 2005. « Identification of a Major Protein on the Cytosolic Face of Caveolae ». *Biochimica et Biophysica Acta (BBA) - Biomembranes* 1717(1):34-40. doi: 10.1016/j.bbamem.2005.09.013.
- Vinten, J., M. Voldstedlund, H. Clausen, K. Christiansen, J. Carlsen, et J. Tranum-Jensen. 2001. « A 60-KDa Protein Abundant in Adipocyte Caveolae ». *Cell and Tissue Research* 305(1):99-106. doi: 10.1007/s004410100389.
- Vitale, Gaetano, Lorenzo Bernardi, et Giorgio Napolitani. 2000. « Susceptibility of Mitogen-Activated Protein Kinase Kinase Family Members to Proteolysis by Anthrax Lethal Factor ». 7.
- Voldstedlund, M., J. Vinten, et J. Tranum-Jensen. 2001. « Cav-P60 Expression in Rat Muscle Tissues ». *Cell and Tissue Research* 306(2):265-76. doi: 10.1007/s004410100439.
- Volonte, Daniela, Charles F. McTiernan, Marek Drab, Michael Kasper, et Ferruccio Galbiati. 2008. « Caveolin-1 and caveolin-3 form heterooligomeric complexes in atrial cardiac myocytes that are required for doxorubicin-induced apoptosis ». *American Journal of Physiology-Heart and Circulatory Physiology* 294(1):H392-401. doi: 10.1152/ajpheart.01039.2007.
- Walser, Piers J., Nicholas Ariotti, Mark Howes, Charles Ferguson, Richard Webb, Dominik Schwudke, Natalya Leneva, Kwang-Jin Cho, Leanne Cooper, James Rae, Matthias Floetenmeyer, Viola M. J. Oorschot, Ulf Skoglund, Kai Simons, John F. Hancock, et Robert G. Parton. 2012. « Constitutive Formation of Caveolae in a Bacterium ». *Cell* 150(4):752-63. doi: 10.1016/j.cell.2012.06.042.

- Wang, Bing-Yuan, Xiao-Hua Ju, Bao-Yu Fu, Jian Zhang, et Yan-Xue Cao. 2005. « Effects of Ethanol on Liver Sinusoidal Endothelial Cells-Fenestrae of Rats ». *Hepatobiliary & Pancreatic Diseases International: HBPD INT* 4(3):422-26.
- Wang, K., et S. J. Singer. 1977. « Interaction of Filamin with F-Actin in Solution. » *Proceedings of the National Academy of Sciences* 74(5):2021-25. doi: 10.1073/pnas.74.5.2021.
- Watanabe, N., T. Kato, A. Fujita, T. Ishizaki, et S. Narumiya. 1999. « Cooperation between MDia1 and ROCK in Rho-Induced Actin Reorganization ». *Nature Cell Biology* 1(3):136-43. doi: 10.1038/11056.
- Watts, C., et M. Marsh. 1992. « Endocytosis: What Goes in and How? » *Journal of Cell Science* 103 (Pt 1):1-8.
- Waugh, R., et E. A. Evans. 1979. « Thermoelasticity of red blood cell membrane. » *Biophysical Journal* 26(1):115-31.
- Way, Michael, et Robert G. Parton. 1995. « M-Caveolin, a Muscle-Specific Caveolin-Related Protein ». *FEBS Letters* 376(1-2):108-12. doi: 10.1016/0014-5793(95)01256-7.
- Weber, K., et U. Groeschel-Stewart. 1974. « Antibody to Myosin: The Specific Visualization of Myosin-Containing Filaments in Nonmuscle Cells ». *Proceedings of the National Academy of Sciences of the United States of America* 71(11):4561-64. doi: 10.1073/pnas.71.11.4561.
- Wegner, A. 1976. « Head to Tail Polymerization of Actin ». *Journal of Molecular Biology* 108(1):139-50. doi: 10.1016/s0022-2836(76)80100-3.
- Wegner, A., K. Aktories, A. Ditsch, I. Just, B. Schoepper, N. Selve, et M. Wille. 1994. « Actin-Gelsolin Interaction ». *Advances in Experimental Medicine and Biology* 358:97-104. doi: 10.1007/978-1-4615-2578-3_9.
- Wells, Claire M., Marita Walmsley, Steen Ooi, Victor Tybulewicz, et Anne J. Ridley. 2004. « Rac1-Deficient Macrophages Exhibit Defects in Cell Spreading and Membrane Ruffling but Not Migration ». *Journal of Cell Science* 117(7):1259-68. doi: 10.1242/jcs.00997.
- Wild, S., G. Roglic, A. Green, R. Sicree, et H. King. 2004. « Global Prevalence of Diabetes: Estimates for the Year 2000 and Projections for 2030 ». *Diabetes Care* 27(5):1047-53. doi: 10.2337/diacare.27.5.1047.
- Williams, Terence M., et Michael P. Lisanti. 2005. « Caveolin-1 in Oncogenic Transformation, Cancer, and Metastasis ». *American Journal of Physiology. Cell Physiology* 288(3):C494-506. doi: 10.1152/ajpcell.00458.2004.
- Wisse, E. 1970. « An Electron Microscopic Study of the Fenestrated Endothelial Lining of Rat Liver Sinusoids ». *Journal of Ultrastructure Research* 31(1):125-50. doi: 10.1016/s0022-5320(70)90150-4.
- Wisse, E., F. Jacobs, B. Topal, P. Frederik, et B. De Geest. 2008. « The Size of Endothelial Fenestrae in Human Liver Sinusoids: Implications for Hepatocyte-Directed Gene Transfer ». *Gene Therapy* 15(17):1193-99. doi: 10.1038/gt.2008.60.
- Wu, Ming-Heng, Tse-Ming Hong, Hui-Wen Cheng, Szu-Hua Pan, Yu-Ray Liang, Hsiao-Chin Hong, Wei-Fan Chiang, Tung-Yiu Wong, Dar-Bin Shieh, Ai-Li Shiau, Ying-Tai Jin, et Yuh-Ling Chen. 2009. « Galectin-1-Mediated Tumor Invasion and Metastasis, Up-Regulated Matrix Metalloproteinase Expression, and Reorganized Actin Cytoskeletons ». *Molecular Cancer Research* 7(3):311-18. doi: 10.1158/1541-7786.MCR-08-0297.
- Xie, Kenan, Yuehua Yang, et Hongyuan Jiang. 2018. « Controlling Cellular Volume via Mechanical and Physical Properties of Substrate ». *Biophysical Journal* 114(3):675-87. doi: 10.1016/j.bpj.2017.11.3785.
- Yamada, Eichi. 1955. « THE FINE STRUCTURE OF THE GALL BLADDER EPITHELIUM OF THE MOUSE ». *The Journal of Biophysical and Biochemical Cytology* 1(5):445-58.
- Yamashiro-Matsumura, S., et F. Matsumura. 1986. « Intracellular Localization of the 55-KD Actin-Bundling Protein in Cultured Cells: Spatial Relationships with Actin, Alpha-Actinin, Tropomyosin, and Fimbrin ». *The Journal of Cell Biology* 103(2):631-40. doi: 10.1083/jcb.103.2.631.
- Yang, Changsong, Lubov Czech, Silke Gerboth, Shin-ichiro Kojima, Giorgio Scita, et Tatyana Svitkina. 2007. « Novel Roles of Formin MDia2 in Lamellipodia and Filopodia Formation in Motile Cells » édité par D. Pellman. *PLoS Biology* 5(11):e317. doi: 10.1371/journal.pbio.0050317.

- Yao, Qing, Jing Chen, Hong Cao, James D. Orth, J. Michael McCaffery, Radu-Virgil Stan, et Mark A. McNiven. 2005. « Caveolin-1 Interacts Directly with Dynamin-2 ». *Journal of Molecular Biology* 348(2):491-501. doi: 10.1016/j.jmb.2005.02.003.
- Yeow, Ivana, Gillian Howard, Jessica Chadwick, Carolina Mendoza-Topaz, Carsten G. Hansen, Benjamin J. Nichols, et Elena Shvets. 2017. « EHD Proteins Cooperate to Generate Caveolar Clusters and to Maintain Caveolae during Repeated Mechanical Stress ». *Current Biology* 27(19):2951-2962.e5. doi: 10.1016/j.cub.2017.07.047.
- Yin, H. L., J. H. Albrecht, et A. Fattoum. 1981. « Identification of Gelsolin, a Ca²⁺-Dependent Regulatory Protein of Actin Gel-Sol Transformation, and Its Intracellular Distribution in a Variety of Cells and Tissues. » *Journal of Cell Biology* 91(3):901-6. doi: 10.1083/jcb.91.3.901.
- Yokomori, Hiroaki, Kazunori Yoshimura, Shinsuke Funakoshi, Toshihiro Nagai, Kayo Fujimaki, Masahiko Nomura, Hiromasa Ishii, et Masaya Oda. 2004. « Rho Modulates Hepatic Sinusoidal Endothelial Fenestrae via Regulation of the Actin Cytoskeleton in Rat Endothelial Cells ». *Laboratory Investigation* 84(7):857-64. doi: 10.1038/labinvest.3700114.
- Yu, F. X., H. Q. Sun, P. A. Janmey, et H. L. Yin. 1992. « Identification of a Polyphosphoinositide-Binding Sequence in an Actin Monomer-Binding Domain of Gelsolin. » *Journal of Biological Chemistry* 267(21):14616-21. doi: 10.1016/S0021-9258(18)42086-8.
- Zaas, David W., Zachary D. Swan, Bethany J. Brown, Guojie Li, Scott H. Randell, Simone Degan, Mary E. Sunday, Jo Rae Wright, et Soman N. Abraham. 2009. « Counteracting Signaling Activities in Lipid Rafts Associated with the Invasion of Lung Epithelial Cells by *Pseudomonas Aeruginosa** ». *Journal of Biological Chemistry* 284(15):9955-64. doi: 10.1074/jbc.M808629200.
- Zapotoczny, Bartłomiej, Filip Braet, Edyta Kus, Katarzyna Ginda-Mäkelä, Beata Klejevska, Roberto Campagna, Stefan Chlopicki, et Marek Szymonski. 2019. « Actin-spectrin Scaffold Supports Open Fenestrae in Liver Sinusoidal Endothelial Cells ». *Traffic* 20(12):932-42. doi: 10.1111/tra.12700.
- Zeng, Dehong, Taras Juzkiw, A. Thomas Read, Darren W. H. Chan, Matthew R. Glucksberg, C. Ross Ethier, et Mark Johnson. 2010. « Young's modulus of elasticity of Schlemm's canal endothelial cells ». *Biomechanics and modeling in mechanobiology* 9(1):19-33. doi: 10.1007/s10237-009-0156-3.
- Zhao, Hongxia, Anette Pykäläinen, et Pekka Lappalainen. 2011. « I-BAR Domain Proteins: Linking Actin and Plasma Membrane Dynamics ». *Current Opinion in Cell Biology* 23(1):14-21. doi: 10.1016/j.ceb.2010.10.005.
- Zhong, Weiliang, Ying Li, Linan Li, Weiguo Zhang, Shouyu Wang, et Xifu Zheng. 2013. « YAP-Mediated Regulation of the Chondrogenic Phenotype in Response to Matrix Elasticity ». *Journal of Molecular Histology* 44(5):587-95. doi: 10.1007/s10735-013-9502-y.
- Zhou, Yong, Nicholas Ariotti, James Rae, Hong Liang, Vikas Tillu, Shern Tee, Michele Bastiani, Adekunle T. Bademosi, Brett M. Collins, Frederic A. Meunier, John F. Hancock, et Robert G. Parton. 2021. « Caveolin-1 and Cavin1 Act Synergistically to Generate a Unique Lipid Environment in Caveolae ». *Journal of Cell Biology* 220(3):e202005138. doi: 10.1083/jcb.202005138.
- Zigmond, Sally H., Marie Evangelista, Charles Boone, Changsong Yang, Arvin C. Dar, Frank Sicheri, Joe Forkey, et Martin Pring. 2003. « Formin Leaky Cap Allows Elongation in the Presence of Tight Capping Proteins ». *Current Biology* 13(20):1820-23. doi: 10.1016/j.cub.2003.09.057.
- Zlotek-Zlotkiewicz, Ewa, Sylvain Monnier, Giovanni Cappello, Mael Le Berre, et Matthieu Piel. 2015. « Optical Volume and Mass Measurements Show That Mammalian Cells Swell during Mitosis ». *The Journal of Cell Biology* 211(4):765-74. doi: 10.1083/jcb.201505056.

VIII. Annexe

1. DHA-PHOSPHOLIPIDS CONTROL MEMBRANE FUSION AND TRANSCELLULAR TUNNEL DYNAMICS

Meng-Chen Tsai¹⁻², Lucile Fleuriot¹, Sébastien Janel³, David Gonzalez-Rodriguez⁴, Camille Morel², Amel Mettouchi², Delphine Debayle¹, Stéphane Dallongeville⁵, Jean-Christophe Olivo-Marin⁵, Bruno Antony¹, Frank Lafont³, Emmanuel Lemichez^{2**} and Hélène Barelli^{1**}
co-last authors: * co-corresponding authors: emmanuel.lemichez@pasteur.fr and

barelli@ipmc.cnrs.fr

¹ Institut de Pharmacologie Moléculaire et Cellulaire, UMR 7275, CNRS and Université Côte d'Azur, 06560, Valbonne, France

² Institut Pasteur, Université de Paris, CNRS UMR2001, Unité des Toxines Bactériennes, 75015 Paris, France

³ Université de Lille, CNRS, Inserm, CHU Lille, Institut Pasteur Lille, U1019 - UMR 9017 - CIIL - Center for Infection and Immunity of Lille, F-59000 Lille, France

⁴ Université de Lorraine, LCP-A2MC, F-57000 Metz, France

⁵ Institut Pasteur, BioImage Analysis Unit, CNRS UMR 3691, Paris, France

Address Correspondence to:

Dr. Hélène BARELLI

Institut de Pharmacologie Moléculaire et Cellulaire

Dynamics of lipid membranes and protein coats

660 Route des Lucioles

06560 Sophia Antipolis, France.

Tel: +33493957774

barelli@ipmc.cnrs.fr

and

Dr. Emmanuel LEMICHEZ

Unité des toxines bactériennes

Institut Pasteur

25 Rue du Docteur Roux

75724 PARIS CEDEX 15

Tél : +33140613044

Emmanuel.lemichez@pasteur.fr

1.1. ABSTRACT

Metabolic studies and animal knockout models point to the critical role of polyunsaturated docosahexaenoic acid (22:6, DHA)-containing phospholipids (PLs) in physiology. Here, we investigated the impact of DHA-PLs on the dynamics of transendothelial cell macroapertures (TEMs) triggered by RhoA inhibition-associated cell spreading. Lipidomic analyses show that human umbilical vein endothelial cells (HUVECs) subjected to DHA-diet undergo a 6-fold enrichment in DHA-PLs at plasma membrane (PM) at the expense of monounsaturated OA-PLs. Consequently, DHA-PLs enrichment at the PM induces a reduction of cell thickness and shifts cellular membranes towards a permissive mode of membrane fusion for transcellular tunnel initiation. We provide evidence that a global homeostatic control of membrane tension and cell cortex rigidity minimizes overall changes of TEM area through a decrease of TEM size and lifetime. Conversely, low DHA-PL levels at the PM leads to the opening of unstable and wider TEMs. Together, this provides evidence that variations of DHA-PLs levels in membranes affect cell biomechanical properties.

Keywords: polyunsaturated phospholipids, docosahexaenoic acid (DHA), membrane fusion, large scale membrane dynamics, endothelium, transendothelial cell macroaperture, bacterial toxins, actin cytoskeleton.

1.2. INTRODUCTION

The plasma membrane attached to the cortical cytoskeleton forms a composite material that undergoes constant reshaping to perform essential cellular processes, including cell division, migration, phagocytosis and epithelial or endothelial semipermeable barrier organization and function (Levayer and Lecuit, 2012; Salbreux et al., 2012). Lipidomic approaches offer ways to quantitatively decipher the impact of fine-tuned changes in the composition of lipid acyl chains on membrane dynamics.

Phospholipids (PLs) often contain an unsaturated acyl chain at the sn-2 position that determines the biophysical properties of cellular membranes. Fatty acids (FA) are classified as saturated (S), monounsaturated (MU), and polyunsaturated (PU) by the number of double bonds present in the hydrocarbon acyl chain. Several glycerophospholipid classes, including phosphatidylcholine (PC), phosphatidylethanolamine (PE) and phosphatidylserine (PS), are the dominant constituents of the plasma membrane in addition to cholesterol (van Meer et al., 2008). Notably, phosphatidylcholine (PC) accounts for 40-50% of total phospholipids at the plasma membrane³. Variations in the length and number of double bonds in acyl chains lead to a remarkably large repertoire of phospholipid variants, such as PC(16:0/18:1), PE(18:0/20:4), and PS(18:0/22:6), conferring different biophysical properties, i.e., fluidity, packing order and curvature (Barelli and Antonny, 2016; Harayama and Riezman, 2018). The double bonds in polyunsaturated phospholipids allow acyl chains to twist at various angles, thereby providing the membrane with remarkably flexible properties (Manni et al., 2018). It is important to decode how the pattern of acyl chain variants in PLs translates into variations in cellular membrane dynamics (Harayama and Riezman, 2018; Pinot et al., 2014).

With 22 carbons and six double bonds, docosahexaenoic acid (DHA) is the most unsaturated form of the omega-3 fatty acids. Given the limited synthesis of this FA from linolenic acid, a dietary supply of DHA is essential to the functions of the retina (Shindou et al., 2017) and for spermatogenesis (Iizuka-Hishikawa et al., 2017) in addition to brain function (Bazinet and Layé, 2014). In particular, animals fed with PUFA-free diets develop reduced visual functions paralleling the low DHA content in their retinas, outcomes that indicate the critical requirement of attaining DHA from the

diet for visual function (Jeffrey and Neuringer, 2009). Lysophosphatidic acid acyltransferase 3 (LPAAT3), which catalyzes the esterification of DHA to generate phosphatidic acid and form precursors of PL, notably DHA-containing PC and PE, is particularly rich in the retina and testis (Yuki et al., 2014). Mice with LPAAT3 knocked out display male infertility and show visual impairment due to structural defects in the membranes of photoreceptors. Much remains to be learned on how DHA impacts the architecture and dynamics of the plasma membrane.

Recent works have shown that polyunsaturated lipids facilitate membrane processes requiring deformations at the nanometer scale. First, incorporation of polyunsaturated acyl chains into PLs facilitates endocytosis in model cellular systems and makes the pure lipid bilayer more flexible and prone to fission mediated by dynamin and endophilin (Manni et al., 2018; Pinot et al., 2014). These effects might explain why PolyUnsaturated PhosphoLipids (PUPLs) are necessary for proper synaptic vesicle formation (Tixier-Vidal et al., 1986). Second, polyunsaturated phosphatidic acid facilitates secretory granule exocytosis in neuroendocrine chromaffin cells, probably by stabilizing intermediates that contribute to a high-curvature membrane during fusion pore formation (Tanguy et al., 2020). Finally, polyunsaturated PLs modulate the activity of several mechanosensitive ion channels, including TRP, TRP-like and Piezo channels (Caires et al., 2017; Randall et al., 2015; Romero et al., 2019). Many of these effects have been proposed to arise from a reduction in the energetic cost of membrane bending and/or from a modulation of the energy required for protein conformational changes within the membrane matrix. However, whether and how the enrichment of cellular membranes with PUPLs modulates large-scale membrane dynamics remain to be elucidated.

Transcellular pores are observed in endothelial cell-lined vessels and form during the transcellular diapedesis of leukocytes (Aird et al., 2007; Braakman et al., 2016; Schimmel et al., 2017). Several toxins from pathogenic bacteria, such as RhoA-inhibitory exoenzymes from *Staphylococcus aureus* and *Clostridium botulinum*, can induce transendothelial cell macroaperture (TEM) tunnels (Lemichez et al., 2013). This TEM formation has been linked to increased vascular permeability and dissemination of *S. aureus* in tissues via the hematogenous route (Boyer et al., 2006; Munro et al., 2010; Rolando et al., 2009). Several bacteria secrete toxins that lower cell actomyosin contractility, thereby promoting cell spreading, which favors close contact between the

dorsal and basal membranes and initiates their self-fusion (Boyer et al., 2006; Ng et al., 2017). This step of fusion between the basal and dorsal membranes determines the very first step of TEM creation named hereafter nucleation. The cellular dewetting physical model is based on the premise that spreading cells generate enough membrane tension for TEM nucleation and growth²⁶. Widening of TEMs is resisted by line tension, which is partially explained by the membrane curvature generated by torus-like pores (Gonzalez-Rodriguez et al., 2012). After nucleation, an imbalance between the membrane and line tension causes TEMs to passively expand up to the maximal equilibrium size, which is stabilized by a newly formed stiff actomyosin cable that encircles TEMs (Stefani et al., 2017). TEMs are eventually sealed by active cytoskeleton-based processes (e.g., lamellipodia formation or purse-string contraction). While considerable progress has been made in understanding the interactions between the membrane and actin cytoskeleton regulatory machinery in the control of TEMs, much remains to be known about the contribution of plasma membrane mechanical properties.

We investigated these areas by analyzing TEM dynamics in primary human endothelial cells subjected to polyunsaturated versus monounsaturated fatty acid diets. We show that membrane enrichment in DHA-containing phospholipids increases the probability of TEM nucleation while decreasing the width and the lifetime of transcellular tunnels leading to conservation of cumulative TEM area. Moreover, we show that impoverishment in DHA-containing PLs has a detrimental impact on TEM stability.

1.3. RESULTS

Comprehensive analysis of the phospholipids in HUVECs fed with fatty acid diets

Recent progress have revealed the importance of whole cell lipidome adaptation to massive incorporation of polyunsaturated fatty acid (PUFAs) in order to maintain cellular viability (Levental et al., 2020). In contrast, little is known about how different cell types adapt their plasma membrane composition to PU-PLs increase, and whether these adaptations fully preserve biomechanical properties of plasma membrane attached to the underneath cortical cytoskeleton network.

Since endothelial cells are physiologically submitted to direct variations of dietary fatty acid chains in plasma, we performed comprehensive lipidome analyses of HUVECs, total membranes and purified plasma membrane, submitted to docosahexaenoic acid (DHA, C22:6) versus oleic acid (OA, C18:1) diets, i.e., the most polyunsaturated acyl chain versus the most abundant monounsaturated acyl chain in PLs, respectively (Harayama and Riezman, 2018). HUVECs were first subjected to medium containing lipoprotein-depleted serum (LPDS) followed by a diet of LPDS supplemented with bovine serum albumin (BSA) complexed either with docosahexaenoic acid (DHA, C22:6) or oleic acid (OA, C18:1). Lipidome analysis was then conducted by comparing relative quantities of lipid species using a Q Exactive mass spectrometer.

While lipid starvation conditions decreased the triglyceride (TG) storing form of acyl chains, we did not detect significant difference in the relative distribution of phospholipid classes (Figure 1A and Figure S1A-C). We monitored the cellular lipidome of HUVECs fed with FA diets for different times. We recorded a massive increase in TG that peaked at 1 hour (Sup. Figure 2A). The incorporation of fatty acids into phospholipids occurred with slower kinetics (Figure S2B-D), reaching a plateau at 6 hours, most notably for DHA incorporation into PC (Figure S2B). Importantly, the relative distribution of phospholipid classes was conserved between conditions, except for PE, which was reduced by 25% in the DHA-treated cells (Figure 1A).

As shown in figure 1B and supplementary figure 1B, in contrast to OA, the DHA diet had an impact on the profile of phospholipids, which show enrichment in DHA-containing PL species. Specifically, DHA was incorporated in large amounts in PC and PE, with a 4-fold increase in PC(16:0/22:6) and a 2-fold increase in PE(18:0/22:6) (Figure 1B). In comparison, the remodeling of the anionic lipids PS and PI was modest, although we recorded an increase in PI(18:0/22:6) at the expense of PI(18:1/20:4), one of the major PI species. In sharp contrast, OA treatment had a narrow and slight impact on the acyl chain profile of phospholipids, inducing a specific increase in PL(18:1/18:1) at the cellular level, which was largely restricted to PC (Figure 1B). Overall, cells fed with DHA displayed considerable enrichment with polyunsaturated phospholipids, which we estimated as a polyunsaturated PC increase from 22% to 47%, at the expense of OA-containing PC (Figure 1C and Figure S2D). Furthermore, the addition of OA to HUVECs had a minor impact on the lipidome, which was already rich in OA-containing PLs and poor in DHA-containing lipids.

Shifting the plasma membrane PL balance from the monounsaturated to the hexa-unsaturated form

The acyl chain profile of phospholipids varies according to subcellular localization (Antonny et al., 2015). Thus, we determined the impact of OA and DHA FA-diet conditions on the composition of PLs at the plasma membrane. For this experiment, we prepared giant plasma membrane vesicles (GPMVs) corresponding to plasma membrane blebs (Figure 2A). We observed the expected enrichment of the plasma membrane markers Annexin-V and Na⁺/K⁺ ATPase in the GPMV fractions (Figure 2B). Markers of internal compartments were observed in the total cell membrane fractions but were largely excluded from the GPMV fractions. The lipidomic analysis of the GPMVs compared to that of the total membrane fractions showed an enrichment in PS and sphingomyelin (SM), which are known to concentrate in the plasma membrane. In contrast, lipids characterizing membranes of internal compartments, such as diglyceride (DG; ER and lipid droplets) and lysobisphosphatidic acid (LBPA; late endosomes), were largely excluded from the GPMV fractions (Figure 2C). Moreover, quantitative analysis of PL classes in the GPMV fraction established the conservation of PL class distribution at the plasma membrane, including PE (Figure 2D).

We analyzed the changes in the acyl chain composition of PLs in the plasma membrane-derived GPMVs prepared from cells subjected to the two fatty acid diets. As observed for the total membrane fraction, the GPMV fraction from DHA-treated cells was enriched in DHA-containing PC, the dominant PL class, by 10-fold (from 1.6% to 16.7%) and PE species by 2-fold (from 8.8% to 18.2%) at the expense of monounsaturated species **as compared to GPMV from OA-treated cells** (Figure 2E). Thus, the DHA diet triggered a 1.9-fold reduction in OA-containing PC compared with OA-treated cells. Interestingly, these variations are accompanied by an increase in saturated PC species in agreement with recent work by Levental et al. (Levental et al., 2020).

Our comprehensive analysis of the HUVEC lipidome establishes that these cells have a plasma membrane intrinsically rich in OA-containing PLs, a profile that can be largely shifted towards polyunsaturated DHA-containing PLs upon exposure to a high-DHA fatty acid diet.

The DHA diet leads to smaller pores in the TEM population

Inhibition of the small GTPase RhoA by bacterial ExoC3-like toxins induces the nucleation and expansion of TEMs (Boyer et al., 2006). The nucleation and growth of TEMs is triggered by a collapse of RhoA-driven actomyosin contractility that leads to a spreading of cells and a reduction of their thickness (Ng et al., 2017). (Figure 3A). We first verified that modification of RhoA signaling had no impact on the proper incorporation of OA or DHA into PLs (Figure S3A-B). To this end, HUVECs were incubated in LPDS medium as the sole treatment or in LPDS containing the RhoA-inhibitory C3-exoenzyme (ExoC3). Next, cells were incubated for 1 to 6 hours in LPDS medium supplemented with bovine serum albumin (BSA) complexed with either OA or DHA fatty acids. We set a treatment of 24 hours with ExoC3 prior DHA/OA incorporation to avoid possible interference of fatty acyl chains incorporation on toxin endocytosis and translocation to the cytosol. To verify ExoC3 action on RhoA in all experimental conditions, we performed sequential ADP-ribosylation experiments showing that RhoA from ExoC3-treated cells becomes refractory to the second step of ADP-ribosylation performed *in vitro* (Figure S3C). In parallel, we observed a disruption of actin stress fibers due to ExoC3 action under the different diet conditions (Figure 3B).

We analyzed the impact of OA or DHA treatment on the spreading of cells induced by ExoC3. Measures of cell area showed no significant difference between the two diet conditions in non-intoxicated cells (Figure 3C). When cells were treated with ExoC3, we recorded a 1.2-fold spreading of both OA- and DHA-treated cells, indicating that cell enrichment in DHA-containing PL did not significantly influence the extent of HUVECs spreading in response to the inhibition of RhoA.

Next, we analyzed TEM parameters on fixed cells stained with FITC-phalloidin to label filamentous actin accumulating around TEMs. We observed that approximately 25% of cells displayed at least one TEM with no significant difference between cells cultured under the two fatty acid diet conditions (Figure 3D). Interestingly, we recorded a significant increase in the density of TEMs per cell in the DHA condition to 3.5 ± 0.3 TEM/cell *versus* 2.5 ± 0.1 TEM/cell for the OA-fed cells (Figure 3E). The increase of TEM density was accompanied by a decrease of the median TEM area in the DHA-treated cells compared with the OA-treated cells, with $A_{\text{DHA}} = 5.6 \mu\text{m}^2$ *versus* $A_{\text{OA}} = 9.9 \mu\text{m}^2$, respectively (Figure 3F and 3G). Consistently, analysis of the distribution of

the size of TEMs showed that the DHA diet induced a major shift toward TEMs of small size ($R < 1 \mu\text{m}$; 21% to 33%) at the expense of large TEMs ($R > 4 \mu\text{m}$; 24% to 14%) (Figure 3H). This first set of data reveals that inhibition of RhoA and incorporation of DHA into phospholipids did not interfere with each other, while the incorporation of DHA affects on TEM biomechanical parameters of density and size.

The DHA diet increases TEM nucleation frequency

TEM tunnels form labile openings (Figure 4A) (Video 1). After nucleation and growth, TEMs reach a stable state in which they oscillate around a maximal area. After this period of latency, TEMs undergo a phase of closure via actin-dependent processes involving either purse-string contraction or membrane wave extension (Maddugoda et al., 2011). Here, we noticed that approximately 70% of the TEMs resealed via a purse-string contraction phenomenon regardless of the fatty acid diet (not shown).

To quantitatively analyze TEM dynamics, we recorded the cycles of TEM opening and closing by time-lapse video in LifeAct-GFP-expressing cells, allowing us to determine the frequency of TEM nucleation and their complete lifetime. Strikingly, this revealed a critical impact of the DHA fatty acid diet on the mechanical control of TEM dynamics. Figure 4B shows that the DHA-fed cells had a higher frequency of opening events during the recording period than OA-fed cells (Video 2 and 3). Mean values were $N=19.3$ events/h for the DHA-fed cells *versus* $N=8.9$ events/h for the OA-fed cells (Figure 4C). Consistent with the impact of DHA on the distribution of TEM sizes, we measured that the lifetime for complete TEM opening and closing cycle was 1.7-fold shorter in the DHA-fed cells than in OA-fed cells, i.e., mean values of 24.6 ± 1.8 min for the DHA-fed cells *versus* 42.0 ± 4.0 min for the OA-fed cells (Figure 4D). TEM cycles encompass dynamic phases of opening and of closure, as well as a phase of latency where the TEM area oscillates within approximately 5% of its maximal size (Figure S4A). While the time for TEM opening was not affected by DHA, we recorded a decrease in the duration of both the latency and closure phases (Table 1). The probability of observing a TEM in a cell depends on the product of TEM nucleation frequency by their lifetime. Despite differences in the opening frequency of TEMs, we have recorded an average conservation in the total TEMs area between OA and DHA conditions. This conservation is interpreted as a consequence of the reduction in the overall lifetime of TEMs. Together our data reveal a striking mechanical coupling

between the nucleation rate of TEMs and their lifetimes that accounts for the observed higher rate of opening of TEMs of smaller size upon membrane enrichment in DHA-PLs (Figure S4B).

The DHA diet decreases cell thickness

We further investigated whether RhoA inhibition and DHA enrichment would affect the cortical elasticity of cells. We used atomic force microscopy (AFM) force mapping with a small colloidal-shaped tip to probe the first 40 nm layer of cell elasticity in the perinuclear region of living cells (Figure 5A). RhoA inhibition greatly reduced Young's modulus, by 1.7-fold, as reported (Ng et al., 2017). However, we measured similar elasticities in cells subjected to OA and DHA treatments (5.1 ± 0.2 kPa *versus* 5.8 ± 0.3 kPa, respectively) (Figure 5C), suggesting negligible impact of DHA enrichment on cortical elasticity. Nor did we observe any significant modification in the homogeneity of elasticity (Figure 5B).

We later measure the topography of the cell thickness at the periphery of TEMs. This was performed using a force feedback imaging mode and computing the zero-force topographical image on fixed, intoxicated cells, with a sharp tip. Cells with TEM showing no fluorescent actin ring were selected. Interestingly, DHA treatment decreased the cell thickness to 1.2-fold; i.e., mean values for the DHA-fed cells was 164 ± 6 nm *versus* 190 ± 6 nm for the OA-fed cells (Figure 5D). As previously reported, the TEM rim is elevated and forms a ridge structure (Maddugoda et al., 2011). In accordance with the measures of cell thickness, the height of the TEM ridge was decreased 1.2-fold in the DHA-enriched cells (Figure 5E). We concluded that DHA enrichment decreases the thickness of TEMs without affecting the cell elasticity contributed by the cellular cortex (Figure 5F).

The impact of DHA-PL enrichment on TEM opening kinetics

The dynamics of TEM opening were analyzed with a custom-made Icy-based program that automatically segments the LifeAct-GFP-decorated actin-rich circumference of TEMs as a function of time (Figures 4A and 6A). This analysis enabled us to study the dynamics and maximal size of parameters of single TEMs.

Interestingly, we observed that, under LPDS conditions, approximately 11% of the TEMs in the OA-treated cells *versus* 3% of the TEMs in the DHA-treated cells resumed

their enlargement 104 ± 33 seconds after stabilization, i.e., after they had reached the first stable state as illustrated in Figure S5A-B and Video 4, suggesting that DHA-PL-rich membranes form pores with greater stability Figure S5C-D In parallel, we performed a comparative super-resolution stimulated emission depletion (STED) microscopy analysis of the actin structures around the TEMs in the OA- and DHA-fed cells; i.e., we examined the typical actomyosin belt and membrane wave-containing dendritic F-actin (Stefani et al., 2017). No significant difference in actin organization around the TEMs between the two conditions was recorded (Figure 6B).

For the quantitative analysis described in the workflow in Figure 6A, we focused on the initial growth up to the first equilibrium state reached by the TEMs, a regime that can be directly compared to predictions of the cellular dewetting physical model, which describes TEM dynamics (Gonzalez-Rodriguez et al., 2012). We recorded and defined the median size of the TEMs over the recording period (Figure 6C). According to cellular dewetting model, the initial speed of TEM opening is primarily dictated by membrane tension while at later timings opening speed progressively integrate forces due to cytoskeleton remodeling along the edge of TEMs (Stefani et al., 2017). A comparative analysis of the initial speeds of opening between 10 and 20 seconds in the OA- and DHA-fed cells revealed no significant difference between the DHA-fed cells ($V_{i-DHA} = 0.39 \mu\text{m}^2 \text{s}^{-1}$) and OA-fed cells ($V_{i-OA} = 0.47 \mu\text{m}^2 \text{s}^{-1}$) (Table 1). In contrast, when we compared the median of late opening speeds over the first 20-70 seconds, the values were 1.4-fold lower for the DHA-fed cells ($V_{0-DHA} = 0.27 \mu\text{m}^2 \text{s}^{-1}$) than for the OA-fed cells ($V_{0-OA} = 0.38 \mu\text{m}^2 \text{s}^{-1}$) (Figure 6D). The cellular dewetting model implies that the nucleation and initial TEM opening speed (at the very first opening stage) are proportional to the membrane tension (Gonzalez-Rodriguez et al., 2012). Because the initial speed was similar between the OA- and DHA-treated cells, the average cell membrane tension is expected to be comparable between the two conditions. This conclusion is further supported by the observation of comparable spreading of the OA- and DHA-fed cells, because the cell spreading area correlates with cell membrane tension and TEM opening (Braakman et al., 2014).

In parallel, we assessed the maximal size of the TEMs during the recording periods. Consistent with measures of the fixed cells, the TEM maximal size was decreased by approximately 1.5-fold in the DHA-treated cells compared with the OA-treated cells, with $S_{\text{max-DHA}} = 25 \pm 2 \mu\text{m}^2$ versus $S_{\text{max-OA}} = 37 \pm 7 \mu\text{m}^2$ (Figure 6E). In accordance with

data on fixed cells, we recorded, in live cells, an increase in small ($R < 3 \mu\text{m}$) TEMs from 38% to 60% at the expense of large ($R > 4 \mu\text{m}$) TEMs (from 42% to 20%) in the DHA-treated cells vs OA-treated cells (Figure 6F). Consistent with the concomitant decrease of TEM size and speed of opening, we recorded for the DHA-fed cells no difference in the time to reach the maximal surface area, i.e., 179 ± 21 seconds for the OA-fed cells and 162 ± 23 seconds for the DHA-fed cells (Figure 6G). Although DHA-PLs had no impact on the initial speed of opening, it reduced the overall TEM opening speed, thereby impacting the maximal TEM size.

The observed decrease in TEM size upon DHA enrichment is in apparent contradiction with a naïve prediction of the cellular dewetting physical model. Indeed, DHA enrichment has been reported to reduce membrane bending rigidity, as measured locally by pulling a membrane tube (Pinot et al., 2014). According to the cell dewetting model, a reduction of membrane bending rigidity would slow down the dynamics of membrane tension relaxation, which should lead to larger TEMs. This apparent contradiction is solved by realizing that TEM opening dynamics are controlled by an effective cortical bending rigidity, which results from joint membrane and cortex properties. According to the physical model, an estimate of this effective membrane bending rigidity is given by

$$\kappa \approx \frac{k_B T A_{cell}}{8\pi N A_{max}},$$

where N is the number of TEMs simultaneously evident per cell, A_{max} is the maximum area of a TEM, k_B is the Boltzmann constant, T is the temperature, and A_{cell} is the total cell spreading area (see Materials and Methods for details). This equation is based on the relaxation of membrane tension during TEM opening, as described by Helfrich's law (Helfrich et al., 1973). Membrane relaxation is larger when the bending rigidity κ is larger. In deriving this equation, we assume a joint effect of N , the number of simultaneous TEMs on membrane, on tension relaxation, which affects each TEM. Because the cell spreading area A_{cell} is the same in the OA- and DHA-fed conditions, this equation indicates that the effective bending rigidity κ is inversely proportional to the product $N \cdot A_{max}$. A comparison between the two conditions leads to

$$\frac{\kappa_{DHA}}{\kappa_{OA}} \approx \frac{N_{OA} \cdot A_{max,OA}}{N_{DHA} \cdot A_{max,DHA}} = 1.05,$$

whose difference from 1 is not statistically significant. Thus, this calculation suggests that the average effective bending rigidity at the cellular scale is similar between cells in the OA- and DHA-fed conditions.

Overall, the interpretation of the experimentally observed TEM dynamics in light of the physical model suggests that average tension and effective bending rigidity, arising from membrane and cortex association that behaves as a composite material, are unchanged in cells subjected to these OA and DHA treatments. This result points to a regulation mechanism of global membrane dynamics controlling TEM opening that is robust despite changes in membrane lipid composition, which dictate the TEM nucleation rate.

1.4. DISCUSSION

Since the discovery of the cellular dewetting phenomenon, the contribution of plasma membrane mechanical properties to the dynamics of TEMs remains to be elucidated. Here, we show that the DHA fatty acid diet induces a shift in the acyl chain composition of phospholipids at the plasma membrane of endothelial cells, with an increase in DHA-PLs, and greatly affects TEM dynamics. Remarkably, DHA-PLs enrichment changes membrane dynamics, i.e., nucleation and lifetime of TEMs, in a coordinated manner to ensure the relative conservation of the overall TEM area per cell, and shifts the size range of the TEMs to a smaller range via reduction of opening speed. Moreover, DHA-PL enrichment reduced uncontrolled resume TEM growth. Collectively, these findings indicate that DHA-PL facilitates the nucleation of smaller TEMs displaying shorter lifetimes. Conversely, deficient DHA-PLs may lead to the opening of unstable and wider TEMs.

DHA-PL enrichment at the plasma membrane leads to a decrease in TEM maximal size and an increase in the number of simultaneous TEMs present in a cell. Strikingly, the total maximum TEM area, obtained as the product of the maximum area per TEM by the number of TEMs, remains constant between OA- and DHA-fed cells. Together with the physical interpretation provided by the cell dewetting model (Boyer et al., 2006; Gonzalez-Rodriguez et al., 2012), this observation suggests a conservation of the global membrane mechanical response at the scale of the entire cell. Essentially, effective membrane tension acting on TEMs behaves as the regulating mechanism.

When several TEMs open simultaneously, the relaxation of membrane tension due to the opening of each TEM impacts the other TEMs, because the available membrane material is shared. Thus, for a larger number of simultaneous TEMs, the membrane relaxation felt by each TEM is more pronounced and the TEMs reach a smaller maximum size on average. Therefore, whereas DHA-PL enrichment promotes the frequency of TEM nucleation events by 2-fold, the regulation of membrane mechanical characteristics at the scale of the whole cell appears sufficiently robust for the cell to cope with these changes, leading to a conserved total TEM area over the cell. To maintain the overall conservation of the TEM area, DHA-PL-enriched cells compensate for the increase in the nucleation rate by reducing the TEM opening speed and thereby maximal size. Moreover, we record a decrease of lifetime that is ascribed to a reduction in both the phase of latency and closure without affecting the initial opening phase (Figure S4A-B).

Enrichment of DHA-PLs at the plasma membrane decreases the speed of opening, while the time to reach the maximal size is not affected. Consistent with the conserved time frame of TEM opening, we observed that actin organization around TEMs formed in the DHA- and OA-fed cells showed no significant difference. Nevertheless, we observed that TEMs were less stable in the OA-fed cells and were more prone to resume their enlargement. Lower TEM stability may reflect defects in the recruitment or activity of actin-crosslinking proteins around the edge of the TEMs that are yet to be identified. Importantly, we previously reported that the absence of TEM stabilization is linked to massive hemorrhage induced by an ExoC3-chimeric toxin derived from the *B. anthracis* lethal toxin (Rolando et al., 2009). This suggests that DHA might play a key function in the appropriate homeostasis of the endothelial barrier, pointing to a likely role in stabilizing large pore structures that are observed along the vascular system (see for review Aird et al., 2007; Lemichez et al., 2010).

Finally, we found a decrease in cell thickness in the DHA-PL-enriched cells. Applying force to the dorsal part of the plasma membrane of normal growing cells is sufficient to bring membranes in close apposition and trigger the nucleation and opening of transcellular pores (Ng et al., 2017). Consistent with this idea, HUVECs intoxicated with ExoC3 were thinner than the control cells, i.e., with medians near the edge of the cells at 332 nm *versus* 462 nm, respectively (Ng et al., 2017). It is therefore reasonable to think that enriching DHA-PLs may enhance close plasma membrane apposition and

increase the probability of pore nucleation by reducing the energy cost to initiate a fusion event. As discussed below, changes in the asymmetric distribution of polyunsaturated phospholipids in DHA-PL-enriched cells might contribute to membrane apposition and fusion.

The plasma membrane is asymmetric in both lipid classes and lipid unsaturation (Lorent et al., 2020). The outer leaflet contains mostly PC and SM, whereas the inner leaflet contains 3 major PL classes, namely, PC, PE and PS. Coarse-grained molecular dynamics simulations on asymmetric phospholipid bilayers show that DHA-PLs facilitate membrane tubulation only when they are located on the convex side of the deformation (Tiberti et al., 2020). This effect is due to the ability of DHA-PLs to switch between several twisted conformations in a convex environment, notably to adopt a conformation in which the polyunsaturated acyl chain occupies voids between polar heads and invades the water-lipid interface. DHA-fed cells showed a 10-fold higher content of DHA-PC species at the plasma membrane than was evident in the OA-fed cells (16.7 and 1.6%, respectively). In contrast, the amount of DHA-PE and DHA-PS species was only approximately 2-fold higher in the DHA-fed HUVECs (18.2% and 14.1%, respectively) than in OA-fed cells (8.8% and 9.5%, respectively). Consequently, the DHA diet might not only increase the overall DHA-PL content of the plasma membrane but might also reduce DHA asymmetry because PC is the most affected PL and is quite evenly distributed between the two leaflets. Such a change coupled with the lack of contractile forces mediated by the cytoskeleton, due to the ExoC3 effect, may favor large undulations in the plasma membrane. High levels of polyunsaturated PLs on the inner and outer sides of the plasma membrane would be beneficial for sustaining large membrane undulations, which are a series of convex and concave deformations. As a prerequisite for hemifusion, the decrease in cell thickness in the DHA-fed cells likely increases the probability of close apposition between the two undulating apical and basal membranes, explaining the increase in the frequency and the number of TEMs. Indeed, as discussed in a review article by Monzel and Sengupta (Monzel and Sengupta, 2016), average membrane undulation amplitudes in nucleated cells have been reported to be of the order of 20-30 nm, and the largest undulations may exceed 100 nm. It is thus reasonable to expect that the largest undulations, whose amplitude are comparable to the cell thickness, facilitate

TEM nucleation. Further experimental work on model membrane systems and coarse-grained simulations of TEM formation will help test this idea.

1.5. MATERIALS AND METHODS

Reagents

LifeAct-GFP-pCMV plasmid was purchased from Ibidi. Antibodies used in this study were mouse anti-Na⁺/K⁺ ATPase (Santa Cruz), Annexin II (BD Transduction Laboratories), Calregulin (Santa Cruz), ERGIC 54 (Santa Cruz), and LAMP1 (BD Transduction Laboratories), and sheep anti-TGN46 (BioRad). Secondary Alexa Fluor-conjugated antibodies were from ThermoFisher and secondary peroxidase-conjugated antibodies were from Jackson ImmunoResearch. For immunofluorescence, hoechst 33342 and Alexa-fluor conjugated FITC-phalloidin were purchased from ThermoFisher. For STED imaging, Star635-phalloidin was purchased from Abberior. C3 toxin was purified as described (Boyer et al., 2006).

OA and DHA fatty acids (Sigma-Aldrich) were conjugated with fatty acid-free BSA (Sigma-Aldrich). Fatty acids were dissolved in warm (60°C) 200 mM NaOH and conjugated with BSA at the molar ratio of 5:1. The FA-BSA was aliquoted and filled with argon to minimalized oxidation. Lipoprotein depleted serum (LPDS) were prepared as described (Renaud et al., 1982). In brief, fetal bovine serum was loaded with NaBr to increase density to 1.21 g/ml followed by ultracentrifugation at 220,000g at 10°C for 48 hours in a Beckman Ti70 rotor. After centrifugation, a greasy layer containing lipoproteins appeared on the top of the tube was removed and the supernatant was centrifuged again at 220,000g at 10°C for 24 hours to remove the remaining lipoprotein. Later the serum was dialyzed intensively with Earle buffer (115 mM NaCl, 5.4 mM KCl, 1.8 mM CaCl₂, 0.8 mM MgSO₄, 5 mM Hepes, pH 7.4) in 14 kD cut-off dialysis membrane (Spectrum) for 72 hours and the buffer was refreshed for at least 5 times.

Cell Culture, Treatment, and Transfection

HUVECs were cultured and electroporated, as described in (Stefani et al., 2017). In brief, HUVECs were trypsinized and suspended in Ingenio Solution (Mirus) containing plasmid DNA (10 µg per 10⁶ cells) in a 4-mm cuvette (CellProjects). Then, cells were electroporated at 300 V, 450 µF, one pulse by GenePulser electroporator (BioRad).

To enrich HUVECs with OA or DHA, cells were washed twice with PBS and lipid starved in LPDS medium (Human endothelial SFM, 20% LPDS, 20 ng/ml FGF, 10 ng/ml EGF, 1 µg/ml Heparin, and Zellshield) overnight with or without 50 µg/ml ExoC3 toxin prepared as described (Boyer et al., 2006). Before experiments, cells were supplemented with 125 µM FA-BSA for 6 hr.

Lipid extraction and Lipidomics

A modified Bligh and Dyer (Bligh and Dyer, 1959) extraction was carried out on cell pellets and purified cell membranes in order to extract lipids. Reverse phase liquid chromatography was selected for lipid separation with an UPLC system (Ultimate 3000, ThermoFisher). Lipid extracts were separated on an Accucore C18 (150x2.1, 2.5µm) column (ThermoFisher) operated at 400 µl/ minutes flow rate. The injection volume was 3 µL. Eluent solutions were ACN/H₂O 50/50 (V/V) containing 10mM ammonium formate and 0.1% formic acid (solvent A) and IPA/ACN/H₂O 88/10/2 (V/V) containing 2mM ammonium formate and 0.02% formic acid (solvent B). The step gradient of elution was in %B : 0.0 min, 35%; 0.0-4.0 min, 35 to 60%; 4.0-8.0 min, 60 to 70%; 8.0-16.0 min, 70 to 85%; 16.0-25.0 min, 85 to 97%; 25-25.1 min 97 to 100% B, 25.1-31 min 100% B and finally the column was reconditioned at 35% B for 4 min. The UPLC system was coupled with a Q-exactive plus Mass Spectrometer (ThermoFisher, CA); equipped with a heated electrospray ionization (HESI) probe. This spectrometer was controlled by Xcalibur software (version 4.1.31.9.) and operated in electrospray positive mode. Data were acquired with dd-MS2 mode at a resolution of 70 000 for MS and 35 000 for MS2 (at 200 m/z) and a normalized collision energy (NCE) of 25 and 30 eV. Data were reprocessed using LipidSearch 4.1.16 (ThermoFisher). The product search mode was used and the identification was based on the accurate mass of precursor ions and MS2 spectral pattern. For quantitative comparison of lipid unsaturation, PCs with indistinguishable sn-1 and sn-2 chains were removed from the data. These PC species account for less than 2 % of the total PC and have negligible impact on the analysis.

Fluorescence microscopy

HUVEC cells were treated as indicated and fixed with 4% paraformaldehyde after 24 hours of ExoC3 toxin treatment and after 6 hours upon DHA or OA diets corresponding

respectively to the maximum of TEMs formation and the maximum of DHA incorporation into PLs. Cells were permeabilized with IF buffer (0.05% saponin, 0.2 % BSA, phosphate-buffered saline, pH 7.4) and stained with 1:500 dilution of phalloidin-594 (Thermo Fisher) for 1 hour at room temperature. Images were acquired with Olympus IX83 inverted microscope equipped with a iXon3 camera (Andor) and an UPlanSApo 40X/1.35 Oil objective (Olympus). The resulting TEM images were analyzed by ImageJ software. The acquired images were segmented by thresholding and the size of cells and TEMs were measured with ImageJ. The number of TEMs per cell was counted manually.

Video Microscopy

HUVECs were electroporated with LifeAct-GFP-pCMV as described above and seeded on gelatin coated polymer coverslip dish (Ibidi). After recovering for 24 hours from transfection, cells were lipid starved in LPDS containing medium overnight. OA-BSA and DHA-BSA were added to the cells to the final concentration of 125 μ M for 6 hours prior to video recording. Cells were supplemented with 25 mM Hepes (pH 7.4) and recorded on a 37°C heated stage of Nikon Ti inverted microscope using Ultraview spinning disk confocal system (Perkin Elmer). For the TEM opening, images were taken every 10 seconds for 1 hour. For TEM closure, images were taken every minute for 3 hours to avoid phototoxicity and bleaching during the acquisition. Acquired videos were analyzed by an Icy based automatic protocol.

Image Analysis

Time-lapse videos were analyzed with the Icy software (de Chaumont et al., 2012) and segmentation plugins (icy.bioimageanalysis.org/plugin). Each TEM was first manually identified as a region of interest (ROI). Considering the gradual recruitment of LifeAct-GFP around TEMs, it was difficult to properly identify the edge of TEMs. Indeed, the non-homogeneous contrast at the TEM border leads to a difficult clipping process. To overcome this challenge, we used advanced image analysis methods like the Active Contour plugin to properly track TEM over time. This allowed us in particular to determine the surface of the TEMs at each time point. We then applied a post-processing analysis to filter the TEMs and automatically eliminate remaining wrong segmentations. For instance, we discarded any TEMs that display excessive growing

area. In the end, this protocol allowed us to provide precise statistics of the TEM dynamics, such as the evolution of the area, the diameters or the sphericity of TEMs over time.

GPMV preparation

Cells were enriched with OA or DHA as described above followed by induction of blebs as described (Segzin et al., 2012). Briefly, cells were washed with GPMV buffer (10 mM HEPES, 150 mM NaCl, 2 mM CaCl₂, pH 7.4) twice and incubated with GPMV buffer containing 25 mM PFA and 2 mM DTT for 1 hour. Blebs were formed and released as GPMVs. Supernatant was collected and centrifuged at 100 g for 5 minutes to remove cell debris. Supernatant containing GPMVs was centrifuged in Beckman Type 70 Ti rotor at 20,000 g at 4 °C for 1 hr. GPMVs appeared as a transparent pellet that was collected for lipidomic analysis or western blot. Otherwise, cells that did not receive the treatment to induce blebs were collected directly to assess total membranes (TM). For western blot, TM or GPMV fractions were lysed in white Leammli buffer (50 mM Tris pH 7.4, EDTA 5mM, 2% SDS) and protein concentration was determined with BCA assay kit (Thermo Fisher) using BSA suspended in Leammli buffer as standard. Total membranes or GPMV lysates were adjusted to the same protein quantity between OA and DHA fed cells. Glycerol, β-mercaptoethanol, and bromophenol blue were added to final concentration of 10%, 5% and 0.004%. Protein samples were analyzed by SDS-PAGE western blot.

STED microscopy

Cells were grown on H1.5 glass coverslips coated with 10 µg/ml fibronectin. After treatment, cells were fixed with 4% PFA/0.1% glutaraldehyde for 15 minutes at room temperature. Cells were washed with PBS, quenched in 50 mM NH₄Cl for 15 minutes followed by permeabilizing in IF buffer (PBS/0.05% saponin/0.2 % BSA) for 30 minutes. Later, the cells were stained with 1 µM Star635-phalloidin (Abberior) for 1 hr followed by 3 washes with IF buffer for 5 minutes and a final wash in H₂O. The cells were mounted in Mount Solid Antifade (Abberior) following manufacturer's instruction. Stimulated Emission Depletion (STED) imaging was performed by TCS STED SP8 (Leica) using a APO 93X/1.3 motCORR lens. The excitation laser was at 633 nm and pulse depletion laser at 775 nm. STED images were deconvolved using Huygens with 5 iterations.

Atomic force microscope measurement of TEM topology

AFM experiments were carried out on a JPK NanoWizardIII mounted on a Zeiss Axio Observer.Z1. For the elasticity measurements PFQNM-LC-A-Cal cantilevers (Bruker) with a 140 nm diameter spherical tip apex were used and calibrated using the SNAP calibration method (Schillers et al., 2017). The AFM was operated in QI mode on the perinuclear region of living cells to record a 10 μm^2 , 20x20 pixels map of force curves with 2 μm ramp length, 200 pN force trigger and 50 $\mu\text{m/s}$ tip velocity. Force maps were computed using in-house software (pyAF) for the fitting of the indentation up to 40 nm using Hertz model. Each dot of the scatter plot corresponds to a different cell (median of a map). For the topography measurements of TEMs sharper Olympus AC40 cantilevers were used with the SADER calibration method (Sader et al., 2016). Cells had to be fixed with 4 % PFA in PBS for 10 min because of the too short window of time available for the measurement with the microscope. A QI map of 150x150 pixels bigger than the size of the TEM was recorded with an 800-nm ramp and 100 $\mu\text{m/s}$ tip velocity. We then computed the zero-force topography by determining the point of contact, and drew several profiles across the TEM to measure its diameter and the height of the rim and the cell at the border. This was all performed on the JPK analysis software v6. Each dot of the scatter plot correspond to a TEM.

RhoA ADP-ribosylation assay

HUVEC were seeded in 15 cm culture plate and treated with or without 50 $\mu\text{g/ml}$ ExoC3 toxin in LPDS or FBS medium (Human endothelial SFM, 20% serum, 20 ng/ml FGF, 10 ng/ml EGF, 1 $\mu\text{g/ml}$ Heparin, and Zellshield) overnight. Before experiments, cells were supplemented with 125 μM FA-BSA for 6 hr. Cells were lysed in ADP-ribosylation buffer (20 mM Tris-HCl, 1 mM EDTA, 1 mM DTT, 5 mM MgCl_2 , cOmpleteTM, pH 7.5) by passing through a 27G syringe 20 times. Cell lysate were collected by centrifuge at 12,000g for 10 min and the protein concentration was determined by BCA assay (Thermo Fisher). Reaction was carried out by incubating 20 μg of cell lysate with 2 μg ExoC3 and 10 μM 6-biotin-17-NAD⁺ (BioLog) at 37°C 30 min. The reaction was terminated by addition of 1 mM DTT and Laemmli buffer (0.3 M Tris-HCl, 10% SDS, 37.5% glycerol, 0.4 mM bromophenol blue) and boiled at 100°C for 5 min. The samples

were subjected to 12% SDS-PAGE and ADP-ribosylated, i.e., biotin-labeled-RhoA was detected by Western blotting using streptavidin–peroxidase.

Physical model of TEM opening

In the physical model for TEM opening dynamics (Gonzalez-Rodriguez et al., 2012), the driving force for opening is given by

$$F_d = 2\sigma - \frac{\tilde{T}}{R},$$

where σ is the membrane tension, \tilde{T} is the line tension and R is the TEM radius. The membrane tension σ depends on R through Helfrich's law, which here we write in a generalized form to account for the coexistence of N simultaneous TEMs in the same cell:

$$\sigma = \sigma_0 \exp\left[-\frac{(\sum_{i=1}^N R_i)^2}{NR_c^2}\right],$$

where $R_c^2 = (R_{\text{cell}}^2 k_B T)/(8\pi\kappa)$ is the so-called critical radius, with R_{cell} the total cell radius, k_B the Boltzmann constant, T the temperature, and κ the effective membrane bending rigidity. Due to actin cable polymerization around the TEM, the line tension is not a constant but rather it increases with time (Stefani et al., 2017), which can be represented by a linear increase $\tilde{T} \sim \alpha t$. The dynamics of TEM opening are governed by a balance between driving force and cell-substrate friction, characterized by a friction coefficient μ . For the case of N identical TEMs, this balance results in the following differential equation:

$$\mu R^2 \frac{dR}{dt} = 2\sigma_0 R \exp\left(-\frac{NR^2}{R_c^2}\right) - \alpha t.$$

This equation can be solved numerically. However, insight can be gained by analytical approximations. First, in the limit of short time, when R is small, the equation can be approximated as

$$v_0 = \frac{dA}{dt} = \frac{4\pi\sigma_0}{\mu},$$

where $A = \pi R^2$ is the TEM area. Therefore, TEM opening speed at short time, v_i , is proportional to the undisturbed cell membrane tension σ_0 .

Second, the dependence of the maximum TEM area $A_{\text{max}} = \pi R_{\text{max}}^2$ on the membrane parameters σ_0 and κ can be estimated by the following approximation. Let us suppose

that the initial opening speed v_i is an acceptable estimate of the average opening speed. Then, the opening time t_{\max} is related to the maximum TEM area by

$$t_{\max} \approx \frac{\mu A_{\max}}{4\pi\sigma_0}.$$

Moreover, at $t = t_{\max}$, the opening stops and $dR/dt=0$. By replacing these two results in the differential equation, we obtain the following approximate relationship:

$$x \exp x^2 = \frac{8 \sqrt{N} \sigma_0^2}{\mu \alpha R_c},$$

where we have defined $x = \sqrt{N}R_{\max}/R_c$. The nondimensional parameter on the right-hand side of this expression is slightly larger than 1, which requires x to be of the order of or somewhat larger than 1. In this range of values, small changes in x yield large changes of the exponential function, implying that x is weakly dependent on the right-hand side. Therefore, x will remain approximately constant for moderate changes of σ_0 , implying that $N^{1/2}R_{\max} \sim R_c \sim 1/\kappa^{1/2}$. This result shows that the maximum TEM size is very sensitive to κ but rather insensitive to σ_0 . We thus obtain the following estimate of the effective membrane bending rigidity:

$$\kappa \approx \frac{k_B T A_{cell}}{8\pi N A_{max}}.$$

Statistical analysis. Data are showed as the medium \pm s.e.m. unless otherwise indicated. The normality distribution of the data was first calculated using Kolmogoro-Smirnov test. For Gaussian distributed data, unpaired, two-sided Student's t-test was used for comparing two groups and one-way ANOVA with Bonferroni post-hoc corrections was used for multiple group comparison. For non-Gaussian distributed data, unpaired, two-tailed Mann-Whitney test was used. P-value for *P<0.05, **P<0.01, ***P<0.001 and ****P<0.0001 were considered statistically significant. The statistical software used was Prism 8 (GraphPad Software, San Diego, CA, USA).

AUTHOR CONTRIBUTIONS. Cell biology experiments were performed by M-C.T. and analyzed by M-C.T., E.L. and H.B.. AFM experiments were performed by S.J. and F.L. Lipidomics was performed by L.F and D.D. Physical model was established by D.J-R. Video and image analyses was performed by M-C.T with the help of Icy software

developped by S.D. and J-C.O-M.; C.M. and A.M.. performed C3 exoenzyme purifications. H.B. and E.L. designed experiments, discussed and supervised the project. H.B., E.L., D.J-R and M-C.T. wrote the manuscript. M.C.T., L.F., S.J., D.G-R., C.M., A.M., D.D., S.D, J-C.O-M, B.A., F.L., E.L. and H.B. reviewed the manuscript.

ACKNOWLEDGEMENTS. This work was supported by a grant from the Fondation pour la Recherche Médicale (Convention DEQ20180339156 Equipes FRM 2018), the Agence Nationale de la Recherche (ANR-11-LABX-0028-01, ANR-15-CE18-0016, ANR 10-EQPX-04-01, ANR- 10-INBS-04, and ANR-10-LABX-62-IBEID) and FEDER 12,001,407 and partially by grants from the France-BioImaging infrastructure (ANR-10-INBS- 04) and the Labex IBEID (ANR- 10- LABX-62-IBEID). MCT was supported by a PhD fellowship from the Labex Signallife PhD Programme and by the Fondation pour la Recherche Médicale (Contrat FDT201904008135). We thank Blandine Madji Hounoum for pilot lipidomics experiments. Frédéric Brau and Sophie Abelanet for support in light and STED microscopy. James Muncey for its helps in time-lapse analyses with Icy software. Marco Lorenzi (INRIA, Sophia Antipolis) for comments on the manuscript and all members of our laboratories for discussion.

DISCLOSURE.

The authors declare no competing interests.

1.6. REFERENCES

- Aird, W.C.** (2007). Vascular bed-specific thrombosis. *Journal of Thrombosis and Haemostasis* **5**, 283-291.
- Antonny, B., Vanni, S., Shindou, H. and Ferreira, T.** (2015). From zero to six double bonds: phospholipid unsaturation and organelle function. *Trends in Cell Biology* **25**, 427-436.
- Barelli, H. and Antonny, B.** (2016). Lipid unsaturation and organelle dynamics. *Current Opinion in Cell Biology* **41**, 25-32.
- Bazinet, R. P. and Layé, S.** (2014). Polyunsaturated fatty acids and their metabolites in brain function and disease. *Nature Reviews Neuroscience* **15**,771-785.
- Bligh, E. G. and Dyer, W. J.** (1959). A rapid method of total lipid extraction and purification. *Canadian Journal of Biochemistry and Physiology* **37**, 911-917.
- Boyer, L., Doye, A., Rolando, M., Flatau, G., Munro, P., Gounon, P., Clément, R., Pulcini, C., Popoff, M. R., Mettouchi, A. et al.** (2006). Induction of transient macroapertures in endothelial cells through Rho inhibition by *Staphylococcus aureus* factors. *The Journal of Cell Biology* **173**, 809-819.

- Braakman, S. T., Pedrigi, R. M., Read, A. T., Smith, J. A. E., Stamer, W. D, Ethier, C. R. and Overby, D. R.** (2014). Biomechanical strain as a trigger for pore formation in Schlemm's canal endothelial cells. *Experimental eye research* **127**, 224-235.
- Braakman, S. T., Moore, J. E., Ethier, C. R. and Overby, D. R.** (2016). Transport across schlemm's canal endothelium and the blood-aqueous barrier. *Experimental Eye Research* **146**, 17-21.
- Caires, R., Sierra-Valdez, F. J., Millet, J. R. M., Herwig, J. D., Roan, E., Vásquez, V. and Cordero-Morales J. F.** (2017). Omega-3 fatty acids modulate trpv4 function through plasma membrane remodeling. *Cell Reports* **21**, 246-258.
- de Chaumont, F., Dallongeville, S., Chenouard, N., Hervé, N., Pop, S., Provoost, T., Meas-Yedid, V., Pankajakshan, P., Lecomte, T, Le Montagner, Y. et al.** (2012). Icy: An open bioimage informatics platform for extended reproducible research. *Nature methods* **9**, 690-696.
- Gonzalez-Rodriguez, D., Maddugoda, M. P., Stefani, C., Janel, S., Lafont, F., Cuvelier, D., Lemichez, E. and Brochard-Wyart F.** (2012). Cellular dewetting: Opening of macroapertures in endothelial cells. *Physical Review Letters* **108**, 218105.
- Harayama, T. and Riezman, H.** (2018). Understanding the diversity of membrane lipid composition. *Nature Reviews Molecular Cell Biology* **19**, 281-296.
- Helfrich W.** (1973). Elastic properties of lipid bilayers: Theory and possible experiments. *Zeitschrift fur Naturforschung. Teil C: Biochemie, Biophysik, Biologie, Virologie* **28**, 693-703.
- Iizuka-Hishikawa, Y., Hishikawa, D., Sasaki, J., Takubo, K., Goto, M., Nagata, K., Nakanishi, H., Shindou, H., Okamura, T., Ito C et al.** (2017). Lysophosphatidic acid acyltransferase 3 tunes the membrane status of germ cells by incorporating docosahexaenoic acid during spermatogenesis. *J Biol Chem.* **292**, 12065-12076.
- Jeffrey, B. G. and Neuringer M.** (2009). Age-related decline in rod phototransduction sensitivity in rhesus monkeys fed an n-3 fatty acid–deficient diet. *Investigative Ophthalmology & Visual Science* **50**, 4360-4367.
- Lemichez, E., Lecuit, M., Nassif, X. and Bourdoulous S.** (2010). Breaking the wall: targeting of the endothelium by pathogenic bacteria. *Nat Rev Micro.* **8**, 93-104.
- Lemichez, E., Gonzalez-Rodriguez, D., Bassereau, P. and Brochard-Wyart, F.** (2013). Transcellular tunnel dynamics: Control of cellular dewetting by actomyosin contractility and I-bar proteins. *Biology of the Cell* **105**, 109-117.
- Levayer, R. and Lecuit, T.** (2012). Biomechanical regulation of contractility: Spatial control and dynamics. *Trends Cell Biol.* **22**, 61-81.
- Levental, K. R., Malmberg, E., Symons, J. L., Fan, Y-Y., Chapkin, R. S., Ernst, R. and Levental I.** (2020). Lipidomic and biophysical homeostasis of mammalian membranes counteracts dietary lipid perturbations to maintain cellular fitness. *Nature Communications* **11**, 1339.
- Lorent, J. H., Levental, K. R., Ganesan, L., Rivera-Longworth, G., Sezgin, E., Doktorova, M., Lyman, E. and Levental I.** (2020). Plasma membranes are asymmetric in lipid unsaturation, packing and protein shape. *Nature Chemical Biology* **16**, 644-652.
- Maddugoda, M. P., Stefani, C., Gonzalez-Rodriguez, D., Saarikangas, J., Torrino, S., Janel, S., Munro, P., Doye, A., Prodon, F., Aurrand-Lions, M. et al.** (2011). cAMP signaling by anthrax edema toxin induces transendothelial cell tunnels, which are resealed by MIM via Arp2/3-driven actin polymerization. *Cell Host & Microbe* **10**, 464-474.

- Manni, M. M., Tiberti, M.L., Pagnotta, S., Barelli, H., Gautier, R. and Antonny, B.** (2018). Acyl chain asymmetry and polyunsaturation of brain phospholipids facilitate membrane vesiculation without leakage. *eLife* **7**, e34394.
- Monzel, C. and Sengupta, K.** (2016). Measuring shape fluctuations in biological membranes. *Journal of Physics D: Applied Physics* **49**, 243002.
- Munro, P., Benchetrit, M., Nahori, M-A., Stefani, C., Clément, R., Michiels, J-F., Landraud, L., Dussurget, O. and Lemichez E.** (2010). The *Staphylococcus aureus* epidermal cell differentiation inhibitor toxin promotes formation of infection foci in a mouse model of bacteremia. *Infection and Immunity* **78**, 3404-3411.
- Ng, W. P., Webster, K. D., Stefani, C., Schmid, E. M., Lemichez, E., Bassereau, P. and Fletcher, D. A.** (2017). Force-induced transcellular tunnel formation in endothelial cells. *Molecular Biology of the Cell* **28**, 2650-2660.
- Pinot, M., Vanni, S., Pagnotta, S., Lacas-Gervais, S., Payet, L-A., Ferreira, T., Gautier, R., Goud, B., Antonny, B. and Barelli H.** (2014). Polyunsaturated phospholipids facilitate membrane deformation and fission by endocytic proteins. *Science* **345**, 693-697.
- Randall, A.S., Liu, C-H., Chu, B., Zhang, Q., Dongre, S. A., Juusola, M., Franze, K., Wakelam, M. J. O. and Hardie, R. C.** (2015). Speed and sensitivity of phototransduction in drosophila depend on degree of saturation of membrane phospholipids. *The Journal of Neuroscience* **35**, 2731-2746.
- Renaud, J-F., Scanu, A. M., Kazazoglou, T., Lombet, A., Romey, G. and Lazdunski M.** (1982). Normal serum and lipoprotein-deficient serum give different expressions of excitability, corresponding to different stages of differentiation, in chicken cardiac cells in culture. *Proc Natl Acad Sci U S A* **79**, 7768-7772.
- Rolando, M., Munro, P., Stefani, C., Auberger, P., Flatau, G. and Lemichez, E.** (2009). Injection of *Staphylococcus aureus* EDIN by the *Bacillus anthracis* protective antigen machinery induces vascular permeability. *Infection and Immunity* **77**, 3596-3601.
- Romero, L.O., Massey, A.E., Mata-Daboin, A.D., Sierra-Valdez, F.J., Chauhan, S.C., Cordero-Morales, J. F. and Vásquez, V.** (2019). Dietary fatty acids fine-tune piezo1 mechanical response. *Nature Communications* **10**, 1200.
- Sader J. E., Borgani R., Gibson C. T., Haviland D. B., Higgins M. J., Kilpatrick J. I., Lu J., Mulvaney P., Shearer C. J., Slattery A. D. et al.** (2016). A virtual instrument to standardise the calibration of atomic force microscope cantilevers. *Review of Scientific Instruments* **87**, 093711.
- Salbreux, G., Charras, G. and Paluch, E.** (2012). Actin cortex mechanics and cellular morphogenesis. *Trends Cell Biol.* **22**, 536-545.
- Schillers, H., Rianna, C., Schäpe, J., Luque, T., Doschke, H., Wälte, M., Uriarte, J. J., Campillo, N., Michanetzis, G. P. A., Bobrowska J. et al.** (2017). Standardized nanomechanical atomic force microscopy procedure (snap) for measuring soft and biological samples. *Scientific Reports* **7**, 5117.
- Schimmel, L., Heemskerk, N. and van Buul, J.D.** (2017). Leukocyte transendothelial migration: A local affair. *Small GTPases* **8**, 1-15.
- Sezgin, E., Kaiser, H-J., Baumgart, T., Schwille, P., Simons, K. and Levental I.** (2012). Elucidating membrane structure and protein behavior using giant plasma membrane vesicles. *Nature Protocols* **7**, 1042-1051.

- Shindou, H., Koso, H., Sasaki, J., Nakanishi, H., Sagara, H., Nakagawa, K. M., Takahashi, Y., Hishikawa, D., Iizuka-Hishikawa, Y., Tokumasu, F. et al. (2017).** Docosahexaenoic acid preserves visual function by maintaining correct disc morphology in retinal photoreceptor cells. *Journal of Biological Chemistry* **292**, 12054-12064.
- Stefani, C., Gonzalez-Rodriguez, D., Senju, Y., Doye, A., Efimova, N., Janel, S., Lipuma, J., Tsai, M. C., Hamaoui, D., Maddugoda, M. P. et al. (2017).** Ezrin enhances line tension along transcellular tunnel edges via NMIIa driven actomyosin cable formation. *Nature Communications* **8**, 15839.
- Tanguy, E., Costé de Bagneaux, P., Kassas, N., Ammar, M-R., Wang, Q., Haeberlé, A-M., Raherindratsara, J., Fouillen, L., Renard, P-Y., Montero-Hadjadje, M. et al. (2020).** Mono- and poly-unsaturated phosphatidic acid regulate distinct steps of regulated exocytosis in neuroendocrine cells. *Cell Reports* **32**, 108026.
- Tiberti, M. L., Antony, B. and Gautier, R. (2020).** The transbilayer distribution of polyunsaturated phospholipids determines their facilitating effect on membrane deformation. *Soft Matter* **16**, 1722-1730.
- Tixier-Vidal, A., Picart, R., Loudes, C. and Bauman, A. F. (1986).** Effects of polyunsaturated fatty acids and hormones on synaptogenesis in serum-free medium cultures of mouse fetal hypothalamic cells. *Neuroscience* **17**, 115-132.
- van Meer, G., Voelker, D. R. and Feigenson, G. W. (2008).** Membrane lipids: Where they are and how they behave. *Nat Rev Mol Cell Biol.* **9**, 112-124.
- Yuki, K., Shindou, H., Hishikawa, D. and Shimizu, T. (2009).** Characterization of mouse lysophosphatidic acid acyltransferase 3: An enzyme with dual functions in the testis. *J Lipid Res.* **50**, 860-869.

Table 1. Summary of TEM measurements presented in the figures

	OA	DHA	Statistics
Cell area (μm^2)	6330 \pm 271	6003 \pm 251	ns
Cell thickness (nm)	190 \pm 6	164 \pm 6	**
% of cells with TEMs	27 \pm 3	26 \pm 3	ns
Number of TEMs/cell	2.5 \pm 0.1	3.5 \pm 0.3	*
TEM frequency (TEMs/hour)	8.9 \pm 1.4	19.3 \pm 3.2	**
TEM max size (μm^2) ^a	37.4 (27.6-59.4)	25.4 (21.2-28.6)	*
Opening time (sec)	179 \pm 21	162 \pm 23	ns
Initial opening speed ($\mu\text{m}^2/\text{sec}$) ^a	0.47 (0.35-0.95)	0.39 (0.29-0.54)	ns

Late opening speed ($\mu\text{m}^2/\text{sec}$) ^a	0.38 (0.22-0.61)	0.27 (0.14-0.37)	*
Latency phase (min)	7.3 \pm 0.6	5.3 \pm 0.4	*
Closure time (min)	16.3 \pm 1.4	11.1 \pm 0.8	**
Closure speed ($\mu\text{m}^2/\text{sec}$) ^a	4.3 (3.4-6.1)	2.7 (2.1-3.3)	***
Lifetime (min)	42.0 \pm 4.0	24.6 \pm 1.8	***

Data show the means \pm SEM; All data were analyzed by Mann-Whitney test

^a data show the median (95% CI, upper-lower)

ns, not significant; * p <0.05, ** p <0.01, *** p <0.001

1.7. FIGURE LEGENDS

FIGURE 1. Analysis of phospholipid classes in HUVEC submitted to oleic acid (OA) versus docosahexaenoic acid (DHA).

(A) Global fold change of phosphatidyl choline (PC), ethanolamine (PE), serine (PS) and inositol (PI) classes from HUVEC submitted to OA- or DHA-diet for 6 hours compared to FBS- or LPDS-cultured HUVEC. Data were compared to FBS-treated cells by one-way ANOVA with Bonferroni correction and were significant with $p < 0.01$ (**) or not significant, not indicated. (B) Lipidic profiles comparison of the different PL classes: PC, PE, PS and PI upon OA-diet, DHA-diet compared to controls (FBS and LPDS). PC with unseparated sn-1 and sn-2 acyl chains represent less than 5% of total PC. Values were normalized individually to the sum of each PL classes. (C) PL species distribution regarding their number of double bond (level of unsaturation): from zero to 6 double bonds as illustrated in figure 1B. OA and DHA contain 1 and 6 double bonds, respectively. LPDS = lipoprotein-depleted serum. (A-C) Data show means \pm SEM; $n > 3$ experiments; 3 biological replicates.

FIGURE 2. Lipidomic analysis of phospholipids from Giant Plasma Membrane Vesicle (GPMV).

(A) 3D-projection of WGA-Alexa488 labeled GPMVs (left) and FM4-64 labelled GPMVs (right) from HUVEC. Scale bars 10 μ m. (B) Western blot of total membrane (TM) and GPMV fractions using different organelles markers. Equal amounts of proteins for TM or GPMV were loaded. Plasma membrane (PM) marker: Na^+/K^+ ATPase and Annexin V, Endoplasmic reticulum (ER) marker: Calregulin, ER-Golgi intermediate compartment (ERGIC) marker: ERGIC53, Golgi complex marker: Trans-Golgi Network 46 (TGN46), Lysosome marker: Lysosomal-associated membrane protein 1 (LAMP1). (C) Lipidomic analyses of GPMVs from OA- or DHA-treated cells. Lipid classes enrichment in GPMVs was calculated by dividing the relative content of each lipid class in GPMVs by those of total membranes. Value bigger than 1 indicate that lipids were enriched in GPMVs, value smaller than 1 indicate that lipids were excluded from GPMVs. SM, sphingomyelin; PC, phosphatidylcholine; PE, phosphatidylethanolamine; PS, phosphatidylserine; PI, phosphatidylinositol; DG, diacylglycerol; LBPA, lysobisphosphatidic acid. (D) Fold change of different PL classes in DHA-treated cells

compared with OA-treated cells. Data were analyzed with Student's t-test and were not significant, n.s. (E). PL species distribution regarding their number of double bond (level of unsaturation): from zero to 6 double bonds as illustrated in figure 1B. AA and DHA contain 4 and 6 double bonds, respectively. (C-E) Data show means \pm SEM; n>3 experiments; 3 biological replicates.

FIGURE 3. The impact of DHA on TEM parameters.

(A) Schematic representations of liquid dewetting physics phenomenon and TransEndothelial cell Macroaperture dynamics. Scale bar 20 μ m. (B-H) HUVEC were treated with C3 exoenzyme or without (Mock) for 16 hours prior to 6-hours fatty acid diet (OA or DHA) as sole source of exogenously added acyl chain. (B) FITC-phalloidin staining of HUVEC in Mock, OA or DHA conditions. Scale bar 100 μ m. (C) Cell area of cells on OA- or DHA-diet. Data show median \pm max to min; cells > 450 / experiments; 2 biological replicates. (D) Percentage of HUVEC with at least one TEM in the population in OA or DHA conditions. Data show means \pm SEM; cells > 200 / experiments; 3 biological replicates. (E) Number of TEMs per cell under OA- or DHA-diet. Data show median \pm max to min of >150 cells from 3 independent experiments (> 50 cells / experiment). (F) Representative FITC-phalloidin staining of OA or DHA-treated cells intoxicated with C3 toxins. Scale bar 20 μ m. (G) Graph shows median values of TEM area in fixed cells treated with either OA or DHA. Data show median \pm max to min of > 450 TEMs from 3 independent experiments (>40 cells / experiments). (H) Distribution of TEM sizes in HUVEC under OA- or DHA-diet. (C, D, E, G) Data were analyzed with nonparametric Mann-Whitney statistical test and p values were indicated.

FIGURE 4. Impact of DHA-enriched membrane on TEM opening dynamics.

(A) Time-lapse images of TEM opening dynamics in OA- or DHA-fed cells using LifAct-GFP as label. Scale bars 10 μ m. (B-C) Frequency of TEM opening events per cell in cells treated with ExoC3 and fed with either OA or DHA. (B) Each row on the Y-axis of the diagram pinpoints all opening events of TEM in a single cell, each black bar is an individual opening event. (C) Graph shows total number of TEM opening events per cell per hour. Data show are median \pm max to min; n>28 cells from 28 independent experiments. (D) Graph shows the distribution of values of TEM opening lifetimes

measured for each TEM. Data are median \pm max to min, $n > 75$ TEMs from > 8 independent experiments. (C-D) Data were analyzed with nonparametric Mann-Whitney statistical test and p values were indicated.

FIGURE 5. Impact of DHA on cell geometry.

(A) Atomic force microscopy (cantilever shape seen in foreground) is used to measure the mechanical parameters of the cell (background in bright field). Scale bar 20 μm . (B) Heatmap of cell elasticity (kPa) on OA- and DHA-treated cells. Scale: 10 μm^2 per field of view. (C) Graph shows the cortical elasticity of Mock or ExoC3-intoxicated cells treated with OA or DHA. Data show median \pm max to min; $n = 40$ TEMs. Data showed Gaussian distribution and were analyzed with one-way ANOVA with Bonferroni correction with p values indicated. (D) AFM zero-force topography measurement of the cell thickness at the periphery of TEMs (E) and thickness of TEMs border (F) were measured by AFM using zero-force topography. (E-F) Data show median \pm max to min; $n > 20$ TEMs. Data were analyzed with Mann-Whitney and p values were indicated. (G) Graph shows the curvature of TEMs derived from the TEM height measurements.

FIGURE 6. Impact of DHA-enrichment on TEM opening parameters.

(A) Experimental workflow. HUVEC cultivated in LPDS medium were transfected with LifeAct-GFP, treated with C3 toxin, and fed with OA- or DHA-BSA for 6 hours. The dynamics of each TEM was recorded by spinning disk confocal microscopy and was analyzed through custom made Icy-based protocol. (B) Super-resolution stimulated emission depletion (STED) microscopy images of phalloidin-StarRed in C3 intoxicated cells treated without any fatty diet (Mock) or with OA- or DHA-diet. Scale bar 5 (upper) and 2 (lower) μm . (C) Graph shows median values of TEM area as a function of time in cells treated with either OA (yellow, $n=71$ TEMs) or DHA (purple, $n=94$ TEMs) as sole source of exogenously added acyl chain. Values correspond to average surface of TEMs. Data show median \pm 95% CI from 28 independent experiments. (D) Distribution of opening speed of TEM between 20-70 seconds. (E) Graph shows median values of TEM maximum area in cells treated with either OA or DHA. (F) Distribution of TEM sizes in HUVEC under OA- or DHA-diet. (G) Graph shows distribution of time durations to reach 95% of maximum area. (D, E, G) Data show

median \pm max to min, n>70 TEMs for each condition from 28 independent experiments. Data were analyzed with Mann-Whitney test and p values were indicated.

FIGURE 7. Impact of unsaturation phospholipids (PL) fatty acyl chains on large scale membrane deformations induced in endothelial cells challenged with the exoenzyme C3 (ExoC3) from *Clostridium botulinum*. The ExoC3 triggers cycles of nucleation, enlargement and closure of transendothelial cell macroaperture TEM tunnels by inhibiting the small GTPase RhoA and inducing a relaxation of the actomyosin cytoskeleton. The diagram summarizes the cellular effects of strict diets in either monounsaturated oleic acid (OA diet) vs polyunsaturated docosahexaenoic acid (DHA diet) on the plasma membrane content in DHA-containing phospholipids (DHA-PLs). Comparative analyses show that high levels of DHA-PLs increase the frequency of TEM tunnel nucleation which we link to a decrease in cell thickness, as a reduction in cell height could promote fusion of the basal and dorsal membranes for TEM nucleation. Moreover, we found that the increase in DHA-PLs also was associated with a reduction of the width of TEM tunnels. Together, this shows that endothelial cells self adapt to changes of polyunsaturated phospholipids by maintaining constant the global area of TEM tunnels through modulating their nucleation and cycling kinetics.

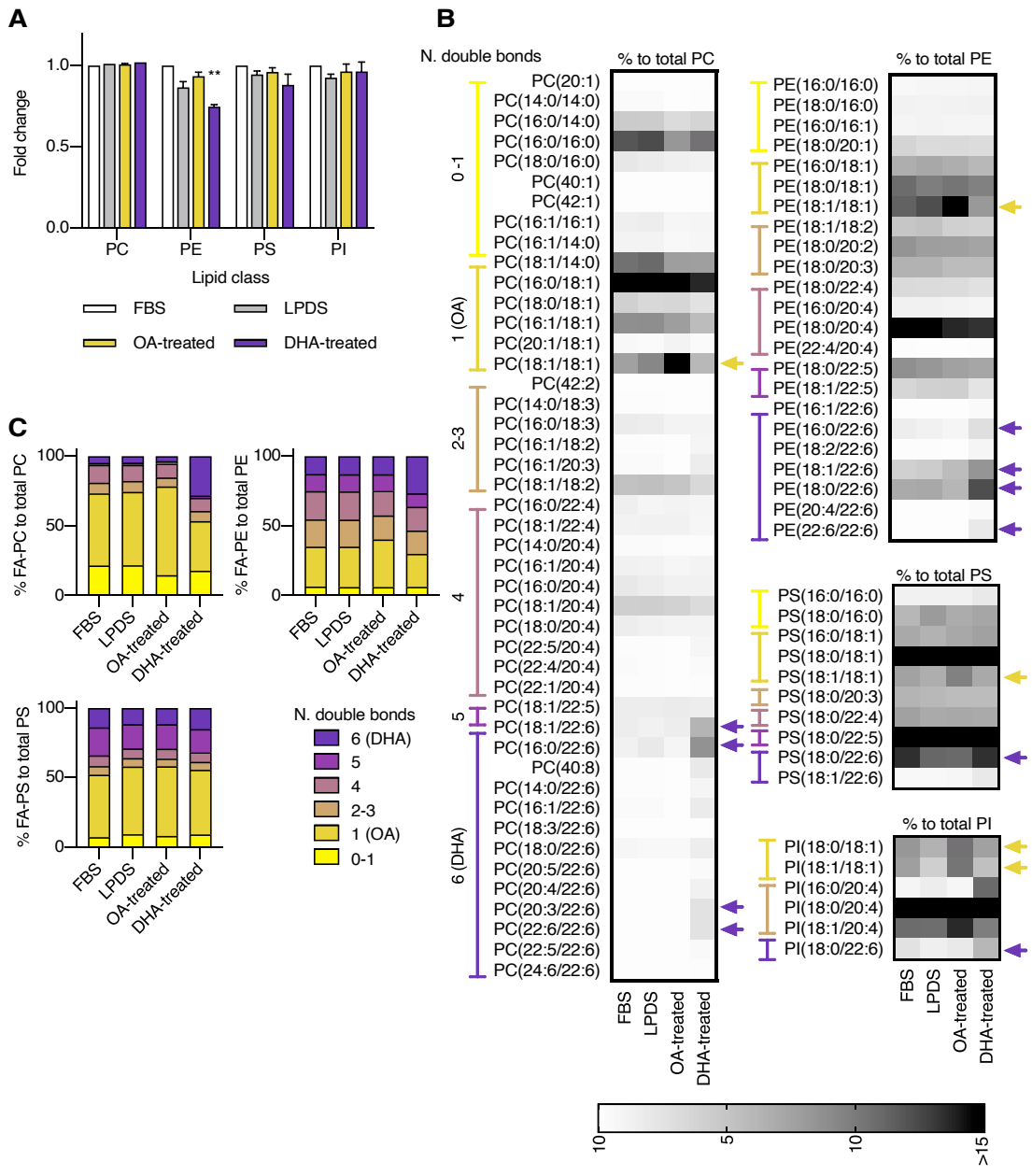


Figure 1

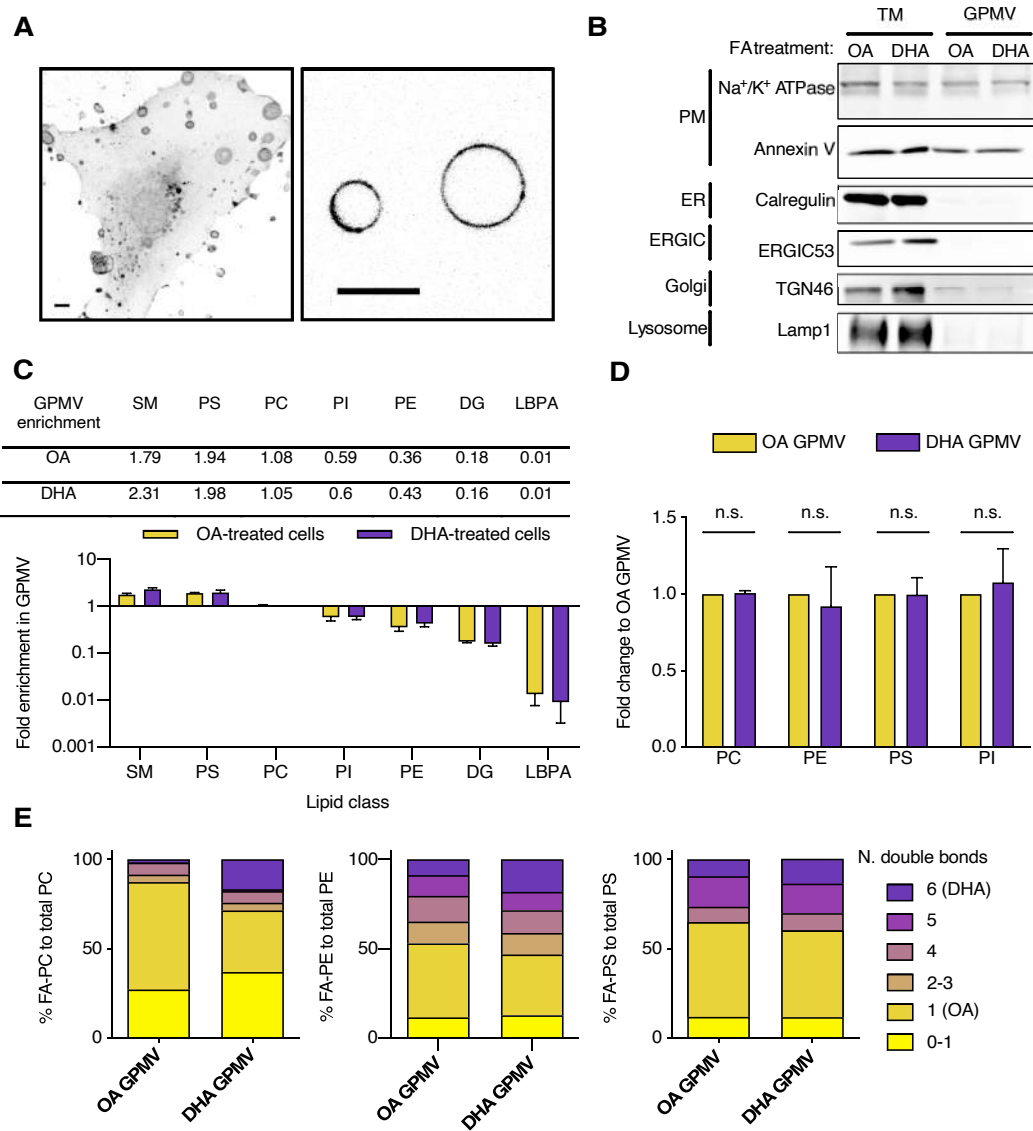


Figure 2

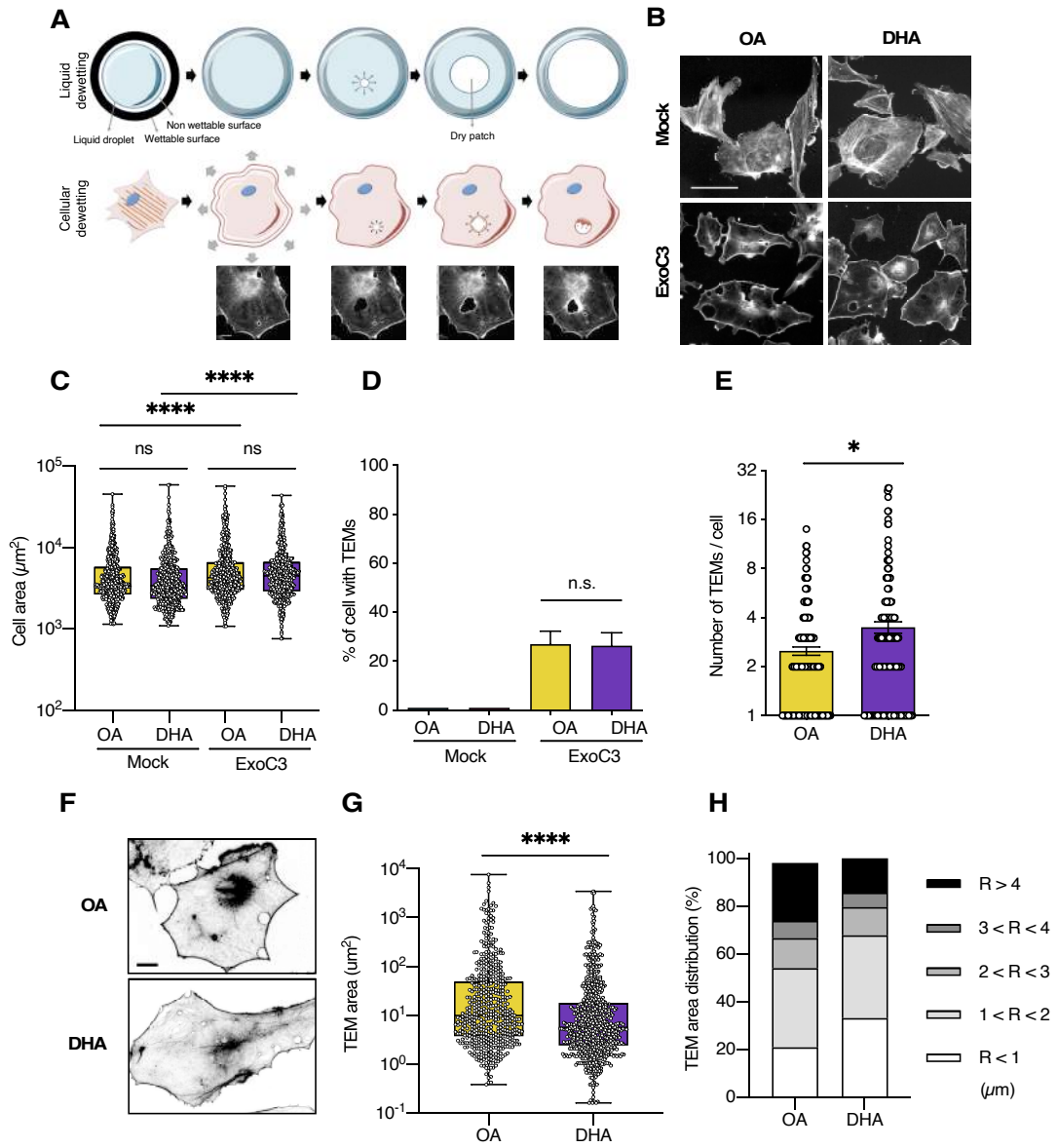


Figure 3

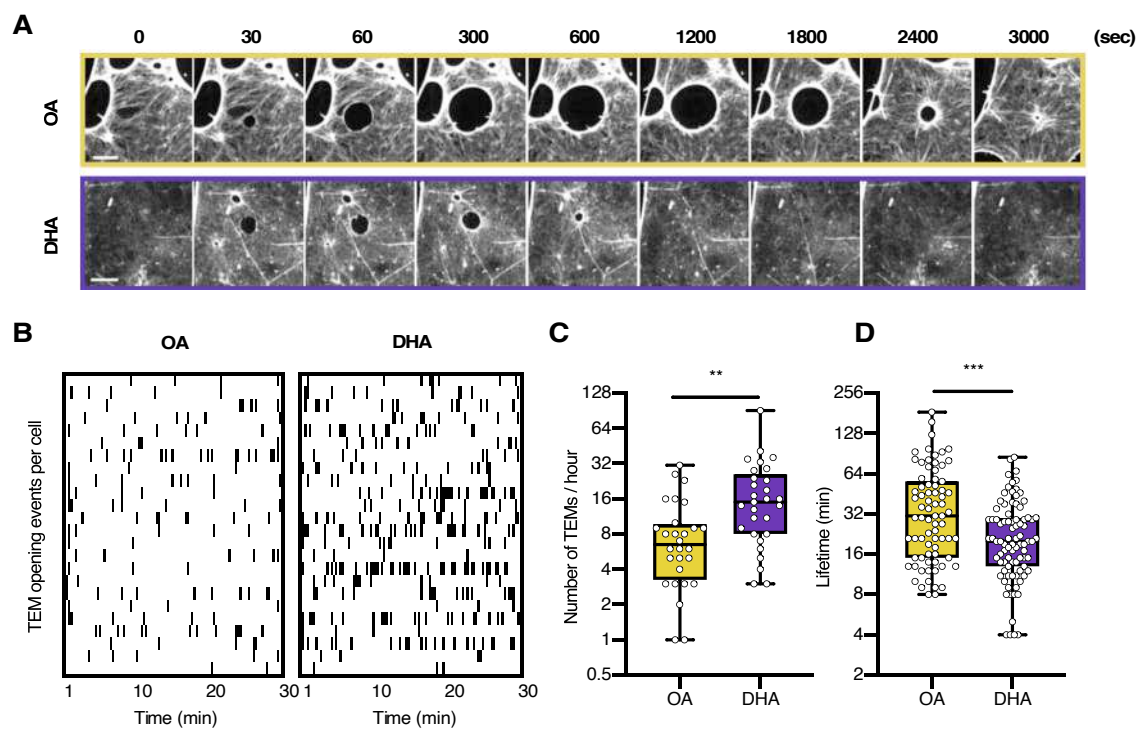


Figure 4

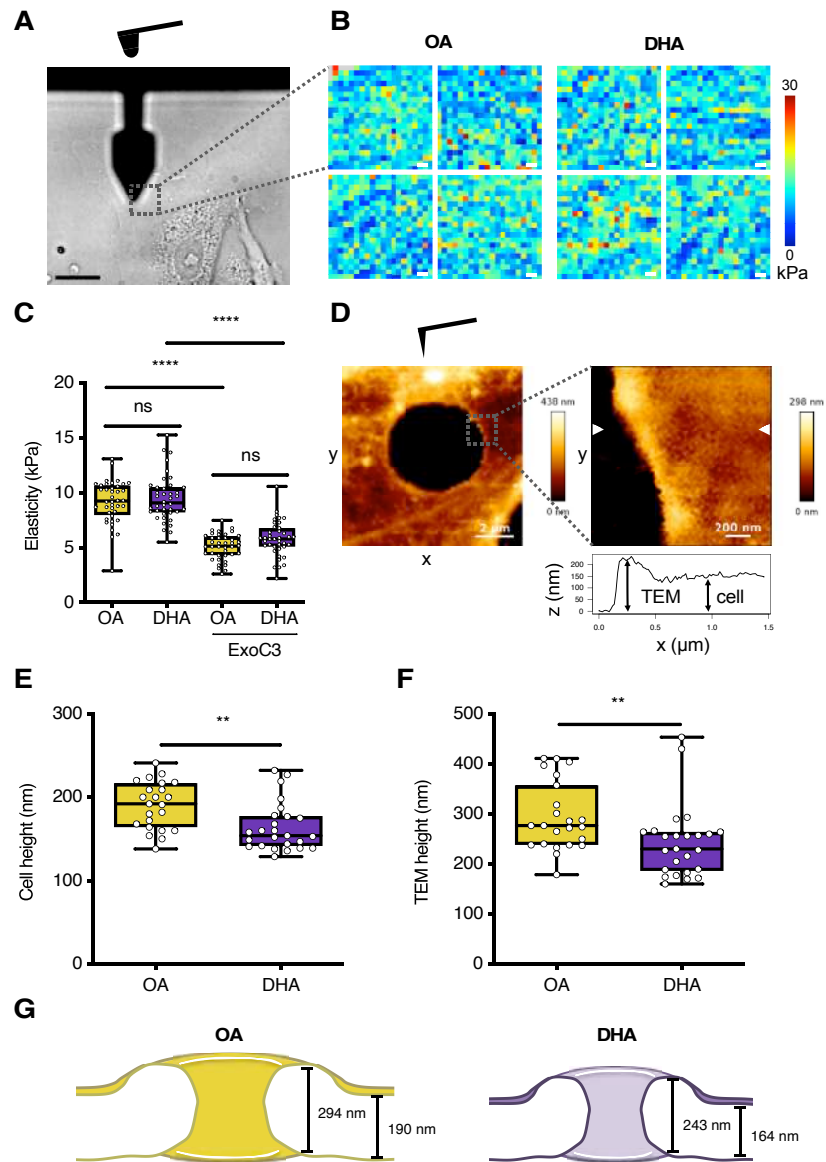


Figure 5

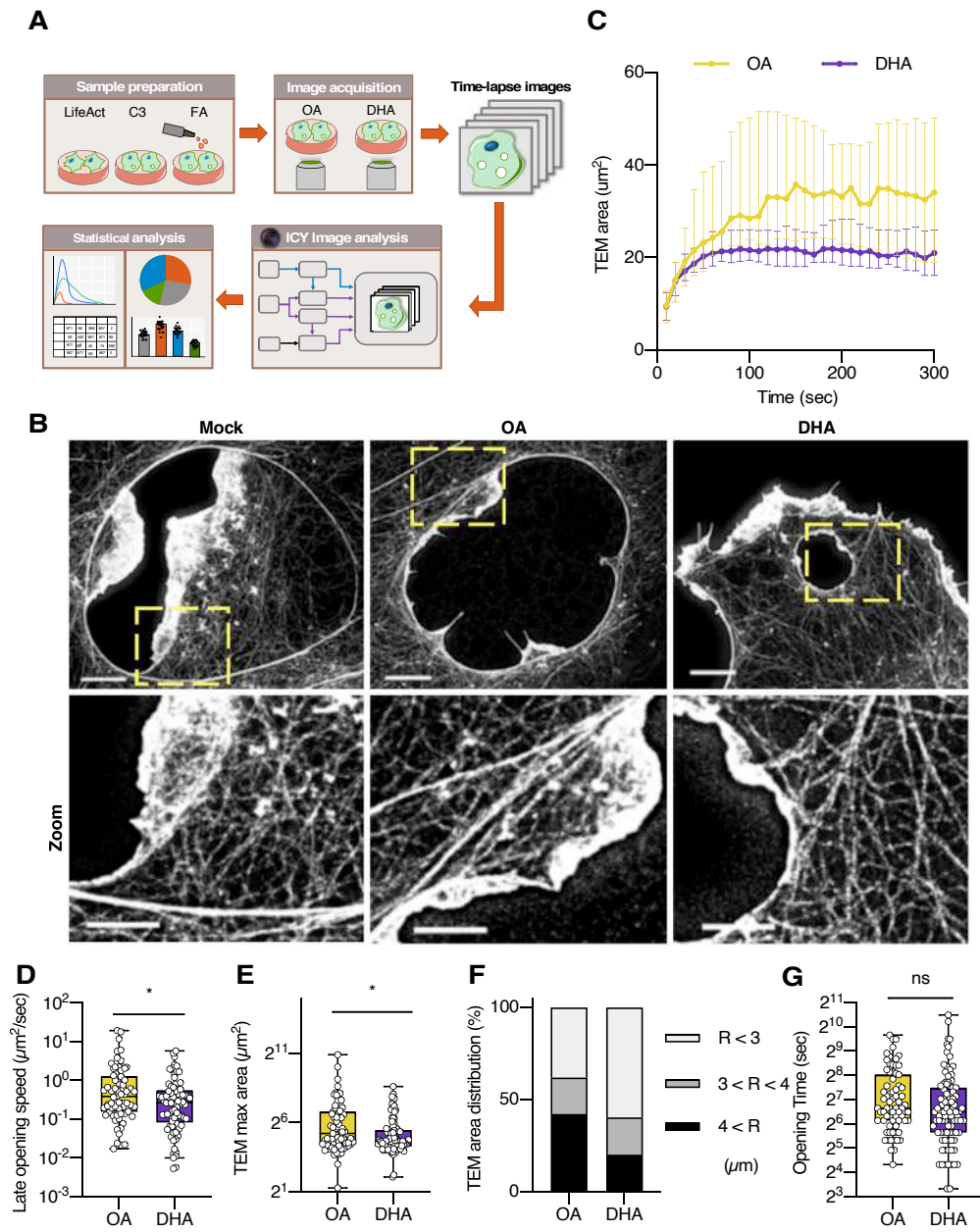


Figure 6

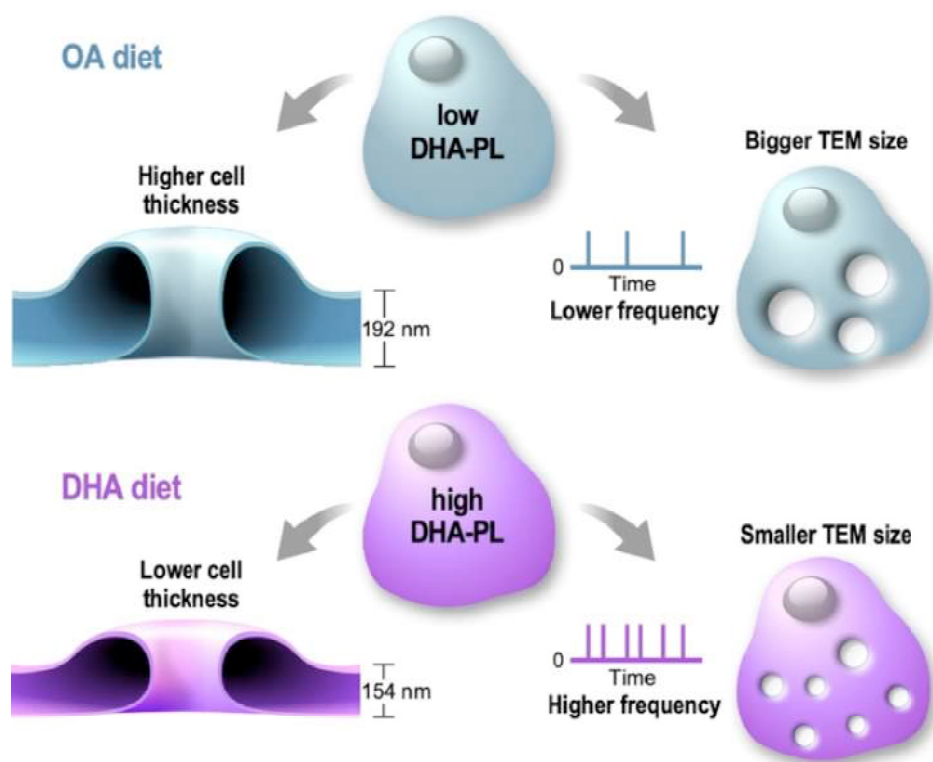


Figure 7

2. DEWETTING: FROM PHYSICS TO THE BIOLOGY OF INTOXICATED CELLS

David Gonzalez-Rodriguez¹, Camille Morel^{2,3} and Emmanuel Lemichez²

1/ LCP-A2MC, Institut Jean Barriol, Université de Lorraine, Metz, 57078 France

2/ Unité des Toxines Bactériennes, Institut Pasteur, ERL 6002, Paris, 75015 France

3/ Paris Diderot, Sorbonne Paris Cité, Paris, France

Corresponding authors : david.gr@univ-lorraine.fr and emmanuel.lemichez@pasteur.fr

2.1. ABSTRACT

Pathogenic bacteria colonize or disseminate into cells and tissues by inducing large-scale remodeling of host membranes. The physical phenomena underpinning these massive membrane extension and deformation are poorly understood. Invasive strategies of pathogens have been recently enriched by the description of a spectacular mode of opening of large transendothelial cell macroaperture (TEM) tunnels correlated to the dissemination of EDIN-producing strains of *Staphylococcus aureus* via a hematogenous route or to the induction of gelatinous edema triggered by the edema toxin from *Bacillus anthracis*. Remarkably, these highly dynamic tunnels close rapidly after they reach a maximal size. Opening and closure of TEMs in cells lasts for hours without inducing endothelial cell death. Multidisciplinary studies have started to provide a broader perspective of both the molecular determinants controlling cytoskeleton organization at newly curved membranes generated by the opening of TEMs and the physical processes controlling the dynamics of these tunnels. Here we discuss the analogy between the opening of TEM tunnels and the physic principles of dewetting, stemming from a parallel between membrane tension and surface tension. This analogy provides a broad framework to investigate biophysical constraints in cell membrane dynamics and their diversion by certain invasive microbial agents.

Abbreviations

BAR Bin Amphiphysin Rvs167 domain

EDIN Epidermal Differentiation Inhibitor
HUVEC Human umbilical vein endothelial cell
I-BAR Inverse-BAR domain
MIM Missing in metastasis
SNARE Soluble NSF attachment protein receptor
TEM Transendothelial cell macroapertures

2.2. INTRODUCTION

Interfacial forces such as surface tension dominate the physics at the micrometric scale, which is characteristic of cellular objects. Indeed, surface tension in liquids has led to two different biophysical analogies in living systems. The first type of analogy has been proposed for multicellular systems, such as multicellular aggregates (Steinberg et al., 1963) or biofilms (Oldewurtel et al., 2015). In this analogy, the cells or bacteria forming the multicellular system are identified to the molecules of a liquid. Such units attract each other through intercellular adhesion, similar to molecular interactions in a liquid. A force imbalance arises at the system's interface, where cells (molecules) only have neighbors to one side. This imbalance is energetically unfavorable and leads the units to spontaneously reorganize to reduce the total surface of the interface. This is the molecular origin of surface tension that describes both the behavior of a liquid drop and of a multicellular system. Thus, surface tension has been characterized and measured for cellular aggregates (Phillips et al., 1978, Forgacs et al., 1998, Guevorkian et al., 2010), soft tissues (Maitre et al., 2015), and bacterial colonies (Rühs et al., 2013). The physical similarities between multicellular systems and liquid drops have led to studying the collective dynamics of multicellular systems through analogies with wetting (Douezan & Brochard-Wyart 2011, Gonzalez-Rodriguez et al., 2012a) and dewetting (Douezan & Brochard-Wyart 2012). A second type of analogy has been proposed at the scale of a single cell. The cell is modeled as a viscous liquid drop (Yeung & Evans 1989) and an analogy is established between liquid surface tension and membrane tension of cells. The idealized picture of a tense membrane to conceptualize liquid surface tension becomes here an actual tense membrane. Importantly, the effective membrane tension in the cell is the sum of two different contributions, one arising from the plasma membrane itself and the other from the actin cortex, to which the plasma membrane is attached (Sheetz & Dai 1996; Diz-Muñoz et al., 2013). The analogy with surface tension is valuable to understand cell shape (Fischer-Friedrich et al., 2014), cell adhesion (Sackmann & Bruinsma 2002), or cell dewetting, which is the topic of this chapter.

A liquid film forced to spread on a non-wettable substrate may spontaneously withdraw from the substrate, leading to the formation of dry patches (Figure 1.1). This phenomenon is known as dewetting. The phenomenon of dewetting is observed for

example when placing a thin layer of oil on a non-sticking pan. Dewetting is driven by a difference in interfacial energies of the liquid between wet and dry regions, the wetting zone being favored. This energy difference translates into tension driving the motion of the liquid surface. The liquid surface can be pictured as a tense membrane whose tension will spontaneously tend to minimize the liquid surface by forming dry patches. By analogy with liquid dewetting, cellular dewetting refers to the process of nucleation and enlargement of transendothelial cell macroapertures (TEM) tunnels observed in endothelial cells (Lemichiez et al., 2013) (Figure 1.1). Several exoenzymes and AB toxins from pathogenic bacteria have the property to induce a cellular dewetting of endothelial cells. They comprise EDIN-like factors from *Staphylococcus aureus* and *Clostridium botulinum* that inactivate RhoA as well as cyclic-AMP producing adenylate cyclase toxins from *Bacillus anthracis* and *Bordetella pertussis*. Formation of TEM tunnels occurs upon relaxation of the actomyosin cytoskeleton as a result of i) inhibition of the small GTPase RhoA by mono-ADP-ribosylating toxins, ii) inhibition of the Rho kinase (ROCK) with the Y27632 compound or iii) a rise of intracellular cyclic-AMP concentration (Boyer et al., 2006; Maddugoda et al., 2011). Video microscopy studies of the dynamics of TEM tunnels formation have revealed the remarkable transient nature of their opening (Figure 1.2). Tunnels open and enlarge in about 2 minutes before reaching a maximal radius of about 10 μm . After the tunnels have stabilized they undergo a phase of closure of about 3 minutes that involves the extension of membrane waves from their edges invading progressively the dry patch up to complete closure (Figure 1.2) (Maddugoda et al., 2011). Cycles of TEM opening and closure occur for hours without induction of cell death or detectable leakage of cytosolic material (Boyer et al., 2006). *In vivo*, the expression of EDIN in a clinically relevant strain of *S. aureus* engineered to emit bioluminescence allows visualizing the resulting increase dissemination of bacteria through the vasculature tree forming more infectious foci in various tissues (Munro et al., 2010). Direct injection of EDIN or of the edema toxin from *B. anthracis* into the vasculature induces the loss of endothelium barrier integrity (Boyer et al., 2006; Maddugoda et al., 2011). *Ex vivo*, EDIN promotes the opening of large tunnels through the endothelium layer of vessels thereby unmasking the extracellular matrix fibers (Boyer et al., 2006). The formation of transcellular tunnels is not just a component of several infectious diseases. More broadly, transendothelial tunnels form during the diapedesis of leukocytes through the

endothelium lining lymphatic and blood vessels (Alon & van Buul, 2017). They also form in cells lining the Schlemm's canal, fulfilling an essential function in the transfer of aqueous humor from the eye chamber to the blood circulation (Braakman et al., 2014).

In this chapter, we review how the analogy with the physics of liquids has allowed a physical interpretation of the opening and enlargement phases of TEMs, yielding the name "cellular dewetting" (Gonzalez-Rodriguez et al., 2012b). While powerful, the analogy between liquid and cellular dewetting is not complete, as some physical aspects of cellular dewetting differ from liquid dewetting due to the intrinsic activity of living matter (Stefani et al., 2017). Here we review the physics of cellular dewetting in parallel to liquid dewetting. Through this parallel, we show the successes of the analogy and we also discuss physical aspects of liquid dewetting for which a cellular dewetting counterpart has not yet been described. This provides clues for future work to address several remaining open questions in the physics of living matter.

2.3. PHYSICAL MODEL OF CELLULAR DEWETTING

In this section we summarize the key ideas for the physical modeling of TEM opening arising from an analogy with liquid dewetting. The driving force for cellular dewetting is

$$F_d = 2\sigma - \frac{T}{R}. \quad (1)$$

Here σ is the membrane tension, which tends to open up a TEM and plays the role of the surface tension in liquid dewetting. Membrane tension is estimated to be of the order of 10^{-5} N/m (Raucher & Sheetz, 2000). The factor of 2 in the equation reflects the existence of upper and lower membranes. T is the line tension that builds up at the edge of TEMs, when they enlarge. It arises from the energetic cost of forming the TEM edge, where the membrane is deformed to a very high curvature. While negligible in liquid dewetting, line tension plays an important role in cellular dewetting. R is the radius of the TEM. Eq. (1) may suggest that the line tension term becomes negligible for large TEMs. This is however not the case, because σ and T do not remain constant during the opening process, as discussed below. Spontaneous dewetting occurs when the driving force F_d is positive. This positive driving force arises from membrane tension

increase due to the spreading of cells, but it can also be enhanced by externally applied equibiaxial strain, *i.e.* a strain of equal magnitude imposed along the two perpendicular directions on the sample plane (Braakman et al., 2014). Eq. (1) shows that $F_d > 0$ requires generating an initial TEM whose radius is larger than a certain threshold, $R > R_n = T/(2\sigma)$. This threshold for initiation of dewetting R_n is known as the nucleation radius. The calculated value of nucleation radius is of the order of 0.1 μm (Gonzalez-Rodriguez et al., 2012b), below photonic microscopy resolution, and its generation mechanisms remain incompletely described so far. As the TEM opens up, the membrane relaxes and membrane tension decreases. It can be assumed that this decrease of membrane tension is rather local given that meanwhile other TEMs open in the cells. Consistent with this notion, recent findings highlighted the local nature of membrane tension in cells (Shi et al., 2018). Moreover, line tension increases due to biological changes occurring around TEM perimeter, such as accumulation of scaffolding proteins (Gonzalez-Rodriguez et al., 2012b) and/or actin assembly (Stefani et al., 2017). As a result, the net driving force decreases and eventually becomes zero. Therefore, the TEM reaches a maximum size, at which spontaneous dewetting stops. Physical models based on Eq. (1) have been developed to explain static aspects of the physics of TEM formation, the maximum size of TEMs, and the role of curvature-sensing proteins (Gonzalez-Rodriguez et al., 2012b, Stefani et al., 2017, Fedorov et al., 2017). Similar to liquid dewetting, the dynamics of TEM opening are governed by a balance between the driving force in Eq. (1) and the dynamic resisting force arising from viscous dissipation (see Eq. 5 below). By using a viscous dissipation model, previous theoretical studies have described the experimentally observed dynamics of TEM opening (Gonzalez-Rodriguez et al., 2012).

2.4. CHARACTERISTICS OF CELL DEWETTING

After having discussed the general framework of the physical modeling of cellular dewetting, in this section we discuss in more detail the building blocks of the model, *i.e.* driving and resisting forces, nucleation, enlargement, reaching of a maximal size and closure of TEMs. We analyze the analogy between liquid dewetting and cellular dewetting and discuss the similarities and differences between the two. The reader

interested in a more detailed overview of the physics of liquid dewetting is referred to the seminal book by P.-G. de Gennes and collaborators (de Gennes et al., 2003).

2.4.1. Driving force

It has been hypothesized that the driving force for a cell to dewet is powered by an abnormal increase of membrane tension, for example during cell stretching. In support of the role of membrane tension increase as a driver for TEM opening, *in vitro* observations highlight that mechanical stretching can induce tunnel formation. A monolayer of endothelial Schlemm's canal cells were cultured on a stretchable substrate and exposed to equibiaxial strain of up to 20%, which induced the formation of transcellular tunnels, as well as paracellular pores at cell junctions (Braakman et al., 2014). Similarly, the bacterial toxin EDIN induces a massive spreading of endothelial cells due to RhoA inhibition and downstream disruption of stress fibers. By analogy, the inhibition of NMII-dependent symmetric traction forces between opposite cell edges induces a sustained spreading of fibroblasts that likely tenses the membrane up to either a rupture of cell edges, which undergo retractions and adopt a C-shape, or the formation of intracellular TEM-like gaps (Cai et al., 2009).

A major difference between TEMs that widen to reach a maximum size and holes in liquids that dewet completely arises from the characteristics of the driving force. The surface tension in liquid dewetting remains constant until the hole enlarges up to a complete disruption of the film. In contrast, membrane tension σ is related to the TEM radius R by Helfrich's law (Helfrich 1975):

$$\sigma = \sigma_0 \exp \left\{ -\frac{R^2}{R_c^2} \right\}, \quad (2)$$

where σ_0 is the undisturbed value of the surface tension, in the absence of a TEM. The characteristic radius in the equation $R_c^2 = R_t^2 (k_B \hat{T}) / (8\pi\kappa)$, where R_t is the radius of the whole cell, $k_B \hat{T}$ is the thermal agitation energy, and κ is the membrane's bending rigidity. Equation (2) is obtained by considering all possible membrane fluctuation modes, whose energy scales as $k_B \hat{T}$ (equipartition theorem). The smallest possible

fluctuation wavelength corresponds to the size of a membrane lipid molecule, whereas the largest possible fluctuation wavelength corresponds to the cell size, R_t . The thermal energy of the membrane fluctuations is used to stretch the membrane (work done against the membrane tension σ) and to bend the membrane (work done against its bending rigidity κ). The mathematical formulation of these concepts leads to Eq. (2) (Helfrich et al., 1975, Helfrich & Servuss, 1984).

Helfrich's law is applicable to membranes subjected to thermal fluctuations. The law is also at play in pore formation in phospholipid vesicles (Sandre et al, 1999, Karatekin et al., 2003), which are also transient. Opening of the hole is limited by reduction of surface tension as the pore opens and by line tension.

By injecting Eq. (2) into Eq. (1) and equating the driving force to zero, two equilibrium solutions for the TEM size are obtained. The smaller of them is the nucleation radius, R_n , and the largest of them is the maximum radius, R_m . For $R_n < R < R_m$, the driving force is positive and cellular dewetting proceeds spontaneously. The first physical model of cell dewetting showed that by combining the dewetting equation, Eq. (1), with Helfrich's law, Eq. (2), one can explain spontaneous TEM opening and the existence of a maximum TEM size (Gonzalez-Rodriguez et al., 2012b). This first result raised the question of the exact nature of line tension around TEMs.

TEM opening does not usually occur in isolation. Rather, it is observed that endothelial cells successively open TEMs at different locations. The opening of one TEM does not significantly impair further TEM opening in the cell. Interestingly, a recent study has provided evidence that membrane tension in cells is a local rather than a global parameter (Shi et al., 2018). According to this study, transmembrane proteins bound to the cytoskeleton act as an obstacle to the propagation of membrane tension variations. Thus, local perturbations in effective cell membrane tension require a time scale of the order of tenths of minutes to propagate to the whole cell, which is the same time scale required for TEMs to close back. This can explain why a local drop in membrane tension due to the opening of a TEM does not preclude subsequent TEM opening elsewhere in the cell.

Laser ablation experiments showed that TEMs having reached their maximum size resume opening when their periphery is perturbed (Stefani et al., 2017). Since laser ablation does not modify membrane tension, these experiments demonstrated that membrane tension reduction does not suffice to explain TEM equilibrium size. This

rather pointed to a key role of cytoskeletal-mediated line tension variations in the arrest of TEM enlargement.

2.4.2. Line tension

Line tension is a force that acts around the edge of a dewetting hole to oppose its widening. In liquids, this force arises from the energetic cost needed to form a highly curved edge. The finding that TEMs stabilize has unveiled the importance of line tension to maintain the cellular integrity, i.e. prevent the extension of a TEM that would finally rupture the edge of cells. The origin of line tension in cell dewetting is a subject of ongoing research. To date, several mechanisms of line tension generation have been proposed: membrane-bending resistance, curvature-sensing proteins forming a scaffold stabilizing the periphery, and actomyosin cable assembly (Gonzalez-Rodriguez et al., 2012b, Stefani et al., 2017).

Membrane bending resistance is responsible for line tension in stretched vesicles (Sandre et al., 1999). When a pore is opened on a vesicle, the lipid molecules along the edge of the pore must curve with a very small radius of curvature that scales as the membrane thickness. This line tension induces the closure of transient pores in vesicles, where it is increased by inclusion of cholesterol and decreased by the addition of detergents (Karatekin et al., 2003). In the case of TEMs, the contribution of membrane bending to line tension is (Gonzalez-Rodriguez et al., 2012b):

$$T_{\text{mb}} = \frac{2\kappa}{h}. \quad (3)$$

As captured by Eq. (3), the relevant radius of curvature of the membrane at the TEM border scales as the cell thickness h . Toxins that induce TEM formation perturb the cell cytoskeleton, leading to a very flat morphology, with a typical thickness $h \sim 50$ nm. Thus, with an estimate of the membrane bending rigidity of $\kappa \sim 40 k_B \hat{T}$, the membrane bending contribution to line tension is of the order of $T_{\text{mb}} \sim 5$ pN. This value is probably greater if one takes into account the force required to deform the cortical cytoskeleton. It is noted that line tension induced by membrane bending rigidity is smaller in TEM opening than it is in pores, because in TEMs the relevant radius for membrane bending is the endothelial cell thickness, whereas at pore edges the lipid membrane bends over

itself to join the inner and outer leaflets. Line tension in TEMs arises from the bending rigidity of the whole membrane, similar to the line tension described at the edges of adherent cells (Oakes et al., 2014). This difference with pore opening leads to a significantly different value of h in Equation (3), and thus to a smaller line tension for TEMs (note that the relevant membrane bending rigidity is also different). However, line tension generation in TEM opening can also be mediated by other mechanisms that are absent in pore formation, as we discuss next.

Curvature-sensing by proteins such as Inverse-BAR domain (I-BAR)-containing proteins may enhance line tension (Saarikangas et al., 2009; Gonzalez-Rodriguez et al., 2012). Association of these proteins to the TEM edge may increase the energetic cost of forming a border. Indeed, these proteins have a preferred spontaneous curvature that may deviate from the actual radius. An increase of the radius may thus force them to an unfavorable configuration, which would translate into a line tension. Interestingly, high-rate video acquisition showed that the I-BAR domain of MIM starts to accumulate along TEM edges a few hundred milliseconds after opening (Maddugoda et al., 2011). The size of TEMs increases upon depletion of the curvature-sensing protein MIM, which can be explained by a decrease of line tension (Maddugoda et al., 2011, Gonzalez-Rodriguez et al., 2012b).

Line tension is primarily provided by local actin reorganization around the TEM edges. It has been shown that an actomyosin cable encircles the TEMs as they open (Stefani et al., 2017). Laser ablation nano-surgery has revealed that cutting the actomyosin cable resumes TEM enlargement up to actomyosin cable formation at the edge of the enlarged zone. Line tension arising from the actomyosin cable limits TEM opening by opposing membrane tension, leading to TEM stabilization at a maximum size. Consistently, the introduction of a break in the cable by a laser nanosurgery-based approach promotes further widening of the hole until a new equilibrium state is reached (Stefani et al., 2017). Indeed, a new break then induces a second phase of TEM enlargement. The role of this cable in limiting TEM size in cellular dewetting can be expressed as an actomyosin contribution to the line tension, T_{am} . The actin scaffold is not present when the TEM nucleates, but rather it is recruited over time, leading to a time-dependent contribution to line tension, $T_{am} = T_{am}(t)$.

Stefani and collaborators have investigated the quantitative dependence of line tension on actomyosin cable formation, by combining physical modeling with experiments of

TEM opening after laser ablation of the cable (Stefani et al., 2017). The predictions of different empirical models of line tension evolution were compared to experimental measurements of TEM opening after ablation. One such model assumed that T_{am} arises from the bending resistance of the cable. Another model supposed that the cable strengthens due to filamentous actin recruitment by convective sweeping of the cell cortex by the moving cable. These two models yielded predictions in contradiction with experimental data showing that the size increase of the TEM after ablation does not depend on its initial size, but it is rather a constant increment. In contrast, good experimental agreement was achieved by a third model that supposed a constant rate of increase of line tension over time, $T_{am} = \alpha t$, corresponding to a constant strengthening of the cable due to actin polymerization and bundling. These descriptions remain empirical, and a full quantitative understanding of the mechanisms by which actomyosin cable assembly leads to line tension generation is still lacking.

2.4.3. Nucleation

The mechanism of nucleation of these structures is probably the most fascinating and difficult question to address. Physical models can guide the response. According to Eq. (1), a TEM will open up if its size is larger than a certain threshold, known as the minimal nucleation radius R_n , which is estimated to be of the order of $0.1 \mu\text{m}$ (Gonzalez-Rodriguez et al., 2012). The mechanism of TEM nucleation, i.e., of formation of the initial tunnel, remains incompletely understood. Even at the cellular scale, a systematic statistical investigation of a population of TEM nucleation events and a comparison with nucleation in classical liquid dewetting is still lacking. At the subcellular scale, TEM nucleation is probably enabled by thermal fluctuations of the two membranes. Because TEMs form in regions where the cells are very thin, the distance between the upper and lower cell membranes (~ 50 to 100 nm) is comparable to the amplitude of membrane fluctuations (Chen et al., 2009), which would allow the two membranes to meet. As the two inner leaflets meet, their fusion may be mediated by fusogenic proteins such as SNAREs (Carman & Springer 2008, Carman et al., 2009) or by cations (Mondal Roy & Sankar 2011). In normal endothelial cells, cytoskeletal resistance to deformation is probably the main barrier to membrane fusion. Indeed, TEMs occur in intoxicated cells whose cytoskeleton is significantly perturbed, leading to a drop of the cell's elastic modulus, as measured by atomic force microscopy

(Ng et al., 2017). Moreover, Ng and collaborators measured a lower penetration work to form TEMs in EDIN-treated cells. In contrast, direct ROCK inhibition has no impact on the penetration force required to form TEMs. This points toward the importance of other RhoA effectors than ROCK for example implicated in actin filaments polymerization and forming a viscous physical barrier to membrane fusion. The contributing role of the dynamics of cortical cytoskeleton in the initiation of tunnels is less defined. More broadly, one can speculate that the formation of a dense network of branched actin filaments triggered by Arp2/3 at the interface of membranes also serves as a natural barrier to prevent membrane interaction and opening of TEMs. Transcellular tunnel opening can also be induced by leukocytes during transmigration, a process in which leukocytes exert forces on endothelial cells through protrusions known as podosomes (Carman et al., 2007, Carman & Springer 2008). By analogy, it has been shown that the application of a mechanical force at the apical side of cells can overcome cytoskeletal resistance to membrane fusion and induce tunnel formation (Ng et al., 2017). In the experiments by Ng et al., compressive forces applied by means of an AFM tip on endothelial cells induced TEM nucleation. Interestingly, control endothelial cells respond to compression by actin polymerization that opposes TEM nucleation, whereas actin polymerization is impaired in intoxicated cells and TEMs open. These tunnels close like those induced by the toxin but are much less wide. The size of the AFM tip is comparable to the size of leukocyte podosomes, and the compression force required to induce TEM opening in AFM experiments (5-100 pN) is also comparable to the forces applied by podosomes during leukocyte transcellular diapedesis (Labernadie et al., 2014).

2.4.4. Maximum size

Typical TEMs open up to a maximum size of the order of several micrometers. TEMs remain at their maximum size for a few tenths of seconds or minutes, before starting to close down. Closure is a slower process, typically lasting for a few minutes, and it is associated to the formation of lamellipodia-like actin-rich membrane waves for a majority of TEMs, whereas other close by a purse-string mechanism (Figure 1.2).

The existence of a maximum size is a specific feature of cellular dewetting. The tunnels remain stably open when the cell is depleted of the MIM protein, showing that cell activity is required for the closure. In contrast, liquid dewetting is irreversible, as dry

patches continue to grow until the liquid has completely withdrawn from the non-wettable surface. In lipid vesicles, pore opening is also transient, but unlike TEMs no durable stabilization at a maximum size is observed between the opening and closure stages (Sandre et al., 1999). Stabilization of a dewetting hole is however observed in liquid dewetting over a rough surface (de Gennes et al., 2003), although such stabilization arises from surface heterogeneities and not from the system itself, as in the process of cellular dewetting.

The maximum size of TEMs results from balance between membrane tension and the kinetics of line tension increase. It corresponds to $F_d=0$ in Eq. (1). In a configuration where membrane tension variations dominate over line tension, the maximum radius would scale as

$$R_m \sim R_c \left(-\ln \frac{T}{2\sigma_0 R_c} \right)^{1/2}. \quad (4)$$

As discussed in the section on line tension above, the assumption of a constant line tension, arising from membrane bending resistance, satisfactorily predicts the typical size attained by TEMs formed *ex novo* (Gonzalez-Rodriguez et al., 2012b). However, this simple picture does not suffice to explain experimental observations of *de novo* TEM opening following laser ablation (Stefani et al., 2017), which requires accounting for a time-varying line tension provided by the assembly of an actin cable around the TEM. With this improvement, the cellular dewetting model can explain quantitatively the increase of TEM size following laser ablation (Stefani et al., 2017). It also provides a physical framework to our hypothesis that ezrin, a member of the FERM-domain containing protein family encompassing ezrin, radixin and moesin, specifically drives the formation of the actin cable encircling TEMs. Ezrin has a tendency to accumulate around TEMs, especially when phosphorylated on T567 (Tsai et al., 2018; Stefani et al., 2017). Ablation of ezrin leads to a higher turnover of F-actin around TEMs and the formation of TEMs of wider size. Taking into account a kinetic parameter in the line tension increase offers a theoretical framework to the observation that a TEM opening *de novo* stabilizes to a maximal size while laser ablation-mediated disruption of the actin cable induced a widening of TEMs that is no longer limited. This particular case indicates that a major difference between viscous liquid dewetting and cellular dewetting comes from cytoskeletal-mediated line tension buildup at curved

membranes, which stabilizes newly formed cell borders generated by the opening of TEMs.

2.4.5. Rim formation

In classical liquid dewetting, the liquid removed from the dry patch accumulates in a rim that forms along the border of the hole (Redon et al., 1991, de Gennes et al., 2003). Such a liquid rim typically has a circular cross-section, and it increases in both height and width as dewetting proceeds, due to mass conservation.

Rim formation is also observed in cellular dewetting, as it has been evidenced by AFM profiles (Maddugoda et al., 2011). The rim appears to correspond to the accumulation of cytoplasmic material that has been displaced as the TEMs open (Gonzalez-Rodriguez et al., 2012b), see Figure 1.1. Typical rim dimensions are about 100 nm in height and about 1 micrometer in width, whereas the cell height at the location of the tunnels is about 50 nm (measured with AFM operated at constant force of 100 pN, 0.3-1 Hz) (Maddugoda et al., 2011). A numerical model that accounts for membrane bending rigidity, membrane tension and cytoplasmic pressure explained the shape of the rim profile by free energy minimization (Fedorov & Shemesh 2017).

2.4.6. Viscous dissipation and opening dynamics

During TEM opening, the driving force in Eq. (1) is positive. At the small length scales of TEM opening, this positive driving force cannot be balanced by inertia as in the macroscopic world. Indeed, the relevant Reynolds number for TEM opening is very small, of the order of 10^{-6} , indicating that inertial effects are negligible. Therefore, the positive driving force must be balanced out by viscous dissipation, same as in viscous liquid dewetting.

In the study of viscous liquid dewetting, different scenarios have been described (de Gennes et al., 2003). For very thin films, where gravity effects are negligible, placed on a smooth and homogeneous solid substrate, liquid removed from the dry patch accumulates in a rim of circular cross-section. Viscous dissipation is mainly due to fluid flow within the rim. This scenario leads to a constant velocity of dewetting, $v = dR / dt = \text{constant}$ (Redon 1991).

A second liquid dewetting scenario arises at longer time scales, once enough liquid has accumulated in the rim and gravity effects are no longer negligible. In this regime, the rim's cross-section becomes a flat pancake, with a maximum thickness equal to e_c , the critical thickness below which a liquid film dewets. This critical thickness scales as the capillary length, of the order of a millimeter. In this regime, viscous dissipation is concentrated at the wedges of the flat pancake, which leads to a law of dewetting of the form $R^2 = D.t$, where D is a constant (Brochard-Wyart et al., 1988).

A third scenario, which inspired the original analogy with cellular dewetting, is the dewetting on a slippery substrate, such as ultra-viscous liquid PDMS on a smooth and passive surface. It has been shown that ultra-viscous liquids slide over smooth, passive surfaces (Redon et al., 1994). Unlike the usual velocity profile of a viscous flow, where velocity vanishes at contact with the substrate due to the no-slip boundary condition, ultra-viscous liquids adopt a plug flow, with a constant velocity profile over the height. In this case, friction dissipation is given by

$$F_v \sim k l v, \quad (5)$$

where l is the width of the rim, $v = dR / dt$ is the velocity, and $k \approx \eta / a$ is a friction coefficient, with η the liquid viscosity and a the size of a monomer in the polymeric liquid. In this scenario, the rim has a circular cross-section. The resulting opening dynamics scale as $R \sim t^{2/3}$ (Redon et al., 1994).

It has been proposed that cellular dewetting resembles this latter scenario (Gonzalez-Rodriguez et al., 2012). As the TEM opens, the rim advances over the substrate. Due to the disturbed cytoskeleton of intoxicated cells, adhesion with the substrate is reduced, and the membrane may slip over the substrate. This is the rationale to model friction dissipation in dewetting using Eq. (5). The friction coefficient k is expected to be of the order of $k \approx 10^8 \text{ Pa.s.m}^{-1}$, an estimate obtained from experiments that measured friction between a cell and a substrate (Guevorkian et al., 2010, Douezan et al., 2011).

Different dynamics are observed in liquid dewetting on a slippery substrate and in cell dewetting, which is attributed to a different shape of the rim. The rim's cross-section is circular in the slippery liquid dewetting and flat in cellular dewetting. This difference modifies the equations of motion, leading to a cellular dewetting law that scales as R

$\sim t^{1/2}$. Thus, cellular dewetting has diffusion-like opening dynamics, same as in the second liquid dewetting scenario discussed above. Interestingly, these two phenomena also share the common feature of a pancake-shaped rim. However, these apparent similarities correspond to different physics: the flat pancake rim in liquid dewetting is due to gravity effects, whereas in cell dewetting it is due to the cell's mechanical properties.

The cellular dewetting dynamics model summarized above is thus based on the assumptions of a pancake-shaped rim of constant height and membrane slipping on the substrate (Gonzalez-Rodriguez et al., 2012b). Its validity is supported by good agreement with the dynamics of opening observed in experiments. However, direct experimental investigation of the rim shape evolution is limited, and the flow field of the cell membrane during TEM opening has not been quantified. Future experiments could aim at experimentally characterizing these two aspects of TEM opening, in order to directly test the model's hypotheses.

2.4.7. Closure

Over longer time scales, of the order of several minutes, TEMs completely close down (Figure 1.2). Unlike transient pore closure in vesicles, the interplay between surface tension and line tension do not suffice to explain the dynamics of TEM closure, which is driven by extension of actomyosin-dependent processes. TEM closure has been related to the formation of lamellipodia-like projections via local Arp2/3-dependent branched-actin polymerization driven by MIM (Maddugoda 2011). Closure driven by actin polymerization has been described by a physical model (Fedorov & Shemesh 2017). This model related actin polymerization dynamics to local curvature of the TEM edge. The model predicted that actin polymerization is slower in regions where the TEM edge has positive curvature (the curvature of a circular TEM) and faster in regions of negative curvature (such as a protrusion). This curvature effect is due to the effect of line tension, which promotes protrusion at a negatively curved edge, and to the lower compressive stress experienced by actin filaments in such regions, which results in a higher polymerization rate. The model successfully explains the observed instability of the circular TEM shape, which forms protrusions during the closure. The TEM closure mechanism described in this model does not require myosin motor activity for TEM repair.

An open question is the role of the actomyosin cable in the dynamics of TEM closure. Although a majority of the TEMs close by extension of membrane waves, we have also observed closure of TEMs by a purse-string phenomenon. Laser ablation experiments have shown that the cable after ablation retains its original length, indicating that it is under tension but does not undergo significant elastic deformation (Stefani et al., 2017). The absence of the contractility of the cable may be dependent on the level of RhoA inactivation in intoxicated cells. In some circumstances the actomyosin cable that forms around the TEM (Stefani et al., 2017) could provide an additional mechanism to drive TEM closure by a purse-string mechanism similar to that described in wound healing of epithelial tissues (Vedula et al., 2015). In this case, it is not excluded that another type of contractile ring forms around TEMs when they stabilize prior to the closure by a purse-string mechanism.

2.5. FUTURE DEVELOPMENTS AND CONCLUSIONS

In this section we discuss several physical phenomena observed in liquid dewetting for which an analogy in cellular dewetting has not yet been identified. These unexplored analogies, if pertinent, may lead to advancements in our understanding of the physics of TEMs.

2.5.1. Critical thickness

Spontaneous dewetting of a liquid film on a solid substrate depends on the value of the spreading parameter S , which is the difference in energy between a wet patch and a dry patch (de Gennes et al., 2003). For $S > 0$ a liquid film is always stable and dewetting does not occur. For $S < 0$ dewetting occurs when the film thickness e is smaller than a critical threshold thickness e_c . The balance between capillarity and gravity defines this critical thickness. For $e < e_c$, a configuration where the liquid accumulates in patches of thickness e_c by leaving dry patches elsewhere is energetically favored, and dewetting can occur spontaneously. The continuous film of thickness $e < e_c$ is thus at a metastable state. Experiments perturbing the film destabilize its metastable state thereby initiating dewetting.

In cellular dewetting, the role of the liquid film is played by the whole cell. In the cell dewetting model, there is no direct analogy with the critical threshold thickness. This is because gravitational forces in liquid dewetting, which set the critical thickness, are negligible in cell dewetting, where they are much smaller than viscous and membrane forces. Nevertheless, it is observed that cellular dewetting occurs in cells that are abnormally thin, of the order of 50 to 100 nm or when pushing on the membranes to bring them in close proximity. This suggests the possible existence of a critical cell thickness for dewetting, although arising from different physics. Existence of a critical thickness would not simply mean that it is harder to nucleate a TEM in a thicker cell. Rather, we suggest that if the cell thickness is larger than a certain threshold, any nucleated tunnel would immediately disappear, implying that TEM opening is observed only when the cell thickness is smaller than this threshold. In physics terms, the cell would be metastable below this critical thickness and stable above. In cellular dewetting, such critical thickness would not be set by gravity, but by a different force opposing TEM opening, such as actin cytoskeletal resistance.

2.5.2. Spinodal dewetting

Very thin liquid films of $e \ll e_c$ are unstable to capillary waves. Driven by van der Waals forces, perturbations get amplified at certain wavelengths, and the liquid films breaks up into multiple droplets. This dewetting mechanism is known as spinodal dewetting (Reiter et al., 1992, de Gennes et al., 2003). It is a different dewetting mechanism from the nucleation and growth of dry patches.

Spinodal dewetting in cells has not been described. Whereas a direct physical analogy may not be pertinent, spinodal decomposition processes may play a role in cell dewetting. Similar to spinodal dewetting arising from the growth of surface perturbations in the liquid film, cellular dewetting appears to arise from perturbations in the cell membrane. Rather than studying out-of-plane perturbations of the film thickness like in spinodal liquid dewetting, it appears more pertinent to investigate heterogeneities in cell membrane composition. Indeed, spinodal decomposition leading to phase separation has been reported in multicomponent lipid vesicles (Veatch & Keller 2003). Such membrane heterogeneities may create preferential spots for TEM nucleation, as well as barriers between membrane domains that limit TEM

opening. These considerations suggest studying how the locations of successive TEM opening within one cell correlate with heterogeneities in membrane composition.

In spinodal dewetting, a thin liquid film may be perturbed by the wavy topography of the substrate, if the wavelength of such geometrical substrate variations is large enough. Similarly, there could be a role of substrate geometry in cellular dewetting. This analogy points to a possible effect of substrate patterning and of substrate curvature on inducing membrane perturbations and TEM nucleation. In the next section, we further consider how surface characteristics may affect cell dewetting.

2.5.3. Irregular and soft substrates

There are large variations in the fibrillar composition and mechanical properties of the extracellular matrix that is in direct contact with endothelial cells (Marchand et al., 2018). Substrate irregularities induce hysteresis in liquid dewetting (de Gennes et al., 2003). The origin for such hysteresis is the existence of two different contact angles for a drop placed on a textured surface, depending on whether the wetting front advances or recedes. Due to hysteresis, liquid dewetting on a textured surface may lead to stable configurations, where a dry patch keeps a constant size, and neither opens up nor closes. Hysteretic effects in cellular dewetting have not yet been described, but they could arise in cellular dewetting over patterned or heterogeneous substrates, which are known to significantly modify cell properties (Curtis & Wilkinson 1997, Anderson & Hinds 2011).

Liquid wetting and dewetting phenomena are also affected by substrate stiffness. If the substrate is sufficiently soft to be deformed by surface tension forces, elasto-capillary phenomena arise (Bico et al., 2018). To date, cellular dewetting on substrates of different stiffness has not been studied. However, we expect that substrate rigidity may affect cellular dewetting through physical mechanisms, such as elasto-capillarity, and through biological mechanisms, such as actin reorganization in response to mechanosensing. We also anticipate the role of biophysical mechanisms by which rigidity modifies the wetting properties of a substrate by a cell. It has been shown that the wetting of cellular aggregates can be equivalently modulated by substrate chemistry (as in classic liquid wetting) or by substrate rigidity (which is specific to biological wetting) (Douezan et al., 2012). Substrate coating and rigidity also affect wetting-dewetting transitions in cellular monolayers (Perez-Gonzalez et al., 2019).

Substrate coating and rigidity are known to affect the height of membrane undulations (Chang et al., 2017), which likely contribute to membrane collision for fusion and opening of TEMs. Taken together, these previous observations suggest an effect of substrate characteristics on cellular dewetting.

In conclusion, the analogy made between the dynamics of TEMs and the physics of liquid dewetting on non-wettable surfaces has been instrumental in deciphering essential parameters of TEM opening and stabilization. A challenge for the upcoming years will certainly encompass the comparison of this phenomenon to leukocyte diapedesis through the endothelium and the study of these phenomena in 3D models reflecting the physiological conditions of vessels. It will also be interesting to define the intrinsic cellular parameters that limit the formation of TEMs in cells. This should ultimately lead to progress in our understanding of spontaneous bleeding vascular diseases not due to platelet deficiencies.

2.6. ACKNOWLEDGEMENTS

We warmly thank all our colleagues who have contributed to unveiling the importance of the cellular dewetting phenomenon and the biophysical mechanisms underlying it. We are particularly grateful to Patricia Bassereau and Françoise Brochard-Wyart for pointing out the analogy between the opening of TEMs and the physics of dewetting and for their contributions to modeling this biological phenomenon. We also thank Cécile Leduc, Patricia Bassereau and two anonymous reviewers, who read earlier versions of this chapter and provided valuable ideas and suggestions. Studies on TEMs are funded by a grant ANR-15-CE18-0016.

References

- Alon R, van Buul JD (2017) Leukocyte Breaching of Endothelial Barriers: The Actin Link. *Trends Immunol* 38, 606-615.
- Anderson DE, Hinds MT (2011) Endothelial cell micropatterning: methods, effects, and applications. *Ann Biomed Eng* 39(9):2329–45.
- Bico J, Reyssat E, Roman B (2018) Elastocapillarity: when surface tension deforms elastic solids. *Annu Rev Fluid Mech* 50:629–659.
- Boyer L, Doye A, Rolando M, Flatau G, Munro P, Gounon P, Clément R, Pulcini C, Popoff MR, Mettouchi A, Landraud L, Dussurget O, Lemichez E (2006) Induction of transient macroapertures in endothelial cells through RhoA inhibition by *Staphylococcus aureus* factors. *J Cell Biol* 173 (5):809–819.
- Braakman ST, Pedrigi RM, Read AT, Smith JAE, Stamer WD, Ethier CR, Overby DR (2014) Biomechanical strain as a trigger for pore formation in Schlemm's canal endothelial cells. *Exp Eye Res* 127:224–235.
- Brochard-Wyart F, Redon C, Rondelez F (1988) Démouillage: régime de gravité. *C R Acad Sci Paris*, 306(II):1143–1146.
- Cai, Y., Rossier, O., Gauthier, N. C., Biais, N., Fardin, M. A., Zhang, X., Miller, L. W., Ladoux, B., Cornish, V. W., and Sheetz, M. P. (2010). Cytoskeletal coherence requires myosin-IIA contractility. *J Cell Sci* 123: 413-423.
- Carman CV, Sage PT, Sciuto TE, de la Fuente MA, Geha RS, Ochs HD, Dvorak HF, Dvorak AM, Springer TA (2007) Transcellular diapedesis is initiated by invasive podosomes. *Immunity* 26:784–797.
- Carman CV, Springer TA (2008) Trans-cellular migration: cell-cell contacts get intimate. *Curr Opin Cell Biol* 20:533–540.
- Carman CV (2009) Mechanisms for transcellular diapedesis: probing and pathfinding by “invadosome-like protrusions.” *J Cell Sci* 122:3025–3035.
- Chen CH, Tsai FC, Wang CC, Lee CH (2009) Three-dimensional characterization of active membrane waves on living cells. *Phys Rev Lett* 103(23):238101.
- Chang CH, Lee HH, Lee CH (2017) Substrate properties modulate cell membrane roughness by way of actin filaments. *Sci Rep* 7:9068.
- de Gennes PG, Brochard-Wyart D, Quéré D (2003) *Capillarity and Wetting Phenomena. Drops, Bubbles, Pearls, Waves.* Springer.
- Curtis A, Wilkinson C (1997) Topographical control of cells. *Biomaterials* 18(24):1573–1583.
- Diz-Muñoz A, Fletcher DA, Weiner OD (2013) Use the force: membrane tension as an organizer of cell shape and motility. *Trends Cell Biol* 23(2):47–53.
- Douezan S, Brochard-Wyart F (2011) Spreading dynamics and wetting transition of cellular aggregates. *Proc Natl Acad Sci USA* 108(18):7315–20.
- Douezan S, Brochard-Wyart F (2012) Dewetting of cellular monolayers. *Eur Phys J E* 35(5):34.
- Douezan S, Dumond J, Brochard-Wyart F (2012) Wetting transitions of cellular aggregates induced by substrate rigidity. *Soft Matter* 8(17):4578–4583.
- Fedorov EG, Shemesh T (2017) Physical model for stabilization and repair of trans-endothelial apertures. *Biophys J* 112(2):388–397.
- Fischer-Friedrich E, Hyman AA, Jülicher F, Muller DJ, Helenius J (2014) Quantification of surface tension and internal pressure generated by single mitotic cells. *Sci Rep* 4:6213.
- Forgacs G, Foty RA, Shafrir Y, Steinberg MS (1988) Viscoelastic properties of living embryonic tissues: a quantitative study. *Biophys J* 74(5):2227–2234.
- Gonzalez-Rodriguez D, Guevorkian K, Douezan S, Brochard-Wyart F (2012a). Soft matter models of developing tissues and tumors. *Science* 338, 910-917.
- Gonzalez-Rodriguez D, Maddugoda MP, Stefani C, Janel S, Lafont F, Cuvelier D, Lemichez E, Brochard-Wyart F (2012b) Cellular dewetting: opening of macroapertures in endothelial cells". *Phys Rev Lett* 108 (21):218105.

- Guevorkian K, Colbert MJ, Durth M, Dufour S, Brochard-Wyart F (2010) Aspiration of biological viscoelastic drops. *Phys Rev Lett* 104:218101.
- Helfrich W (1975) Out-of-Plane Fluctuations of Lipid Bilayers. *Zeitschrift für Naturforschung C*, 30(11-12):841–842.
- Helfrich W, Servuss RM (1984) Undulations, steric interaction and cohesion of fluid membranes. *Il Nuovo Cimento D*, 3(1):137–151.
- Karatekin E, Sandre O, Guitouni H, Borghi N, Puech PH, Brochard-Wyart F (2003) Cascades of Transient Pores in Giant Vesicles: Line Tension and Transport. *Biophys J* 84(3):1743–1749.
- Labernadie, A., Bouissou, A., Delobelle, P., Balor, S., Voituriez, R., Proag, A., Fourquaux, I., Thibault, C., Vieu, C., Poincloux, R., Charrière, G. M., and Maridonneau-Parini, I. (2014). Protrusion force microscopy reveals oscillatory force generation and mechanosensing activity of human macrophage podosomes. *Nat Commun* 5:5343.
- Lemichez E, Gonzalez-Rodriguez D, Bassereau P, Brochard-Wyart F (2013) Transcellular tunnel dynamics: Control of cellular dewetting by actomyosin contractility and I-BAR proteins. *Biol Cell* 105 (3):109–117.
- Maddugoda MP, Stefani C, Gonzalez-Rodriguez D, Saarikangas J, Torino S, Janel S, Munro P, Doye A, Prodon F, Aurrand-Lions M, Goossens PL, Lafont F, Bassereau P, Lappalainen P, Brochard F, Lemichez E (2011) cAMP signalling by anthrax edema toxin induces transendothelial cell tunnels, which are resealed by MIM via Arp2/3-driven actin polymerization. *Cell Host Microbe* 10 (5):464–474.
- Maitre JL, Niwayama R, Turlier H, Nédélec F, Hiragi T (2015) Pulsatile cell-autonomous contractility drives compaction in the mouse embryo. *Nat Cell Biol* 17(7):849–855.
- Marchand M, Monnot C, Muller L, Germain S (2018) Extracellular matrix scaffolding in angiogenesis and capillary homeostasis. *Semin Cell Dev Biol* S1084-9521(17):30578–30575.
- Mondal Roy S, Sarkar M (2011) Membrane fusion induced by small molecules and ions. *J Lipids* e528784.
- Munro P, Benchetrit M, Nahori MA, Stefani C, Clement R, Michiels JF, Landraud L, Dussurget O, Lemichez E (2010) *Staphylococcus aureus* EDIN toxin promotes formation of infection foci in a mouse model of bacteremia. *Infect Immun* 78:3404–3411.
- Ng WP, Webster KD, Stefani C, Schmid EM, Lemichez E, Bassereau P, Fletcher DA (2017) Force-induced transcellular tunnel formation in endothelial cells. *Mol Biol Cell* 28(20):2589–2745.
- Oakes PW, Banerjee S, Marchetti MC, Gardel ML (2014) Geometry regulates traction stresses in adherent cells. *Biophys J* 107(4): 825-833.
- Oldewurtel ER, Kouzel N, Dewenter L, Henseler K, Maier B (2015) Differential interaction forces govern bacterial sorting in early biofilms. *eLife* 4:e10811.
- Pérez-González C, Alert R, Blanch-Mercader C, Gómez-González M, Kolodziej T, Bazellieres E, Casademunt J, Trepast X (2019) Active wetting of epithelial tissues. *Nat Phys* 15:79–88.
- Phillips HM, Steinberg MS (1978) Embryonic tissues as elasticoviscous liquids. I. Rapid and slow shape changes in centrifuged cell aggregates. *J Cell Sci* 30:1–20.
- Raucher D, Sheetz MP (2000) Cell spreading and lamellipodial extension rate is regulated by membrane tension. *J Cell Biol* 148:127–136.
- Redon C, Brochard-Wyart F, Rondelez F (1991) Dynamics of dewetting. *Phys Rev Lett* 66(6):715–718.
- Redon C, Brzoska JB, Brochard-Wyart F (1994) Dewetting and slippage of microscopic polymer films. *Macromolecules* 27:468–471.
- Reiter G (1992) Dewetting of thin polymer films. *Phys Rev Lett* 68(1):75–78.
- Rühs PA, Böni L, Fuller GG, Inglis RF, Fischer P (2013) In-situ quantification of the interfacial rheological response of bacterial biofilms to environmental stimuli. *PLoS One* 8(11):e78524.
- Saarikangas, J., Zhao, H., Pykalainen, A., Laurinmaki, P., Mattila, P. K., Kinnunen, P. K., Butcher, S. J., and Lappalainen, P. (2009). Molecular mechanisms of membrane deformation by I-BAR domain proteins. *Curr Biol* 19:95-107.
- Sackmann E, Bruinsma RF (2002) Cell adhesion as wetting transition? *Chem Phys Chem* 3:262–269.
- Sandre O, Moreaux L, Brochard-Wyart F (1999) Dynamics of transient pores in stretched vesicles. *Proc Natl Acad Sci USA*, 96(19):10591–10596.

Sheetz, M. P., and Dai, J. (1996). Modulation of membrane dynamics and cell motility by membrane tension. *Trends Cell Biol* 6: 85-89.

Shi Z, Graber ZT, Baumgart T, Stone HA, Cohen AE (2018) Cell membranes resist flow. *Cell* 175:1769–1779.

Stefani C, Gonzalez-Rodriguez D, Senju Y, Doye A, Efimova N, Janel S, Lipuma J, Tsai MC, Hamaoui D, Maddugoda MP, Cochet-Escartin O, Prévost C, Lafont F, Svitkina T, Lappalainen P, Bassereau P, Lemichez E (2017) Ezrin enhances line tension along transcellular tunnel edges via NMIIa driven actomyosin cable formation. *Nat Commun* 23(8):15839.

Steinberg MS (1963) Reconstruction of tissues by dissociated cells. *Science* 141(3579):401–408.

Tsai, F. C., Bertin, A., Bousquet, H., Manzi, J., Senju, Y., Tsai, M. C., Picas, L., Miserey-Lenkei, S., Lappalainen, P., Lemichez, E., Coudrier, E., and Bassereau, P. (2018). Ezrin enrichment on curved membranes requires a specific conformation or interaction with a curvature-sensitive partner. *eLife* 7:e37262.

Veatch SL, Keller SL (2003) Separation of Liquid Phases in Giant Vesicles of Ternary Mixtures of Phospholipids and Cholesterol. *Biophys J* 85(5):3074–3083.

Vedula SR, Peyret G, Cheddadi I, Chen T, Brugués A, Hirata H, Lopez-Menendez H, Toyama Y, de Almeida LN, Trepát X, Lim CT, Ladoux B (2015) Mechanics of epithelial closure over non-adherent environments. *Nat Commun* 6:6111.

Yeung A and Evans E (1989) Cortical shell-liquid core model for passive flow of liquid-like spherical cells into micropipets. *Biophys J* 56:139–149.

Figures

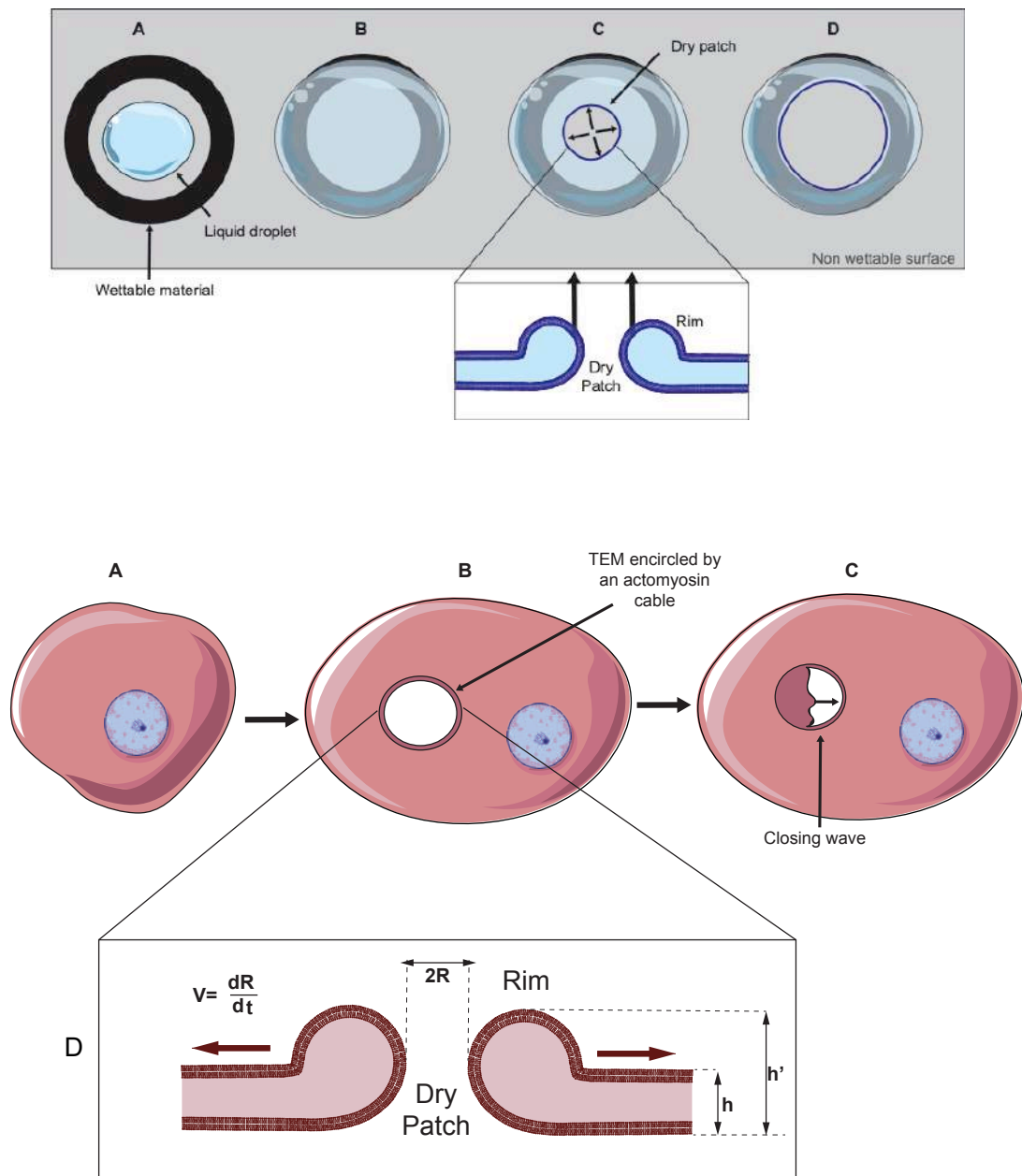


Fig. 1.1 Physical process of liquid dewetting compared to biological cellular dewetting

Upper panel: dewetting phenomenon. **(A)** A liquid droplet is deposited at the center of a non-wettable surface, surrounded by a black region that has been rendered wettable. **(B)** The droplet is mechanically forced to spread and gets pinned by the wettable region, created by a localized substrate treatment. Thus, a metastable state is reached. **(C)** Nucleation of a dry patch destabilizes the system. The dry patch opens up spontaneously so that free energy is minimized. **(D)** The dry patch grows until it fully withdraws from the non-wettable zone. The liquid removed from the dry zone accumulates in a rim.

Lower panel: cellular dewetting phenomenon. **(A)** An untreated cell with its nucleus (in blue). **(B)** Upon RhoA inhibiting exoenzyme treatment, the cell spreads thereby increasing membrane tension. A TEM forms and enlarges up to a maximal size, also displaying the formation of a rim along the TEM. The formation of a rigid actin cable encircling the TEM allows its stabilization. **(C)** TEMs open transiently owing to the formation of membrane waves invading the dry patch up to complete resealing of the TEM. **(D)** Schematic side-view showing characteristic dimensions ($h=50$ nm, $h'=100$ nm, t : time, R : radius, V : opening speed).

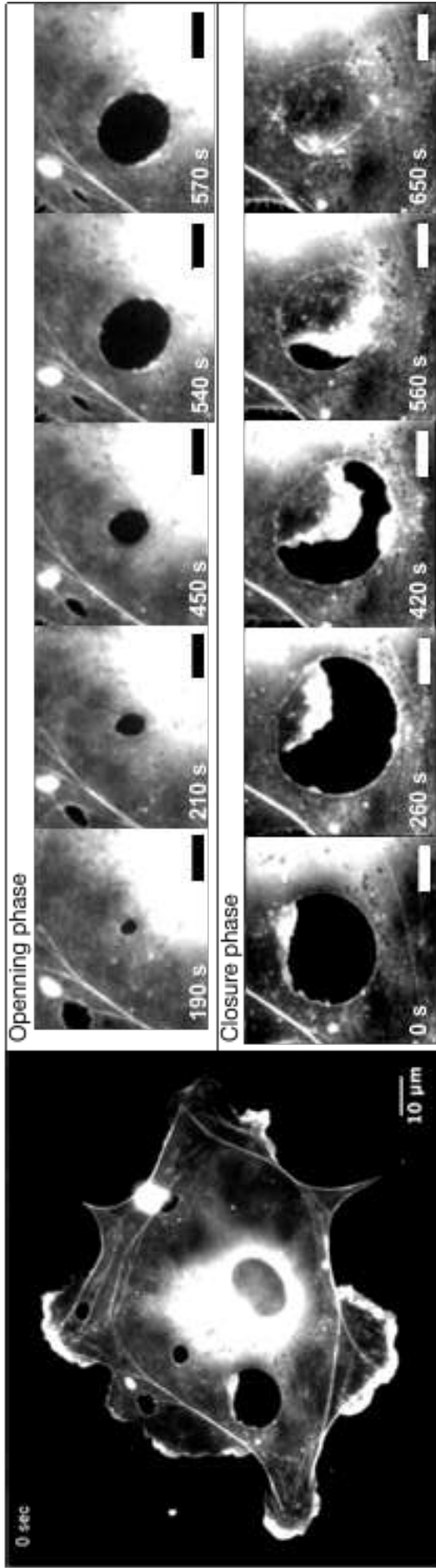


Fig. 1.2 Human Umbilical Vein Endothelial cell (HUVEC) expressing pLifeAct-GFP intoxicated 24h with edema toxin (ET) from *Bacillus anthracis* was imaged with a spinning-disk microscope (60x) at a rate of one image every 10 seconds during 1h (Published in Maddugoda et al., 2011). Right panels show series of snapshots taken at the indicated time. It displays the opening (upper panel) and closure (lower panel) phase of two TEMs. The TEM opens and reaches its maximum size in a few tenths of seconds. Closure typically involves lamellipodia-like actin-rich membrane extension. Note the presence after closure of a persistent actin cable encircling TEMs. Scale bar represent 5 μm.